Wrocław University
of Science and Technology

Theoretical studies on photoinduced charge and electron transfer processes in nucleobase pairs and their prebiotic precursors

by

Kinga Szkaradek

DISSERTATION

submitted in partial fulfillment
for the doctoral degree in

CHEMICAL SCIENCES

at the

Faculty of Chemistry

Wrocław, September, 2024

Supervisor:
Robert W. Góra, Ph.D., D.Sc.
Co-Supervisor:
Prof. RNDr. Jiří Šponer, DrSc.

Contents

Acknowledgments

I would like to take this opportunity to express my gratitude to all those who contributed to this doctoral dissertation. I am grateful to my supervisor, Professor Robert Góra, for being an endless source of knowledge. I thank Dr Rafał Szabla for his inspiring scientific discussions and constructive criticism. Special thanks also go to Dr Petr Stadlbauer for assisting with the linguistic aspects of this dissertation. I would like to express my gratitude for some such crucial motivating words of Dr Robert Zaleśny in the time of need. Last but not least, I wish to thank my parents for their constant support.

This work was supported by a grant from National Science Centre Poland (Preludium no 2021/42/N/ST4/04532) and BioTechNan fellowship. The authors acknowledge the resources granted by the Wrocław Centre of Networking and Supercomputing (WCSS).

List of Abbreviations

CoI	Conical intersection
CT	Charge transfer
EDPT	Electron-driven proton transfer
FC	Franck-Condon
HS	Hoogsteen
IC	Internal conversion
ISC	Intersystem crossing
LE	Locally excited
LIIC	Linear interpolation in internal coordinates
MECI	Minimum-energy conical intersection
MECP	Minimum-energy crossing point
MO	molecular orbital
NTO	Natural Transition Orbitals
PCET	Proton-coupled electron transfer
PES	Potential energy surface
SA	State-averaged

SCS Spin-component scaling variant

TS Transition state

WC Watson-Crick

Abstract

The photochemistry and photophysics of the canonical guanine-cytosine (G-C) and adenine-thymine (A-T) nucleobase pairs have been the subject of intensive research by numerous experimental and theoretical groups. However, there is still no consensus in the literature regarding the nature of the relaxation processes that occur after the absorption of UV radiation. Theoretical studies on the behavior of canonical Watson–Crick (WC) base pairs under photoexcitation have led to the suggestion that proton-coupled electron transfer (PCET), also known as electron-driven proton transfer (EDPT), processes seem to play a significant role in the radiationless deactivation of photoexcitation through the intersection of the dark repulsive $^1\pi\pi^*$ charge-transfer (CT) state with a locally excited bright state (LE) and subsequently with a ground state.

Although much is already known about these processes, the proposed proton transfer mechanism as a result of electron transfer has not been confirmed experimentally for the WC-A-T canonical base pair. It could be a result of spectroscopic failure to measure the ultra-short lifetimes (<100fs) or wrong assumptions about the nature of this process. The computational studies carried out within this thesis have led to the research hypothesis that **there are several alternative relaxation channels through charge and electron transfer due to interaction between nucleobases**. The latter not only enables EDPT or PCET processes but also alters the intramolecular photoexcitation decay pathways through heterocyclic ring deformation or bond stretching. The processes involving intersections of the LE $^1\pi\pi^*$ bright states with the dark $^1n\pi^*$ states and the alternative EDPT channel through the population of $^1n\pi^*_{CT}$ states were identified and described here for the first time.

Simultaneously, a significant part of the research is devoted to alternative non-canonical base pairs. Comparative analysis and verification of the mechanisms of nonradiative deactivation of excited states in canonical and non-canonical nucleobases paired in the WC scheme

deepen the insight into the role of photoinduced charge transfer processes in nucleic acids after UV absorption. They also contribute to a better understanding of why living organisms use such a narrow set of building blocks of genetic material, which interestingly share a common feature of high photostability.

Scientific research conducted within the confines of this thesis is divided into several stages. First, the research on the photophysics and photochemistry of the canonical and noncanonical nucleobases, both isolated and paired in the WC scheme, is reviewed. The selection of non-canonical nucleobases was inspired by research reports on the synthesis of nucleotides and their prebiotic precursors under reliable abiotic conditions. The analysis of the potential energy surface profiles for low-lying excited states of the systems studied along the proton transfer coordinates is discussed and the role of $^1n\pi^*$ states in these processes is established. Theoretical studies of potential energy surfaces (PESs) and conical intersections between them were performed using state-of-the-art single- and multireference ab initio methods.

This dissertation describes for the first time the conical intersections of intermolecular CT $^1n\pi^*$ with the ground state in canonical and alternative base pairs, which may allow efficient deactivation through a new type of EDPT mechanism. This indicates that long-lived, reactive $^1n\pi^*$ states, previously considered as potential sources of photodamage in isolated pyrimidine nucleosides, may actually facilitate efficient photodeactivation.

Two possible types of nonradiative deactivation channels have been identified and described occurring on the potential energy surfaces of $^1n\pi^*$ states. It may be a one-step process in which the pyrimidine ring is deformed after photoexcitation and, as a result, the conical intersection with a ground state is reached. The population of the $^1n\pi^*$ states may also initiate a two-step EDPT process in some WC-type base pairs, in particular the G-C, H-C and oxoG-C pairs. It was also noticed that in all systems studied, the population of the $^1\pi\pi^*$ charge transfer state should lead to effective photorelaxation through the EDPT process.

1 Introduction

1.1 Theoretical background

Time-dependent phenomena of the excitation decay

The photophysical and photochemical processes lead to the time-dependent evolution of the state and geometry of an excited molecule, respectively. The molecule under UV irradiation is supplied with a large amount of excess energy that needs to be dissipated on a relatively short timescale. The excited molecule eventually must reach its ground state, and it is through vibrational relaxation, quenching, or radiative and nonradiative transitions.[1] The loss of oscillatory energy is highly correlated with collisions, which cause this energy to be converted to kinetic energy and transferred to other particles.[1] The quenching is attributed to internal (as nonradiative transitions) or external factors. It is often connected with the quencher: the substance that accelerates the higher-to-lower electronic-state deactivation or the relaxation to the ground state. The oxygen molecule is, for example, one of the most effective quenchers. Furthermore, this process is often related to excimer formation, manifested by an increase in the concentration of the emitting substance with a decrease in the fluorescence quantum yields.[1]

Fluorescence is one of the radiative transition processes between states of the same multiplicity. It is a relatively fast spin-allowed process, unlike phosphorescence, which is due to the transition between states of different multiplicity (usually $T_1 \rightarrow S_0$). However, one should remember that there are faster decay channels; thus, the fluorescence is vital only while they are unavailable. In particular, the dissipation of excess energy can occur through radiationless deactivation processes that occur between degenerate levels of different states.

[1] J. A. Barltrop and J. D. Coyle, *Principles of photochemistry*, Wiley, 1978.

In order to better understand these intertwining photophysical phenomena, the Jabłoński diagram is often used. The diagram marks the electronic states and vibrational levels with bold and thin horizontal lines, respectively. The solid vertical lines represent the absorption or emission of a photon, whereas the dashed arrows depict nonradiative processes. The first step, absorption, is usually characterized as vertical electronic excitation because the electrons respond much faster to the absorbed photon than the nuclei.[2] According to the Frank–Condon principle, the nuclei, which are much heavier, require more time to react to the change in the electronic structure; thus, the excitation occurs through a vertical transition in an ultra-fast process.[2]

Further energy dissipation processes may compete with each other, and the relative rate constants determine their contribution to the excitation deactivation. In the diagram presented, the second excited state in the singlet manifold is an optically allowed state, often called the bright state. Its characteristic is a large magnitude of transition dipole moment ($\boldsymbol{\mu}_{if}$) between initial (i) and final (f) states, and consequently a high oscillator strength (in atomic units):[2]

$$f_{if} = \tfrac{2}{3}(E_f - E_i)|\boldsymbol{\mu}_{if}|^2. \tag{1}$$

[2] P. Atkins, *Shriver and Atkins' inorganic chemistry*, Oxford University Press, USA, 2010.

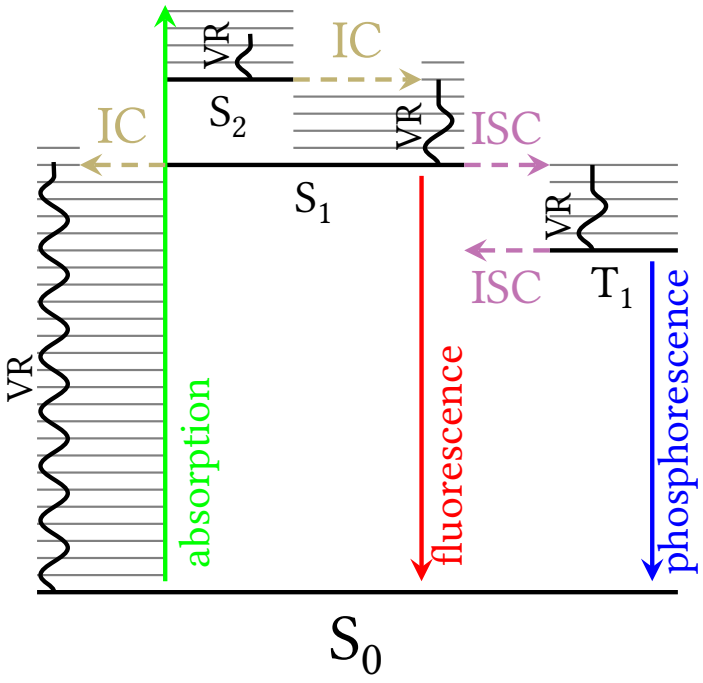

Figure 1. Schematic representation of the Jabłoński diagram. IC stands for internal conversion, ISC denotes intersystem crossing, and VR vibrational relaxation.

The vertical wavy lines in Figure 1 depict the vibrational relaxation processes that occur after transitions between electronic states. The dipole-allowed transition to a bright state through the absorption of a quantum of electromagnetic radiation initiates excited state dynamics, which leads to deactivation through competing radiative and nonradiative processes. Radiationless internal conversion (IC) between the higher-lying states is very fast. However, it is usually much slower or even impossible from the lowest excited singlet state due to a generally large adiabatic separation from the ground state. Therefore, fluorescence is often the main mechanism of deactivation to the ground electronic state, even if it occurs on a nanosecond time scale.[3] As mentioned, its quantum yield may be decreased due to the IC to the ground electronic state via conical intersection (CoI) or intersystem crossing (ISC), leading to the population of the electronic states having a different multiplicity (usually triplet). Since the $T_1 \rightarrow S_1$ transition usually requires thermal activation, from the triplet state, the radiationless deactivation $T_1 \rightarrow S_0$ competes with phosphorescence. Substantial luminescence generally occurs only from the S_1 or T_1 states, according to Kasha's rule.[1]

Potential energy surface

It is essential to introduce a fundamental theoretical concept of the potential energy surface (PES) to understand how photochemical and photobiological processes occur at the molecular level. This notion results from the Born–Oppenheimer (BO) approximation, which assumes that the motion of electrons and nuclei can be treated independently due to the significant mass differences.[4] Essentially, this means that within this approximation, the electrons move in the static external electric potential of the clamped nuclei and instantaneously adapt to any changes in the nuclear configuration within a molecule due to the separate time scales of these motions. The solution of the corresponding electronic Schrödinger equation (2) is the wavefunction ψ_{el}, which depends on the electronic coordinates **r** and only parametrically on the nuclear coordinates **R**.

$$\hat{H}_{el}\psi_{el}(\boldsymbol{r};\boldsymbol{R}) = E_{el}(\boldsymbol{R})\psi_{el}(\boldsymbol{r};\boldsymbol{R}) \tag{2}$$

The electronic Hamiltonian $\hat{H}_{el}$ contains the electronic kinetic energy operators $\hat{T}_{el}$ and potentials due to the nuclear attraction of electrons and interelectronic and internuclear repulsion. The corresponding electronic energy E_{el} depends on the nuclear configuration,

[3] S. Boldissar and M. S. d. Vries, *Physical Chemistry Chemical Physics*, **2018**, *20*, 9701–9716.
[4] C. J. Cramer, *Essentials of computational chemistry: theories and models*, John Wiley & Sons, 2013.

thus defining a $3N - 6$ ($3N - 5$ for linear molecules) dimensional potential energy (PE) hypersurface for nuclear motion.[5]

$$i\hbar \frac{\delta \mid \psi_{nuc}(\boldsymbol{R})\rangle}{\delta t} = \hat{H} \mid \psi_{nuc}(\boldsymbol{R})\rangle = \left[\hat{T}_{nuc}(\boldsymbol{R}) + E_{el}(\boldsymbol{R})\right] \mid \psi_{nuc}(\boldsymbol{R})\rangle \tag{3}$$

Thus, analysis of the PES provides direct mechanistic insight into the chemical reactions occurring in the ground or excited states. A thorough understanding of the shape of the PE surfaces and their key stationary points is essential to determine plausible reaction mechanisms along minimum energy paths. This knowledge bridges the photophysical and photochemical perspectives, and even chemistry in general, with quantum mechanics. The complexity of PESs requires suitable visualization techniques and clarification of the relationship between the changes in molecular geometry and their energetic implications for the processes studied. Intuitively, PES is simply a surface defined by the electronic energy of a given adiabatic state that depends on the nuclear coordinates.[6] However, in general, PESs are too complex to visualize in a complete form; thus, instead, the potential energy surface cuts of reduced dimensionality are presented along specific internal coordinates.[6] In the photochemical and photophysical context, the initial step involves the characterization of the Franck–Condon region and the topology of bright excited states in the proximity of a ground-state equilibrium geometry. The subsequent location of the key stationary points on the excited-state PE hypersurfaces involving local minima, saddle points, and minimum energy crossing points (MECPs) on the intersection seams between two PE surfaces allows one to estimate the PE energy profile corresponding to a hypothetical reaction path and speculate on its plausibility.[4,7] Less approximate but more computationally demanding approaches include various approximate methods of simulation of non-adiabatic nuclear dynamics to study the time evolution of the population of electronic states.[8]

Although the Born-Oppenheimer approximation yields valid results for a single potential energy surface, it is, by definition, inadequate to describe photochemical processes involving varying populations of several electronic states through their crossings.[9] When the energy

[5] L. González and R. Lindh, eds., *Quantum Chemistry and Dynamics of Excited States: Methods and Applications*, 1st edition. Wiley, 2021.

[6] E. Lewars, *Introduction to the theory and applications of molecular and quantum mechanics*, **2011**, *318*.

[7] L. Piela, *Ideas of quantum chemistry*, Elsevier, 2006.

[8] R. Crespo-Otero and M. Barbatti, *Chemical Reviews*, **2018**, *118*, 7026–7068.

[9] W. Domcke, D. Yarkony, and H. Köppel, *Conical intersections: electronic structure, dynamics & spectroscopy*, vol. 15. World Scientific, 2004.

levels of two electronic states become degenerate, the wavefunction in the adiabatic expansion should be determined as the linear combination of the adiabatic wavefunctions of at least these two states (ψ_1 and ψ_2).

$$\hat{H}\Psi(\boldsymbol{r}, \boldsymbol{R}) = E(\boldsymbol{R})[c_1(\boldsymbol{R})\psi_1(\boldsymbol{r}; \boldsymbol{R}) + c_2(\boldsymbol{R})\psi_2(\boldsymbol{r}; \boldsymbol{R})] \tag{4}$$

Due to the different mixing of these states for varying geometries, the coefficients c_1 and c_2 depend on the nuclear coordinates and thus act as nuclear wavefunctions. The Hamiltonian operator in the time-independent Schrödinger equation (4) includes the electronic Hamiltonian and $\hat{T}_{nuc}$ (nuclear repulsion is often included in $\hat{H}_{el}$ to render a correct topology of the PE surface $E(\boldsymbol{R})$).[4] Multiplying the above equation from the left by the adiabatic wave functions and integrating over electronic coordinates leads to a set of nuclear Schrödinger equations.

Since the Born–Oppenheimer approximation implies neglecting all the derivatives of electronic wavefunctions concerning nuclear coordinates (the so-called non-adiabatic couplings), crossings between PE surfaces are not allowed – which is inconsistent with physical reality. When two electronic states are nearly degenerate, their non-adiabatic coupling becomes stronger.[10] This coupling enables transitions between the two adiabatic states. Thus, to theoretically describe nonradiative decay, it is vital to move beyond the BO approximation.[10,11] On the other hand, to draw qualitative conclusions regarding the possible deactivation channels, it is often sufficient to locate the minimum energy structures at the crossing seams.

[10] C. E. Crespo-Hernández, B. Cohen, P. M. Hare, and B. Kohler, *Chemical Reviews*, **2004**, *104*, 1977–2020.
[11] S. H. Lin, *The Journal of Chemical Physics*, **1966**, *44*, 3759–3767.

Conical intersection

In diatomic molecules, the adiabatic PE curves of the same symmetry may become close in energy but do not cross and display an *avoided crossing*; however, in larger systems they may become degenerate. This crossing of two or more PE surfaces is called a conical intersection if their degeneracy is lifted linearly from the intersection.[9] The degeneracy is lifted along two nuclear displacements that form the so-called *branching space* whereas displacements in the orthogonal directions do not lift the degeneracy. Thus, in polyatomic species, the crossing PE surfaces form more of a seam of conical intersections.[7,9] The minimum-energy crossing point (MECP) is usually identified with a CoI.[5,9] At CoI, the transition from the upper to the lower electronic state is almost instantaneous and provides an efficient internal conversion route. Regarding photoinduced reactions, these crossings serve a purpose similar to transition states in thermal reactions.[7,12] Therefore, identifying the crossings with the ground electronic state, accessible from the FC region, is crucial to determine the photorelaxation pathways. It is worth mentioning that many factors, including their topography, can characterize conical intersections.[9] Usually, with the *peaked intersection*, the excited state minimum of the upper electronic state coincides with a maximum on the lower state PES; therefore, this CoI is easily accessible within mere tens or hundreds of femtoseconds. This ultra-fast process typically occurs without any barriers. Another extreme is a *sloped topography* in which both the upper and lower surfaces raise to CoI, which is neither a local maximum nor a minimum. This implies a much slower relaxation time scale and may result in trapping the molecule at a minimum on the excited-state PES before it finally goes through radiationless deactivation to the ground state. In this scenario, the excited-state lifetimes of the molecule can last several tens of picoseconds.

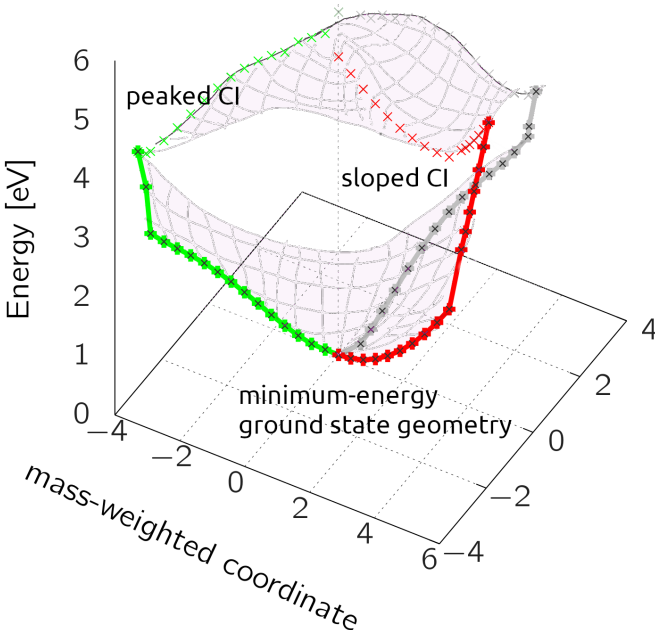

Figure 2. The schematic representation of the two potential energy surfaces in the ground and the excited electronic state, which cross along three different coordinates

[12] B. G. Levine, J. D. Coe, and T. J. Martinez, *The Journal of Physical Chemistry B*, **2008**, *112*, 405–413.

After reaching the conical intersection, the molecule relaxes further on the S_0 hypersurface. When its momentum is low, it may return to its original form. Otherwise, it falls to the nearest minimum, associated with a new photoproduct.[7] For example, in the deactivation process of the WC G-C base pair, in which the transfer of a proton is involved, the molecular structure mostly remains intact after UV light exposure.[13,14] Although the internal conversion results in imino-enol or imino-oxo tautomers (depending on the hydrogen bonds involved), there are several plausible paths on the ground-state PES that drive the system to its initial canonical structure.[15,16]

[13] K. Röttger, H. J. B. Marroux, M. P. Grubb, P. M. Coulter, H. Böhnke, A. S. Henderson, M. C. Galan, F. Temps, A. J. Orr-Ewing, and G. M. Roberts, *Angewandte Chemie International Edition*, **2015**, *54*, 14719–14722.

[14] A. Francés-Monerris, H. Gattuso, D. Roca-Sanjuán, I. Tuñón, M. Marazzi, E. Dumont, and A. Monari, *Chemical Science*, **2018**, *9*, 7902–7911.

[15] J. P. Gobbo, V. Sauri, D. Roca-Sanjuan, L. Serrano-Andres, M. Merchan, and A. C. Borin, *The Journal of Physical Chemistry B*, **2012**, *116*, 4089–4097.

[16] V. Sauri, J. P. Gobbo, J. J. Serrano-Perez, M. Lundberg, P. B. Coto, L. Serrano-Andres, A. C. Borin, R. Lindh, M. Merchan, and D. Roca-Sanjuan, *Journal of Chemical Theory and Computation*, **2013**, *9*, 481–496.

1.2 Literature review

1.2.1 Canonical nucleobases under UV irradiation

The photochemistry of canonical nucleobases has been extensively studied in the past, both theoretically and experimentally.[10,17–22] The main reason for this is that they are the building blocks of DNA and RNA polymers essential for the storage and inheritance of genetic information. However, they also have quite unique photophysical properties. In particular, they exhibit the shortest excited state lifetimes among other purines and pyrimidines (with a few notable exceptions).[18] This process involves a rapid internal conversion of photoexcited nucleobases to their ground states through a chain of conical intersections.[10,18,23–25] The fact that all canonical nucleobases are exceptionally photostable is particularly revealing in the context of the origins of these molecules. The earliest signs of life date to the period when the conditions on the surface of Earth were extremely harsh, including harmful ultraviolet (UV) radiation reaching the surface of the early Earth without the protective ozone layer. Sunlight could have been a strong selection factor favouring more photostable molecules in the early stages of chemical evolution, which ultimately led to the emergence of life.[26–28] Therefore, a detailed characterization of the mechanisms of excited-state deactivation and identification

[17] C. T. Middleton, K. d. L. Harpe, C. Su, Y. K. Law, C. E. Crespo-Hernández, and B. Kohler, *Annual Review of Physical Chemistry*, **2009**, *60*, 217–239.

[18] K. Kleinermanns, D. Nachtigallová, and M. S. de Vries, *International Reviews in Physical Chemistry*, **2013**, *32*, 308–342.

[19] M. Barbatti, A. C. Borin, and S. Ullrich. "Photoinduced Processes in Nucleic Acids". In: *Photoinduced Phenomena in Nucleic Acids I.* ed. by M. Barbatti, A. C. Borin, and S. Ullrich. Vol. 355. Cham: Springer International Publishing, 2014. 1–32. DOI: 10.1007/128_2014_569.

[20] A. Giussani, J. Segarra-Martí, D. Roca-Sanjuán, and M. Merchán. "Excitation of Nucleobases from a Computational Perspective I: Reaction Paths". In: *Photoinduced Phenomena in Nucleic Acids I: Nucleobases in the Gas Phase and in Solvents.* Ed. by M. Barbatti, A. C. Borin, and S. Ullrich. Topics in Current Chemistry. Cham: Springer International Publishing, 2015. 57–97. DOI: 10.1007/128_2013_501.

[21] S. Mai, M. Richter, P. Marquetand, and L. González. "Excitation of Nucleobases from a Computational Perspective II: Dynamics". In: *Photoinduced Phenomena in Nucleic Acids I: Nucleobases in the Gas Phase and in Solvents.* Ed. by M. Barbatti, A. C. Borin, and S. Ullrich. Topics in Current Chemistry. Cham: Springer International Publishing, 2015. 99–153. DOI: 10.1007/128_2014_549.

[22] R. Improta, F. Santoro, and L. Blancafort, *Chemical Reviews*, **2016**, *116*, 3540–3593.

[23] P. R. Callis, *Annual Review of Physical Chemistry*, **1983**, *34*, 329–357.

[24] N. Ismail, L. Blancafort, M. Olivucci, B. Kohler, and M. A. Robb, *Journal of the American Chemical Society*, **2002**, *124*, 6818–6819.

[25] M. Barbatti, A. J. A. Aquino, J. J. Szymczak, D. Nachtigallová, P. Hobza, and H. Lischka, *Proceedings of the National Academy of Sciences*, **2010**, *107*, 21453–21458.

[26] A. L. Sobolewski and W. Domcke, *Europhysics News*, **2006**, *37*, 20–23.

[27] D. Shemesh, A. L. Sobolewski, and W. Domcke, *Journal of the American Chemical Society*, **2009**, *131*, 1374–1375.

[28] N. J. Green, J. Xu, and J. D. Sutherland, *Journal of the American Chemical Society*, **2021**, *143*, 7219–7236.

of the structural changes that follow these processes is required to understand the origins of the natural preselection of nucleic acid building blocks. Furthermore, understanding the mechanisms of nonradiative photorelaxation of nucleobases can help develop strategies to prevent DNA damage and promote DNA repair.

Photoexcited DNA and RNA nucleobases are characterized by ultra-short subpicosecond decay time constants and, consequently, vanishingly small fluorescence quantum yields.[10,18,23,25] Generally, they show strong $\pi^* \leftarrow \pi$ transitions in the UV range that could potentially induce structural damage; however, out-of-plane deformations of aromatic rings lead to the formation of accessible conical intersections that allow rapid internal conversion (IC) and thus photostability.[19,26] Such a ring distortion, or the bending of a ring structure, is commonly referred to as ring puckering. The origins of this phenomenon may differ for each nucleobase, because their structural features, electronic properties, spectra, and general behavior under UV irradiation differ. In particular, the photodynamics of pyrimidines is considerably richer than that of purines due to the participation of $n\pi^*$ states.[19,21,25] It has also been shown that the environment surrounding a nucleobase can significantly affect its photorelaxation decay.[18,29–31] The most relevant studies that have provided insights into the dynamics of the photorelaxation process of canonical nucleobases and the factors that influence it are briefly reviewed below. This topic has recently been thoroughly reviewed.[19–21]

Guanine

Guanine is claimed to have the simplest photodynamics among the canonical nucleobases. Time-resolved ion yield (TR-IY) and photoelectron (TR-PES) spectra recorded after 267 nm excitation reveal[32,33] biexponential decay for both purine bases. It was originally interpreted as the initial population of the $^1\pi\pi^*$ state, followed by relaxation on the $^1n\pi^*$ surface to the CoI with the electronic ground state; however, the assignment was based on the results of the TD-DFT calculations and the authors noted that the numerical fitting of the experimental data does not always lead to an unambiguous interpretation.

[29] H. Langer, N. L. Doltsinis, and D. Marx, *ChemPhysChem*, **2005**, *6*, 1734–1737.
[30] D. Tuna, A. L. Sobolewski, and W. Domcke, *The Journal of Physical Chemistry A*, **2014**, *118*, 122–127.
[31] A. Alexandrova, J. Tully, and G. Granucci, *Biophysical Journal*, **2010**, *98*, 43a.
[32] S. Ullrich, T. Schultz, M. Z. Zgierski, and A. Stolow, *Physical Chemistry Chemical Physics*, **2004**, *6*, 2796–2801.
[33] C. Canuel, M. Mons, F. Piuzzi, B. Tardivel, I. Dimicoli, and M. Elhanine, *The Journal of Chemical Physics*, **2005**, *122*, 074316.

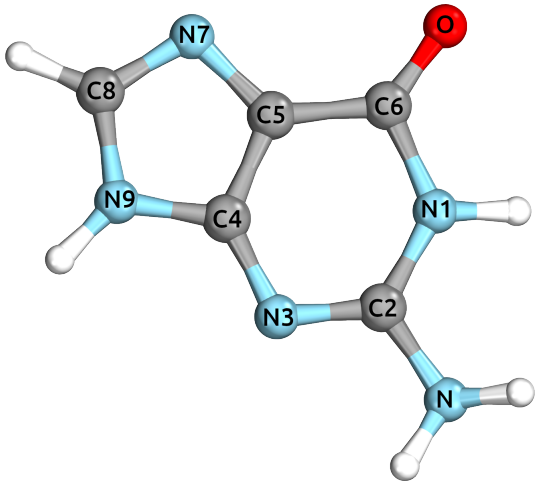

Figure 3. Equilibrium geometry of 9H-Guanine tautomer with the labeling of atoms.

It should also be noted that guanine has 36 different tautomers, which detection may be susceptible to the experimental setup, but the most stable 7H-keto and 9H-keto are usually considered.[21] Later theoretical studies of potential energy profiles[34–36] and, in particular, nonadiabatic dynamics simulations[25,37–39] indicate that the longer time constant of 360 fs may be attributed to the direct dynamics of 9H-guanine on the repulsive $^1\pi\pi^*$ PE surface crossing with the ground state. This deactivation channel manifests itself mainly in the puckering of the guanine C2 atom with the NH_2 group distorted out-of-plane.[35,36,39] Other deactivation channels through the population of $^1n\pi^*$ and $^1\pi\sigma^*$ states were also suggested[34,36,40] but were later ruled out as not accessible under experimental conditions. Only 5% of the trajectories in nonadiabatic dynamics simulations at the MRCIS level followed a channel through $^1\pi\pi^*/^1n\pi^*$ and $^1n\pi^*/S_0$ minimum energy crossing points (MECPs).[25] Therefore, the internal conversion on the $^1\pi\pi^*$ PE surface likely dominates the photophysics of isolated guanine.

Adenine

Adenine shows similar dynamics to guanine after photoexcitation with biexponential decay and slightly larger time constants (τ_2 amounts to 1.2 ps).[25,32,33] Only one experimental TR-PES study reports an additional 1 ns time constant. The shorter time constant estimated below

[34] H. Chen and S. Li, *The Journal of Chemical Physics*, **2006**, *124*, 154315.
[35] C. M. Marian, *The Journal of Physical Chemistry A*, **2007**, *111*, 1545–1553.
[36] L. Serrano-Andrés, M. Merchán, and A. C. Borin, *Journal of the American Chemical Society*, **2008**, *130*, 2473–2484.
[37] Z. Lan, E. Fabiano, and W. Thiel, *ChemPhysChem*, **2009**, *10*, 1225–1229.
[38] N. L. Doltsinis, P. R. L. Markwick, H. Nieber, and H. Langer. "Ultrafast Radiationless Decay in Nucleic Acids: Insights From Nonadiabatic Ab Initio Molecular Dynamics". In: *Radiation Induced Molecular Phenomena in Nucleic Acids: A Comprehensive Theoretical and Experimental Analysis*. Ed. by M. K. Shukla and J. Leszczynski. Challenges and Advances In Computational Chemistry and Physics. Dordrecht: Springer Netherlands, 2008. 265–299. DOI: 10.1007/978-1-4020-8184-2_10.
[39] M. Barbatti, J. J. Szymczak, A. J. Aquino, D. Nachtigallová, and H. Lischka, *The Journal of Chemical Physics*, **2011**, *134*, 01B606.
[40] S. Yamazaki, W. Domcke, and A. L. Sobolewski, *The Journal of Physical Chemistry A*, **2008**, *112*, 11965–11968.

100 fs is most likely associated with a population of dark $^1n\pi^*$ states,[41] which is consistent with the landscape of the calculated potential energy profiles.[36,42] Despite similar deactivation mechanisms, their efficiency differs as a result of the different character of the lowest excited states in the Franck–Condon region.

Serrano-Andres et al.[36] compared the photoexcitation decay channels of 9H-adenine and 9H-guanine, demonstrating that for adenine, the repulsive $^1\pi\pi^*$ state is accessible at higher excitation energies. The authors suggested that photorelaxation of adenine might occur through a cascade of crossings with the $^1n\pi^*$ states.[43] Later nonadiabatic dynamics simulations contradicted this, as most of the trajectories in Tully's surface-hopping nonadiabatic dynamics simulations followed a direct deactivation pathway through C2-atom puckered $^1\pi\pi^*/S_0$ CoI.[25] However, the $^1n\pi^*$ states are so close to the $^1\pi\pi^*$ states that they can borrow some of their intensity,[18] so that the lowest $^1n\pi^*$ state could be directly populated after photoexcitation. The crossing seam of the $^1n\pi^*$ and S_0 states is reached after the out-of-plane distortion of the NH_2 group at the C6 atom position.[44]

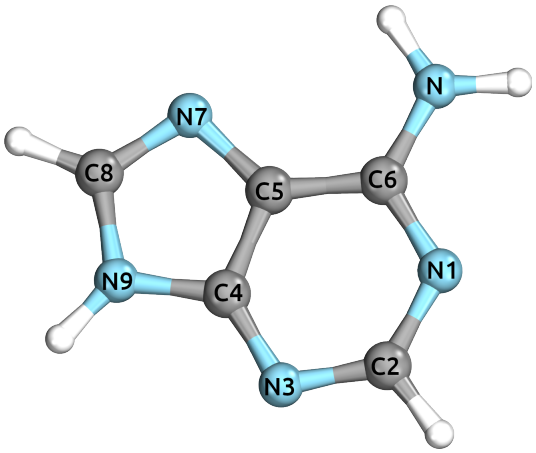

Figure 4. Equilibrium geometry of 9H-Adenine tautomer with the labeling of atoms.

Similarly to guanine, the population of the $^1\pi\pi^*$ state of 9H-adenine leads to a minimum on the S_1 PE surface, which is located near the crossing point with the ground state and the $^1\pi\pi^*/S_0$ conical intersection associated with puckering of the C2 atom can be reached without an energy barrier.[36,42,44–46] It is interesting to note that base pairing, which results in the formation of hydrogen bonds, may reduce the availability of this channel. Likewise, the abstraction of the H atom from the N9 position (discussed below) is impossible in nucleosides because ribose is attached to this position in nucleic acid.

[41] N. L. Evans and S. Ullrich, *The Journal of Physical Chemistry A*, **2010**, *114*, 11225–11230.
[42] L. Serrano-Andres, M. Merchan, and A. C. Borin, *Proceedings of the National Academy of Sciences*, **2006**, *103*, 8691–8696.
[43] H. Chen and S. Li, *The Journal of Physical Chemistry A*, **2005**, *109*, 8443–8446.
[44] S. Perun, A. L. Sobolewski, and W. Domcke, *Journal of the American Chemical Society*, **2005**, *127*, 6257–6265.
[45] L. Blancafort, *Journal of the American Chemical Society*, **2006**, *128*, 210–219.
[46] M. Barbatti, Z. Lan, R. Crespo-Otero, J. J. Szymczak, H. Lischka, and W. Thiel, *The Journal of Chemical Physics*, **2012**, *137*, 22A503.

Other conical intersections have been found[42,47–49] that involve $^1n\pi^*$ or $^1\pi\sigma^*$ states, but these are either energetically unavailable in typical experimental setups or unlikely to be observed in the larger nucleic acid fragments. For example, the $\pi \rightarrow \sigma^*$ transition has been considered vital in the internal conversion of irradiated adenine.[47,48] This state is dissociative with respect to the abstraction of hydrogen atoms from the amino group or from the azole N9 atom.[50] However, the most accurate nonadiabatic dynamics simulations using MRCIS and XMS-CASPT2 Hamiltonians[25,46,49,51] indicate that there are two deactivation funnels responsible for ultrafast deactivation, which correspond to the folding of the purine ring. The main one is the C2 ring-puckered $^1\pi\pi^*/S_0$ CoI with the C6 ring-puckered channel of secondary importance. However, the results of surface hopping ADC(2) dynamics[52] find the latter mechanism to be equally contributing to the photodynamics of isolated adenine. Furthermore, in the solvated purine and polymeric $(dA)_{10}$ structure, the C6 folding prevails over the C2 atom puckering channel in the semiempirical MRCI dynamics.[53] The hydrogen bonding introduced by the complementary pyrimidine can, however, completely suppress this channel.[54]

It is note-worthy that none of these pathways involves the participation of $^1n\pi^*$ or $^1\pi\sigma^*$ states. Simulations assuming an increased excitation energy (250 nm) reduce the excited-state lifetime but without any change in the decay mechanism. Still, although the results of recent time-resolved mass spectroscopy (TR-MS) and velocity-map ion imaging (VMI) confirm that the role of the $^1\pi\sigma^*$ states after excitation at 266 nm is negligible, the data obtained after excitation at 200 nm indicate the participation of the azole and amino $^1\pi\sigma^*$ states.[55]

It should be underlined that the discussed mechanisms of photodeactivation concern isolated adenine in the gas phase. Interestingly, the extensively studied intramolecular proton

[47] A. L. Sobolewski and W. Domcke, *The European Physical Journal D-Atomic, Molecular, Optical and Plasma Physics*, **2002**, *20*, 369–374.
[48] A. L. Sobolewski, W. Domcke, C. Dedonder-Lardeux, and C. Jouvet, *Physical Chemistry Chemical Physics*, **2002**, *4*, 1093–1100.
[49] M. Barbatti and H. Lischka, *Journal of the American Chemical Society*, **2008**, *130*, 6831–6839.
[50] I. Hünig, C. Plützer, K. A. Seefeld, D. Löwenich, M. Nispel, and K. Kleinermanns, *A European Journal of Chemical Physics and Physical Chemistry*, **2004**, *5*, 1427–1431.
[51] J. W. Park and T. Shiozaki, *Journal of Chemical Theory and Computation*, **2017**, *13*, 3676–3683.
[52] F. Plasser, R. Crespo-Otero, M. Pederzoli, J. Pittner, H. Lischka, and M. Barbatti, *Journal of chemical theory and computation*, **2014**, *10*, 1395–1405.
[53] Y. Lu, Z. Lan, and W. Thiel, *Journal of computational chemistry*, **2012**, *33*, 1225–1235.
[54] Y. Lu, Z. Lan, and W. Thiel, *Angewandte Chemie*, **2011**, *123*, 6996–6999.
[55] K. L. Wells, D. J. Hadden, M. G. Nix, and V. G. Stavros, *The Journal of Physical Chemistry Letters*, **2010**, *1*, 993–996.

transfer in nucleosides contributed to the extent of the range of relaxation pathways of this molecule. For example, it has been shown that the transfer of a proton from the 5'-OH ribose group to the N3 atom of adenosine occurs without an energy barrier. However, the conical intersection that arises through this process can be located at a higher energy level than the crossing points connected with the puckering of the C2 and C6 atoms of adenosine.[30]

Cytosine

The availability of several cytosine tautomers in the gas phase makes it difficult to interpret the results of time-resolved experiments in molecular beams.[19,21] TR-IY measurements allow to discriminate between the photodynamics of the keto and enol tautomeric forms based on their unique absorption spectra.[56] The available experimental data indicate a τ_2 time constant of about 1 ps and a longer one of a few ps (τ_3 = 1.86 − 3.2 ps) that strongly increases with the excitation wavelength (up to 150 ps). Most experimental studies also report a very short decay constant (<200 fs).[19,21]

Various studies on radiationless deactivation mechanisms in cytosine proposed different pathways for IC from $^1\pi\pi^*$ to S_0.[20] The first ab initio studies suggested a path that goes through states $^1n_O\pi^*$ and $^1n_N\pi^*$[24] or a direct path.[57] The latter MECP was related to pyramidalization of the C6 atom and stretching of the C=O bond. Subsequently, a similar ethylenic path was proposed involving the twist of the C5-C6 bond[58,59] and yet another through torsion of the N3-C4 bond resulting in puckering of the amino group.[59] The disagreement in the literature regarding the dominant decay path was amplified by Blancafort and Robb, who proposed an interesting decay mechanism in which the bright state decays through a three-state CoI between the ground state and the $^1\pi\pi^*$ and $n_O\pi^*$ states.[60] However, further computational studies of excited-state PE profiles using a more accurate methodology appear to consistently support a direct $^1\pi\pi^*/S_0$

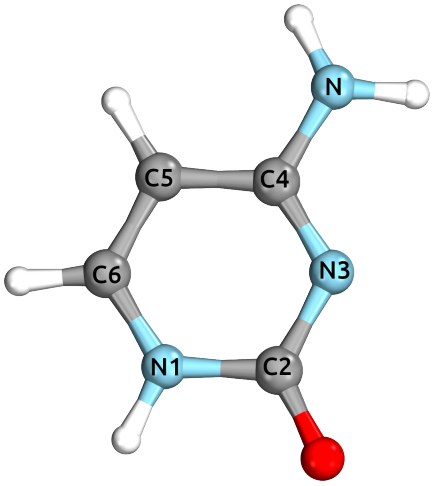

Figure 5. Equilibrium geometry of Cytosine with the labelling of atoms.

[56] J.-W. Ho, H.-C. Yen, W.-K. Chou, C.-N. Weng, L.-H. Cheng, H.-Q. Shi, S.-H. Lai, and P.-Y. Cheng, *The Journal of Physical Chemistry A*, **2011**, *115*, 8406–8418.
[57] M. Merchán and L. Serrano-Andrés, *Journal of the American Chemical Society*, **2003**, *125*, 8108–8109.
[58] L. Blancafort, *Photochemistry and Photobiology*, **2007**, *83*, 603–610.
[59] K. A. Kistler and S. Matsika, *The Journal of Physical Chemistry A*, **2007**, *111*, 2650–2661.
[60] L. Blancafort and M. A. Robb, *The Journal of Physical Chemistry A*, **2004**, *108*, 10609–10614.

decay mechanism after surmounting a small energy barrier.[20,59,61–63]

The complexity of the PE landscape of low-lying states in cytosine has been confirmed by the first nonadiabatic dynamics study on this topic conducted by Hudock and Martínez,[64] which utilized the on-the-fly SA-CASSCF multiple spawning dynamics. This study demonstrated that various decay paths could be operational simultaneously, involving all the mentioned states at different time scales. Finally, the dynamics studies performed by Barbatti et al.[65] provided a quantitative analysis of the relaxation decay paths. Indeed, the strongly coupled $^1\pi\pi^*$ and $^1n\pi^*$ states cross directly the ground state, but in the majority, the relaxation proceeds through the minimum S_1 of $n_O\pi^*$ character. The crossing with a ground state is reached in 62% cases through a population of mixed $^1\pi\pi^*$ and $^1n\pi^*$ states (semi-planar MECP), and in 18% directly on $^1n\pi^*$ or $^1\pi\pi^*$ hypersurface (out-of-plane distortion of the C4-amino group via N3-C4 torsion and puckering at the C6 atom position, respectively). The remaining 20% of the trajectories revealed no relaxation within 1.2 ps dynamics. Thus, the question arises whether the longer time constant (τ_3) results from the intersystem crossing to a triplet state or population of a dark $^1n\pi^*$ state.[21,62,66,67]

It should be underlined again that the mechanisms mentioned above concern cytosine in the gas phase and only in its keto-tautomeric form (while it is known that cytosine also exists in the gas phase in the forms of imino and enol tautomers).[21] However, different deactivation channels can contribute to the photophysics of this chromophore in bulk or more complex molecular structures. For example, Alexandrova et al.[31] in their study of nonadiabatic dynamics of nucleosides indicate a significant tendency for cytidine to decay through stretching of the N1-C2 bond, which has not previously been reported for the isolated cytosine molecule. The authors conclude that this channel may be activated as a result of the presence of sugar. However, in the DNA/RNA context, this pathway is likely hindered by

[61] M. Z. Zgierski, S. Patchkovskii, T. Fujiwara, and E. C. Lim, *The Journal of Physical Chemistry A*, **2005**, *109*, 9384–9387.

[62] R. Gonzalez-Luque, T. Climent, I. Gonzalez-Ramirez, M. Merchan, and L. Serrano-Andres, *Journal of Chemical Theory and Computation*, **2010**, *6*, 2103–2114.

[63] A. Nakayama, Y. Harabuchi, S. Yamazaki, and T. Taketsugu, *Physical Chemistry Chemical Physics*, **2013**, *15*, 12322–12339.

[64] H. R. Hudock and T. J. Martinez, *ChemPhysChem*, **2008**, *9*, 2486–2490.

[65] M. Barbatti, A. J. Aquino, J. J. Szymczak, D. Nachtigallova, and H. Lischka, *Physical Chemistry Chemical Physics*, **2011**, *13*, 6145–6155.

[66] M. Merchán, L. Serrano-Andrés, M. A. Robb, and L. Blancafort, *Journal of the American Chemical Society*, **2005**, *127*, 1820–1825.

[67] A. J. Pepino, J. Segarra-Martí, A. Nenov, I. Rivalta, R. Improta, and M. Garavelli, *Physical Chemistry Chemical Physics*, **2018**, *20*, 6877–6890.

stabilization owing to complementary nucleobase introduction.

Thymine

Most of the experimental studies report three time scales observed for a gas phase thymine: <50 fs, 490 fs and >5 ps.[18,21,32] Similarly to cytosine, two general pathways of deactivation of thymine were proposed.[20,21] One is direct decay on the $^1\pi\pi^*$ PE surface, which further crosses the ground state through the ethylenic MECP with a twisted C5-C6 bond.[68,69] This mechanism, however, does not explain the experimentally observed slow (5–7 ps) time constant. The alternative pathway involves initial population trapping at a minimum on the S_2 PES that has $\pi\pi^*$ character and subsequent decay to the $^1n\pi^*$ state that eventually crosses with the ground state.[70,71] Asturiol et al. also suggested that the biexponential decay could be explained by the splitting of the population into a rapid, direct route through $^1\pi\pi^*/S_0$ MECP and a slower, indirect route that involves a population of the $^1n\pi^*$ state. It is generally agreed that the latter mechanism is the most probable and consistent with experimental observations.[21,22,71,72]

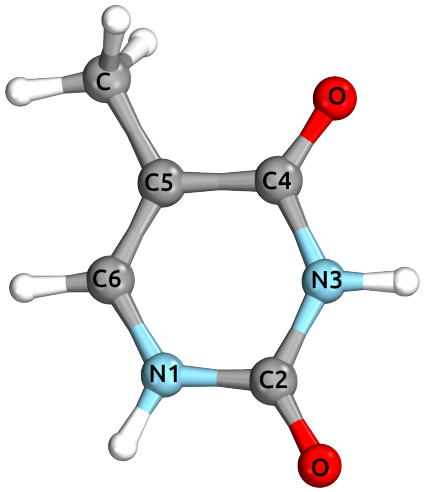

Figure 6. Equilibrium geometry of Thymine with the labeling of atoms.

The $^1\pi\pi^*/S_0$ MECP arises due to the twist of the C5-C6 bond resulting in an out-of-plane distortion of the CH_3 group.[73,74] Whereas the second path proceeds via $^1\pi\pi^*/^1n\pi^*$ crossing due to puckering of the C6 atom and shortening of the carbonyl bond, and subsequently $^1n_O\pi^*/S_0$ MECP involving pyramidalization of the C4 atom and the out-of-plane distortion of

[68] M. Merchan, R. Gonzalez-Luque, T. Climent, L. Serrano-Andres, E. Rodríguez, M. Reguero, and D. Pelaez, *The Journal of Physical Chemistry B*, **2006**, *110*, 26471–26476.
[69] Z. Lan, E. Fabiano, and W. Thiel, *The Journal of Physical Chemistry B*, **2009**, *113*, 3548–3555.
[70] J. J. Szymczak, M. Barbatti, J. T. Soo Hoo, J. A. Adkins, T. L. Windus, D. Nachtigallová, and H. Lischka, *The Journal of Physical Chemistry A*, **2009**, *113*, 12686–12693.
[71] D. Asturiol, B. Lasorne, M. A. Robb, and L. Blancafort, *The Journal of Physical Chemistry A*, **2009**, *113*, 10211–10218.
[72] H. R. Hudock, B. G. Levine, A. L. Thompson, H. Satzger, D. Townsend, N. Gador, S. Ullrich, A. Stolow, and T. J. Martinez, *The Journal of Physical Chemistry A*, **2007**, *111*, 8500–8508.
[73] S. Perun, A. L. Sobolewski, and W. Domcke, *The Journal of Physical Chemistry A*, **2006**, *110*, 13238–13244.
[74] S. Yamazaki and T. Taketsugu, *The Journal of Physical Chemistry A*, **2012**, *116*, 491–503.

carbonyl oxygen.[22,72,75] The longer, a few picosecond time constant was interpreted as either the result of trapping long-living singlet $n\pi^*$ state in S_1 minimum,[73] or trapping thymine in the S_2 state of $\pi\pi^*$ character. An ab initio nonadiabatic dynamic study conducted by Szymczak et al.[70] concluded that both scenarios could contribute to the excited-state lifetime elongation. Zechmann et al.[76] in their comprehensive ab initio study confirmed these findings and discovered eight different MECPs between the low-lying states of thymine. The latter are distinguished by various modes of ring puckering and bond length alterations. The authors concluded that direct relaxation on the hypersurface of the $^1\pi\pi^*$ state is not favorable and that thymine relaxes through CI arising on the $^1n\pi^*$ PES of ascending character. Finally, a very recent nonadiabatic MD study of Park et al.[77] employing the mixed reference spin-flip TDDFT method suggested that the S_2 trapping, which has thus far been assumed to determine the photophysics of thymine, may be an artifact of insufficient dynamic electron correlation inclusion and dynamics simulations limited to CASSCF surfaces. Instead, the authors propose that after the population of the S_2 $\pi\pi^*$ state, thymine undergoes a rapid relaxation through a bond length alteration MECP to the minimum on the S_1 $n_O\pi^*$ PES where it is trapped (τ_2 = 6.1 ps), which also explains the long decay lifetime. Ab initio molecular dynamics simulations based on the CASPT2 method also ruled out population trapping in the S_2 $\pi\pi^*$ state.[78]

It is worth mentioning that the UV-excited thymine in the gas phase has the longest decay time of all canonical nucleobases.[19,32,33] This makes it prone to photodimerization in DNA due to its less efficient photoreversibility.[79,80]

[75] L. Blancafort, B. Cohen, P. M. Hare, B. Kohler, and M. A. Robb, *The Journal of Physical Chemistry A*, **2005**, *109*, 4431–4436.
[76] G. Zechmann and M. Barbatti, *The Journal of Physical Chemistry A*, **2008**, *112*, 8273–8279.
[77] W. Park, S. Lee, M. Huix-Rotllant, M. Filatov, and C. H. Choi, *The Journal of Physical Chemistry Letters*, **2021**, *12*, 4339–4346.
[78] A. Nakayama, G. Arai, S. Yamazaki, and T. Taketsugu, *The Journal of Chemical Physics*, **2013**, *139*, 214304.
[79] J. J. Serrano-Pérez, I. Gonzalez-Ramirez, P. B. Coto, M. Merchan, and L. Serrano-Andres, *The Journal of Physical Chemistry B*, **2008**, *112*, 14096–14098.
[80] N. J. Kim, J. Chang, H. M. Kim, H. Kang, T. K. Ahn, J. Heo, and S. K. Kim, *ChemPhysChem*, **2011**, *12*, 1935–1939.

Uracil

Uracil is an analogue of thymine found mainly in RNA. Most experimental studies agree on bi-exponential decay with fast (<130 fs) and slow (1.0-3.2 ps) components.[21,33,81,82] The character of the vertical excitation energy profile in the Franck-Condon region and the minima on PESs of the low-lying excited states of uracil are very similar compared to thymine, and a similar decay mechanism has been found.[68,83]

Static calculations have predicted the same direct path of $^1\pi\pi^*$ character to the C5-C6 ethylenic MECP,[61,83] and a relaxation path that involves trapping in the S_1 minimum of $n_O\pi^*$ character,[83,84] or trapping in the S_2 $^1\pi\pi^*$ state minimum.[68,72]

The nonadiabatic dynamics calculations based on the multiple spawning method[72] suggested that trapping in the S_2 state is the dominant relaxation mechanism for uracil. Nachtigallová et al.[85] conducted the dynamics simulations under the same conditions as for thymine and discovered an aforementioned process for most trajectories, with time constants consistent with experimental observations. The remaining trajectories quickly reached the S_1 excited state and either relaxed through C6-atom puckering on the $^1\pi\pi^*$ hypersurface or, to a small extent, through a ring-opening CoI at the N3-C4 bond. The latter channel involved an admixture of $^1n\pi^*$ electronic configuration into the wavefunction that was not observed for thymine and was later confirmed in a separate study.[86] Although the C5-substituted derivatives of uracil (thymine among others) generally have longer lifetimes,[87]

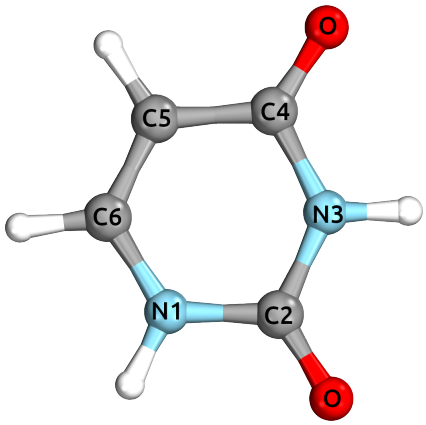

Figure 7. Equilibrium geometry of Uracil with the labeling of atoms.

[81] M. Kotur, T. C. Weinacht, C. Zhou, and S. Matsika, *IEEE Journal of Selected Topics in Quantum Electronics*, **2012**, *18*, 187–194.

[82] S. Matsika, M. Spanner, M. Kotur, and T. C. Weinacht, *The Journal of Physical Chemistry A*, **2013**, *117*, 12796–12801.

[83] S. Matsika, *The Journal of Physical Chemistry A*, **2004**, *108*, 7584–7590.

[84] Y. Mercier, F. Santoro, M. Reguero, and R. Improta, *The Journal of Physical Chemistry B*, **2008**, *112*, 10769–10772.

[85] D. Nachtigallová, A. J. Aquino, J. J. Szymczak, M. Barbatti, P. Hobza, and H. Lischka, *The Journal of Physical Chemistry A*, **2011**, *115*, 5247–5255.

[86] M. Richter, S. Mai, P. Marquetand, and L. González, *Physical Chemistry Chemical Physics*, **2014**, *16*, 24423–24436.

[87] T. Gustavsson, A. Bányász, E. Lazzarotto, D. Markovitsi, G. Scalmani, M. J. Frisch, V. Barone, and R. Improta, *Journal of the American Chemical Society*, **2006**, *128*, 607–619.

the similarities of the dynamics of uracil and thymine challenge the possibility of population trapping in S_2 state minimum.[77]

In conclusion, all five canonical nucleobases are characterized by ultrafast nonradiative decay in the gas phase. Static calculations and analysis of potential energy profiles allow one to speculate only on the possible deactivation mechanism. The results of nonadiabatic dynamics simulations, in turn, are often a compromise between the accuracy of the method used to compute the potential energy and its derivatives and the computational costs. Hence, differences in the interpretation can be found for all canonical nucleobases, and the most likely scenario is usually deduced based on the results of static and dynamic calculations compared to the experimental data. For instance, although it is generally agreed that the short time constant is due to the $^1\pi\pi^*$ to $^1n\pi^*$ transition, the longer τ_2 is assigned to direct deactivation on the $^1\pi\pi^*$ surface through C2-puckered CoI or population transfer to the $^1n\pi^*$ state and C6-puckered CoI. In the case of pyrimidines, the close proximity of the bright $^1\pi\pi^*$ state and the lower-lying $^1n\pi^*$ states makes the results of static and dynamic calculations strongly dependent on the chosen methodology. For example, all nonadiabatic dynamics simulations based on the CASSCF wavefunction predict relaxation on the $^1\pi\pi^*$ PES and population trapping in the S_2 state, which is most likely an artifact of inadequate dynamic electron correlation treatment, as it does not occur in CASPT2,[78,88] TDDFT[77] and semiempirical MRCI[69] studies. In general, the results of ab initio calculations indicate that the deactivation mechanism in the case of purines adenine and guanine is due to direct decay through puckering on $^1\pi\pi^*$ PE surfaces (with a possible minor contribution from $n\pi^*$ states in adenine); however, even in the case of these molecules, there are discrepancies between various methods regarding the mechanistic details. It is also evident that the pyrimidine nucleobases cytosine, uracil, and thymine have far more intricate decay mechanisms, involving both the $^1\pi\pi^*$ and the $^1n\pi^*$ states. Despite apparent structural and spectral similarities, it is obvious that a unified deactivation mechanism would be, at best, an oversimplification. However, most of the MECPs located between $^1\pi\pi^*$, $^1n\pi^*$ and the ground state show a significant degree of ring puckering. It is also generally agreed that the longest time constants of a few picoseconds reported for all pyrimidine nucleobases are either due to population trapping (most likely in the S_1 $^1n\pi^*$ state) or due to an intersystem crossing to a triplet state (particularly in cytosine).

[88] D. Picconi, V. Barone, A. Lami, F. Santoro, and R. Improta, *ChemPhysChem*, **2011**, *12*, 1957–1968.

However, it should be noted that deactivation mechanisms may strictly depend on environmental influence and constraints, such as adjacent solvent molecules,[13,38,78,89] the sugar moiety attached,[30,31,90] and base pairing in macromolecular structures, among others. Therefore, additional radiationless deactivation mechanisms arise when investigated monomers are integral to larger nucleic acid fragments.[10,17,22,91,92] In general, two predominant types of noncovalent interactions can influence the described mechanisms: base stacking[22,92–95] and hydrogen bonding.[13,96–98] The hydrogen bonds stiffen the structures and may open an efficient decay path associated with an exchange of hydrogen atoms between the H-bond donor and acceptor leading to ultrafast decay.[96–99] Given that base stacking associated with the formation of exciplex states results in considerably longer decay, this thesis focuses on the proton transfer phenomena in the excited states.

1.2.2 Electron-driven-proton-transfer in base pairs

When the photochemical behavior of the base pairs arranged according to the Watson-Crick scheme is studied, it can be observed that the local nonradiative decay processes compete with the intermolecular processes as a result of the formation of charge-transfer states. The situation becomes much more complex in nucleic acids, where additional processes occur, including delocalized excitonic states and energy transfer, intrastrand and interstrand electron and proton transfer, formation of excimeric states, and possible photoproduct formation (e.g.

[89] M. Dargiewicz, M. Biczysko, R. Improta, and V. Barone, *Physical Chemistry Chemical Physics*, **2012**, *14*, 8981–8989.
[90] M. J. Janicki, R. Szabla, J. Šponer, and R. W. Góra, *Physical Chemistry Chemical Physics*, **2022**, *24*, 8217–8224.
[91] B. Marchetti, T. N. V. Karsili, M. N. R. Ashfold, and W. Domcke, *Physical Chemistry Chemical Physics*, **2016**, *18*, 20007–20027.
[92] L. Martinez Fernandez, F. Santoro, and R. Improta, *Accounts of Chemical Research*, **2022**, *55*, 2077–2087.
[93] C. E. Crespo-Hernández, B. Cohen, and B. Kohler, *Nature*, **2005**, *436*, 1141–1144.
[94] Y. Zhang, K. de La Harpe, A. A. Beckstead, R. Improta, and B. Kohler, *Journal of the American Chemical Society*, **2015**, *137*, 7059–7062.
[95] V. A. Spata, W. Lee, and S. Matsika, *The Journal of Physical Chemistry Letters*, **2016**, *7*, 976–984.
[96] A. Abo-Riziq, L. Grace, E. Nir, M. Kabelac, P. Hobza, and M. S. De Vries, *Proceedings of the National Academy of Sciences*, **2005**, *102*, 20–23.
[97] A. L. Sobolewski, W. Domcke, and C. Hattig, *Proceedings of the National Academy of Sciences*, **2005**, *102*, 17903–17906.
[98] A. L. Sobolewski and W. Domcke, *A European Journal of Chemical Physics and Physical Chemistry*, **2006**, *7*, 561–564.
[99] E. Nir, K. Kleinermanns, and M. S. de Vries, *Nature*, **2000**, *408*, 949–951.

thymine dimerization).[17,22,100] In fact, the major deactivation channels of isolated nucleobases may be quenched entirely in the nucleic acid environment that imposes the structural restrictions and general planarity of the base pairs, which may consequently block the deactivation mechanisms associated with significant structural distortion of the individual nucleobases.[22] Although the intrastrand coupling between stacked nucleobases appears stronger than the interstrand base pair excimeric states, there is still evidence for both.[22] This thesis focuses on the latter.

In the G-C base pair, the charge-transfer state lies low on the potential energy profile. Various methods based on wave function theory determined that the CT state is lying only $\sim$ 0.4 eV above the lowest bright state in the FC region.[22] It is firmly established that in this WC dimer the population of the dark $^1\pi_G\pi_C^*$ CT state leads to a very efficient photoexcitation decay within $\sim$ 100 fs,[96,97,101,102] which is observed as a broad UV spectrum in the gas phase.[96] Following the crossing of the $^1\pi_G\pi_C^*$ CT state with a locally-excited bright $^1\pi_G\pi_G^*$ state, a significant charge density is transferred from the purine to the pyrimidine. The latter is considered to be the driving force for the subsequent transfer of a proton and dissipation of energy through a conical intersection with the ground state.[96,103–106] This mechanism was first proposed by Sobolewski and Domcke,[97,104] which they called electron-driven proton transfer (EDPT), even though it closely resembles the proton-coupled electron transfer process described earlier (PCET).[107,108] The most likely is the transfer of a proton from the N1 atom of guanine to the N3 atom of cytosine, along which coordinate the CT state is stabilized and eventually crosses with the ground state in a barrierless manner.[22,26,91,97]

Even in the presence of water, this process is assumed to contribute to the photostability of

[100] F. Plasser, A. J. A. Aquino, H. Lischka, and D. Nachtigallová. "Electronic Excitation Processes in Single-Strand and Double-Strand DNA: A Computational Approach". In: *Photoinduced Phenomena in Nucleic Acids II: DNA Fragments and Phenomenological Aspects*. Ed. by M. Barbatti, A. C. Borin, and S. Ullrich. Topics in Current Chemistry. Cham: Springer International Publishing, 2015. 1–37. DOI: 10.1007/128_2013_517.
[101] P. R. Markwick and N. L. Doltsinis, *The Journal of Chemical Physics*, **2007**, *126*, 05B603.
[102] G. Groenhof, L. V. Schäfer, M. Boggio-Pasqua, M. Goette, H. Grubmüller, and M. A. Robb, *Journal of the American Chemical Society*, **2007**, *129*, 6812–6819.
[103] A. L. Sobolewski and W. Domcke, *Physical Chemistry Chemical Physics*, **2004**, *6*, 2763–2771.
[104] T. Schultz, E. Samoylova, W. Radloff, I. V. Hertel, A. L. Sobolewski, and W. Domcke, *Science*, **2004**, *306*, 1765–1768.
[105] N. K. Schwalb and F. Temps, *Journal of the American Chemical Society*, **2007**, *129*, 9272–9273.
[106] V. G. Stavros and J. R. Verlet, *Annual Review of Physical Chemistry*, **2016**, *67*, 211–232.
[107] S. Hammes-Schiffer, *Accounts of Chemical Research*, **2001**, *34*, 273–281.
[108] S. Hammes-Schiffer, *Journal of the American Chemical Society*, **2015**, *137*, 8860–8871.

G-C.[22] A series of papers, both experimental and theoretical, validate this conclusion.[13,99,109] However, the results of calculations considering the presence of a polar solvent indicate that the EDPT process might be obscured by a non-negligible energy barrier,[22] thus, regarding timescales of this decay path and a complete equilibration of the system in the solvent, intramonomer deactivation mechanisms may be ahead of the EDPT in bulk.[110] On the contrary, in their Car-Parrinello MD studies, Markwick et al. suggested that the water solvent does not substantially affect the dynamics of G-C, and if it does, it slightly enhances the stability of the charge-transfer state.[111] A few separate trajectory-based MD studies also concluded that the solvation effect is minor.[16,101] According to the dynamics studies in the gas phase, the majority of these studies, regardless of the chosen methodology, predict a dominating role of the deactivation process associated with the proton transfer in the photodynamics of the G-C.[16,31,101,102,112] Some of these works identified not only a single proton transfer path along the central hydrogen bond but also a second involving the H-bond formed between amino and carbonyl groups.[14,16,102]

According to ab initio calculations, the EDPT process should also be possible in the WC base pair of adenine-thymine.[15,91,113,114] However, its experimental verification was hindered due to the A-T complex having a different equilibrium geometry in the gas phase.[115] Theoretical predictions did suggest that the photoexcited WC A-T dimer might decay via an EDPT coordinate in a barrierless manner,[15,114] through the $^1\pi_A\pi_T^*$ CT state.[91] The plausibility of the EDPT process in A-T is also amplified by experimental evidence that photorelaxation involving proton transfer occurs in the adenine dimer.[50] However, recent computational results[116] did not yield the population of the CT state in the nonadiabatic dynamics, which is too far apart from the optically accessible LE state in the Franck–Condon region. Instead, the authors claim that the main decay path of A-T involves a $\pi^* \leftarrow \pi$ transition on the thymine.

[109] J. A. Green, S. Gómez, G. Worth, F. Santoro, and R. Improta, *Chemistry–A European Journal*, **2022**, *28*, e202201731.
[110] L. Biemann, S. A. Kovalenko, K. Kleinermanns, R. Mahrwald, M. Markert, and R. Improta, *Journal of the American Chemical Society*, **2011**, *133*, 19664–19667.
[111] P. R. Markwick, N. L. Doltsinis, and J. Schlitter, *The Journal of Chemical Physics*, **2007**, *126*, 01B623.
[112] J. A. Green, M. Yaghoubi Jouybari, H. Asha, F. Santoro, and R. Improta, *Journal of Chemical Theory and Computation*, **2021**, *17*, 4660–4674.
[113] G. Villani, *Chemical Physics*, **2005**, *316*, 1–8.
[114] S. Perun, A. L. Sobolewski, and W. Domcke, *The Journal of Physical Chemistry A*, **2006**, *110*, 9031–9038.
[115] K. Röttger, H. J. Marroux, A. F. Chemin, E. Elsdon, T. A. Oliver, S. T. Street, A. S. Henderson, M. C. Galan, A. J. Orr-Ewing, and G. M. Roberts, *The Journal of Physical Chemistry B*, **2017**, *121*, 4448–4455.
[116] M. Y. Jouybari, J. A. Green, R. Improta, and F. Santoro, *The Journal of Physical Chemistry A*, **2021**, *125*, 8912–8924.

Indeed, given the vertical excitation energy of the CT state in WC A-T computed using various methods, it can be concluded that this state is substantially separated from the lowest bright state (0.6-0.8 eV) and less stable than the respective CT state in the G-C canonical base pair.[22] Processes involving excited states of pyrimidines, including $n \longrightarrow \pi^*$ transitions, may also block the channel of relaxation by proton exchange along hydrogen bonds. However, it is generally known that the population of the $^1n\pi^*$ state of thymine is strongly reduced in the polar solvent[117] and base pairing also destabilizes these transitions.[118,119] Recently, transient electronic and vibrational absorption spectroscopies[115] indicated that monomer-like decay processes likely dominate the excited state photodynamics of chemically-modified A-T (8-(tert-butyl)-9-ethyladenine-thymine), but the authors did not exclude the possibility that an ultrafast EDPT process is still accessible in this dimer. Although Jouybari et al.[116] suggested relaxation of the A-T base pair through the $^1\pi\pi^*$ LE state of thymine, it was concluded that isolated thymine decays rather on the $^1n\pi^*$ surface and that population trapping in the S_2 $^1\pi\pi^*$ state discussed above may be an artifact of inadequate treatment of dynamical electron correlation.[77,120,121]

On the other hand, A-T in the nucleic acid duplex may behave quite differently than that in the gas phase or solution. For example, Zhang et al. suggested that the EDPT channel appears to be inaccessible in both the gas phase A-T and the double-stranded $d(A)_n \cdot d(T)_n$ duplex; however, an electron transfer between the stacked bases in the nonalterating chain may be subsequently followed by a proton transfer in the radical-ion A-T base pair.[94] The effect of a polar solvent on the CT state may also increase the population of this state; however, proton transfer makes it less polar. Consequently, the EDPT process becomes endoergonic[89] and involves an energy barrier.[22] Given the apparent similarities of the uracil and thymine discussed in Sec. 1.2.1 on page 8, the same obstacle in detecting EDPT should be assumed in the A-U base pair. However, Chan et al.[122] in their recent findings of ultra-fast time-resolved fluorescence (TRF) with fluorescence anisotropy (TRFA), observed proton-coupled electron

[117] J. Cerezo, Y. Liu, N. Lin, X. Zhao, R. Improta, and F. Santoro, *Journal of Chemical Theory and Computation*, **2018**, *14*, 820–832.
[118] F. Santoro, V. Barone, and R. Improta, *ChemPhysChem*, **2008**, *9*, 2531–2537.
[119] F. Santoro, V. Barone, and R. Improta, *Journal of the American Chemical Society*, **2009**, *131*, 15232–15245.
[120] L. Stojanović, S. Bai, J. Nagesh, A. F. Izmaylov, R. Crespo-Otero, H. Lischka, and M. Barbatti, *Molecules*, **2016**, *21*, 1603.
[121] H. Lischka, M. Barbatti, F. Siddique, A. Das, and A. J. Aquino, *Chemical Physics*, **2018**, *515*, 472–479.
[122] R. C.-T. Chan, C. Ma, A. K.-W. Wong, C. T.-L. Chan, J. C.-L. Chow, and W.-M. Kwok, *The Journal of Physical Chemistry Letters*, **2022**, *13*, 302–311.

transfer within the A-U pair in the A-form RNA double helix. As can be concluded from numerous studies,[122–125] the RNA environment can influence the photostability mechanisms of the canonical base pair A-U. Finally, it is worth noting that the availability of a specific nonradiative deactivation channel depends to some extent on the wavelength of the irradiation, thus the EDPT mechanism may still be active after excitation to higher-lying electronic states. All this suggests that in the case of A-T and A-U base pairs, the availability of the EDPT channel may depend on environmental constraints and cannot be entirely ruled out.

Interestingly, the EDPT mechanism has been suggested to occur not only in the base pairs. Several studies of photochemical reactions concerning microsolvated nucleobases indicate the possibility of EDPT from a water molecule to an adjacent nucleobase or nucleoside[90,126,127] and from a nucleobase to a sugar moiety in nucleoside.[30] The plausibility of the EDPT process has also been suggested in computational studies of non-canonical nucleobase analogues.[128,129] This thesis is, to our knowledge, the first attempt to compare the possible photorelaxation channels among a set of dimeric structures closely related to canonical base pairs.

1.2.3 Non-canonical nucleobases and base pairs

Since ultrafast radiationless decay reduces the possibility of photodegradation of nucleobases and their aggregates, it is interesting to investigate whether the same applies also to their analogues. It is known that the five canonical nucleobases discussed thus far are not unique in their ability to form stable duplexes. Even contemporary living organisms contain a number of modified noncanonical nucleobases and nucleosides in their DNA and RNA,[130] and the range of molecules having similar properties that could have been the building

[123] K. H. Johnson, D. M. Gray, and J. C. Sutherland, *Nucleic Acids Research*, **1991**, *19*, 2275–2280.
[124] M. Pollum, L. Martinez-Fernandez, and C. E. Crespo-Hernandez, *Photoinduced Phenomena in Nucleic Acids I: Nucleobases in the Gas Phase and in Solvents*, **2015**, 245–327.
[125] S. Reiter, D. Keefer, and R. de Vivie-Riedle, *Journal of the American Chemical Society*, **2018**, *140*, 8714–8720.
[126] R. Szabla, H. Kruse, J. Šponer, and R. W. Góra, *Physical Chemistry Chemical Physics*, **2017**, *19*, 17531–17537.
[127] R. Mansour, J. M. Toldo, and M. Barbatti, *The Journal of Physical Chemistry Letters*, **2022**, *13*, 6194–6199.
[128] A. Kumar and M. D. Sevilla, *Photochemical & Photobiological Sciences*, **2013**, *12*, 1328.
[129] X. Wu, T. Karsili, and W. Domcke, *Molecules*, **2017**, *22*, 135.
[130] T. Carell, C. Brandmayr, A. Hienzsch, M. Müller, D. Pearson, V. Reiter, I. Thoma, P. Thumbs, and M. Wagner, *Angewandte Chemie International Edition*, **2012**, *51*, 7110–7131.

blocks of pre-nucleic acid is far greater.[131–134] It is reasonable to assume that even if the canonical nucleobases appeared in the early stages of chemical evolution, other derivatives and analogues might as well. This conclusion is supported by studies on the stability of oligonucleotide duplexes in which the noncanonical base pairs isoguanine-isocytosine (iG-iC) were successfully incorporated.[135–137] Other examples of stable oligonucleotide duplexes consisting of alternative all-purine nucleobases, including the base pairs of DAP-xanthine (DAP-X) and G-iG, were also reported.[138,139] These studies are related to an idea proposed in 1968 by Crick that a purine-purine genetic system, consisting of adenine paired with hypoxanthine (H), could have preceded the contemporary paradigm.[140] Hypoxanthine is a particularly interesting molecule, as it is claimed to be an essential prebiotic ancestor of canonical nucleobases due to its participation in the same prebiotic path as adenine[141] and the direct formation of the nucleoside inosine.[142] This molecule has also been identified in carbonaceous meteorites,[143–145] confirming its prebiotic availability. However, when paired with cytosine, its interaction energy is substantially lower than that of the parent G-C base pair.[146]

Recently, efficient self-assembly of hydrogen-bonded nucleobase analogues was demonstrated, which could be relevant for the origin of RNA-like polymers.[131,132] In this context, particularly interesting are heterocycles whose prebiotic availability on Young Earth is plausi-

[131] N. V. Hud, B. J. Cafferty, R. Krishnamurthy, and L. D. Williams, *Chemistry & Biology*, **2013**, *20*, 466–474.
[132] B. J. Cafferty, I. Gállego, M. C. Chen, K. I. Farley, R. Eritja, and N. V. Hud, *Journal of the American Chemical Society*, **2013**, *135*, 2447–2450.
[133] A. C. Rios and Y. Tor, *Israel journal of chemistry*, **2013**, *53*, 469–483.
[134] S. Becker, C. Schneider, A. Crisp, and T. Carell, *Nature Communications*, **2018**, *9*, 5174.
[135] C. Switzer, S. E. Moroney, and S. A. Benner, *Journal of the American Chemical Society*, **1989**, *111*, 8322–8323.
[136] J. A. Piccirilli, S. A. Benner, T. Krauch, S. E. Moroney, and S. A. Benner, *Nature*, **1990**, *343*, 33–37.
[137] C. Roberts, R. Bandaru, and C. Switzer, *Journal of the American Chemical Society*, **1997**, *119*, 4640–4649.
[138] K. Groebke, J. Hunziker, W. Fraser, L. Peng, U. Diederichsen, K. Zimmermann, A. Holzner, C. Leumann, and A. Eschenmoser, *Helvetica Chimica Acta*, **1998**, *81*, 375–474.
[139] B. D. Heuberger and C. Switzer, *ChemBioChem*, **2008**, *9*, 2779–2783.
[140] F. Crick, *Journal of Molecular Biology*, **1968**, *38*, 367–379.
[141] S. Miyakawa, H. J. Cleaves, and S. L. Miller, *Origins of Life and Evolution of the Biosphere*, **2002**, *32*, 209–218.
[142] J. Xu, V. Chmela, N. J. Green, D. A. Russell, M. J. Janicki, R. W. Góra, R. Szabla, A. D. Bond, and J. D. Sutherland, *Nature*, **2020**, *582*, 60–66.
[143] C. Hartel and M. Göbel, *Helvetica Chimica Acta*, **2000**, *83*, 2541–2549.
[144] Y. Y. Guan, N. Fray, P. Coll, F. Macari, D. Chaput, F. Raulin, and H. Cottin, *Planetary and Space Science*, **2010**, *58*, 1327–1346.
[145] M. P. Callahan, K. E. Smith, H. J. Cleaves, J. Ruzicka, J. C. Stern, D. P. Glavin, C. H. House, and J. P. Dworkin, *Proceedings of the National Academy of Sciences*, **2011**, *108*, 13995–13998.
[146] J. Šponer, P. Jurečka, and P. Hobza, *Journal of the American Chemical Society*, **2004**, *126*, 10142–10151.

ble and which are characterized by certain structural features, in particular their photostability and ability to form multiple hydrogen bonds. A good example of numerous heterocycles that are being investigated according to these criteria is 2,6-diaminopurine (DAP), which is soluble in water, prebiotically plausible,[141,143,145] and is also found in meteorite matter.[132,145] In aqueous solution, DAP exists mainly in the 9H- and 7H-diamino tautomeric forms, precisely like the canonical purine nucleobases.[147] DAP is a derivative of adenine (2-amino-A), having an extra amino exocyclic group at the C2 position, which retains the base pairing ability with T and U that is even strengthened with an additional hydrogen bond. It is not the only "modified" base that could easily fit into nucleic acids. Cafferty and Hud considered an interesting set of heterocycles.[131,132] They followed the substitution of extant nucleobases into nucleic acids suggested by Benner,[135,136] investigating more than 80 different heterocycles. The authors focused on finding alternative nucleobases capable of glycosylation and self-assembling, given that the WC-base pairs do not form in water.[131,132] The authors found that barbituric acid (B) and 2,4,6-triaminopyrimidine (TAP) met the criteria for viable protonucleobases (cf. Figure 22), including having certain exocyclic groups that can form in an abiotic environment, compatible H-bonding patterns for self-assembly, being water-soluble and being capable of glycosylation. Surprisingly, the authors did not consider photostability as a selection factor, which, as mentioned before, should have been an essential feature of such compounds. Interestingly, TAP and B are relatively photostable in aqueous solution.[148] The same applies to melamine (M) which was also considered by Cafferty and Hud as the pyrimidine nucleobases analogue.[149]

As was already mentioned, one of the most striking features of photoexcited DNA/RNA nucleobases are their ultra-short excited-state lifetimes.[18] Many heterocycles that are structurally very similar to them evince much longer lifetimes, causing them to be more prone to photodegradation. Figure 8 presents the excitation lifetimes of canonical nucleobases and their selected derivatives. Many attempts have been made to understand this phenomenon[3,18,147,156,157]

[147] Z. Gengeliczki, M. P. Callahan, N. Svadlenak, C. I. Pongor, B. Sztaray, L. Meerts, D. Nachtigallova, P. Hobza, M. Barbatti, H. Lischka, et al., *Physical Chemistry Chemical Physics*, **2010**, *12*, 5375–5388.

[148] M. M. Brister, M. Pollum, and C. E. Crespo-Hernández, *Physical Chemistry Chemical Physics*, **2016**, *18*, 20097–20103.

[149] Y. Zhang, A. A. Beckstead, Y. Hu, X. Piao, D. Bong, and B. Kohler, *Molecules*, **2016**, *21*, 1645.

[156] D. Nachtigallova, H. Lischka, J. J. Szymczak, M. Barbatti, P. Hobza, Z. Gengeliczki, G. Pino, M. P. Callahan, and M. S. De Vries, *Physical Chemistry Chemical Physics*, **2010**, *12*, 4924–4933.

[157] L. Martinez-Fernandez, S. Arslancan, D. Ivashchenko, C. E. Crespo-Hernandez, and I. Corral, *Physical Chemistry Chemical Physics*, **2019**, *21*, 13467–13473.

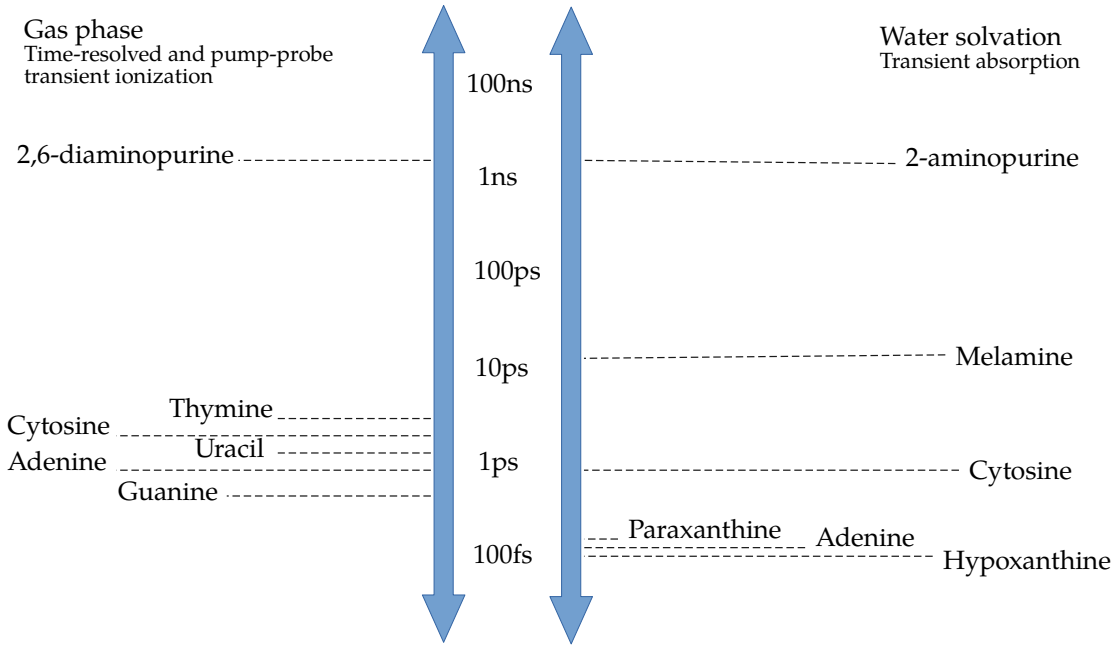

Figure 8. Excited state lifetimes estimated with the time-resolved transient ionization, pump-probe transient ionization and the femtosecond transient absorption methods for canonical[150–154] *and selected non-canonical nucleobases.*[3,149,154,155]

and identify the key aspects that affect the diversity of the photodynamics of these compounds. In the perspective of Boldissar and de Vries,[3] a few critical aspects have been raised and a systematic analysis of the influence of particular substitutions has been proposed. Generally, the authors attribute the changes in the lifetimes to changes in the PE surfaces and the topology of relevant CoIs. For example, purines substituted at the C2 position (as in DAP) have a substantially longer excited-state lifetime than adenine and hypoxanthine. Uracil and thymine (5-methyl-U) have excited-state lifetimes of a few picoseconds, while 5-hydroxy-U and 5-amino-U have lifetimes in the range of nanoseconds. Ab initio calculations show that functionalization of a heterocyclic compound can lead to profound changes in the topography of excited-state PE surfaces. In particular, MS-CASPT2 calculations demonstrated that substitution of purines at the C6 position leads to the disappearance of a minimum along the $^1\pi\pi^*$ PES which facilitates the decay of the excited-state population to the ground state and thus increases photostability of a substituted purine.[157] Another interesting example is hypoxanthine, whose excited-state lifetime is even shorter than those reported for canonical nucleobases (see Figure 8).[157] While its isomer 2-aminopurine (2AP), which has the amino group at C2 instead of C6 position, has a considerably longer excited-state lifetime.[3,158]

[158] M. Barbatti and H. Lischka, *Physical Chemistry Chemical Physics*, **2015**, *17*, 15452–15459.

The conclusions of these studies shed light on why living organisms use such a narrow set of building blocks of genetic material and contribute to expanding the scope of functional genomics. Naturally, base pairs and larger aggregates of nucleobases may photorelax differently, and this feature should be investigated alongside the terms of stability and molecular recognition. As was already discussed, the iG-iC base pair is structurally very similar to G-C[137,159] and can be incorporated into DNA. The photostability of isocytosine is comparable to that of cytosine;[160] however, the lower photostability of the biologically relevant keto form of isoguanine could explain its reduced functionality,[161] which could be traced to UV-rich prebiotic conditions. This could at least partially explain why this alternative base pair did not become the nucleic acid building block.

With regard to the photochemistry and photophysics of alternative nucleobase pairs, the literature lacks a comprehensive description of probable photodeactivation mechanisms. The study on the photochemistry of the 2AP-T base pair in the WC and Hoogsteen (HS) conformations is a rare example of such an attempt.[162] An incentive for the latter study was the fact that 2AP is commonly used as an intrinsic fluorescent probe in nucleic acid research. The authors concluded, based on the results of time-resolved spectroscopy and ab initio calculations, that the observed dynamic fluorescence quenching of 2AP is likely influenced by H-bonding between strands according to both WC and HS patterns. Interestingly, the authors suggested excited-state proton transfer as an efficient deactivation pathway of photoexcited 2AP-T dimer, but only in the HS conformation. Particular attention has been paid to canonical base pairs in which purine is oxidized at the C8 position, leading to 8-oxo-guanine (8-oxoG) and 8-oxo-adenine (8-oxoA),[128,129] as it is a common oxidative DNA lesion.[163] UV absorption was shown to create a long-lived (~60 ps) radical ion pair by transferring an electron from 8-oxo-G to A in a dinucleotide.[164] The authors suggested that 8-oxo-G thus might have been a plausible prebiotic agent capable of repairing cyclobutane pyrimidine dimers (CPD) lesions of pyrimidines and a precursor of modern flavine cofactors. A separate study indicated that

[159] A. Jaworski, J. S. Kwiatkowski, and B. Lesyng, *International Journal of Quantum Chemistry*, **2009**, *28*, 209–216.
[160] R. Szabla, R. W. Góra, and J. Šponer, *Physical Chemistry Chemical Physics*, **2016**, *18*, 20208–20218.
[161] G. Gate, R. Szabla, M. R. Haggmark, J. Šponer, A. L. Sobolewski, and M. S. de Vries, *Physical Chemistry Chemical Physics*, **2019**, *21*, 13474–13485.
[162] H. Böhnke, K. Röttger, R. A. Ingle, H. J. Marroux, M. Bohnsack, N. K. Schwalb, A. J. Orr-Ewing, and F. Temps, *The Journal of Physical Chemistry B*, **2019**, *123*, 2904–2914.
[163] S. Kanvah, J. Joseph, G. B. Schuster, R. N. Barnett, C. L. Cleveland, and U. Landman, *Accounts of Chemical Research*, **2010**, *43*, 280–287.
[164] Y. Zhang, J. Dood, A. A. Beckstead, X.-B. Li, K. V. Nguyen, C. J. Burrows, R. Improta, and B. Kohler, *Proceedings of the National Academy of Sciences*, **2014**, *111*, 11612–11617.

it could also contribute to the protection of the DNA of contemporary living organisms by removing highly oxidizing hydroxide radicals.[165] However, the presence of the oxidized form of guanine in DNA may have an indirect mutagenic effect, as it leads to mispairing during replication. In particular, the 8-oxoG-A dimer can be formed in both the HS and WC conformations.[129] The 8-oxoG-A and 8-oxoG-C base pairs in their neutral forms were investigated by Kumar and Sevilla.[128] The authors investigated the possibility of an EDPT deactivation process in these complexes using TD-DFT computations. They showed that in 8-oxoG-C the population of a low-lying charge-transfer $^1\pi\pi^*$ state in the FC region is feasible and that further stabilization of this state along the proton-transfer coordinate leads to barrierless deactivation to the ground state. However, in the case of the 8-oxoG-A dimer, the authors concluded that such a deactivation channel is not available because of the much larger energy gap between the CT and the ground state. In a follow-up study by Wu et al.[129] it was suggested based on the results of the ADC(2) calculations that an ultra-fast EDPT deactivation channel should be available in complexes with deprotonated 8-oxoG. This implies that photoexcited 8-oxoG$^-$-C and 8-oxoG$^-$-A base pairs are too short-lived to be an efficient electron transfer repair agent. Therefore, only isolated 8-oxoG or its nucleoside can serve in this role.[129]

This thesis is an attempt to supplement these findings with a thorough computational photochemical analysis of selected canonical and noncanonical base pairs.

1.3 Scientific goal and significance of the thesis

As discussed in the Introduction, all nucleic acid building blocks share a characteristic of relatively high photostability.[10,98] Single nucleobases, their dimers, nucleosides and even small fragments of nucleic acid strands undergo a series of structural changes under the influence of UV light, leading to ultrafast deactivation of the precarious excited state.[19] It is not certain whether RNA and DNA appeared in the Archean and remained unchanged since then or, more likely, their precursors underwent a sort of prebiotic chemical evolution. Still, the focus on the photostability characteristic seems valid regardless of whether the protonucleotides

[165] S. Steenken, S. V. Jovanovic, M. Bietti, and K. Bernhard, *Journal of the American Chemical Society*, **2000**, *122*, 2373–2374.

were assembled from nucleobases, ribose, and phosphates[166] or appeared in direct synthesis from prebiotic feedstock molecules.[167] The earliest signs of life date from the period when conditions on the surface of Earth were extremely harsh for organic molecules due to considerably higher than today internal heat flow, volcanic activity and sunlight, including harmful ultraviolet (UV) radiation reaching yet unprotected surface of Earth.[167] It is generally believed that sunlight was a decisive selection factor back to the beginning of life, favoring more photostable molecules in the early stages of chemical evolution, eventually leading to life's emergence.[10,26–28,168–170] Therefore, a thorough characterization of the probable mechanisms of excited-state deactivation and identification of the structural changes associated with these processes are required to understand the origin of photostability as an important criterion for the preselection of nucleic acid building blocks. Furthermore, understanding the mechanisms of nonradiative deactivation of nucleobases and base pairs can help develop strategies to prevent DNA damage and promote DNA repair.

The aim of the thesis is **to determine the mechanisms of charge transfer between canonical and non-canonical nucleobases paired according to the Watson-Crick scheme, which are induced by UV irradiation**. As discussed above, the excited-state energy profiles in the Franck–Condon region for G-C and A-T pairs have been documented in many studies. However, there is no consensus in the available literature on the mechanisms of energy and charge transfer after UV absorption of base pairs, which description is often incomplete and debatable. In particular, resonance-enhanced multiphoton ionization spectroscopy (REMPI) measurements revealed the ultrafast deactivation channel of the photoexcited G-C base pair,[99,114] distinguished from that observed for the A-T base pair,[171] for which the lifetime of the excited state extended from a few hundreds of femtoseconds to a few picoseconds.[19,172,173]

[166] B. J. Cafferty, D. M. Fialho, J. Khanam, R. Krishnamurthy, and N. V. Hud, *Nature communications*, **2016**, *7*, 11328.
[167] J. D. Sutherland, *Angew. Chem. Int. Ed.*, **2016**, *55*, 104–121.
[168] P. Ehrenfreund, M. Bernstein, J. Dworkin, S. Sandford, and L. Allamandola, *The Astrophysical Journal*, **2001**, *550*, L95.
[169] R. Szabla, D. Tuna, R. W. Góra, J. Šponer, A. L. Sobolewski, and W. Domcke, *The Journal of Physical Chemistry Letters*, **2013**, *4*, 2785–2788.
[170] S. A. Sandford, P. P. Bera, T. J. Lee, and M. Nuevo. "Photosynthesis and photo-stability of nucleic acids in prebiotic extraterrestrial environments". In: *Photoinduced Phenomena in Nucleic Acids II.*. Springer, 2014. 123–164.
[171] C. Plützer, I. Hünig, K. Kleinermanns, E. Nir, and M. S. de Vries, *ChemPhysChem*, **2003**, *4*, 838–842.
[172] E. Samoylova, H. Lippert, S. Ullrich, I. V. Hertel, W. Radloff, and T. Schultz, *Journal of the American Chemical Society*, **2005**, *127*, 1782–1786.
[173] E. Samoylova, T. Schultz, I. Hertel, and W. Radloff, *Chemical Physics*, **2008**, *347*, 376–382.

The main premises to discuss this research topic are the results of previous reports on the importance of the EDPT process[97,104] in nonradiative relaxation of photoexcited base pairs to the ground state. Studies of the influence of exocyclic groups -OH, -NH_2, -NH on photoexcitation of Watson-Crick type canonical base pairs have led to the assumption of great importance of the aforementioned EDPT/PCET mechanisms for the photophysics of these systems.[97] Although much is already known about these processes, the proposed proton transfer mechanism caused by electron transfer has yet to be experimentally confirmed for the WC A-T canonical base pair. It could be the result of spectroscopic failure to measure the ultra-short lifetimes (<100fs),[174] influence of solvation in bulk on the character of the EDPT and the direction of proton transfer,[89,175] or incorrect assumptions about the nature of this process.

According to the working hypothesis, **several alternative relaxation channels induced by charge transfer phenomena may exist simultaneously** as a result of the interaction of nucleobases in electronically excited states. Hydrogen bonds provide an obvious coordinate for effective nonradiative deactivation of the excited state owing to the possible proton transfer between the acceptor and donor moieties. On the basis of the theoretically determined potential energy profiles, it was postulated that the EDPT process is a plausible and effective relaxation channel of the excited state in the A-T canonical base pair, although the lowest singlet state of this dimer is of $^1n\pi^*$ character. The presence of low-lying, long-living $^1n\pi^*$ states can be a significant factor in the observed relaxation handicap[172] because the population of these states can lead to other internal conversion processes and intersystem crossing to triplet states in pyrimidines.[67,176] Presumably, these channels may compete or even dominate in nonradiative deactivation processes of these species, which may result in blocking the proton transfer channel. Taking into account experimental evidence of photorelaxation through the EDPT channel in the adenine homodimer,[50] it is worth considering that processes involving pyrimidines are indeed an obstacle to effective relaxation through the exchange of protons along hydrogen bonds. Experimental results indicate that in the case of adenine and thymine monomers, after excitation to the lowest $^1\pi\pi^*$ state, internal conversion leads to a lower $^1n\pi^*$ state, with a lifetime of ~2.4 ps.[172] On the other hand, for the adenine monomer,

[174] K. Röttger, H. J. B. Marroux, A. F. M. Chemin, E. Elsdon, T. A. A. Oliver, S. T. G. Street, A. S. Henderson, M. C. Galan, A. J. Orr-Ewing, and G. M. Roberts, *The Journal of Physical Chemistry B*, **2017**, *121*, 4448–4455.
[175] R. Szabla, R. W. Góra, M. Janicki, and J. Šponer, *Faraday Discussions*, **2016**, *195*, 237–251.
[176] P. M. Hare, C. E. Crespo-Hernández, and B. Kohler, *Proceedings of the National Academy of Sciences*, **2007**, *104*, 435–440.

population transfer from the bright $^1\pi\pi^*$ state to the dark $^1n\pi^*$ state occurs at an ultrafast pace (<50 fs).[172]

Thus, the scope of the thesis also includes **elucidation of the disputed role of non-absorbing (dark) $^1n\pi^*$ states in the process of nonradiative deactivation after photoexcitation and consequently the identification of other pathways of photoexcitation decay, previously not considered**. For instance, we have reasons to suggest the existence of yet another type of EDPT relaxation channel activated after the population of $^1n\pi^*$ charge-transfer state. Our preliminary calculations for the guanine-cytosine and hypoxanthine-cytosine (H-C) base pairs seem to confirm the plausibility of this mechanism. To verify these assumptions, PE surface profiles for low-lying excited states are analyzed, and possible conical intersections with the ground state are located using state-of-the-art computational chemistry *ab initio* methods. Furthermore, the thesis aims **to investigate the mechanisms of nonradiative deactivation processes in non-biological base pairs that are hypothetical prebiotic precursors of protonucleic acids**. Although verifying the existence of known photoexcitation channels for plausible prebiotic precursors of nucleotides is an essential part of this thesis, the main focus is on investigating new competitive deactivation processes.

If resistance to UV irradiation was indeed an important selecting factor, comparative analysis and verification of the mechanisms of nonradiative deactivation of excited states, either in canonical or non-canonical bases paired in the WC scheme, should contribute to our understanding of the role and significance of charge-transfer processes upon excitation. It could also shed light on the perplexing question of why living organisms use such a narrow set of building blocks of genetic material that interestingly share a common feature of high photostability.

1.4 Methodology

In this section, a brief overview of the theoretical methods and models used in this thesis is given. Most of the results were obtained using wavefunction theory methods that stem from the Hartree–Fock self-consistent field method.

Hartree-Fock

The physically correct many-electron wavefunction must obey the Schrödinger equation and the **Pauli principle**, which implies that ψ has to be antisymmetric with respect to the interchange in the electronic coordinates x_i, defined in terms of position r_i and spin s_i coordinates.[177] Therefore, two electrons with the same spin cannot occupy the same position in space. Typically, the electronic wave functions of many-electron atoms and molecules are represented as a linear combination of products of one-electron functions $\varphi_j(r_i)$, referred to as atomic or molecular orbitals (AOs or MOs), depending on the context. This is because the Schrödinger equation is exactly solvable in the case of one-electron atoms and selected model potentials. In fact, one of the first approximations of many electron wavefunctions was proposed by Hartree in 1927 as a product of one-electron atomic orbitals, which were determined according to a procedure he called the self-consistent field method (SCF).

$$\psi(\boldsymbol{r}) = \varphi_1(r_1) \cdots \varphi_n(r_n) = \prod_{i=1}^{n} \varphi_i(r_i) \tag{5}$$

However, such a wavefunction was not antisymmetric. Therefore, this approach was later redefined independently by Fock and Slater by formally applying the variational principle and ensuring the correct permutational symmetry of the wave function to meet Pauli's exclusion principle.[2] The resulting Hartree–Fock method is essentially an independent particle model in which the electronic degrees of freedom are coupled through an effective mean field. In practical applications, it relies on the representation of an electronic wave function with the so-called Slater determinant, which corresponds to a particular distribution of electrons among spin orbitals $\phi(x_i)$ defined as a product of one-electron spatial and spin functions $\varphi(r_i)\sigma(s_i)$ that are usually expanded in terms of predefined atomic orbitals called basis functions (i.e. linear combination of atomic orbitals, LCAO).[4,177]

$$\psi_0(x_1 \ldots x_n) = |\phi_1 \cdots \phi_n\rangle \coloneqq \frac{1}{\sqrt{n!}} \begin{vmatrix} \phi_1(x_1) & \phi_2(x_1) & \cdots & \phi_n(x_1) \\ \phi_1(x_2) & \ddots & & \phi_n(x_2) \\ \vdots & & \ddots & \vdots \\ \phi_1(x_n) & \cdots & \cdots & \phi_n(x_n) \end{vmatrix} \tag{6}$$

The variational principle states that the energy expectation value of any trial wave function should be equal to or greater than that of the ground state wave function for a given time-

[177] A. Szabo and N. S. Ostlund, *Modern quantum chemistry: introduction to advanced electronic structure theory*, Courier Corporation, 2012.

independent Hamiltonian. Application of this principle to a Slater determinant composed of spin orbitals that are a linear combination of AOs (typically Gaussian-type functions, GTOs) leads to the Hartree–Fock–Roothan equations, which are solved through iterative minimization.[2,177] At convergence, a set of spin orbitals $\{\phi_i\}$ is obtained corresponding to the lowest electronic energy for a given Slater determinant. Such spin orbitals are eigenfunctions of the Fock operator with eigenvalues ϵ_i:

$$f(i)\phi_i(x_i) = \epsilon_i\phi_i(x_i). \tag{7}$$

The Fock operator is an effective one-electron operator defined as:[7]

$$f(i) = -\frac{1}{2}\nabla_i^2 - \sum_\alpha \frac{Z_\alpha}{r_{i\alpha}} + v_i^{HF}, \tag{8}$$

where the first term on the right hand side is an electronic kinetic energy operator, followed by a electron-nuclear attraction (Z_α is the atomic number of nucleus α), whereas the last term represents the effective potential due to electronic repulsion experienced by the i-th electron. The latter is defined in terms of Coulomb (J) and exchange (K) one-electron operators expanded in terms of spin orbitals that represent classical electron repulsion and its correction due to the antisymmetry of the determinantal wavefunction, respectively. In the HF method, the extremely complicated many-electron problem is approximated with an effective one-particle model, allowing a wide range of effects to be covered, including spin correlation (or Fermi correlation).[177]

In essence, the HF method is a method of obtaining the best Slater determinant. However, the latter is only a convenient approximation of many electron wavefunctions, and the HF theory has many drawbacks. The major issue is that, even though the motion of the same spin electrons is correlated due to proper antisymmetrization, the motion of the opposite spin electrons is not. Hence, the HF method lacks the so-called Coulomb electron correlation. Furthermore, since it depends on a single-determinantal representation, imposing a particular distribution of electrons among the orbitals (i.e. electronic configuration), it is also incapable of describing the essentially multi-configurational character of the wavefunction.[4,178] As a result, the HF method has a significant bias in the electronic energy, which results in unreliable predictions of molecular properties or energetics and is rather ineffective on its own. Nevertheless, the HF method is a starting point for more sophisticated methods that

[178] F. Jensen. *Introduction to computational chemistry*. 2016.

account for the Coulomb correlation and approach an adequate solution of the problem defined by the Schrodinger equation.[4]

Multiconfigurational Self-Consistent Field Theory

The electronic structure of most molecules in their ground electronic state at equilibrium geometry is reasonably well rendered by a closed-shell single determinantal wave function. However, in the case of biradical species, molecules in open-shell excited electronic states and when electronic states become energetically degenerate, such a description becomes unreliable. An extension of the HF approach that was proposed to adequately describe such problems is the so-called Multiconfigurational Self-Consistent Field method (MCSCF), in which the wavefunction is represented as a linear combination of more than one Slater determinant. The latter are usually obtained by populating unoccupied (virtual) MOs instead of occupied in the HF determinant (ψ_0).[4,177,178]

$$\psi^{MCSCF} = c_0\psi_0 + c_1\psi_1 + c_2\psi_2 + \dots \tag{9}$$

For example, in doubly degenerate electronic states, at least two different determinants will significantly contribute to the representation of the wavefunction according to the weights reflected by the variationally optimized coefficients c. In the more complex cases, even more determinants are required to properly represent the wave function. Note that in the MCSCF method, both the configuration weights and the MO coefficients are optimized simultaneously. This should not be confused with the configuration interaction (CI) method, in which the wavefunction is also expanded in terms of "excited" determinants; however, the LCAO coefficients of MOs remain fixed.

$$\psi^{CI} = c_0\psi_0 + \sum_{i}^{occ}\sum_{a}^{virt} c_i^a\psi_i^a + \sum_{i<j}^{occ}\sum_{a<b}^{virt} c_{ij}^{ab}\psi_{ij}^{ab} + \dots \tag{10}$$

The indices i, j and a, b denote occupied and virtual MOs, respectively, and the consecutive terms in the summations run over all singly, doubly, triply, etc. substituted determinants. Truncation of this expansion on single, double, etc. substitutions leads to CIS, CISD etc. wavefunctions, respectively. In the case of a complete CI expansion (i.e. full CI, FCI) both formulations are equivalent; however, in the case of truncated expansions, applications of both methods differ. MCSCF is generally applied to address the aforementioned deficiencies of a single-determinantal wavefunction (often referred to as static correlation), whereas truncated CI methods are more suitable to treat the deficiencies of the mean-field approach, that is the

lack of the Coulomb (dynamic) electron correlation.[4,178] There are many variants of the MCSCF approach; however, the method that gained particular popularity is the Complete Active Space variant of SCF (CASSCF).[179,180] In general, the CASSCF wavefunction corresponds to an expansion of determinants formed by all possible substitutions of a chosen subset of electrons among the so-called active orbitals (i.e. FCI in a selected orbital subspace).[4,178] The remaining orbitals are either unoccupied or doubly occupied. Such an approach has many advantages and provides a qualitatively good description for many multi-configurational problems. However, quantitative agreement with reference data is lacking, and the increasing complexity of the wavefunction with the size of the active space quickly becomes intractable. Occupation restrictions based on orbital groups can be implemented to alleviate this problem.[181]

Generally, following a rule of thumb proposed by Veryazov et al.,[182] only orbitals having occupation numbers in the range between 0.02 and 1.98 are typically selected in active space, and the missing dynamical correlation effects are included using either perturbational approaches (CASPT2, NEVPT2 etc. discussed later) or multireference CI (MRCI), usually a truncated CI expansion based on the CASSCF reference (e.g. MRCISD).[4,183]

Since the same active space renders slightly different performance for electronic states of a distinct character, it is often used in the so-called state-averaged variant (SA-CASSCF). The latter allows for a balanced description of several roots of the CI matrix. The undeniable advantage of the SA-CASSCF approach is the qualitatively correct description of relative energies and the regions of state crossing or avoided crossing of electronic states, despite the loss of accuracy for individual states.[184,185]

Although the CASSCF method has some undeniable advantages, such as size consistency and proper description of degenerate states,[2,7,178] it is based on arbitrary selection of the active space,[182] and does not account for dynamical correlation that can significantly impact the

[179] B. O. Roos, P. R. Taylor, and P. E. Sigbahn, *Chemical Physics*, **1980**, *48*, 157–173.
[180] P.-Å. Malmqvist and B. O. Roos, *Chemical Physics Letters*, **1989**, *155*, 189–194.
[181] K. P. Lawley, *Ab Initio Methods in Quantum Chemistry, Volume 69, Part 2*, John Wiley & Sons, 2009.
[182] V. Veryazov, P. Å. Malmqvist, and B. O. Roos, *International Journal of Quantum Chemistry*, **2011**, *111*, 3329–3338.
[183] B. O. Roos, K. Andersson, M. P. Fülscher, P.-â. Malmqvist, L. Serrano-Andrés, K. Pierloot, and M. Merchán. "Multiconfigurational Perturbation Theory: Applications in Electronic Spectroscopy". In: *Advances in Chemical Physics*. Ed. by I. Prigogine and S. A. Rice. John Wiley & Sons, Inc., 1996. 219–331.
[184] H. Lischka, M. Dallos, P. G. Szalay, D. R. Yarkony, and R. Shepard, *The Journal of Chemical Physics*, **2004**, *120*, 7322–7329.
[185] F. Plasser, "Quantum mechanical simulations of defect dynamics in DNA and model systems", PhD Thesis, University of Vienna, **2012**.

calculated molecular properties.[4] Consequently, it may not be the most reliable method for geometry optimization.

Many-body perturbation theory

Single reference

Perturbation methods for electronic structure calculations rely on the arbitrary partitioning of a Hamiltonian into the so-called zeroth-order component, for which an exact or approximate solution is known, and the remainder, called perturbation. The eigenenergy and eigenfunction are then obtained as a sum of zeroth-order and perturbational corrections, determined consecutively. Partitioning of a Hamiltonian proposed by Møller and Plesset (MP) is commonly used to account for a missing electronic correlation in the (MC)SCF wavefunctions.[177] In the single reference case, the HF wavefunction ψ_0 is the zeroth-order wavefunction $\psi^{(0)}$, and the sum of one-electron Fock operators adds up to the zeroth-order Hamiltonian:

$$H^{(0)} = \sum_i f(i). \tag{11}$$

The perturbation (fluctuation) operator is defined as its deviation from the exact Hamiltonian (more precisely, the difference of the HF potential v^{HF} from the exact electron repulsion operator) $V = H - H^{(0)}$. The zeroth-order energy is, thus, the sum of the occupied orbital energies ($e_0 = \sum_i^{occ} \epsilon_i$):

$$H^{(0)}\psi^{(0)} = \left(\sum_i^{occ} \epsilon_i\right)\psi^{(0)} \tag{12}$$

Since the orbital energies take into account the interaction of a given electron with the mean field of the remaining electrons, e_0 counts each electron-electron repulsion twice. The first-order correction to the energy cancels this double counting and retrieves the correct HF energy:

$$e_0 + e_1 = \langle\psi^{(0)}|H^{(0)}\psi^{(0)}\rangle + \langle\psi^{(0)}|V\psi^{(0)}\rangle = \langle\psi^{(0)}|H\psi^{(0)}\rangle = E_{HF}. \tag{13}$$

Thus, the first correction to the HF energy due to electron correlation appears in the second order, e_2, which in the standard notation in spin orbital basis is

$$e_2 = \frac{1}{4}\sum_{ijab}\frac{|\langle ij||ab\rangle|^2}{\epsilon_i + \epsilon_j - \epsilon_a - \epsilon_b}, \tag{14}$$

where the indices i, j and a, b denote occupied and virtual orbitals, respectively.[177] The sum of e_0, e_1, and e_2 defines the MP2 method, which has become widely popular in the 1980s and is still being used today due to recent developments that have significantly reduced the time-consuming aspects of these calculations, such as the resolution-of-the-identity (RI) or density-fitting approximation. The latter expands two-electron integrals in terms of the auxiliary basis that approximates products of Gaussian functions, decreasing computational storage and computing time. MP2 is known to provide reliable geometries and energies for organic molecules when used with a sufficiently large base set, with relatively modest scaling against the number of basis functions N of roughly N^5. Moreover, unlike the truncated CI methods, it is a size-extensive approach that scales correctly with the number of electrons. Due to its non-variational character, it can overestimate the electron correlation energy; however, as it slowly converges with the basis set size, these effects usually cancel out. Higher orders than second in the MP*n* formalism generally offer a significant improvement in terms of electronic energy (particularly MP4) but not necessarily in terms of other molecular properties and are generally much more computationally demanding. Moreover, higher-order MP implementations often lack analytic gradients and, thus, may not be an adequate choice to explore PES.[4] Consequently, when higher accuracy of the results is required, the Coupled Cluster methods discussed below are usually the methods of choice.

Multireference

As with any single reference approach, MP*n* methods also fail when the electronic ground state of the investigated system has a significant multi-reference character. However, when combined with the MCSCF wavefunction, the MP perturbation approach was shown to adequately address the multireference problems. Furthermore, it substantially improves the description of the dynamical electron correlation, largely omitted in MCSCF or CASSCF calculations (even with relatively large active spaces).

Among the variants of multireference many-body perturbation theory (MRPT), the complete active space perturbation theory to the second order (CASPT2) gained the most attention. One of the most undeniable advantages of this method is the compensation of deficiencies resulting from the usually incomplete active space; thus, the relative energies and properties of the system are less sensitive to the size of the chosen active space.[4] Therefore, the results of CASPT2 calculations are generally more reliable than those obtained at the CASSCF level, and this approach became routine for the description of the electronic structure of molecules

in their excited states.[4,183,186,187] It was shown that this approach is inclined to underestimate excitation energies in the vertical spectrum.[187] It is also prone to the intruder state problem and divergencies due to the near-degeneracies of perturber states and eigenvalues of the zeroth-order Hamiltonian.[183] Both of these deficiencies may be avoided with level-shifting[188] or amplitude regularization techniques.[189] In particular, the so-called IPEA shift improves the agreement of CASPT2 excitation energies in the FC region,[187] even though its performance in the case of medium-sized organic molecules is debatable.[188,190] An alternative formulation of MRPT that is free from the intruder state problem due to a particular choice of zeroth-order Hamiltonian is the n-electron valence state perturbation theory to the second order (NEVPT2).[191–193] In order to correctly describe state-crossings and quasi-degeneracies with the CASPT2 or other MRPT methodology, the various multi-state variants (MS) were proposed, of which the extended multi-state approach (XMS) is particularly appropriate for the description of conical intersections.[194–196] In the case of NEVPT2 a corresponding quasi-degenerate variant (QD-NEVPT2) is also available. The main limitation of both CASPT2 and NEVPT2 lies in the arbitrary selection of active spaces in the CASSCF wavefunction, whose size is currently limited to a dozen or so orbitals due to computational feasibility. Thus, currently, a system roughly the size of three nucleobases can be adequately described using the CASPT2 or NEVPT2 methods.[22]

Coupled-cluster methods

The coupled cluster (CC) is another post-Hartree-Fock technique to account for the missing electron correlation. The CC approach is based on the following exponential wavefunction

[186] M. R. Silva-Junior, M. Schreiber, S. P. A. Sauer, and W. Thiel, *The Journal of Chemical Physics*, **2010**, *133*, 174318.
[187] R. Sarkar, P.-F. Loos, M. Boggio-Pasqua, and D. Jacquemin, *Journal of Chemical Theory and Computation*, **2022**, *18*, 2418–2436.
[188] J. P. Zobel, J. J. Nogueira, and L. González, *Chemical Science*, **2017**, *8*, 1482–1499.
[189] S. Battaglia and R. Lindh, *Journal of Chemical Theory and Computation*, **2020**, *16*, 1555–1567.
[190] Ł. Wolański, D. Grabarek, and T. Andruniów, *Journal of Computational Chemistry*, **2018**, *39*, 1470–1480.
[191] C. Angeli, R. Cimiraglia, and J.-P. Malrieu, *The Journal of Chemical Physics*, **2002**, *117*, 9138–9153.
[192] C. Angeli, R. Cimiraglia, and J.-P. Malrieu, *Chemical Physics Letters*, **2001**, *350*, 297–305.
[193] C. Angeli, R. Cimiraglia, S. Evangelisti, T. Leininger, and J.-P. Malrieu, *The Journal of Chemical Physics*, **2001**, *114*, 10252–10264.
[194] A. A. Granovsky, *The Journal of Chemical Physics*, **2011**, *134*, 214113.
[195] T. Shiozaki, W. Győrffy, P. Celani, and H.-J. Werner, *J. Chem. Phys.*, **2011**, *135*, 081106.
[196] Q. M. Phung, Y. Komori, T. Yanai, T. Sommerfeld, and M. Ehara, *Journal of Chemical Theory and Computation*, **2020**, *16*, 2606–2616.

ansatz:

$$\psi^{CC} = e^{T}|\psi_0\rangle, \tag{15}$$

where ψ_0 is the reference wavefunction (usually HF determinant) and T is the cluster operator defined as a sum of operators generating all singly T_1, doubly T_2 etc. excited determinants weighted by the so-called cluster amplitudes. The main advantage of CC over the CI expansion is the size-extensivity of truncated expansions. However, a variational solution to the coupled cluster eigenproblem would be intractable. Thus, practical implementation relies on the projection onto the excited determinant space and the iterative solution of the resulting linear equations for the cluster amplitudes.[4,7]

$$E_{CC} = \langle\psi_0|H|e^{T}\psi_0\rangle. \tag{16}$$

Truncation of the cluster operator on T_1, T_2, etc. and Taylor expansion of the exponential operator lead to a family of CC methods (CCS, CCSD, etc., respectively). In practical applications, the most popular approach is CCSD(T), in which the effect of T_3 amplitudes is approximated perturbatively. The full CCSDT method scales as N^8 and is computationally tractable only for small molecules. Fortunately, CCSD(T) calculations in sufficiently saturated basis sets often provide very accurate results and have become the effective golden standard for single reference systems.[4]

The coupled cluster formalism is essentially a ground-state method; however, excitation energies may be computed using the equation of motion (EOM-CC) or linear response (LR-CC) approaches.[5,197] An approximate coupled cluster singles and doubles model, CC2, was later introduced, in which the double excitation amplitudes have a form similar to the MP2 equations. The CC2 method has the same accuracy as MP2, but when combined with the linear response formalism, it provides a reliable and computationally inexpensive approach (scaling as N^5) for excited-state calculations.[198] In general, the CC2 method allows for semi-quantitative prediction of vertical excitation energies and excited-state potential energy surfaces of single reference states. However, the agreement of any EOM-CC or LR-CC method

[197] M. Musiał. "Equation-of-Motion Coupled-Cluster Models". In: *Quantum Chemistry and Dynamics of Excited States*. John Wiley & Sons, Ltd, 2020. 77–108. DOI: 10.1002/9781119417774.ch4.

[198] C. Hättig. "Structure Optimizations for Excited States with Correlated Second-Order Methods: CC2 and ADC(2)". In: *Advances in Quantum Chemistry*. Ed. by H. J. A. Jensen. Vol. 50. Response Theory and Molecular Properties (A Tribute to Jan Linderberg and Poul Jørgensen). Academic Press, 2005. 37–60. DOI: 10.1016/S0065-3276(05)50003-0.

deteriorates as state crossings are approached and their performance in these regions should be tested against reliable multiconfugurational method.[198]

Algebraic Diagrammatic Construction up to second-order

The CC2 model was designed to describe the excitation energies of electronic states dominated by a single configuration. In such a case the excitation energies are correct through the second order in the fluctuation potential. However, in the linear response LR-CC approach the excitation energies are obtained as eigenvalues of a non-Hermitian Jacobi matrix. This leads to a particularly poor performance in the regions of state crossings. The latter problem was resolved to some extent with the introduction of the Algebraic Diagrammatic Construction to Second-Order (ADC(2)) in which the excitation energies are obtained as eigenvalues of a Hermitian secular matrix.[199,200] This leads to a physically correct description of conical intersections between states of the same symmetry. Although ADC(2) remains a single reference method and fails in the case of near degeneracies with the ground state.[198] The relation of the CC2, ADC(2) and CIS(D_∞) method was discussed in detail by Hättig.[198] In short, the CC2 Jacobian includes some terms that are not necessary to obtain excitation energies that are correct through second-order in the fluctuation operator. Neglect of these terms corresponds to an iterative variant of the perturbatively corrected CIS(D) method introduced by Head-Gordon et al. CIS(D_∞). Although developed within the polarization propagator approach, the secular matrix in the ADC(2) method corresponds to a symmetrized variant of the latter Jacobian:[198,201]

$$J^{ADC(2)} = \frac{1}{2}\left(J^{CIS(D_\infty)} + (J^{CIS(D_\infty)})^\dagger\right). \tag{17}$$

All the discussed second-order methods: CC2, ADC(2) and CIS(D_∞) produce almost identical results in the FC region that on average show even better agreement with the experimental data than CCSD. However, ADC(2) has some particular advantages in other regions of PESs and is particularly well suited to describe regions of state crossings. It is much more robust than the CC and CI methods and is size-extensive when combined with the MP2 description of the ground state. However, it is a single reference approach what limits its usage

[199] A. B. Trofimov and J. Schirmer, *Journal of Physics B: Atomic, Molecular and Optical Physics*, **1995**, *28*, 2299.
[200] A. Dreuw and M. Wormit, *Wiley Interdisciplinary Reviews: Computational Molecular Science*, **2015**, *5*, 82–95.
[201] R. Lindh and L. González, *Quantum Chemistry and Dynamics of Excited States: Methods and Applications*, John Wiley & Sons, 2020.

to systems adequately described by the HF method. Organic photochemistry generally meets this requirement, unless one deals with bond breaking or significant structural distortions, for which a multiconfigurational description is needed. When used in those cases, the CC model often yields a better description of the ground state; however, recent advances in the multireference ADC scheme provide a solution to overcome these limitations.[202]

Spin Component Scaling (SCS) approach

Since the same–spin and opposite–spin contributions to the correlation energy scale differently, most second-order methods like MP2, CC2 or ADC(2) can be modified by introducing empirical scaling factors to improve their performance. Grimme proposed the first empirical Spin Component Scaling (SCS) variant of MP2 that increases the weight of the opposite-spin contribution by a factor of 1.20 and reduces the same-spin contribution by 0.33.[203] Other variants of such an approach were proposed, like the Scaled Opposite Spin (SOS), which neglects the same spin contributions since Fermi correlation is already included at the HF level and scales the opposite spin term by a factor of 1.3. The latter results also in a significant computational speedup.[204] Although the SCS augmented methods are by definition semi-empirical, it was shown that this approach improves the quantitative agreement of the calculated thermochemical parameters[204] and excitation energies.[205]

Hybrid variational-perturbational interaction energy decomposition scheme

The ground-state interaction energies of complementary nucleobases were calculated using a supermolecular approach with a full counterpoise correction of the basis set superposition error (BSSE).[206]

$$\Delta E_{\mathrm{AB}} = E_{\mathrm{A}} - E_{\mathrm{B}}. \tag{18}$$

[202] A. Dreuw, A. Papapostolou, and A. L. Dempwolff, *The Journal of Physical Chemistry A*, **2023**.
[203] S. Grimme, *J. Chem. Phys.*, **2003**, *118*, 9095–9102.
[204] S. Grimme, L. Goerigk, and R. F. Fink, *Wiley Interdisciplinary Reviews: Computational Molecular Science*, **2012**, *2*, 886–906.
[205] A. Tajti and P. G. Szalay, *Journal of Chemical Theory and Computation*, **2019**, *15*, 5523–5531.
[206] S. Boys and F. Bernardi, *Molecular Physics*, **1970**, *19*, 553–566.

The energies of the dimer and its components (marked A and B) were calculated using the MP2 and SCS-MP2 methods implemented in Gaussian 16 software,[207] assuming the dimer-centered cc-pVTZ and aug-cc-pVTZ basis sets.

To gain a more detailed understanding of the origins of interactions, the hybrid variational-perturbational interaction energy decomposition scheme (HVPT-EDS), interfaced with the GAMESS package,[208] was used. This method, introduced by Gutowski et al.[209] and further developed,[210–213] enables the partitioning of the interaction energies into physically meaningful components.

In this scheme, the total MP2 interaction energy of a dimer is partitioned into the Hartree–Fock (HF) and the electron correlation components:

$$\Delta E^{\mathrm{MP2}} = \Delta E^{\mathrm{HF}} + \Delta E^{\mathrm{MP2}}_{corr}. \tag{19}$$

The HF term can be partitioned into the Heitler–London (ΔE^{HL}) and the delocalization energy ($\Delta E^{\mathrm{HF}}_{del}$) components. The HL term involves electrostatic interactions of the charge densities of the unperturbed monomers ($\epsilon^{(10)}_{el}$) and the associated exchange repulsion ($\Delta E^{\mathrm{HL}}_{ex}$). The delocalization term accounts for the induction and exchange-induction effect.

$$\Delta E^{\mathrm{HF}} = \Delta E^{\mathrm{HL}} + \Delta E^{\mathrm{HF}}_{del} \tag{20}$$

$$= \epsilon^{(10)}_{el} + \Delta E^{\mathrm{HL}}_{ex} + \Delta E^{\mathrm{HF}}_{del} \tag{21}$$

The second order electron correlation term ($\Delta E^{\mathrm{MP2}}_{corr}$) comprises the second order dispersion interaction ($\epsilon^{(20)}_{disp}$) as well as the electron correlation correction to the first order electrostatic

[207] M. J. Frisch, G. W. Trucks, H. B. Schlegel, G. E. Scuseria, M. A. Robb, J. R. Cheeseman, G. Scalmani, V. Barone, G. A. Petersson, H. Nakatsuji, X. Li, M. Caricato, A. V. Marenich, J. Bloino, B. G. Janesko, R. Gomperts, B. Mennucci, H. P. Hratchian, J. V. Ortiz, A. F. Izmaylov, J. L. Sonnenberg, D. Williams-Young, F. Ding, F. Lipparini, F. Egidi, J. Goings, B. Peng, A. Petrone, T. Henderson, D. Ranasinghe, V. G. Zakrzewski, J. Gao, N. Rega, G. Zheng, W. Liang, M. Hada, M. Ehara, K. Toyota, R. Fukuda, J. Hasegawa, M. Ishida, T. Nakajima, Y. Honda, O. Kitao, H. Nakai, T. Vreven, K. Throssell, J. A. Montgomery Jr., J. E. Peralta, F. Ogliaro, M. J. Bearpark, J. J. Heyd, E. N. Brothers, K. N. Kudin, V. N. Staroverov, T. A. Keith, R. Kobayashi, J. Normand, K. Raghavachari, A. P. Rendell, J. C. Burant, S. S. Iyengar, J. Tomasi, M. Cossi, J. M. Millam, M. Klene, C. Adamo, R. Cammi, J. W. Ochterski, R. L. Martin, K. Morokuma, O. Farkas, J. B. Foresman, and D. J. Fox. *Gaussian~16 Revision C.01*. Gaussian Inc. Wallingford CT. 2016.

[208] M. W. Schmidt, K. K. Baldridge, J. A. Boatz, S. T. Elbert, M. S. Gordon, J. H. Jensen, S. Koseki, N. Matsunaga, K. A. Nguyen, S. Su, et al., *Journal of Computational Chemistry*, **1993**, *14*, 1347–1363.

[209] M. Gutowski, F. B. Van Duijneveldt, G. Chałasiński, and L. Piela, *Molecular Physics*, **1987**, *61*, 233–247.

[210] W. A. Sokalski, S. Roszak, and K. Pecul, *Chemical physics letters*, **1988**, *153*, 153–159.

[211] G. Chałasiński and M. Szcześniak, *Molecular Physics*, **1988**, *63*, 205–224.

[212] S. Cybulski, G. Chal/asiński, and R. Moszyński, *The Journal of chemical physics*, **1990**, *92*, 4357–4363.

[213] R. W. Gora, W. Bartkowiak, S. Roszak, and J. Leszczynski, *The Journal of chemical physics*, **2004**, *120*, 2802–2813.

interaction ($\epsilon_{el,r}^{(12)}$) and the remaining electron correlation effects ($\Delta E_{ex}^{(2)}$). The latter term accounts mainly for the uncorrelated exchange-dispersion and electron correlation corrections to the Hartree–Fock exchange repulsion.

$$\Delta E_{corr}^{\mathrm{MP2}} = \epsilon_{el,r}^{(12)} + \epsilon_{disp}^{(20)} + \Delta E_{ex}^{(2)} \tag{22}$$

Employed ab initio methods and auxiliary schemes

This dissertation focuses on the theoretical investigations of the photochemistry of selected pairs of canonical and non-canonical nucleobases. The MP2 method with the correlation-consistent cc-pVTZ basis set[214] was employed for the optimization of the equilibrium geometries. In general, no symmetry constraints were imposed, unless otherwise noted. The stationary points on the ground and the excited PE surfaces were located using the Turbomole 7.3 package.[215] The vertical excitation energies and transition dipole moments at equilibrium geometries were obtained using ADC(2)/cc-pVTZ and SCS-ADC(2)/cc-pVTZ methodology. Most of the discussion focuses on the results obtained for the isolated systems in the gas phase. However, when the analysis of the solvation effects was relevant, the polarizable continuum model (PCM)[216] was used to incorporate the electrostatic effects of bulk water and chloroform on the selected properties in the FC region.

The relevant MECPs were located using the sequential penalty-constrained optimization implemented in the CIOpt package.[12] This approach, proposed by Levine, Martínez and Coe, utilizes penalty functions to guarantee that the energies of two intersecting states are equal while minimizing their overall value. This approach has a great advantage, as it eliminates the requirement to compute the nonadiabatic couplings in the optimization process of the MECP. The MECPs reported in this dissertation were located using the MP2 and ADC(2) methods (or their SCS variants) for the ground and the S_1 excited states, respectively in cc-pVTZ basis set. This approach was denoted as either the MP2/ADC(2)/cc-pVTZ or SCS-MP2/SCS-ADC(2)/cc-pVTZ.

The potential energy profiles were computed by linear interpolation in internal coordinates (LIIC) between stationary points using the same electronic structure calculation methods, i.e.

[214] T. H. Dunning, *The Journal of Chemical Physics*, **1989**, *90*, 1007–1023.
[215] *TURBOMOLE v7.3 2018, a development of University of Karlsruhe and Forschungszentrum Karlsruhe GmbH, 1989-2007, TURBOMOLE GmbH, since 2007; available from www.turbomole.com.*
[216] J. Tomasi, B. Mennucci, and R. Cammi, *Chemical reviews*, **2005**, *105*, 2999–3094.

the MP2 and ADC(2) methods or their SCS variants in the cc-pVTZ basis set. The reliability of the MP2/ADC(2) PE profiles for representative systems was tested against the NEVPT2 or XMS-CASPT2 results. The selected MECP geometries were compared with the structures located using the XMS-CASPT2 method. The intermolecular charge transfer character of the electronic states was assigned based on the transition density matrix analysis proposed by Plasser et al.[217]

The charge transfer numbers defined as partial summations over squared transition density matrix elements of molecular fragments were calculated using the TheoDore 1.5.1 package.[217–219] These numbers were computed based on the Mulliken type analysis[220] and were used to determine the weight of charge transfer configurations for a given state (denoted as Ω_{CT}). This quantity vanishes for localized or delocalized Frenkel excitonic states and approaches unity for charge transfer or charge resonance states.

The ionization potentials and electron affinities of the isolated nucleobases were computed to investigate their relative stability and ability to receive or donate electronic density. Electron affinities were calculated as the difference between the total energies of the neutral and anionic forms ($EA = E_{neutral} - E_{anion}$). The vertical electron affinities (VEAs) were calculated assuming the equilibrium geometry, whereas the adiabatic electron affinities (AEAs) were computed assuming the optimized geometries of the neutral and anionic species. These calculations were performed using the UMP2/aug-cc-pVTZ method in the gas phase. The PCM model[216] was used to estimate solvation effects. Vertical (VIE) and adiabatic (AIE) electron detachment (ionization) energies were calculated accordingly as $IE = E_{cation} - E_{neutral}$.

The transition rates of radiative and nonradiative processes were calculated using the thermal vibration correlation function (TVCF) formalism for excited state decay, developed by Shuai et al.[221–223] employing MOMAP software.[224] Due to the availability of non-adiabatic coupling terms, these calculations were performed using the TD-DFT approach, assuming ωB97X-D3 exchange-correlation functional and def2-SVP basis set available in the QChem 6.1

[217] F. Plasser, M. Wormit, and A. Dreuw, *The Journal of Chemical Physics*, **2014**, *141*, 024106.
[218] F. Plasser, S. A. Bäppler, M. Wormit, and A. Dreuw, *The Journal of Chemical Physics*, **2014**, *141*, 024107.
[219] F. Plasser, *The Journal of Chemical Physics*, **2020**, *152*, 084108.
[220] R. S. Mulliken, *The Journal of chemical physics*, **1955**, *23*, 1833–1840.
[221] Q. Peng, Y. Yi, Z. Shuai, and J. Shao, *The Journal of Chemical Physics*, **2007**, *126*, 114302.
[222] Y. Niu, Q. Peng, C. Deng, X. Gao, and Z. Shuai, *The Journal of Physical Chemistry A*, **2010**, *114*, 7817–7831.
[223] Z. Shuai, *Chinese Journal of Chemistry*, **2020**, *38*, 1223–1232.
[224] Y. Niu, W. Li, Q. Peng, H. Geng, Y. Yi, L. Wang, G. Nan, D. Wang, and Z. Shuai, *Molecular Physics*, **2018**, *116*, 1078–1090.

package.[225] The rotationally invariant spin-orbit coupling constants (SOCC) were computed including mean-field treatment of the two-electron part of the Breit–Pauli Hamiltonian and Wigner-Eckart theorem (as implemented in QChem 6.1)[226] by summing over all projections M of spin S according to:

$$\mathrm{SOCC} = \sqrt{\sum_{M'M''} |\langle S'M'|H^{SO}|S''M''\rangle|^2}. \tag{23}$$

[225] Y. Shao, Z. Gan, E. Epifanovsky, A. T. Gilbert, M. Wormit, J. Kussmann, A. W. Lange, A. Behn, J. Deng, X. Feng, et al., *Molecular Physics*, **2015**, *113*, 184–215.

[226] S. Kotaru, P. Pokhilko, and A. I. Krylov, *The Journal of Chemical Physics*, **2022**, *157*, 224110.

2 Discussion of results

2.1 Radiationless deactivation of the canonical nucleobase pairs

Equilibrium geometries of the three canonical Watson–Crick (WC) base pairs: guanine-cytosine (G-C), adenine-thymine (A-T) and adenine-uracil (A-U) are presented in Figure 9 with the corresponding bond lengths. Geometries on ground state potential energy (PE) surfaces were located using the MP2 method with the correlation-consistent cc-pVTZ basis set.[214] Geometry optimization without symmetry constraints generally yields planar structures with minor deviations of amino and (obviously) methyl groups outside the plane of heterocyclic rings. The located equilibrium geometries were assumed in consecutive single-point calculations of vertical excitation energies for 15 lowest-lying excited states. Natural Transition Orbitals (NTO) analysis[227] was used to determine the character of electronic transitions and the weight of charge transfer configurations for a given state (denoted Ω_{CT}). As mentioned in the methodology section, the latter quantity approaches unity for charge transfer or charge resonance states. Table 1 presents vertical excitation energies for selected low-lying electronic states with corresponding oscillator strengths and assigned transition characters for canonical nucleobase pairs.

For the G-C base pair, the lowest singlet excited state is of $\pi\pi^*$ character, and this transition is located mainly on guanine. There are several other locally-excited (LE) bright $^1\pi\pi^*$ states lying below the S_5 $^1\pi\pi^*$ state that has a clear charge transfer (CT) character (the Ω_{CT} weight amounts to 0.91). In the Franck-Condon region, this CT state lies 5.67 eV above the ground state.

[227] R. L. Martin, *The Journal of Chemical Physics*, **2003**, *118*, 4775–4777.

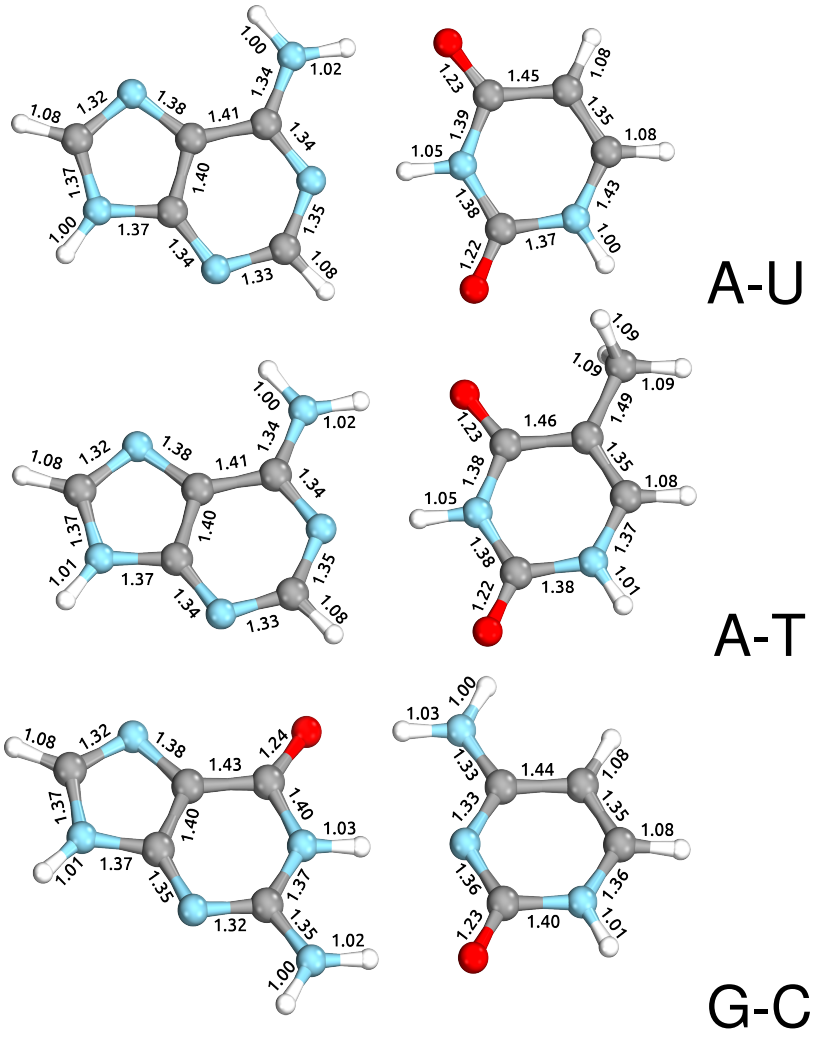

Figure 9. Geometries of canonical nucleobases paired in the Watson-Crick scheme, optimized at the MP2/cc-pVTZ level of theory.

Such a composition of low-lying electronic states leads to interesting and unique dynamics of photoexcited WC G-C, which is well known in the literature. In particular, the time-resolved gas-phase IR-UV spectrum of this base pair has a characteristic distinct broad-band feature and is qualitatively different from the sharp UV spectrum exhibited by other base pairs.[96] Furthermore, it is now firmly established that for the G-C base pair, the transfer of an electron in the CT state leads to the transfer of a proton (or two) and, consequently, nonradiative subpicosecond deactivation to the ground state.[96,103–106] This mechanism, called electron-driven proton transfer (EDPT), was first proposed by Sobolewski and Domcke in 2005[97] and may be considered as a particular case of a proton-coupled electron transfer (PCET) process.[108]

Table 1. Properties of selected low-lying electronic states of canonical base pairs A-T, A-U and G-C, calculated using SCS-ADC(2)/cc-pVTZ method assuming the ground-state equilibrium geometries optimized using MP2/cc-pVTZ method. The oscillator strengths (f_{osc}), vertical excitation energies in eV (E_{exc}) and the weights of the CT configurations (Ω_{CT}) are reported. The last column shows the reference values of excitation energies calculated at the EOM-CC level.[a]

Base pair	State / Transition	f_{osc}	E_{exc}	Ω_{CT}	E_{exc}^{EOM-CC}
G-C	S_1 $\pi_G\pi_G^*$	0.077	4.99	0.042	4.85
	S_2 $\pi_C\pi_C^*$	0.084	5.06	0.017	4.92
	S_3 $\pi_C\pi_C^*$	0.356	5.55	0.098	5.37
	S_4 $\pi_G\pi_G^*$	0.334	5.59	0.015	5.48
	S_5 $\pi_G\pi_C^*$	0.028	5.67	**0.906**	5.36
	S_6 $n_C\pi_C^*/n_G\pi_C^*$	0.001	5.76	0.136	5.65
A-T	S_1 $n_T\pi_T^*$	$5.334 \cdot 10^{-5}$	5.11	0.050	5.24
	S_2 $\pi_A\pi_A^*$	0.015	5.19	0.008	5.34
	S_3 $\pi_T\pi_T^*/\pi_A\pi_A^*$	0.284	5.30	0.012	5.52
	S_4 $\pi_A\pi_A^*/\pi_T\pi_T^*$	0.239	5.39	0.009	5.60
	S_5 $n_A\pi_A^*$	$3.558 \cdot 10^{-4}$	5.64	0.044	5.65
	S_9 $\pi_A\pi_T^*$	0.292	6.60	**0.428**	
	S_{11} $\pi_A\pi_T^*$	0.238	6.66	**0.505**	
	S_{13} $n_T\pi_T^*$	$1.569 \cdot 10^{-4}$	6.90	0.102	
A-U	S_1 $n_U\pi_U^*$	$9.254 \cdot 10^{-5}$	5.09	0.049	
	S_2 $\pi_A\pi_A^*$	0.017	5.19	0.007	
	S_3 $\pi_A\pi_A^*/\pi_U\pi_U^*$	0.338	5.33	0.008	
	S_4 $\pi_U\pi_U^*/\pi_A\pi_A^*$	0.178	5.46	0.009	
	S_5 $n_A\pi_A^*$	$3.288 \cdot 10^{-4}$	5.65	0.041	
	S_9 $\pi_A\pi_U^*$	0.152	6.57	**0.659**	
	S_{11} $\pi_A\pi_U^*$	0.373	6.65	**0.260**	
	S_{14} $n_U\pi_U^*$	$1.638 \cdot 10^{-4}$	6.93	0.137	

[a] Results adopted from Szalay et al.[228,229] EOM-CCSD(T)/TZVP values for G-C and EOM-CCSD/cc-pVDZ results for A-T in the arrangement denoted WW1.

Interestingly, less than 0.1 eV above the $^1\pi_G\pi_C^*$ CT state, a reactive $^1n\pi^*$ state is found that is located mainly on cytosine moiety but with a partial CT character. These states often do not receive the deserved attention, as they have low transition strengths and $n\pi^*$ CT states are rarely seen. However, they are significant for the dynamics of photoexcited molecules, as they can be populated by crossing with the LE $^1\pi\pi^*$ state, leading to rich photodynamics

of pyrimidine bases.[19] Nevertheless, in G-C, because of the ordering of electronic states in the Franck-Condon region, they probably do not play a significant role in the nonradiative deactivation of this complex.

A different situation is observed for the A-T and A-U base pairs for which $^1n\pi^*$ states appear in the low-energy range of the UV spectrum. In these base pairs, the first excited state in the singlet manifold is the LE $^1n\pi^*$ state at about 5.1 eV, which is associated with the electronic transition from the carbonyl oxygen lone pair to the π^* orbital localized on the aromatic ring of pyrimidine. Experimental results[172] indicate that in the case of the adenine-thymine dimer, after excitation to the lowest $^1\pi\pi^*$ state, internal conversion leads to the population of the $^1n\pi^*$ state having lower energy, with a lifetime of 2.4 ps. The same study shows that the nonradiative transition from $^1\pi\pi^*$ to $^1n\pi^*$ state through a conical intersection occurs at an ultrafast pace (< 100 fs). However, it should be noted that the assignment was based on the Koopmans' ionization correlations calculated at the TD-B3LYP/6-31++G(d,p) level. The ordering of states and the position of $n\pi^*$ states in the singlet manifold are particularly important because they lie below both the CT and the lowest bright state, which increases the probability of their population in photodynamics. Although $^1n\pi^*$ states usually have very weak spectral features due to negligible oscillator strength, trapping a molecule for tens to hundreds of nanoseconds in a dark reactive state could have significant consequences. Particularly interesting in this context is that $^1n\pi^*$ states can contribute to both photostability and photodamage of nucleic acids due to their long-lived character and the possibility of a population of triplet states in pyrimidines via efficient ISC.[67,126,176,230]

In A-T and A-U, the charge transfer state of $^1\pi\pi^*$ character is also found that has properties similar to the dark CT state in G-C; however, its excitation energy is much higher, as it amounts to about 6.6 eV in the Franck-Condon region (cf. Table 1, Perun et al. reported 6.26 eV at CC2/cc-pVDZ level[114] whereas Szalay et al.[228] EOM-CCSD(T)/TZVP estimate is 5.88 eV). Consequently, the excited state dynamics of this base pair is likely dominated by intramolecular processes (puckering of the C2 or C6 atom of adenine and deactivation through the $^1n\pi^*$ states of pyrimidines (see Sect. 1.2.1 on page 8). Indeed, a recent computational study of the ultrafast dynamics of the photoexcited A-T base pair using the Fragment Diabatization Linear Vibronic Coupling Model at the TD-DFT level shows that the CT state, lying ~0.7 eV

[230] J. Dezalay, M. Broquier, S. Soorkia, and G. Grégoire, *The European Physical Journal D*, **2021**, *75*, 1–11.
[228] P. G. Szalay, T. Watson, A. Perera, V. Lotrich, and R. J. Bartlett, *The Journal of Physical Chemistry A*, **2013**, *117*, 3149–3157.

above the bright LE state in the FC region, was not populated,[116] in contrast to the results obtained using the same approach for G-C.[112]

Although, in principle, all of the above intra and intermolecular deactivation channels are available in the canonical base pairs, their relative importance depends on many factors. The vertical electronic spectrum in the Franck-Condon region and the relative energies of the relevant states are just indications of these factors. For instance, Green et al. reported that H-bonding leads to destabilization of $^1n\pi^*$ states and stabilization of $^1\pi\pi^*$ states in the WC G-C and A-T.[112,116] Therefore, to obtain a more detailed understanding, the relevant potential energy surfaces should be analyzed, since photodynamics strongly depends on the topology and location of the particular conical intersections.

2.1.1 EDPT in WC G-C — population of $^1\pi_G\pi_C^*$ CT state

Schultz et al.[104] have shown using femtosecond time-resolved mass spectroscopy of 2-aminopyridine (2AP) clusters and ab initio calculations that the excited state lifetime of a hydrogen-bonded 2AP dimer is significantly shorter than the lifetime of either the monomer or the larger nonplanar clusters. They attributed this to internal conversion through an intermolecular channel formed by the $^1\pi\pi$ CT state, which is strongly stabilized by the transfer of a proton in the hydrogen-bonded dimer. The results of nonadiabatic dynamics simulations at the XMS-CASPT2 level later confirmed it.[231] Schultz et al. also indicated that a similar mechanism should be available in the WC G-C with an even faster excited state decay, as the corresponding CT state is energetically closer to the lowest-lying bright state. Indeed, the lowest CT state in the FC region in G-C is closer to the lowest bright state than in any other canonical WC base pair (0.68 eV above S_1 at the SCS-ADC(2)/cc-pVTZ level and 0.51 eV at the EOM-CCSD(T)/TZVP level[228]). This was later confirmed by time-resolved IR-UV studies of gas-phase base-pair complexes discussed above.[96]

EDPT mechanism is thus the most plausible explanation for the ultra-fast subpicosecond deactivation of photoexcited WC G-C due to spontaneous proton transfer from guanine to cytosine through the population of the $^1\pi_G\pi_C^*$ CT state. To construct the corresponding potential energy profile along the proton-transfer coordinate in the base pair, one must consider the possibility of transferring protons corresponding to the different hydrogen bonds in the system. Therefore, the PE profiles of the states of interest were calculated as

[231] J. Ray and S. G. Ramesh, *Physical Chemistry Chemical Physics*, **2022**, *24*, 7274–7292.

functions of the N-H bond distances (simultaneous double proton transfer was not taken into consideration). Because the CT state is strongly stabilized by proton transfer, this allowed us to locate the minimum energy structures on its PE surface. Subsequently, S_1/S_0 minimum energy crossing points (MECPs) were located employing sequential penalty-constrained optimization as implemented by Levine et al. in the CIOpt package[12] that was interfaced with the TURBOMOLE 7.3 package.[215]

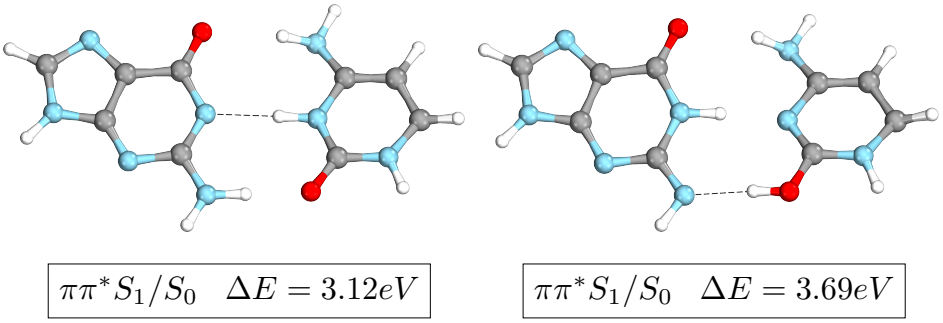

Figure 10. Minimum energy S_1/S_0 crossing points corresponding to two different protons transferred, located at the SCS-MP2/SCS-ADC(2)/cc-pVTZ level. The ΔE with respect to the ground state energy is shown.

As shown in Figure 10 the MECP corresponding to the transfer of imino N1 proton to N3 nitrogen of cytosine is significantly lower in energy than the one associated with the transfer of amino proton to carbonyl oxygen of cytosine. This can be rationalised by the lower pK_a value of the N1-H imino proton.[232] Further investigation of the PE surfaces of the relevant states was based on linear interpolation in the internal coordinates (LIIC) between the ground state equilibrium geometry and the minimum-energy structure of S_1 excited state, corresponding to the intermolecular CT state. Subsequently, the S_1 $^1\pi_G\pi_C^*/S_0$ MECP was located, which was structurally and energetically very close to the optimized S_1 minimum geometry.

It should be underlined that initially the PE profiles were computed using the MP2 method for the ground state and the ADC(2) method for the excited states. These were further compared with the results obtained using the spin component scaling variants[233] of these methods (that is, SCS-MP2 and SCS-ADC(2)), assuming the same interpolated geometries. Recent studies indicated that the SCS variant of the CC2 method essentially alleviates the underestimation of excitation energies (i.e. excessive stabilization) of CT, Rydberg and $n\pi^*$ states.[205] Since the ADC(2) method suffers from similar problems, considering the formal

[232] X. Zhang, J. Jie, D. Song, and H. Su, *The Journal of Physical Chemistry A*, **2020**, *124*, 6076–6083.
[233] A. Hellweg, S. A. Grün, and C. Hättig, *Physical Chemistry Chemical Physics*, **2008**, *10*, 4119–4127.

similarities between the ADC(2) and CC2 methods, the SCS variant should produce a more balanced description of the valence and CT states.

The SCS variant of the ADC(2) method increases the excitation energies and shifts the potential energy profiles both inside and outside the Franck-Condon region. Regarding the vertical excitations of the G-C base pair, the blueshift of 0.13-0.34 eV has been observed along with a change in the order of the electronic states. In particular, the CT state in the ADC(2) method lies lower on the PE profile, and even the first excited state in the FC region exhibits a partial CT character. This characteristic is confirmed when the ADC(2) results are compared to the results obtained at the CC2 level of theory (see Table 2 for reference). The $^1\pi_G\pi_C^*$ state of a clear CT character, which the ADC(2) method predicts to be the third excited state in the singlet manifold, becomes fifth in the SCS-ADC(2) results. It is interesting to note that the results obtained with the ADC(2) method are very similar to those reported using the EOM-CCSD(T)/TZVP method.[228] Likewise, the MECPs presented in Figure 10 differ energetically by ~0.6 eV compared to the results of the ADC(2) method.

The accuracy of the chosen methodology was tested against the results obtained using the multiconfigurational second-order *n*-electron valence state perturbation theory (NEVPT2) with the state-averaged complete active space SA-2-CASSCF(4,4)/cc-pVTZ reference wave function. Two π orbitals located on guanine and cytosine and two respective π^* orbitals were included in the active space. Molecular orbitals with occupations ranging from 0.02 to 1.98 were considered, as suggested by Veryazov et al.[182] It can be concluded from Figure 11 that the excitation energies obtained using the SCS-ADC(2) method agree well with the NEVPT2 results for this system, in stark contrast to the ADC(2) approach, which systematically underestimates the energies of the $^1\pi_G\pi_C^*$ CT and $^1n\pi^*$ states. The interpolated PE profiles of the S_0 state calculated using different methods (shown with green lines and triangles) are virtually identical. The hypersurfaces of the lowest-lying $^1\pi\pi^*$ bright state (shown with red lines) are also very close, with the SCS-ADC(2) energies being slightly lower than the ADC(2) values. However, there is a substantial difference between the SCS-ADC(2) or NEVPT2 results and the ADC(2) results for the CT state (black lines or triangles) and the $^1n\pi^*$ state (gray lines), for which the ADC(2) results are significantly underestimated compared to the reference NEVPT2 results. It shows that although the choice of theoretical approach does not affect the description of the PE surface in the ground state, it is essential to determine the PE surfaces of the CT and $^1n\pi^*$ states, and hence the MECPs with these surfaces. Therefore, in the following discussion, all reported MECPs were located assuming the SCS-MP2 energies and gradients for the ground state and the SCS-ADC(2) results for the excited states (an approach denoted as SCS-MP2/SCS-ADC(2)).

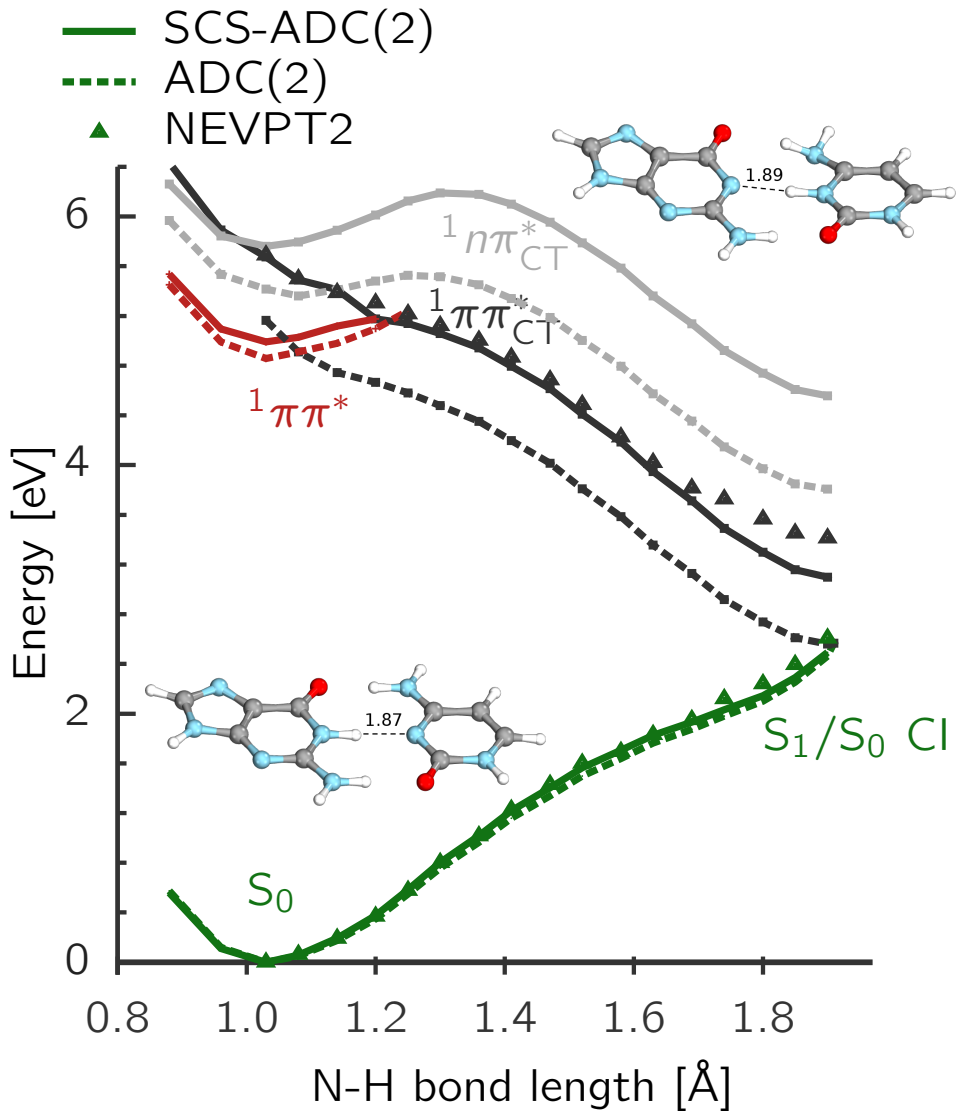

Figure 11. Potential energy cut for low-lying electronic states of G-C plotted by linear interpolation in internal coordinates along the proton transfer coordinate between the S_0 and S_1 minimum energy structures.

As discussed previously by other authors,[26,97,234] stabilization of the $^1\pi_G\pi^*_C$ CT state by proton transfer results in two conical intersections: 1) with the optically accessible locally excited $^1\pi_G\pi^*_G$ state and 2) with the ground state after proton transfer. The energy of the latter lies lower on the PE profile than the vertical excitation energy of any of the locally excited (LE) states; therefore, this CT state serves as a pathway connecting the LE states with S_0 and drives the radiationless deactivation by which photoexcited base pairs may return to the ground

[234] A. L. Sobolewski and W. Domcke, *The Journal of Physical Chemistry A*, **2007**, *111*, 11725–11735.

state in a nondestructive manner. Upon returning to the ground state, charge recombination occurs, and the transferred proton may return to guanine, recovering its initial structure, or some other tautomer may be formed. It should be emphasized that the reported PE profiles were obtained by interpolation in internal coordinates instead of constrained optimization and do not correspond to minimum energy paths. Hence, the observed PE barriers are likely overestimated. However, the goal was to obtain useful qualitative information on possible deactivation mechanisms by inspecting the correlations of the adiabatic states.

EDPT vs. intramolecular ring-puckering

Since the S_1 state in the FC region is the bright $^1\pi_G\pi_G^*$ LE state localized at the guanine moiety, an alternative decay channel may be available after the population of this state. Previous nonadiabatic dynamics simulations indicated that the population of the corresponding state in isolated guanine leads to a very efficient deactivation due to puckering of the C2 atom.[25] Figure 12 shows a qualitative overview of the corresponding decay channel along the mass-weighted deformation coordinate of the guanine ring compared to the EDPT process.

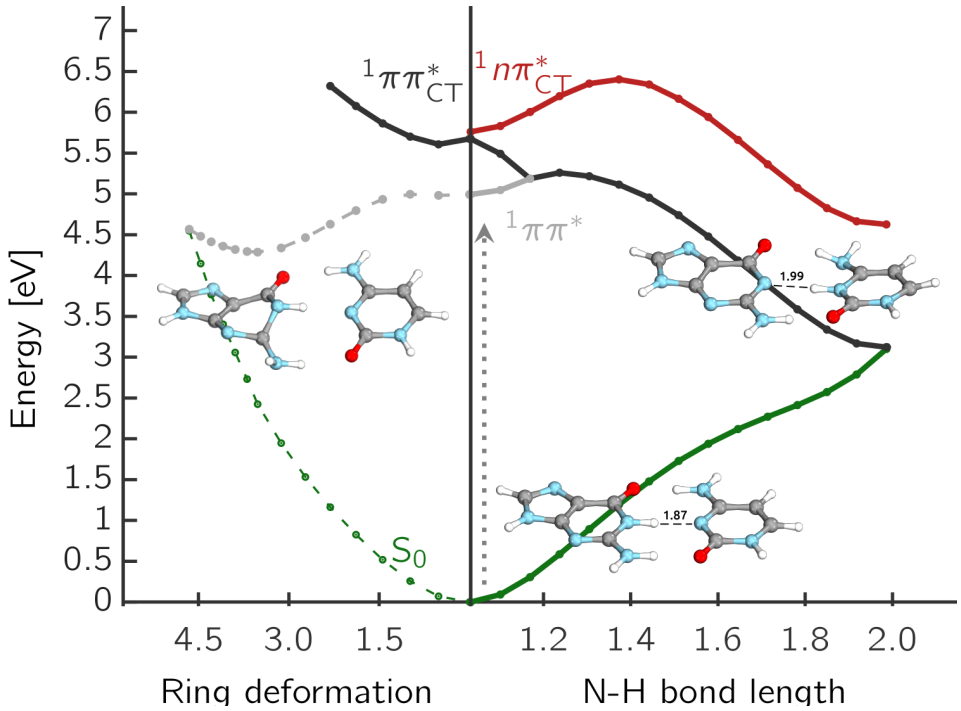

Figure 12. Comparison of PE profiles obtained by LIIC for photorelaxation along ring deformation (plotted in mass-weighted coordinates in Å · $\sqrt{amu}$) and proton transfer coordinates (in Å). The ground state structure and the corresponding MECP structures are shown.

The PE profiles of the low-lying states between the FC region and the corresponding $S_1(\pi_G\pi_G^*)/S_0$ MECPs, calculated using the SCS-ADC(2) and SCS-MP2/SCS-ADC(2) methods, respectively, are presented along with the S_0 and MECP structures. The S_1/S_0 minimum energy crossing with the LE $^1\pi_G\pi_G^*$ state is associated with puckering of the C2 atom of the purine ring of guanine. This MECP lies 0.28 eV higher in energy than the corresponding minimum on the S_1 PE surface, indicating that it has a sloped topology. However, a similar PE barrier is found near the LE/CT conical intersection for the EDPT process. Unfortunately, we were unable to locate the geometry of this MECP, and the PE barrier is probably overestimated in LIIC. Although it is difficult to assess the relative availability of intermolecular EDPT and intramolecular ring-puckering channels based solely on the analysis of PE profiles, our calculations indicate that both seem to be accessible after the population of the LE $^1\pi_G\pi_G^*$ state.

2.1.2 EDPT in wobble G-C — population of $^1n_G\pi_C^*$ CT state

In the WC G-C, the $^1n\pi^*$ pyrimidine LE state lies higher than in A-U and A-T, but only slightly above the $^1\pi_G\pi_C^*$ CT state (less than 0.1 eV at the SCS-ADC(2)/cc-pVTZ level and about 0.3 eV at the EOM-CCSD(T)/TZVP level[228]). Moreover, this $^1n\pi^*$ state exhibits a partial charge-transfer character that could have an intriguing consequence for the photorelaxation of G-C, as it can contribute to yet another photodeactivation mechanism, which has not been reported before.

Although the $^1n\pi^*$ states contribute similarly to the photodynamics of the three canonical pyrimidine RNA and DNA nucleobases,[176] cytosine was found to be the least prone to photodamage formation in nucleic acid strands.[235] Thus, the lowest $^1n_C\pi_C^*$ state of cytosine may facilitate efficient photorelaxation channels unavailable in the WC A-T and A-U base pairs. The G-C base pair was investigated to verify this hypothesis, focusing on electron transfer processes that could occur on the $^1n_C\pi_C^*$ PE hypersurface through the corresponding state crossings. The calculations started with imposed planar symmetry constraints (C_s point group). In this way, the $^1n\pi^*$ state with a partial CT character was the lowest excited singlet state that belongs to the A″ irreducible representation. In preliminary calculations discussed below, the spin component scaling variants of the MP2 or ACD(2) methods were used only as a reference (cf. Figure 16 and its discussion).

[235] S. Mouret, C. Baudouin, M. Charveron, A. Favier, J. Cadet, and T. Douki, *Proceedings of the National Academy of Sciences*, **2006**, *103*, 13765–13770.

Table 2. Selected vertical excitation energies calculated at the equilibrium geometry of the G-C dimer using ADC(2) and CC2 methods in the cc-pVTZ basis set. Subscripts G and C indicate localization of a given molecular orbital on a particular nucleobase. The oscillator strengths (f) and the weights of CT configurations (Ω_{CT}) are shown for each state.

State / Transition		E_{exc}/[eV]	f	Ω_{CT}
G-C in C_S symmetry – ADC(2) results				
$S_1(A')$	$\pi_G\pi_G^*$ / $\pi_G\pi_C^*$(CT)	4.86	$6.99 \cdot 10^{-2}$	0.215
$S_2(A')$	$\pi_C\pi_C^*$	4.91	$5.65 \cdot 10^{-2}$	0.024
$S_3(A')$	$\pi_G\pi_C^*$ (CT)	5.16	$2.84 \cdot 10^{-2}$	**0.766**
$S_4(A'')$	$n_C\pi_C^*/n_G\pi_C^*$(CT)	5.37	$6.45 \cdot 10^{-4}$	0.169
$S_5(A')$	$\pi_C\pi_C^*$	5.37	0.234	0.033
$S_6(A')$	$\pi_C\pi_C^*$	5.42	0.407	0.011
$S_7(A'')$	$n_G\pi_G^*$	5.58	$2.12 \cdot 10^{-4}$	0.086
$S_8(A'')$	$n_C\pi_C^*$	5.68	$5.07 \cdot 10^{-5}$	0.110
$S_9(A'')$	$n_C\pi_C^*$	6.17	$1.60 \cdot 10^{-6}$	0.060
$S_{10}(A'')$	$n_C\pi_C^*$	6.31	0.001	**0.268**
$S_{11}(A'')$	$n_C\pi_C^*/n_G\pi_C^*$(CT)	6.34	$9.80 \cdot 10^{-5}$	**0.525**
$S_{12}(A'')$	$\pi_G\sigma_G^*$	6.43	$8.80 \cdot 10^{-4}$	0.004
$S_{13}(A')$	$\pi_G\pi_C^*$(CT)	6.46	$1.27 \cdot 10^{-1}$	**0.470**
G-C in C_S symmetry – CC2 results				
$S_1(A')$	$\pi_G\pi_G^*$ / $\pi_G\pi_C^*$(CT)	4.94	$6.17 \cdot 10^{-2}$	**0.278**
$S_2(A')$	$\pi_C\pi_C^*$	5.04	$6.20 \cdot 10^{-2}$	0.010
$S_3(A')$	$\pi_G\pi_C^*$ / $\pi_G\pi_G^*$	5.24	$2.29 \cdot 10^{-2}$	**0.737**
$S_4(A'')$	$n_C\pi_C^*$/ $n_G\pi_C^*$(CT)	5.49	$7.38 \cdot 10^{-4}$	0.169
$S_5(A')$	$\pi_G\pi_G^*$	5.52	0.509	0.006
$S_6(A')$	$\pi_C\pi_C^*$	5.52	0.095	0.022
$S_7(A'')$	$n_C\pi_C^*$	5.77	$3.39 \cdot 10^{-5}$	0.145
$S_8(A'')$	$n_G\pi_G^*$	5.852	$7.48 \cdot 10^{-6}$	0.066
$S_9(A'')$	$n_G\pi_G^*$	6.356	$5.72 \cdot 10^{-4}$	0.027
$S_{10}(A')$	$\pi_G\sigma_G^*$	6.371	$1.26 \cdot 10^{-3}$	0.011
$S_{11}(A'')$	$n_C\pi_C^*$	6.420	$2.85 \cdot 10^{-6}$	0.056
$S_{12}(A')$	$\pi_G\pi_C^*$(CT)	6.50	$6.10 \cdot 10^{-2}$	**0.664**
$S_{13}(A'')$	$n_C\pi_C^*/n_G\pi_C^*$(CT)	6.51	$1.03 \cdot 10^{-4}$	**0.790**

The selected vertical excitation energies calculated for the minimum energy structure of G-C using the ADC(2)/cc-pVTZ method are shown in Table 2. They indicate that the $^1n_C\pi_C^*$ state lies 0.21 eV above the $^1\pi_G\pi_C^*$ CT state and 0.51 eV above the lowest bright state S_1. Transition density analysis shows that the weight of charge transfer configurations for this

state amounts to 0.17, indicating its partial CT character due to the transfer of the electronic density from the carbonyl lone pair of guanine to the antibonding π^* orbital located on cytosine. The ADC(2) results were compared against the CC2 method[236] with the same basis set that produced a qualitatively similar spectrum of low-lying states with CC2 excitation energies shifted systematically by roughly 0.1 eV towards higher values.

Geometry optimization in the lowest ^{1}A″ state that has a partial $n_G\pi_C$ CT character leads to a significant rearrangement of the G-C base pair, resulting in a wobble-shaped structure (shown in the right panel of Figure 13) with the N1-H proton transferred from guanine to the carbonyl oxygen atom of cytosine. The CT character of this state is evident upon inspection of the corresponding hole and particle molecular orbitals presented in Figure 13 below the molecular structure. To further investigate the mechanism of this process, a constrained geometry optimization was performed, with the guanine N1-H bond kept frozen, resulting in the plateau geometry on the now S_1 $^1n_G\pi_C$ CT PE surface. The charge transfer character of this state in the plateau region is substantially enhanced as Ω_{CT} increases to 0.57. The subsequent proton transfer process occurs spontaneously as a result of the mutual displacement of the two nucleobases and the formation of the excited-state complex (exciplex). This geometry is very similar to the G-T wobble base pairing scheme that occurs in A, B and Z-DNA structures[237,238] or G-U in RNA,[239,240] suggesting its structural availability.

The minimum energy structures of S_1 ($n\pi^*$ CT) and S_1 ($\pi\pi^*$ CT) states, optimized using the ADC(2)/cc-pVTZ method, are presented in Figure 13 with the corresponding hole and particle molecular orbitals. It shows that the wobble G-C exciplex is formed by N$\cdots$O interaction and a short hydrogen bond between the guanine N3 atom and the hydroxyl group of protonated cytosine. The latter is due to the interaction of the electron-deficient carbonyl n_O molecular orbital of guanine that shares the electron density with the n_N molecular orbital of cytosine, thus increasing the charge-transfer character of this electronic state. This interaction enables the excited-state proton transfer to the cytosine carbonyl group, forming a hydrogen bond. The short length of the latter (1.57 Å) may indicate its strength. This type of synthon should be further investigated as it may be a structural characteristic that allows proton transfer on

[236] O. Christiansen, H. Koch, and P. Jørgensen, *Chemical Physics Letters*, **1995**, *243*, 409–418.
[237] O. Kennard, *Journal of Biomolecular Structure and Dynamics*, **1985**, *3*, 205–226.
[238] T. Brown, O. Kennard, G. Kneale, and D. Rabinovich, *Nature*, **1985**, *315*, 604–606.
[239] J. E. Ladner, A. Jack, J. D. Robertus, R. S. Brown, D. Rhodes, B. F. Clark, and A. Klug, *Proceedings of the National Academy of Sciences*, **1975**, *72*, 4414–4418.
[240] G. Varani and W. H. McClain, *EMBO reports*, **2000**, *1*, 18–23.

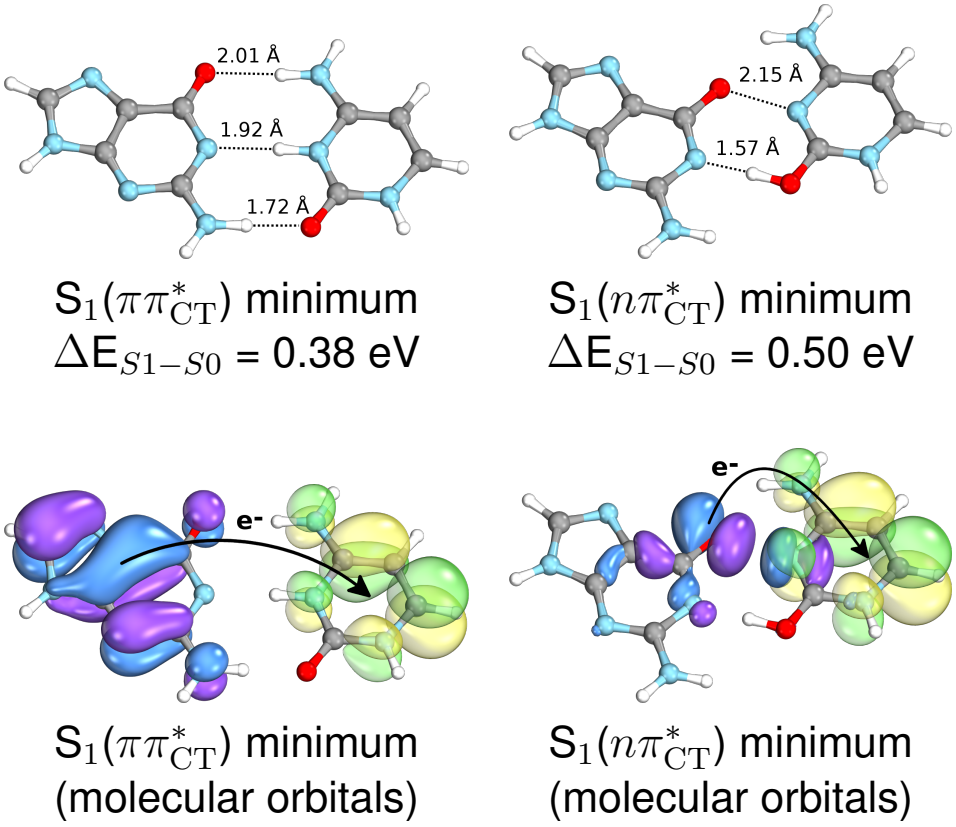

Figure 13. Minimum energy structures at the ${}^1n_G\pi_C$ and ${}^1\pi_G\pi_C$ PE surfaces optimized using the ADC(2)/cc-pVTZ method. The canonical hole (solid blue and violet) and particle (translucent yellow and green) molecular orbitals are shown, with arrows indicating the charge transfer direction.

the ${}^1n\pi^*$ hypersurface and subsequent nonradiative deactivation to the ground state. Indeed, the $\Delta E_{S_1-S_0}$ energy gap at the corresponding excited state minimum amounts to 0.5 eV which indicates that the MECI is almost reached.

The LIIC between the S_0 minimum energy structure, the plateau on the S_1 ${}^1n_G\pi^*_C$ PE surface and the located S_1/S_0 MECP is presented in Figure 14. The EDPT mechanism that occurs on the hypersurface of the ${}^1n\pi^*$ state is likely sequential. On the left side of Figure 14, a process associated with partial charge transfer from the lone pair of carbonyl oxygen of guanine to the π^* orbital localized at cytosine is shown that leads to the formation of the wobble exciplex in a barrier-free manner. The gradual dislocation of nucleobases in the plane results in an increasing CT character of the electronic state, which eventually leads to the complete transfer of an electron once the plateau geometry on the S_1 potential energy surface is reached. This induces the transfer of the guanine N1-H proton to the cytosine carbonyl oxygen atom, and along this coordinate, the S_1/S_0 conical intersection is reached.

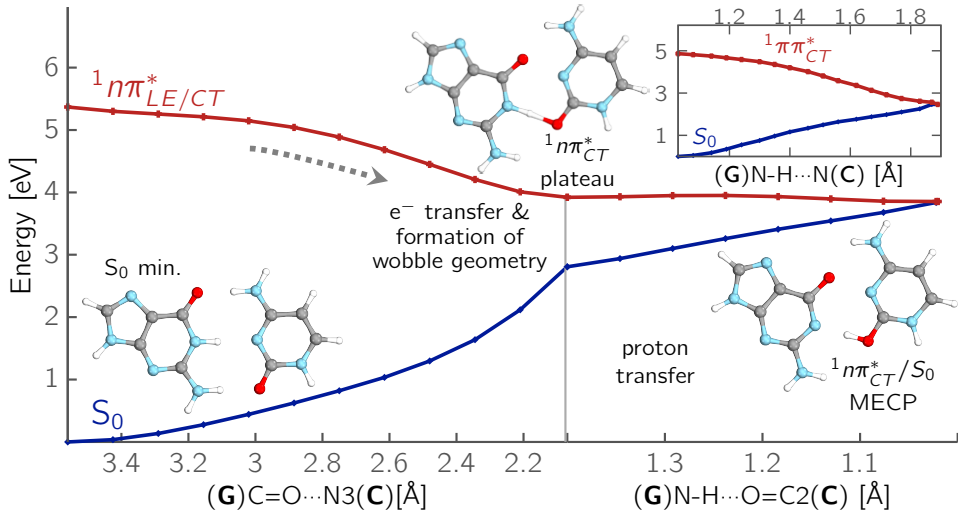

Figure 14. PE cross-sections presenting the EDPT process occurring on the $^1n\pi^*$ state having partial CT character. The left-hand side of the plot shows LIIC along O···N3 distance between FC region and $^1n_G\pi^*_C$ plateau structure optimized with frozen N1-H bond distance. The right-hand side of the graph shows the PE profile for the proton transfer obtained by LIIC between the plateau and S_1/S_0 MECP. The inset shows the EDPT process, which follows the population of $^1\pi_G\pi^*_C$ CT state.

This mechanism is quite different from the EDPT process discussed above, which was mediated by the $^1\pi_G\pi^*_C$ CT state, where only a one-stage mechanism was suggested (PE profile shown in the inset of Figure 14).

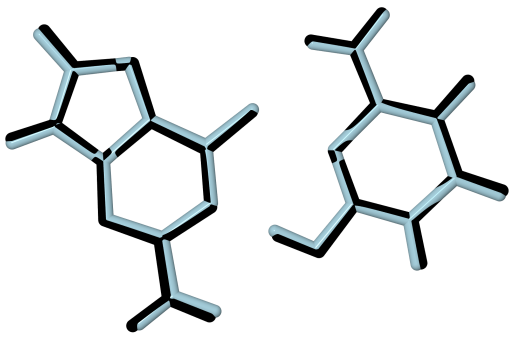

Figure 15. Aligned minima of the S_1 $(n\pi^*_{CT})/S_0$ state crossings located using the ADC(2)/MP2 (navy) and XMS-CASPT2(6,6) (black) methods.

Due to the bias of the ADC(2) method that was discussed earlier the results were tested against the XMS-CASPT2/SA-2-CASSCF(6,6) data calculated using the BAGEL code.[241] The superimposed minimum energy structures for crossing between S_1 $(n_G\pi^*_C)$ and S_0 electronic states calculated at the MP2/ADC(2) and XMS-CASPT2 levels are presented in Figure 15. The excellent alignment of both structures demonstrates that the more approximate ADC(2) approach performed consistently with the XMS-CASPT2 method, and the differences between the corresponding N···O and hydrogen bond distances are negligible.

[241] *BAGEL, Brilliantly Advanced General Electronic-structure Library. http://www.nubakery.org under the GNU General Public License.*

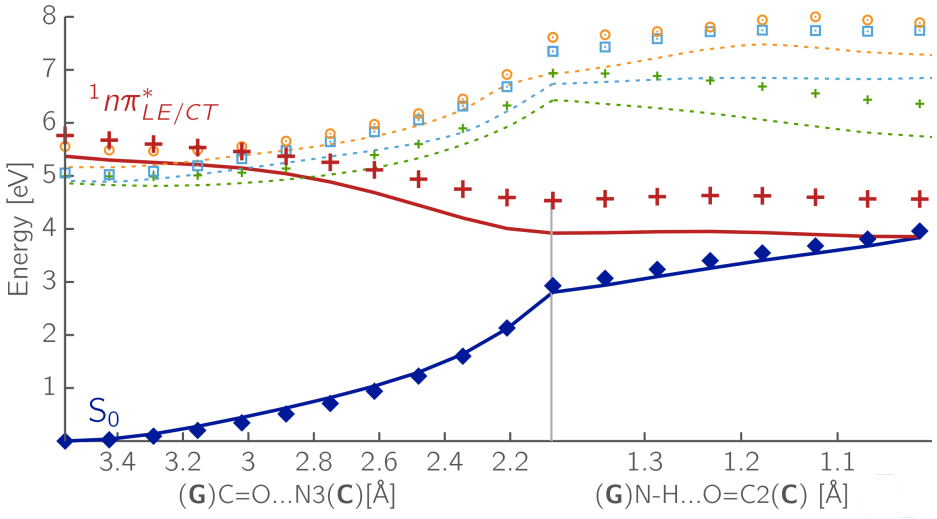

Figure 16. PE surface cuts presenting the EDPT process on the $^1n_G\pi^*_C$ PE surface calculated at the ADC(2)/cc-pVTZ (lines), and SCS-ADC(2)/cc-pVTZ results (symbols). The identical colors mark the corresponding states.

The $\Delta E_{S_1-S_0}$ energy gap in the plateau region calculated using MP2/ADC(2) and XMS-CASPT2 methods amounts to 1.11 eV and 1.55 eV, respectively.

Although the ADC(2) method quite accurately describes the phenomenon studied, previous studies showed that the use of the SCS-variant may essentially eliminate the biases of the ADC(2) method. For this reason, the ADC(2) results were compared with the data calculated using the corresponding spin-component scaled variant. Figure 16 shows that the ADC(2) method systematically underestimates the $^1n_G\pi^*_C$ CT state energies. However, the order of the low-lying states is maintained, and the PE surface cuts are qualitatively similar and lead to the same conclusions. Furthermore, the geometry of $^1n_G\pi^*_C/S_0$ MECP located with the SCS-ADC(2) method does not differ markedly from those obtained with the ADC(2) or XMS-CASPT2 methods.

It can be concluded that the long-lived singlet states of the $n\pi^*$ character widely associated with the photodamage of isolated pyrimidines may, in fact, contribute to efficient nonradiative deactivation via a sequential two-stage EDPT process. It has already been demonstrated that the population of $^1n\pi^*$ state after photoirradiation of cytidine leads to the abstraction of hy-

drogen atom from the sugar moiety and subsequently to photoanomerisation.[242] Furthermore, it has been proposed that the $^1n\pi^*$ state participates in a water splitting reaction in which the nucleobase enables the removal of a hydrogen atom from neighboring water molecules, thus generating hydroxyl radicals.[126,243] Hydrated chromophore radicals could be further approached by OH radicals, consequently leading to the formation of photohydrates, another type of photodamage, which can significantly affect the function of nucleic acids.[126]

The EDPT channel described in this subsection is complementary to the EDPT process on the $^1\pi_G\pi_C^*$ CT hypersurface. According to previous computational studies, similar processes have also been reported on the $^1n\pi^*$ PE surfaces for hydrated cytidine and adenine.[126,243] The experimental results for cytosine and its N1 derivatives in aqueous solution indicate a long-lived species with ~33-39 ps lifetime attributed to a population of the dark $^1n\pi^*$ state.[67,176,244,245] A similar lifetime was determined with the transient infrared absorption spectrum of $[poly(dGdC)]_2$.[246] The latter study identified two long-lived transients, of which one was assigned to the $^1n_N\pi^*$ dark state of the 2'-deoxycytidine. The potential energy surface shown in Figure 14 indicates that this dark $^1n\pi^*$ LE state can easily acquire the charge transfer character and consequently significantly shorten the excitation lifetime through a highly efficient EDPT channel. The results described in this subsection have already been published[247] and were supplemented with molecular dynamics (MD) simulations used to assess the plausibility of the required displacement from the WC to the Wobble base pairing mode under the constraints of the sugar-phosphate backbone. The B-DNA fragments 3'-GGGCCC-5' and 3'-GGHCCC5' were tested by replacing one of the cytosine bases with thymine. In most of the trajectories, a Wobble base pair formed in the first 5 ps. Therefore, we postulated that the timescale of formation of the $^1n\pi^*$ CT excimer is probably much shorter than the lifetime of the $^1n\pi^*$ state in the cytidine monomer, and this process should be readily available.[247]

[242] R. Szabla, J. Campos, J. E. Šponer, J. Šponer, R. W. Góra, and J. D. Sutherland, *Chemical Science*, **2015**, *6*, 2035–2043.

[243] X. Wu, T. N. V. Karsili, and W. Domcke, *ChemPhysChem*, **2016**, *17*, 1298–1304.

[244] P. M. Keane, M. Wojdyla, G. W. Doorley, G. W. Watson, I. P. Clark, G. M. Greetham, A. W. Parker, M. Towrie, J. M. Kelly, and S. J. Quinn, *Journal of the American Chemical Society*, **2011**, *133*, 4212–4215.

[245] C. Ma, C. C.-W. Cheng, C. T.-L. Chan, R. C.-T. Chan, and W.-M. Kwok, *Physical Chemistry Chemical Physics*, **2015**, *17*, 19045–19057.

[246] G. W. Doorley, D. A. McGovern, M. W. George, M. Towrie, A. W. Parker, J. M. Kelly, and S. J. Quinn, *Angewandte Chemie*, **2009**, *121*, 129–133.

[247] K. E. Szkaradek, P. Stadlbauer, J. Šponer, R. W. Góra, and R. Szabla, "UV-induced hydrogen transfer in DNA base pairs promoted by dark nπ^* states", *Chemical Communications* **2020**, *56*, 201–204. DOI: 10.1039/C9CC06180K.

2.1.3 Relaxation mechanisms of A-T/A-U base pairs

In the case of the A-T and A-U base pairs, forming a wobble exciplex interaction that facilitates the subsequent proton transfer is impossible because of a different hydrogen-bonding pattern. It may be one of the reasons why both thymine and uracil are more vulnerable to photodamage than cytosine in the nucleic acid duplex.

As discussed in Section 1.2.2 on page 19, the availability of the EDPT mechanism in the $^1\pi_A\pi_T^*$ CT state for the A-T base pair is also debatable. Although the results of computational studies indicate that such a process could be available in WC A-T,[15,91,114] its experimental verification was obscured due to the different equilibrium geometry assumed by the A-T complex in the gas phase.[115] The results of femtosecond pump-probe spectroscopy of the A-T base pairs in the gas phase indicate an additional time constant of about 40 ps that was tentatively assigned to an intermolecular process, possibly involving conversion via the $^1\pi\pi^*$ CT state through proton transfer. However, the results of transient electronic and vibrational absorption spectroscopies of the substituted A-T base pair indicate the predominance of monomer-like excited state dynamics.[115] This conclusion is also supported by the results of a recent computational study of the ultrafast dynamics of the photoexcited A-T base pair.[116] Therefore, excitation decay through the EDPT channel in A-T seems unlikely or of secondary importance.[50,93,115,116]

Considering experimental evidence that photorelaxation via the EDPT channel is available in adenine dimer,[50] it is worth investigating whether the processes involving excited states of pyrimidines are an obstacle to effective relaxation by proton exchange along hydrogen bonds in base pairs. As can be concluded from several studies,[122–125] the RNA environment can change the photostability mechanisms of the A-U canonical base pair. The isolated WC A-T and A-U base pairs have very similar electronic states spectra (see Figure 24 discussed later). However, a recent study by Chan et al.[122] shows that in the polymeric $r(A)_n{\cdot}r(U)_n$ RNA helical duplex there are strong indications of the EDPT decay channel involving H-bonded A-U base pairs with a relatively short timescale of 2.9 ps, which is virtually identical to that reported by Röttger et al.[13] for the G-C WC base pair. This is rather unexpected considering that a corresponding channel seems inaccessible in both the gas phase A-T and the double-stranded $d(A)_n{\cdot}d(T)_n$ duplex.[94]

Consequently, it is interesting to investigate the EDPT process in the WC A-U and A-T base pairs relative to the intramonomer radiationless deactivation mechanisms involving nucleobases within these dimers. The calculations started with optimization of the minima on the S_1 PE surfaces for A-T and A-U using the SCS-ADC(2)/cc-pVTZ method, initiated with the

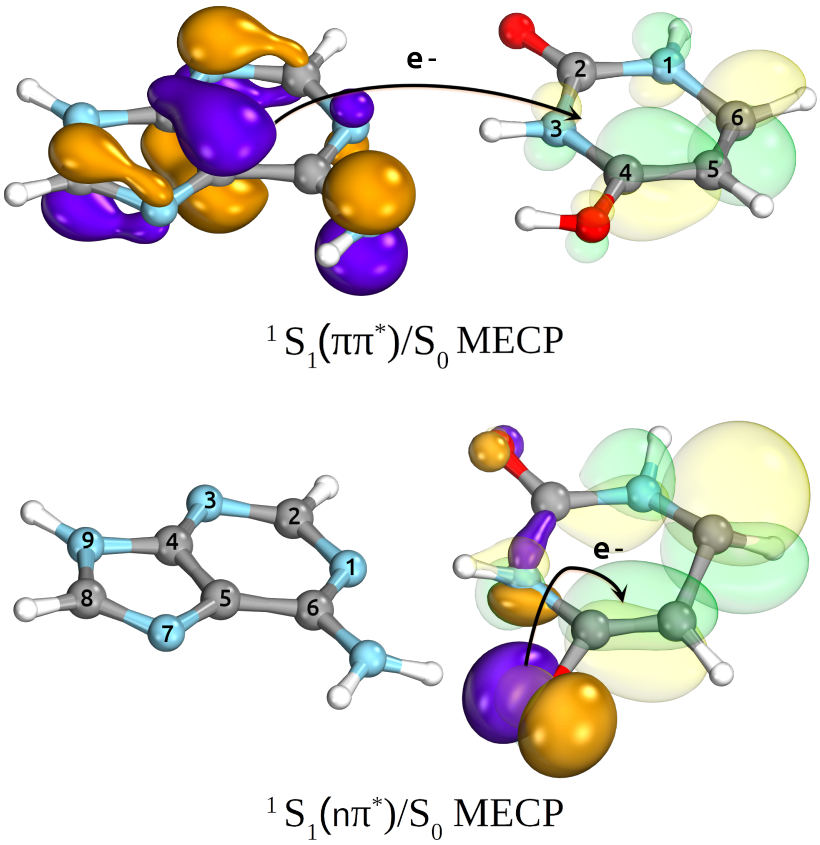

Figure 17. Structures of the $^1\pi_A\pi_U^*/S_0$ and $^1n_U\pi_U^*/S_0$ minimum energy crossing points located using SCS-MP2/SCS-ADC(2)/cc-pVTZ method for A-U. Occupied (solid purple and orange) and virtual (translucent green and yellow) molecular orbitals for the leading amplitudes are shown indicating the orbital character of the corresponding S_1 state.

forced transfer of a proton from adenine to thymine or uracil. The S_1/S_0 energy gaps dropped below 1 eV at the located S_1 minima; therefore, these geometries provided an excellent starting point to determine the minimum energy crossing points (MECPs) between the S_1 and S_0 PE surfaces. Considering that the $^1n\pi^*$ dark LE state located on the pyrimidine moiety is the lowest-lying singlet state for the A-U and A-T systems, the subsequent MECP optimization was performed in search of the photorelaxation channel on the $^1n\pi^*$ LE hypersurface.

A comparison of $^1\pi_A\pi_U^*/S_0$ and $^1n_U\pi_U^*/S_0$ MECPs found on the S_1 potential energy surface of the A-U base pair is presented in Figure 17. The former, shown in the top panel, corresponds to the EDPT channel. The amino hydrogen transfer that follows the $\pi_U^* \leftarrow \pi_A$ CT transition stabilizes the structure, and the most noticeable difference in geometry is the elongation of the C4-O bond of U by 0.14 Å due to keto-enol tautomerization and the change in dihedral angle $\delta_{H_5-C_5-C_6-H_6}$ by almost 20°. In the latter intramolecular $^1n_U\pi_U^*/S_0$ conical intersection depicted in the lower panel, the WC A-U base pair undergoes local structural changes within

the uracil molecule similar to those reported for S_1/S_0 of isolated uracil by Matsika[83] or CI_1 and CI_3 conical intersections of isolated thymine reported by Perun et al.[73] Compared to the S_0 minimum energy structure in the Franck-Condon region, this MECP shows pyramidalization of the pyrimidine ring atoms N3 and C6. Despite some similarities, the observed structural changes in the base pair are not as pronounced as in bare nucleobases, presumably due to the stabilization provided by the complementary base.

Further investigation included LIIC between three stationary points: S_0 and S_1 minimum energy structures and S_1/S_0 MECP using MP2/ADC(2) methodology. The PE cuts obtained were further tested against the SCS variants of MP2 and ADC(2) as well as the state-averaged n-electron valence perturbation method (SA-NEVPT2) assuming the same interpolated geometries. The complete active space in NEVPT2 calculations included 10 electrons correlated in 8 orbitals (3 occupied π, 2 occupied n and 3 virtual π^*).

As in the case of G-C, the ADC(2) method systematically underestimates the energies of excited $^1n\pi^*$ states but returns reliable energies of the $^1\pi\pi^*$ states that agree well with the NEVPT2 results. It is well documented that hydrogen bonding destabilizes the $^1n\pi^*$ states in WC base pairs,[162,229] and their description is more demanding than the $^1\pi\pi^*$ states. Note that the SCS correction does not significantly affect the relative energies of the ground state. It has already been indicated that the dispersion interaction is substantial in the A-T system[248,249] and is overestimated at the MP2 level, which is to some extent corrected when the SCS-MP2 variant is used. The results of SCS-MP2/SCS-ADC(2) calculations will be further considered, as they generally better reflect the potential energy profiles in the ground and excited states of the base pairs.

The potential energy profiles of the low-lying electronic state for the canonical A-U are shown in Figure 18. There are two competing mechanisms that can lead to internal conversion to the ground state. On the right side of the plot, the potential energy cuts along the amino N-H distance indicate an efficient decay path through LE/CT and CT/S_0 crossings via EDPT process. Interestingly, the two lowest-lying locally excited states, namely dark $^1n\pi^*$ and bright $^1\pi\pi^*$ are nearly degenerate in the FC region and along a few first steps of interpolation at the SCS-ADC(2) level. NEVPT2 results also show a close proximity of these states, which indicates a possibility of internal conversion from the bright to the dark $^1n\pi^*$

[229] Z. Benda and P. G. Szalay, *Physical Chemistry Chemical Physics*, **2016**, *18*, 23596–23606.
[248] S. M. Cybulski and M. L. Lytle, *The Journal of Chemical Physics*, **2007**, *127*, 141102–141102–4.
[249] P. R. Horn, Y. Mao, and M. Head-Gordon, *Physical Chemistry Chemical Physics*, **2016**, *18*, 23067–23079.

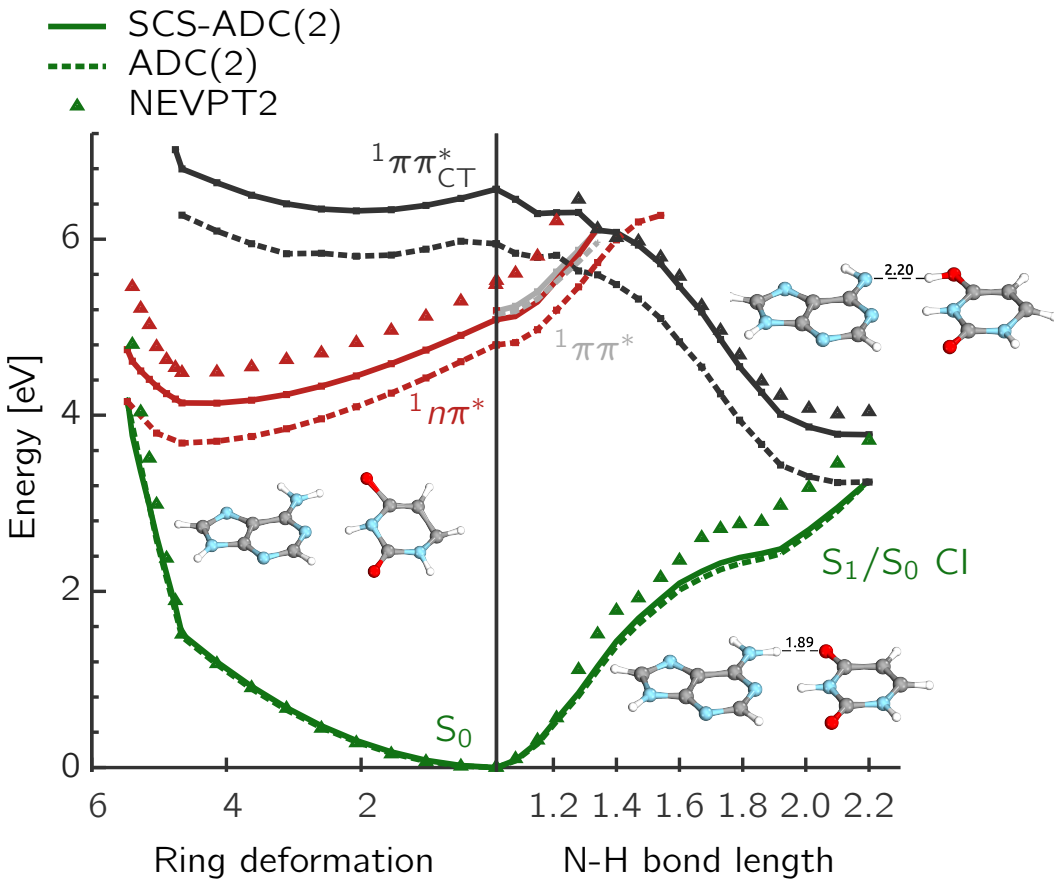

Figure 18. Selected mechanism of nonradiative deactivation of photoexcited A-U. On the right PE cut along the amino N-H transfer shows EDPT via LE/CT and CT/S_0 and on the left relaxation through U puckering on the $^1n\pi^*$ surface is schematically presented with respect to the interpolated ring-puckering plotted in mass-weighted Cartesian coordinates in Å · $\sqrt{amu}$.

state. Although both LE states cross with the dark $^1\pi_A\pi^*_U$ CT state ($^1\pi\pi^*_{CT}$), these CoIs have a sloped topology, suggesting that the EDPT relaxation channel becomes operational at higher excitation energies. Thus, it may not be the most plausible and effective decay path of the excited state in A-U.

The locally excited $^1n\pi^*$ state lies 0.1 eV below the bright state of $^1\pi\pi^*$ character in the FC region. Thus, after photoexcitation to the bright state, there is the opportunity to cross with the lower lying $^1n\pi^*$ in a barrierless manner and trigger the competing deactivation mechanism presented on the left side of the figure. In this scenario, the system evolves on the hypersurface of the S_1 $^1n\pi^*$ state toward the S_1 PE minimum along the pyrimidine ring deformation coordinate and then to the S_1/S_0 MECP. The latter lies 0.86 eV above the S_1 minimum and has a sloped topology; however, considering that the energy of the bright state in the FC region lies above this MECP, internal conversion through this channel could be

possible. On the other hand, the population of the $^1n\pi^*$ state could lead to population trapping and possibly ISC to a triplet manifold. The credibility of $S_1 \rightarrow T_2$ ISC is supported by the change in the molecular orbital character of the initial and final states and a substantial spin-orbit coupling between them (see further analysis in the text). According to the SCS-ADC(2) calculations, the S_1 $^1n\pi^*$ and T_2 $^3\pi\pi^*$ states at the minimum of S_1 PES are nearly degenerate (cf. Table 3).Geometry optimization using the SCS-ADC(2) method on the T_2 PE surface leads to the S_1/T_2 states crossing at 4.12 eV. Thus, considering the steeply sloped character of the corresponding S_1/S_0 MECP, the population of the S_1 state could decay through ISC to the T_2 state and subsequent T_2/T_1 CoI.

Table 3. Selected excitation energies calculated at the respective minimum-energy geometries of the first excited $^1n_U\pi_U^*$ state of A-U dimer using the SCS-ADC(2)/cc-pVTZ and ωB97X-D3/def2-SVP methods (in parentheses, excitation energies obtained using the ωB97X-V/def2-SVP method are shown). Subscripts A and U indicate the localization of a given molecular orbital on a particular nucleobase.

State / Transition		E_{exc}/[eV]	f	State / Transition		E_{exc}/[eV]	f
ωB97X-D3/def2-SVP				SCS-ADC(2)/cc-pVTZ			
T_1	$^3\pi_U\pi_U^*$	3.23 (3.28)	0.00	T_1	$^3n_U\pi_U^*$	2.77	0.000
T_2	$^3n_U\pi_U^*$	3.83 (3.89)	0.00	S_1	$^1n_U\pi_U^*$	2.83	$1.47 \cdot 10^{-4}$
T_3	$^3\pi_A\pi_A^*$	3.98 (4.03)	0.00	T_2	$^3\pi_U\pi_U^*$	2.90	0.000
S_1	$^1n_U\pi_U^*$	4.21 (4.30)	$5.98 \cdot 10^{-4}$	S_2	$^1\pi_U\pi_U^*$	3.79	0.179
T_4	$^3\pi_U\pi_U^*$	4.37 (4.46)	0.00	T_3	$^3\pi_U\pi_U^*$	4.14	0.000
S_2	$^1\pi_U\pi_U^*$	5.44 (5.52)	0.25	T_4	$^3\pi_A\pi_A^*$	4.19	0.000

The transition rates of radiative and nonradiative processes were calculated using MOMAP software.[224] Due to the availability of nonadiabatic coupling terms, these calculations were performed using the TD-DFT approach, assuming ωB97X-D3 exchange-correlation functional and def2-SVP basis set available in the QChem 6.1 package.[225]

Thus, the minimum energy structure of the A-U WC base pair in the first excited state of $^1n\pi^*$ character was also determined using the ωB97X-D3/def2-SVP method. A comparison of the characters of the low-lying states at this geometry shows different orderings of excited states in the TD-DFT and SCS-ADC(2) results. These are shown in Table 3 and reveal that the order of the T_1 and T_2 states is reversed in the TD-DFT calculations, and both states lie below the S_1 state. The minimum energy structures of the S_1 $^1n_U\pi_U^*$ state and the T_1 $^3\pi_U\pi_U^*$ (corresponding to the T_2 state in SCS-ADC(2)/cc-pVTZ calculations) obtained using the TD-DFT approach were very similar to those located at the SCS-ADC(2)/cc-pVTZ level,

with RMSD of 0.109 and 0.184, respectively. This and a similar character of the respective excited states justify the use of the TD-DFT approach for the transition-rate calculations.

The SOCC values computed between the $S_1(n\pi^*)$ and $T_1(\pi\pi^*)$ states amount to 30.3 cm^{-1} for both the ωB97X-D3/def2-SVP and ωB97X-V/def2-TZVP methods at the respective S_1 minimum energy geometries. These are similar to the corresponding values obtained at the SCS-ADC(2)/cc-pVTZ S_1 minimum energy geometry (39.0 and 38.8 cm^{-1}, respectively) as well as the SA-CASPT2(12,10)/cc-pVTZ-DK estimate of 58.3 cm^{-1} obtained at the same geometry using RASSI-SO approach implemented in OpenMolcas v22.10 (the active space consisted of 3 n_U, 2 π_A, 1 π_U and 4 virtual orbitals: 2 π_U^* and 2 π_A^*; and the density was averaged over the two lowest-lying states). In fact, the larger magnitudes of these couplings only strengthen our conclusions.

The transition rate between these states amounts to 1.60×10^{10} s^{-1}, which is consistent with the k_{ISC} rate calculated for isolated uracil by Etinski et al. (2.60×10^{10} s^{-1}).[250] The calculated reverse ISC rate k_{RISC} of 3.99×10^{-3} s^{-1} is negligible. The corresponding internal conversion S_1-S_0 k_{IC} rate is an order of magnitude smaller (1.29×10^9 s^{-1}) while the radiative rate of this transition is very small (1.91×10^3 s^{-1}). According to the ωB97X-D3 method, the $T_1(\pi\pi^*)$ state lies 0.98 eV below the $S_1(n\pi^*)$ state. However, the geometries obtained from the optimization of T_1 and S_1 in this methodology correspond to the geometries of T_2 and S_1 obtained using SCS-ADC(2) approach, for which the energy gap in the calculated potential energy profile is smaller than 0.2 eV. In addition, the SA-2-CASPT2(12,10)/cc-pVTZ-DK calculations indicate a much more substantial spin-orbit coupling between these states. These results imply that the intersystem crossing to a triplet manifold may be of great importance in WC A-U, especially since the $S_1(n\pi^*)\longrightarrow S_0$ k_{IC} rate is an order of magnitude lower than the k_{ISC} rate calculated using the ωB97X-D3/def2-SVP method. The rates of selected radiative and nonradiative transitions calculated at the ωB97X-D3/def2-SVP level are shown in Table 4.

The suggested process occurring on the $^1n\pi^*$ state hypersurface is similar to that discussed by Böhnke et al.[162] in the WC 2-aminopurine-thymine dimer. In their findings based on time-resolved fluorescence and transient vibrational absorption spectroscopy supplemented with CC2 calculations, the authors conclude that one of the decay paths after excitation to $^1\pi\pi^*$ proceeds to a short-lived (<100 fs) intermediate state of $^1n\pi^*$ character, the population of which is partially recovered to the electronic ground state and partially transferred via ISC to the $^3\pi\pi^*$ state.[162]

[250] M. Etinski, *Journal of the Serbian Chemical Society*, **2011**, *76*, 1649–1660.

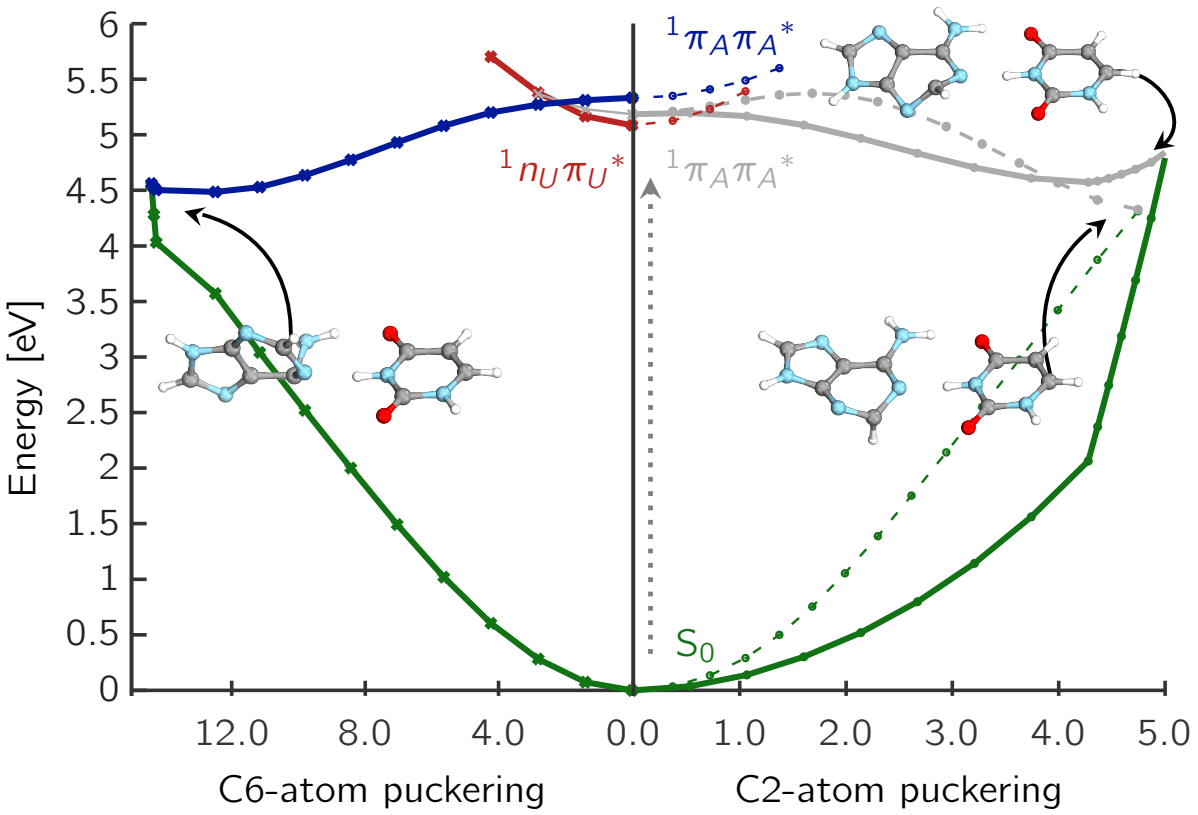

Figure 19. Potential energy cuts presenting radiationless deactivation mechanisms associated with the ring-puckering deformation of adenine in the A-U base pair. The relative energies in eV are plotted against the respective interpolated ring-puckering mass-weighted coordinates in Å · $\sqrt{amu}$.

At this point, it is relevant to investigate whether deactivation by puckering of the purine ring on the $^1\pi\pi^*$ PE surface is plausible in A-U and A-T. A similar process associated with purine C2-puckering was discussed earlier for G-C. A total of three MECP structures were located on the S_1 $^1\pi_A\pi_A^*$ PES, corresponding to LE transitions of adenine. All these structures correspond to puckering of the adenine ring at the position of the C2 or C6 atoms distorted out of plane (denoted as A C6-oop or C2-oop in the schemes in Figures 20-21).

Table 4. Rates of selected nonradiative (IC or ISC) and radiative transitions computed using the TVCF approach based on ωB97X-D3/def2-SVP data.

	k_{IC}/k_{ISC} $[\frac{1}{s}]$	Lifetime [s]	k_r $[\frac{1}{s}]$	Lifetime [s]
S_0/S_1	$1.29 \cdot 10^9$	$7.75 \cdot 10^{-10}$	$1.91 \cdot 10^3$	$5.25 \cdot 10^{-4}$
S_0/T_1	$1.61 \cdot 10^8$	$6.21 \cdot 10^{-9}$	$9.29 \cdot 10^{-2}$	10.7
S_1/T_1	$1.60 \cdot 10^{10}$	$6.23 \cdot 10^{-11}$	$9.31 \cdot 10^{-4}$	$1.07 \cdot 10^3$
S_1/T_2	$6.64 \cdot 10^7$	$1.51 \cdot 10^{-8}$	$7.73 \cdot 10^{-5}$	$1.29 \cdot 10^4$

The first two MECPs shown on the right part of Figure 19 correspond to different modes of C2 atom distortion, either above or below the plane of purine rings. The corresponding $^1\pi_A\pi_A^*/S_0$ MECPs have been located and are shown together with the interpolated PE cuts from the FC region with respect to the mass-weighted displacement of the Cartesian coordinates. Both MECPs are easily accessible from the FC region, even though the LIIC path plotted with a dashed line shows a negligible PE barrier of 0.04 eV. The latter is likely an artifact of the interpolation procedure and is probably overestimated. The corresponding $^1\pi_A\pi_A^*$ LE/S_0 MECP is shown as the bottom right structure in Figure 19. It is characterized by an out-of-plane distortion of the C2 atom with a slight elongation of the C2-N3 and C2-N1 bonds of adenine, by 0.09 Åand 0.08 Å, respectively. The dihedral angle $\delta_{N_1C_2N_3C_4}$ of adenine changes from 0° to 63.4° with respect to the structure of the ground state. This MECP is located 4.33 eV above the ground state, which is 0.49 eV lower than the other C2-puckered MECP and is easily accessible from the FC region. However, even this MECP is located above the $^1\pi_A\pi_U^*$ CT/S_0 state crossing. The alternative higher-lying C2-puckered MECP geometry is presented in the top right of Figure 19. It shows a significant displacement along the C2-N3 bond of adenine (elongated by 0.17 Å) and the dihedral angle $\delta_{N_1C_2N_3C_4}$ that changed from 0° to −81.6°, compared to the equilibrium geometry. This MECP features a slightly sloped topography; however, the energy barrier from the corresponding S_1 PE minimum to S_1/S_0 MECP amounts only to 0.28 eV, which is roughly a third of that found for $^1n\pi^*/S_0$.

Similarly as in the case of isolated adenine (see 1.2.1 on page 10) the C6-puckered MECP was also located in the A-T and A-U base pairs. The corresponding structure and interpolated PE profile are shown in the left of Figure 19. This MECP is characterized by the elongation of the adenine N1-C6 bond by 0.13Å and the change in the dihedral angle $\delta_{C_2N_1C_6C_5}$ from 0° to −42.2°. This MECP structure features out-of-plane distortion of the -NH_2 group and is the most distorted of all puckered structures, as indicated by the mass-weighted displacement of the Cartesian coordinates. However, since the A-U dimer has only two hydrogen bonds when the NH_2 group bends, the complementary uracil twists to preserve the interaction between the functional groups of the complementary nucleobases (the dihedral angle between the N9-C8 bond of adenine and the N1-C2 bond of uracil, $\delta_{(A)N_9C_8-N_1C_2(U)}$, changes from 0° to 88.8°). As with the previously discussed C2-puckering paths, the C6-puckering mechanism appears to be easily accessible from the FC region. The corresponding MECP has a peaked topography. This makes it easily accessible, even though it lies 0.23 eV higher than the MECP associated with puckering of the C2 atom.

According to the findings of Jouybari et al.[116] we also attempted to find the photorelaxation mechanisms that may occur on the $\pi\pi^*$ PE hypersurfaces of T and U. Unfortunately, the MECPs $\pi_U\pi_U^*/S_0$ were localized at 6.3 eV in the potential energy profiles of A-U and A-T. This fact, combined with a significant admixture of the $\pi_U\pi_U^*$ and $\pi_A\pi_A^*$ states caught in the FC region, indicates the inaccessibility of this deactivation mechanism in these dimers. Furthermore, optimization of the geometry of the $^1n_A\pi_A^*$ excited state for A-U and A-T leads to the $^1\pi_A\pi_A^*$ minimum, even though we were able to locate the corresponding $^1n_A\pi_A^*$ minimum energy structure of isolated adenine. This may be a consequence of the formation of hydrogen bonds involving the N1 lone electron pair, which results in an increased energy of $n\pi^*$ transitions.[229] All of this indicates that the discussed minima are inaccessible from the FC region of A-U/A-T, particularly since these states lie higher than those previously discussed (cf. Table 1).

The mechanisms discussed thus far relate to the A-U WC base pair. The results obtained for A-T are qualitatively similar. The relevant critical points are schematically plotted for both base pairs in Figures 20-21, showing the relative energies of the excited-state minima and MECPs. The differences in these data between A-U and A-T are within 0.01-0.05 eV. In general, all PE cuts indicate that $^1n_U\pi_U^*/S_0$ or $^1n_T\pi_T^*/S_0$ as well as C2- and C6-puckered $^1\pi_A\pi_A^*/S_0$ MECPs should be accessible from the FC region in the gas phase. C6 and C2-puckered adenine MECPs with peaked topography appear to be slightly more plausible than the C2-puckered adenine and N3/C6 puckered uracil or thymine $^1n\pi^*/S_0$ MECPs with a sloped topography. Furthermore, the close proximity of two $^1\pi_A\pi_A^*$ bright states (shown in blue and gray lines) strengthens the possibility of nonradiative deactivation by puckering of adenine. However, it should be underlined that experimental studies of A-T photodynamics conclude that it is dominated by intramonomer processes, involving a population of $^1n\pi^*$ states.[172,251] Indeed, there is no barrier on $^1n\pi^*$ A/U PE surfaces between the FC region and S_1 minimum. On the other hand, the corresponding LE/S_0 MECPs have a strongly sloped topography with a substantial barrier of 0.86-0.87 eV. These findings, as well as the near-degeneracy of the S_1 and T_2 states that are strongly coupled through spin-orbit interaction, imply an efficient ISC to triplet manifold.

The strong distortion from the planar structure of all intramolecular MECPs raises the question of the plausibility of these paths in DNA and RNA structures. To explore whether

[251] C. Canuel, M. Mons, F. Piuzzi, B. Tardivel, I. Dimicoli, and M. Elhanine, *The Journal of Chemical Physics*, **2005**, *122*, 074316.

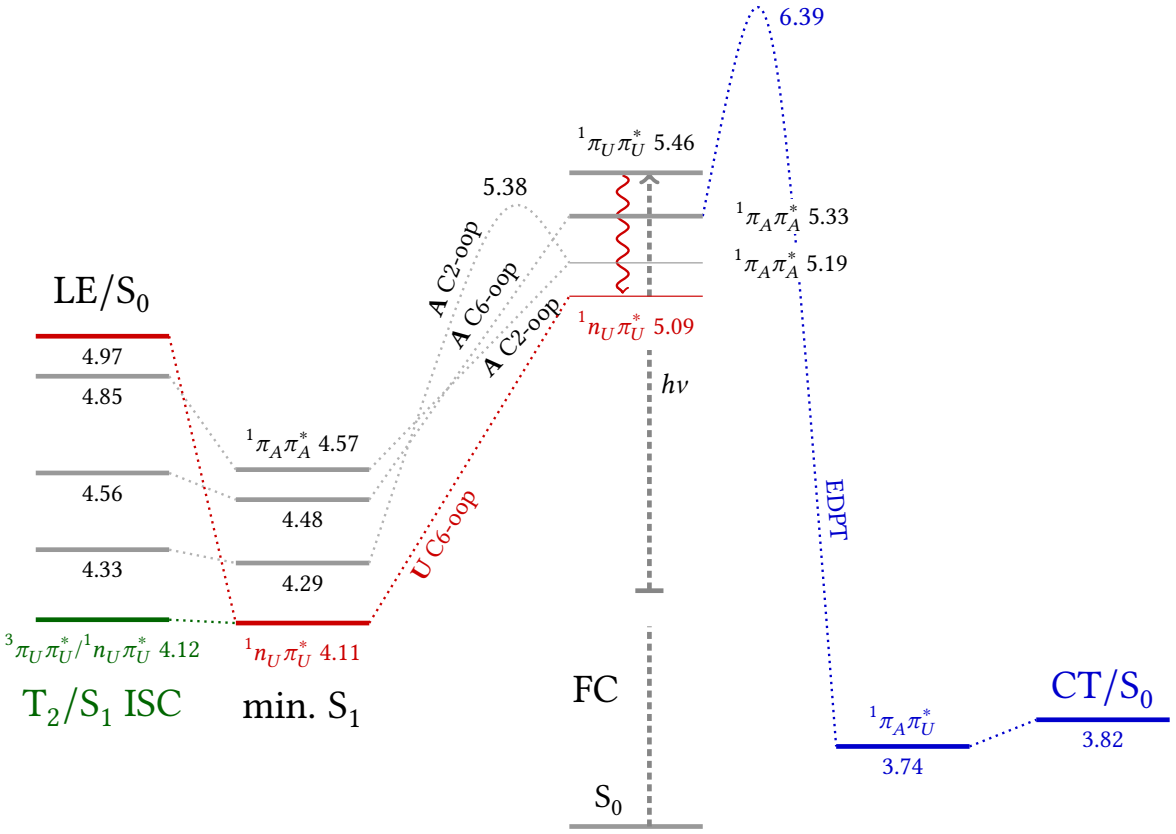

Figure 20. Schematic representation of the investigated radiationless deactivation mechanisms in the A-U base pair. Values show energies relative to the ground state in eV. Ring-puckering paths are labeled with puckered base and the most distorted ring atom, e.g. U C6-oop indicates uracil atom C6 distorted out of plane.

the puckered structures are accessible in DNA and RNA, we performed a search of the experimental B-DNA structures. Taking into account the structural deformations of puckered MECPs, the propeller twist parameter seems to most reliably reflect the change of mutual orientation of the nucleobases. The average value of this parameter for A-T in the experimental results collected from the nucleic acid database[252,253] is 22.9°, while the BIGNASim molecular dynamics simulations database,[254] employing Nucleic Acids Flexibility Server,[255] shows that this parameter can change up to 53.6°. The data presented relate only to a bare B-DNA duplex

[252] H. M. Berman, W. K. Olson, D. L. Beveridge, J. Westbrook, A. Gelbin, T. Demeny, S.-H. Hsieh, A. Srinivasan, and B. Schneider, *Biophysical Journal*, **1992**, *63*, 751.
[253] B. Coimbatore Narayanan, J. Westbrook, S. Ghosh, A. I. Petrov, B. Sweeney, C. L. Zirbel, N. B. Leontis, and H. M. Berman, *Nucleic Acids Research*, **2014**, *42*, D114–D122.
[254] A. Hospital, P. Andrio, C. Cugnasco, L. Codo, Y. Becerra, P. D. Dans, F. Battistini, J. Torres, R. Goni, M. Orozco, et al., *Nucleic Acids Research*, **2016**, *44*, D272–D278.
[255] A. Hospital, I. Faustino, R. Collepardo-Guevara, C. Gonzalez, J. L. Gelpí, and M. Orozco, *Nucleic Acids Research*, **2013**, *41*, W47–W55.

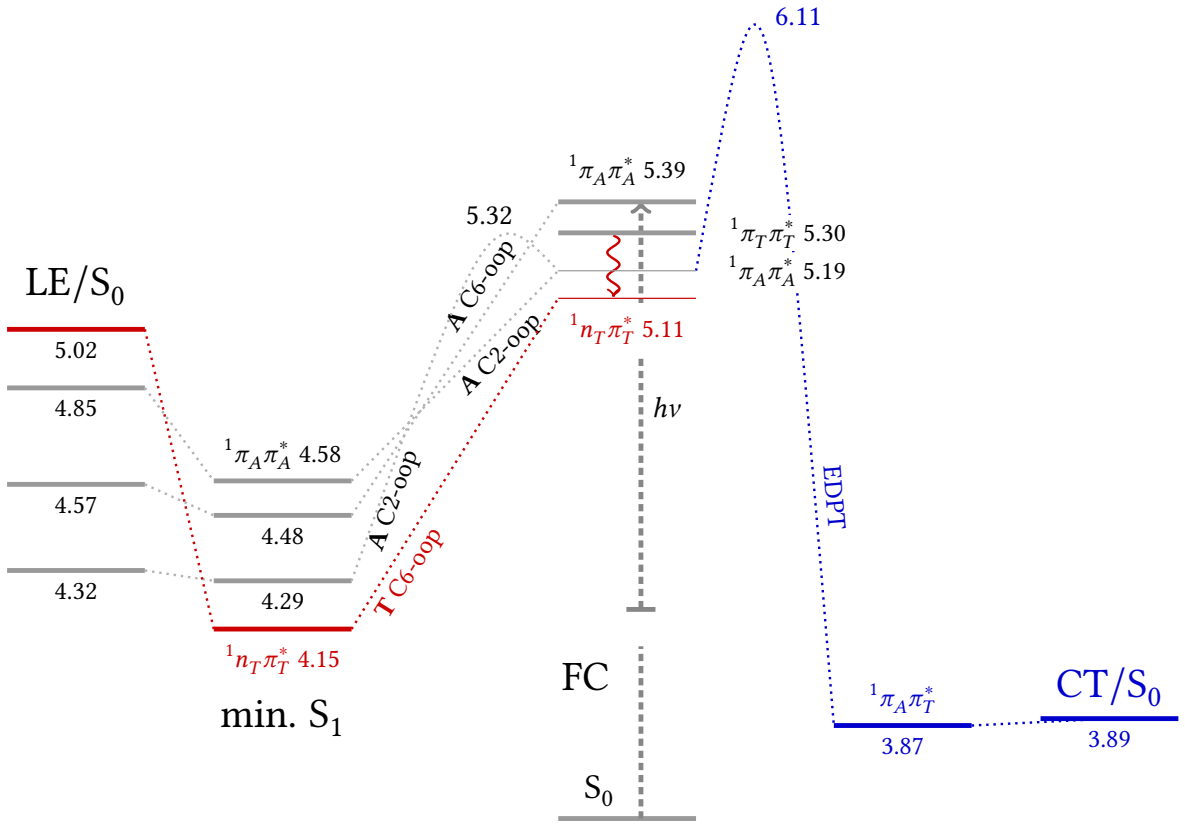

Figure 21. Schematic representation of the investigated radiationless deactivation mechanisms in the A-T base pair. Values show energies relative to the ground state in eV. Ring-puckering paths are labeled with puckered base and the most distorted ring atom, e.g. T C6-oop indicates thymine atom C6 distorted out of plane.

with at least two A-T base pairs in a sequence. The average and extreme values of the propeller twist parameter could be compared to the values of the dihedral angle $\delta_{(A)N_9C_8-C_2N_1(U)}$ which amounts to 21.8° and 5.1° for the two C2-oop(A) MECPs, and 88.8° and 31.4° for the C6-oop(A) and C6-oop(U) MECPs, respectively.

2.2 Investigation of alternative base pairs

In the previous section, it has been shown that the EDPT process is one of the key nonradiative relaxation channels in canonical base pairs. Even though the experimental data support population decay through this channel only for G-C, the lack of experimental evidence in the case of A-T is most likely due to a different binding mode of A-T in the gas phase. Therefore,

its availability could be one of the criteria for selecting particular nucleobases during prebiotic evolution. The question worth investigating is thus whether it is also accessible in selected WC-like pairs of alternative (non-canonical) nucleobases. Since ultrafast radiationless decay reduces the likelihood of photodegradation of nucleobases and their aggregates, **the working hypothesis is that the rate of nonradiative photorelaxation would be highest among a set of structures closely related to canonical forms**.

The nonbiological base pairs chosen to investigate are relevant in the context of the photochemistry of nucleic acids and their hypothetical prebiotic ancestors. The particular choice of complexes also allows one to examine how specific chemical modifications change the photochemistry of chromophores, thus continuing the broad discussion on this topic.[256] The set contains alternative nucleobase pairs consisting of bases with purine oxidized at the C8 position, namely: 8-oxo-guanine (**8-oxoG** or in short oxoG), 8-oxo-adenine (**8-oxoA** or oxoA) and 8-oxo-hypoxanthine (**8-oxoH** or oxoH); those with the modified exocyclic group at the C2 position: hypoxanthine (**H**), 2,6-diaminopurine (**DAP**) and xanthine (**X**); barbituric acid (**B**), that is, 6-hydroxyuracil; isomers of canonical nucleobases: isoguanine and isocytosine (**iG** and **iC**) and pyrimidine analogs of purines: 2,4,6-triaminopyrimidine (**TAP**) and melamine (**M**) with canonical nucleobases that constitute the reference.

The molecular structures of the studied complexes are shown schematically in Figure 22 along with selected geometric parameters. Equilibrium geometries on the ground state PE surfaces were located using the MP2/cc-pVTZ method without any symmetry constraints. The optimized ground-state geometries generally have planar or nearly planar symmetry with minor deviations of amino and methyl groups and form WC-type pairs by relatively strong double or triple hydrogen bonds. The hydrogen bond distance differences for complexes with the same H-bonding motif (e.g. A-T, A-U, A-B, A-H, and H-C) are smaller than 0.1 Å.

[256] C. E. Crespo-Hernández, L. Martínez-Fernández, C. Rauer, C. Reichardt, S. Mai, M. Pollum, P. Marquetand, L. González, and I. Corral, *Journal of the American Chemical Society*, **2015**, *137*, 4368–4381.

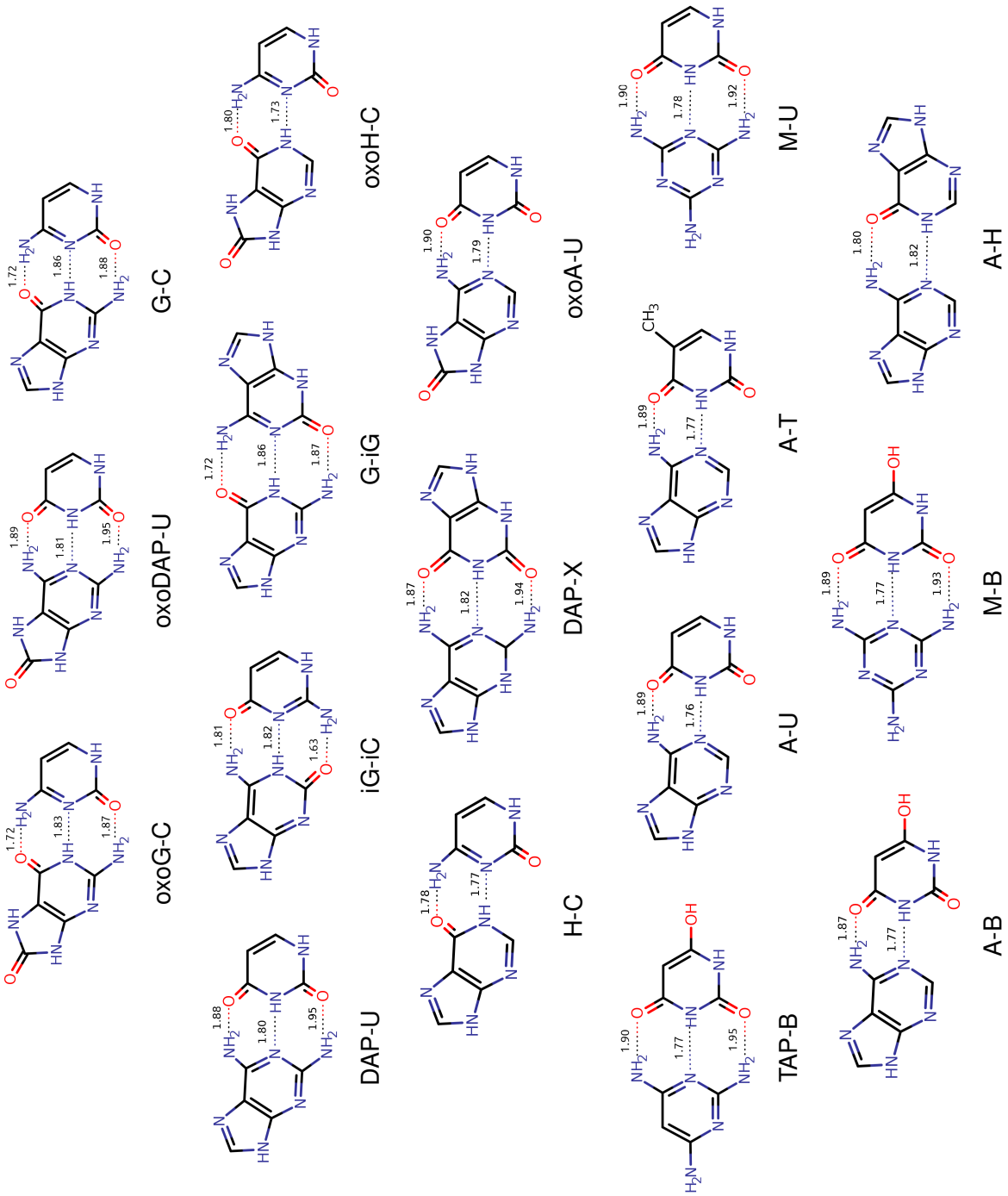

Figure 22. The structures of 17 canonical and alternative nucleobase pairs studied that were optimized using the MP2/cc-pVTZ method. Selected distances are given in Å.

2.2.1 The Franck-Condon region

Relative stability of the base pairs

The studies on the chosen set started by determining the relative stability of canonical and noncanonical base pairs. The interaction energy has been calculated using selected methods implemented in the Gaussian 16 program assuming the counterpoise procedure to correct for the basis set superposition error (BSSE).[206]

Table 5. The counterpoise-corrected interaction energies between nucleobases. Acronym (sp) refers to the geometry of the complex optimized using the MP2 method. All values are given in kJ/mol

Base pair	Synthon	MP2/cc-pVTZ	SCS-MP2/ aug-cc-pVTZ	SCS-MP2(sp)/ aug-cc-pVTZ
iG-iC[a]	O ··· H-N	-153.4	-140.4	-143.8
oxoG-C	N-H ··· N	-125.8	-116.7	-118.5
G-C	N-H ··· O	-122.6	-115.8	-115.6
G-iG		-121.9	-114.9	-114.6
oxoH-C	O··· H-N	-98.4	-90.8	-92.4
H-C	N-H ··· N	-95.3	-88.0	-89.8
M-B		-78.8	-70.9	-72.0
M-U	N-H ··· O	-78.3	-70.4	-71.6
TAP-B	N ··· H-N	-75.4	-67.5	-68.8
DAP-U	N-H ··· O	-74.4	-66.7	-67.7
oxoDAP-U		-73.1	-65.8	-66.7
DAP-X		-73.1	-65.8	-66.7
A-H		-71.9	-65.1	-66.1
A-B	N-H ··· O	-64.7	-58.7	-59.7
A-U	N ··· H-N	-64.1	-58.0	-59.1
A-T		-63.6	-57.5	-58.6
oxoA-U		-61.0	-55.3	-56.3

[a] Synthon in the iG-iC complex is, in fact, a mirror image of that specified, corresponding rather to iC-iG.

The interaction energies of the studied complexes calculated using MP2 and SCS-MP2 methods assuming cc-pVTZ and aug-cc-pVTZ basis sets are shown in Table 5. The SCS-MP2/aug-cc-pVTZ interaction energy of the G-C pair bound by three hydrogen bonds amounts to ~116 kJ/mol in contrast to the other two canonical pairs of A-T and A-U connected by two

hydrogen bonds, with the interaction energy roughly half of that (~58 kJ/mol). This 2:1 ratio has been observed in the literature related to ab initio studies on the nature of interaction in these complexes.[257–259] The hydrogen bonding motif is correlated to some extent with the interaction energies; however, it is not necessarily a decisive factor. For instance, the interaction energy in G-C is significantly weaker than that in iG-iC, despite the fact that both complexes have the same H-bonding synthon. It shows that the properties of the monomers, particularly the magnitude and orientation of permanent molecular multipole moments and the polarizability, are equally important. In the case of G-C and iG-iC, analysis of the interaction energy components discussed further indicates that the induction interaction is relatively much stronger in the latter (since the net first-order attraction is, in fact, smaller in iG-iC and the stabilization due to the correlation energy is only slightly larger), which brings the monomers much closer and increases the absolute magnitude of all interaction energy terms due to their asymptotic behavior. Nonetheless, the complexes with three hydrogen bonds are generally stronger than those with two. The only exceptions among the studied set are the H-C and 8-oxoH-C base pairs. The study of Šponer et al.[146] also indicated an essentially lower interaction energy of H-C compared to G-C.

Although the same motif of synthons appears in the corresponding purine-purine and purine-pyrimidine dimers A-H and H-C, the interaction energies of H-C and oxoH-C are notably larger. Presumably, it is due to a much smaller dipole moment of A compared to H (2.5 D vs. 5.2 D) and a less favorable orientation of permanent molecular dipole moments. Particularly since the corresponding isotropic polarizabilities of purines are comparable ($\langle\alpha\rangle$ amounts to 89 a.u. and 96 a.u. for H and A, respectively) while C is the most polarizable among canonical pyrimidine bases ($\langle\alpha\rangle$ = 78 a.u.).[260,i] The latter affects both the attractive forces of induction and dispersion.

The origins of the intermolecular interactions in the complexes studied were analyzed using the HVPT-EDS scheme. We used the custom implementation[261] in the GAMESS software package.[208] The interaction energy decomposition has been performed at the MP2/cc-pVDZ

[257] P. Jurečka, J. Šponer, J. Černỳ, and P. Hobza, *Physical Chemistry Chemical Physics*, **2006**, *8*, 1985–1993.
[258] A. Hesselmann, G. Jansen, and M. Schütz, *Journal of the American Chemical Society*, **2006**, *128*, 11730–11731.
[259] Y. Mo, *Journal of Molecular Modeling*, **2006**, *12*, 665–672.
[260] A. Alparone, *Chemical Physics*, **2013**, *410*, 90–98.
[i] The discussed magnitudes of dipole moments and average polarizability are the MP4/aug-cc-pVDZ values reported by Alparone.[260]
[261] R. W. Góra. *EDS package, revision 2.8.3*. 1998.

level of theory. It yields the total interaction energy at the MP2 level (ΔE^{MP2}) divided into Hartree-Fock (ΔE^{HF}) and the Coulomb electron correlation components ($\epsilon^{(2)}_{MP}$). Further partitioning of these terms along with their description can be found in the Methodology Section 1.4 on page 41.

The selected components of the interaction energy are shown schematically in Figure 23 as the relative contribution to the total interaction energy. The corresponding values of the interaction energy terms are given in Table 6.

The main difference in the origins of interactions can be observed between the dimers that are alternative to the G-C base pair and those that resemble the A-T and A-U base pairs. In the former, induction interactions ($\Delta E^{\mathrm{HF}}_{\mathrm{del}}$) are decisive, as they constitute roughly 85% of the total interaction energy (cf. Figure 23b). This term collectively accounts for interactions of induced multipole moments and the corresponding exchange terms. First-order interactions (ΔE^{HL}) are weakly stabilizing, with the electrostatic attraction slightly larger than the corresponding exchange repulsion. The latter is also unique to the G-C-like base pairs, with relatively small net stabilization as a result of electron correlation effects. The iG-iC base pair shows the strongest interactions, but the origins of interactions are similar to that of 8-oxoG-C, G-C and G-iG. The H-C and 8-oxoH-C base pairs also show a similar nature of interactions. However, having one hydrogen bond less than the other alternatives of G-C makes the overall interaction noticeably weaker. The total Hartree-Fock interaction energy in H-C is nearly twice as large as in other systems with similar synthons (A-H, A-T, and others) because of much larger stabilization from induction interactions.

A significant reduction in the role of inductive interactions can be observed in the remaining systems. $\Delta E^{\mathrm{HF}}_{\mathrm{del}}$ remains the main component, but its relative contribution to ΔE^{MP2} drops in most complexes below 60%. The first-order electrostatic interactions are completely quenched by exchange repulsion, which makes the Heitler-London term repulsive. Simultaneously, the stabilization from electron correlation effects increases in both the absolute magnitude and the relative contribution to the interaction energy. In the base pairs A-T, A-U, and their alternatives, the importance of dispersion, which is invariably stabilizing, increases. Interestingly, in these systems, one base always lacks the carbonyl group and has only electron-donating groups. Base pairs composed of monomers with electron-withdrawing carbonyl and electron-donating amino functional groups show stronger interactions with the first-order electrostatic attraction that prevails over exchange repulsion and with considerable stabilization from electronic density delocalization.

Table 6. The interaction energy components analysis is based on the HVPT-EDS method. The values are given in kJ/mol.

base pair	$\epsilon_{el}^{(10)}$	ϵ_{ex}^{HL}	ΔE_{del}^{HF}	ΔE^{HF}	$\epsilon_{disp}^{(20)}$	$\Delta E_{ex-del}^{(2)}$	$\epsilon_{el,r}^{(12)}$	$\epsilon_{MP}^{(2)}$	ΔE^{MP2}
iG-iC	-254.04	244.58	-119.16	-128.62	-59.44	44.53	5.94	-8.97	-137.59
oxoG-C	-214.81	199.52	-92.87	-108.16	-52.28	38.74	9.51	-4.02	-112.19
G-C	-207.98	194.00	-89.66	-103.64	-51.27	38.14	7.95	-5.19	-108.82
G-iG	-206.86	194.87	-90.01	-102.00	-51.91	37.90	7.52	-6.49	-108.49
oxoH-C	-175.95	168.70	-78.17	-85.42	-44.69	32.71	10.05	-1.93	-87.35
H-C	-168.16	161.04	-73.59	-80.71	-43.34	31.92	8.21	-3.22	-83.93
M-B	-162.73	176.54	-65.54	-51.72	-47.21	34.01	-0.84	-14.03	-65.76
M-U	-161.51	175.33	-64.88	-51.06	-47.01	33.78	-0.88	-14.12	-65.18
TAP-B	-159.08	175.53	-64.99	-48.54	-47.93	34.56	-0.49	-13.86	-62.40
DAP-U	-155.38	170.38	-62.23	-47.23	-47.38	33.79	-0.79	-14.38	-61.61
oxoDAP-U	-153.31	166.22	-59.71	-46.80	-46.79	33.04	0.40	-13.36	-60.16
DAP-X	-151.88	165.82	-59.85	-45.90	-47.21	33.17	-0.37	-14.41	-60.31
A-H	-133.53	143.47	-59.45	-49.51	-39.07	27.04	-1.19	-13.21	-62.72
A-B	-131.21	144.73	-56.31	-42.79	-39.77	27.80	0.53	-11.44	-54.23
A-U	-129.57	143.32	-55.54	-41.79	-39.59	27.57	0.27	-11.75	-53.54
A-T	-128.86	142.84	-55.11	-41.13	-39.82	27.61	0.16	-12.05	-53.18
oxoA-U	-123.07	133.84	-50.09	-39.31	-38.08	25.94	1.10	-11.04	-50.35

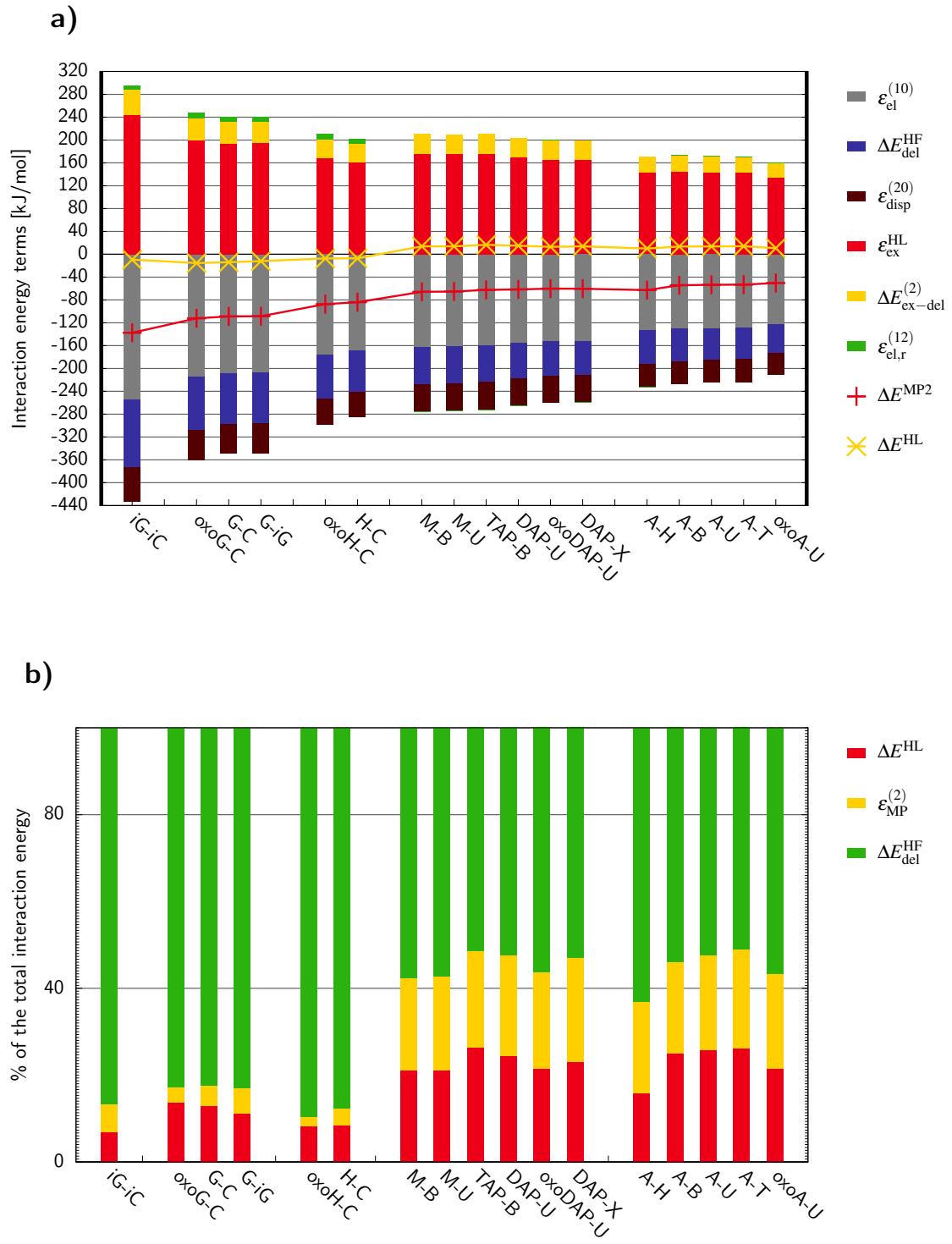

Figure 23. The interaction energy in the studied base pairs shown as a) histogram of its components, and b) relative contributions of the Heitler-London, delocalization, and correlation interaction energies to the total interaction energy. Base pairs are grouped according to decreasing interaction energy and H-bonding motifs, as in Table 6.

Since it is well known that the MP2 method tends to overestimate dispersion forces[248] the interaction energies were recalculated using the SCS-MP2 method with an expanded basis set aug-cc-pVTZ augmented with a set of diffuse functions. Equilibrium geometries optimized using the SCS-MP2/cc-pVTZ method are very similar to MP2/cc-pVTZ structures, with slightly longer hydrogen bonds (by 0.01-0.07 Å). The corresponding interaction energies are on average less attractive by 9%, but this did not affect the conclusions regarding the relative stability or nature of the interactions in the studied base pairs. It should be noted that the change in interaction energies is primarily due to the SCS procedure. Comparing the last two columns in Table 6 shows that the change in the interaction energy due to structural differences is for all complexes but one below 2 kJ/mol (only for iG-iC it amounts to 3.4 kJ/mol). It indicates that the differences between the SCS-MP2 and MP2 equilibrium geometries should not affect the interpretation of the interpolated PES profiles.

Ionization potentials and electron affinities of the nucleobases

Since some of the nonradiative deactivation processes discussed thus far occur on the PESs of charge-transfer states, it is interesting to investigate whether their availability can be predicted on the basis of the properties of isolated nucleobases. Thus, in this section, the selected electronic properties of the subsystems studied are discussed. In particular, the ionization potential and electron affinity of the studied nucleobases show their relative capability to transfer and receive an electron. An accurate description of the distribution of excess electrons is essential for predicting electron- and hole-transfer in nucleic acids. In Table 7 the computed gas-phase ionization energies and electron affinities of the studied nucleobases are gathered, arranged according to increasing vertical ionization energies (VIEs). The SCS-MP2 method has previously been reported as a reliable method for estimating canonical nucleobase ionization potentials (IP),[262] since it reproduces the experimentally determined adiabatic ionization energies (AIEs) quite accurately[263] and produces a relatively small mean average relative error compared to the results obtained using the IP-EOM-CCSD method.[262] Comparison of the results of spin-unrestricted UMP2 and its SCS variant shows differences in VIEs below 0.22 eV (cf. Table 7) and almost the same order of nucleobases in terms of their ionization energies, with the exception of reversed ordering of melamine

[262] S. Śmiga, S. Siecińska, and I. Grabowski, *New Journal of Physics*, **2020**, *22*, 083084.
[263] V. Orlov, A. Smirnov, and Y. M. Varshavsky, *Tetrahedron Letters*, **1976**, *17*, 4377–4378.

and isocytosine. The acronym P-UMP2 indicates that the spin contamination projection was applied as implemented in the Gaussian 16 package. The experimentally determined magnitudes of IPs for biological nucleobases are in the following relation: G<A<C<T<U, which was maintained for both variants of UMP2. However, compared to the reference results, the SCS-P-UMP2 data generally agree better with the IP-EOM-CCSD method and the experimentally determined IP values.

Table 7. Spin contamination projected results of detachment (ionization) energy and electron affinity of nucleobases, calculated using P-UMP2/aug-cc-pVTZ method.

	P-UMP2		SCS-P-UMP2		IP-EOM-CCSD	Experimental
Base	VEA [eV]	VIE [eV]	VEA [eV]	VIE [eV]	VIE [eV]	VIE [eV]
oxoDAP	-0.25	7.96	-0.31	7.88		
iG	-0.10	8.03	-0.17	7.90		
DAP	-0.41	8.06	-0.45	7.92		
oxoG	-0.07	8.12	-0.12	7.99		
TAP	-0.43	8.21	-0.47	8.11		
G	-0.20	8.53	-0.24	8.35	8.15[a],8.08[b]	8.24[c]
oxoH	-0.22	8.58	-0.26	8.43		
oxoA	-0.18	8.63	-0.24	8.52		
A	-0.36	8.72	-0.38	8.72	8.37[a],8.39[b]	8.47[b],8.44[c]
C	-0.24	9.01	-0.28	8.80	8.78[a],8.86[b]	8.89[b],8.94[c]
H	-0.29	9.06	-0.33	8.86		8.89[c]
X	0.15	9.10	0.10	8.92		8.89[c]
M	-0.52	9.13	-0.56	8.98		
iC	0.02	9.18	-0.05	8.96		
T	-0.25	9.29	-0.29	9.17	9.13[a],9.25[b]	9.19[b],9.14[c]
B	-0.14	9.56	-0.19	9.42		
U	-0.21	9.69	-0.25	9.53	9.66[b]	9.50[c]

[a] The cc-pVTZ/IP-EOM-CCSD results for A,T,C and aug-cc-pVTZ/IP-EOM-CCSD for G.[264]
[b] The results of IP-EOM-CCSD/cc-pVTZ extrapolated to CBS limit from Śmiga et al.[262]
[c] Adopted from Trofimov et al.[265]

Accordingly, it is established that the most prominent electron donor in the studied set is the oxoDAP nucleobase. Purines in general show smaller magnitudes of VIEs. This characteristic of purines can be understood by reference to earlier studies by Rehm and Weller,[266,267] where the authors established a connection between the rates of excited-state

[266] S. Farid, J. P. Dinnocenzo, P. B. Merkel, R. H. Young, D. Shukla, and G. Guirado, *Journal of the American Chemical Society*, **2011**, *133*, 11580–11587.
[267] D. Rehm and A. Weller, *Israel Journal of Chemistry*, **1970**, *8*, 259–271.

electron transfer reactions and the oxidation and reduction potentials. In this context, the relatively low IP of the TAP nucleobase is surprising, since it is below IPs of some of the purines studied. On the other hand, hypoxanthine is a purine moiety with relatively large ionization potential, which is a unique observation regarding its ultrafast radiationless decay.[157,268] The same conclusion applies to xanthine.

Interestingly, Takaya et al.[269] observed that the excited state lifetimes of base-stacked dinucleosides correlate with the difference between the ionization potentials of the electron-donating nucleobase and the electron affinities of the electron-accepting nucleobase. Thus, it would be interesting to investigate the correlation between the ionization potential values, or rather the sum of the ionization potential of the absorbing monomer and the electron affinity of the acceptor nucleobase, and the CT energy value in the Franck-Condon region of each base pair. It could be a simple indicator of the ease of population of such a state. To examine such a possibility, the IP/EA values calculated using the SCS-UMP2 method compared to the energies of the CT state of the base pairs calculated on the SCS-ADC(2) level of theory. However, it did not show a clear correlation with the determination coefficient that amounted to roughly R^2=0.65. Intuitively, the pyrimidines should be more capable of receiving an electron as a complementary base to the electron-donating purines; however, no such correlation has been noticed either. The purines, from which it is relatively easy to detach an electron, accept it as easily.

The generally higher ionization potential of purines may be connected to the antiaromatic model introduced by Karas et al.,[270] where authors claim that the antiaromaticity gained by purine upon excitation is released by electron transfer. Subsequently, the proton transfer may occur as well. Therefore, for further analysis, the ionization potential alone may suggest the direction of the electron and potentially proton transfer from one base to another.

Vertical excitation energies

The selected vertical excitation energies computed in the Franck-Condon (FC) region using the SCS-ADC(2)/cc-pVTZ method are shown in Fig. 24. These include the lowest-lying locally excited bright $^1\pi\pi^*$ states, dark ^{1}nπ^* states, and $^1\pi\pi^*_{\mathrm{CT}}$ states that are relevant in the

[268] J. P. Villabona-Monsalve, R. Noria, S. Matsika, and J. Peón, *Journal of the American Chemical Society*, **2012**, *134*, 7820–7829.
[269] T. Takaya, C. Su, K. de La Harpe, C. E. Crespo-Hernández, and B. Kohler, *Proceedings of the National Academy of Sciences*, **2008**, *105*, 10285–10290.
[270] L. J. Karas, C.-H. Wu, H. Ottosson, and J. I. Wu, *Chemical Science*, **2020**, *11*, 10071–10077.

Table 8. Properties of selected vertical excitations of the studied dimers in FC region; orbital character, oscillator strengths, excitation energies in eV and the weights of CT configurations greater than 0.1 are reported.

Base pair	State Transition	f_{osc}	E_{exc}	Ω_{CT}	Base pair	State Transition	f_{osc}	E_{exc}	Ω_{CT}
iG-iC	S_1 $\pi\pi^*_{iG}$	0.150	4.457	-	oxoG-C	S_1 $\pi\pi^*_{oxoG}$	0.136	4.434	-
	S_2 $n\pi^*_{iC}$	$2.09 \cdot 10^{-5}$	4.925	-		S_2 $\pi\pi^*_{C}$	0.091	5.008	-
	S_3 $\pi\pi^*_{iG}$	0.337	5.512	-		S_3 $\pi\pi^*_{CT}$	0.007	5.338	0.982
	S_5 $\pi_{mix}\pi^*_{iC}$	0.076	5.853	0.152		S_4 $\pi\pi^*_{oxoG}$	0.421	5.517	-
	S_7 $\pi\pi^*_{CT}$	0.022	5.965	0.851		S_6 $n_{mix}\pi^*_{C}$	0.002	5.758	0.122
	S_9 $\pi\pi^*_{CT}$	0.101	6.428	0.417		S_{13} $\pi\pi^*_{CT}$	0.033	6.744	0.659
						S_{15} $\pi\pi^*_{CT}$	0.117	6.831	0.330
A-B	S_1 $\pi\pi^*_{A}$	0.023	5.182	-	oxoA-U	S_1 $\pi\pi^*_{oxoA}$	0.108	4.812	-
	S_2 $\pi\pi^*_{A}$	0.374	5.343	-		S_2 $n\pi^*_{U}$	$1.81 \cdot 10^{-4}$	5.050	-
	S_3 $n\pi^*_{B}$	$2.01 \cdot 10^{-4}$	5.426	-		S_3 $\pi\pi^*_{U}$	0.261	5.363	-
	S_4 $n\pi^*_{A}$	$3.17 \cdot 10^{-4}$	5.653	-		S_{10} $\pi\pi^*_{CT}$	0.025	6.218	0.772
	S_5 $\pi\pi^*_{B}$	0.189	5.668	-					
	S_{14} $\pi\pi^*_{CT}$	0.006	7.061	0.893					
TAP-B	S_1 $\pi\pi^*_{TAP}$	0.103	5.015	-	M-U	S_1 $n\pi^*_{U}$	$1.04 \cdot 10^{-4}$	5.055	-
	S_2 $n\pi^*_{B}$	$3.56 \cdot 10^{-4}$	5.345	-		S_2 $\pi\pi^*_{U}$	0.144	5.480	-
	S_3 $\pi\pi^*_{B}$	0.183	5.561	-		S_3 $\pi\pi^*_{M}$	0.036	5.620	-
	S_4 $\pi\pi^*_{TAP}$	0.155	5.923	-		S_4 $n\pi^*_{M}$	$4.05 \cdot 10^{-5}$	6.226	-
	S_7 $n_{mix}\pi^*_{B}$ / $\pi\pi^*_{CT}$	0.001	6.441	0.140		S_{11} $\pi\pi^*_{CT}$	0.030	6.767	0.893
	S_8 $\pi\pi^*_{CT}$ / $\pi\pi^*$	0.295	6.490	0.528		S_{12} $\pi\pi^*_{CT}$	0.007	6.876	0.684
	S_9 $\pi\pi^*_{CT}$	0.152	6.516	0.405		S_{14} $\pi\pi^*_{CT}$	0.039	6.907	0.311
oxoDAP-U	$S_1\pi\pi^*_{oxoDAP}$	0.153	4.542	-	DAP-X	S_1 $\pi\pi^*_{DAP}$	0.162	4.897	-
	S_2 $n\pi^*_{U}$	$1.77 \cdot 10^{-4}$	5.092	-		S_2 $n\pi^*_{X}$	$3.22 \cdot 10^{-4}$	5.313	-
	S_3 $\pi\pi^*_{U}$	0.071	5.445	-		S_3 $\pi\pi^*_{DAP}$	0.350	5.434	-
	$S_4\pi\sigma^*_{oxoDAP}$	0.176	5.496	0.106		S_7 $\pi\pi^*_{DAP}$ / $\pi\pi^*_{CT}$	0.270	6.254	0.328
	S_6 $\pi\pi^*_{CT}$	0.010	5.617	0.835		S_8 $\pi\pi^*_{CT}$	0.127	6.310	0.688
	$S_{15}\pi\pi^*_{CT}$	0.017	6.936	0.857					
A-H	S_1 $\pi\pi^*_{H}$	0.141	5.071	-	M-B	S_1 $n\pi^*_{B}$	$2.03 \cdot 10^{-4}$	5.395	-
	S_2 $\pi\pi^*_{A}$	0.041	5.134	-		S_2 $\pi\pi^*_{M}$	0.009	5.614	-
	S_3 $\pi\pi^*_{A}$	0.449	5.306	-		S_3 $\pi\pi^*_{B}$	0.220	5.696	-
	S_4 $n\pi^*_{H}$	$3.73 \cdot 10^{-4}$	5.622	-		S_4 $n\pi^*_{M}$	$1.43 \cdot 10^{-4}$	6.228	-
	$S_{17}\pi\pi^*_{CT}$	0.095	7.058	0.759		S_{15} $\pi\pi^*_{CT}$	0.026	7.220	0.521
G-iG	S_1 $\pi\pi^*_{G}$	0.084	5.030	-	H-C	S_1 $\pi\pi^*_{C}$	0.096	4.917	-
	S_2 $\pi\pi^*_{iG}$	0.241	5.101	-		S_2 $\pi\pi^*_{H}$	0.080	5.100	-
	S_3 $\pi\pi^*_{G}$	0.543	5.581	-		S_3 $\pi\pi^*_{C}/\pi\pi^*_{H}$	0.261	5.500	-
	S_5 $n\pi^*_{G}$	0.001	5.780	-		S_4 $n\pi^*_{mix}$	0.013	5.660	0.116
	S_6 $\pi\pi^*_{CT}$	0.024	6.004	0.906		S_5 $\pi\pi^*_{H}/\pi\pi^*_{C}$	0.241	5.668	-
	S_8 $n_{mix}\pi^*_{iG}$	0.013	6.123	0.154		S_8 $n\pi^*_{C}$	$1.60 \cdot 10^{-4}$	6.057	0.955
						S_9 $\pi\pi^*_{CT}$	0.004	6.145	-
DAP-U	S_1 $\pi\pi^*_{DAP}$	0.147	4.886	-	oxoH-C	S_1 $\pi\pi^*_{oxoH}$	0.067	4.617	-
	S_2 $n\pi^*_{U}$	$1.68 \cdot 10^{-4}$	5.048	-		S_2 $\pi\pi^*_{C}$	0.092	4.961	-
	S_3 $\pi\pi^*_{DAP}$	0.282	5.437	-		S_3 $\pi\pi^*_{oxoH}$	0.248	5.271	-
	S_4 $\pi\pi^*_{U}$	0.167	5.466	-		S_4 $\pi\pi^*_{C}$	0.199	5.622	-
	S_5 $\pi\pi^*_{CT}$	0.002	5.804	0.986		S_5 $n_{mix}\pi^*_{C}$	0.001	5.754	0.132
	$S_{13}\pi\pi^*_{CT}$	0.010	6.827	0.870		S_7 $\pi\pi^*_{CT}$	0.004	6.009	0.975
	$S_{15}n\pi^*_{CT}$	0.002	6.948	0.512		S_8 $n\pi^*_{C}$	$2.88 \cdot 10^{-4}$	6.135	-

context of the nonradiative deactivation of the complexes studied. The presented results are arranged according to the increasing excitation energy of the CT state. A more detailed juxtaposition of the properties of the selected low-lying excited states can be found in Table 8. The presence of low-lying intermolecular CT excimeric states in purine-pyrimidine systems is consistent with previous studies.[26,91,97,103,104,114,129] Interestingly, such CT states are also found in purine-purine and pyrimidine-pyrimidine type complexes. Between one and four CT states were identified in the base pairs studied. The only exception is the adenine-hypoxanthine (A-H) dimer, for which no intermolecular CT states were observed among the 15 lowest-lying excited states.

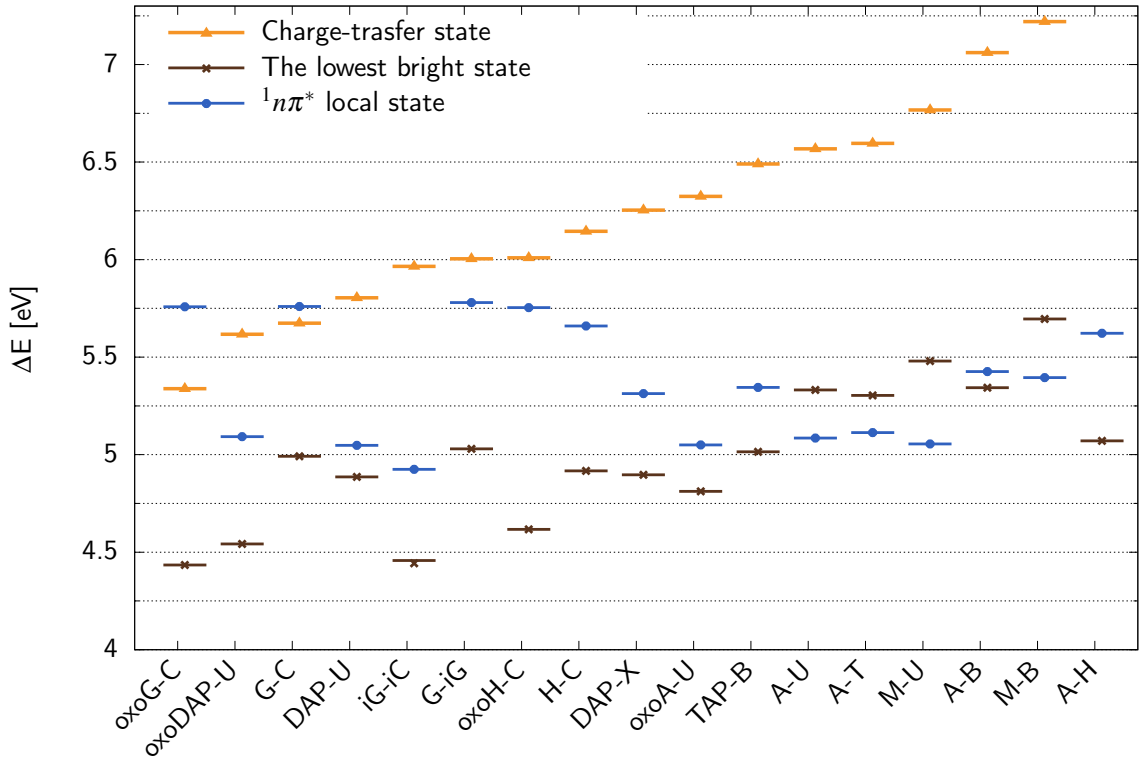

Figure 24. The profile of vertical excitation energies of the lowest-lying $^1\pi\pi^*$ bright states, the dark $^1n\pi^*$ states and the charge transfer states for the studied complexes.

In further analysis, a given excitation is considered to have the CT character when the weight of the charge transfer configurations (Ω_{CT}) exceeds 0.25. Based on this threshold, the oxoG-C base pair was identified as the best electron donor-acceptor complex, for which the S_3 state at 5.34 eV has an evident CT character with Ω_{CT} of 0.98. The lowest optically allowed S_1 state in oxoG-C lies at 4.43 eV. Therefore, both the bright and the low-lying CT

states have excitation energies in the FC region that are lower than the corresponding states of G-C, for which the occurrence of ultrafast deactivation through EDPT is firmly established. Therefore, the same should be expected for oxoG-C. Guanine and its 8-oxo derivative paired with complementary cytosine are also the only base pairs with a dark state of $^1n\pi^*$ character lying above the charge-transfer state. In stark contrast, the potential energy profiles of A-T, A-U, M-U, and M-B indicate that in these base pairs the locally excited $^1n\pi^*$ state is located below the lowest bright state. This ordering of the excited states in the FC region may determine the mechanism of nonradiative deactivation of these complexes.

The locally excited $^1n\pi^*$ transitions discussed are associated with the shift in electronic density from the carbonyl C=O group to the aromatic ring of pyrimidines. Figure 24 shows that, in general, the substitutions of purine or pyrimidine rings only slightly alter the excitation energies of the locally excited $^1n\pi^*$ states. However, modifications of the purine moiety may significantly alter the energy of the optically allowed LE state, which often leads to a change in the ordering of LE excited states. This situation is clearly seen when vertical spectra of A-U are compared with those of DAP-U and 8-oxo-A-U. In fact, in all the studied cases, the introduction of carbonyl in the C8 atom position of the purine ring leads to a substantial decrease in the excitation energy of the lowest absorbing state of the $^1\pi\pi^*$ character. It also leads to an interesting decrease in the CT state excitation energy (cf. Figure 24).

As discussed before ring puckering or pyramidalization at the C2 position of purines are important processes for the photophysics of these species,[18,26,157] thus, the introduction of a functional group in this position should significantly affect these processes and consequently the excitation energy and excited state lifetime.[3] For example, the removal of -NH_2 exocyclic group in the C2 position of guanine significantly impacts the CT state energy which increases substantially in every studied complex of hypoxanthine or its oxidative derivative. However, the introduction of the -NH_2 group in the C2 position of adenine and the formation of 2,6-diaminopurine (DAP) has the opposite effect.

DAP is interesting and unique in some ways. It is the only nucleobase that does not fit in the evident correlation in Figure 24, where the structures alternative to the G-C base pair are characterized, in general, by low-lying CT state, contrary to those similar to A-U or A-T base pairs. DAP may form triply hydrogen-bonded WC-like pairs with U, T, or X with binding energies intermediate between G-C and A-U or A-T. DAP is also a much better electron donor than adenine because of the two electron-donating substituents. It has even lower detachment (ionization) energy than guanine (see Table 7 on page 82). These features make base pairs with DAP an interesting object for studying the interplay of EDPT and intramolecular deactivation processes.

2.2.2 Isosteres of G-C

To investigate the mechanism of excitation decay along the EDPT path, potential energy profiles along each hydrogen bond were calculated. For the oxidative form of G-C, exactly like in the canonical base pair, the most likely is transfer of a proton from N1 site of 8-oxo-G to the N3 of cytosine. The interpolated PE surface cuts in Figure 25 indicate an efficient EDPT process that results in the crossing of the low-lying $^1\pi\pi^*_{CT}$ and S_0 states.

oxoG-C

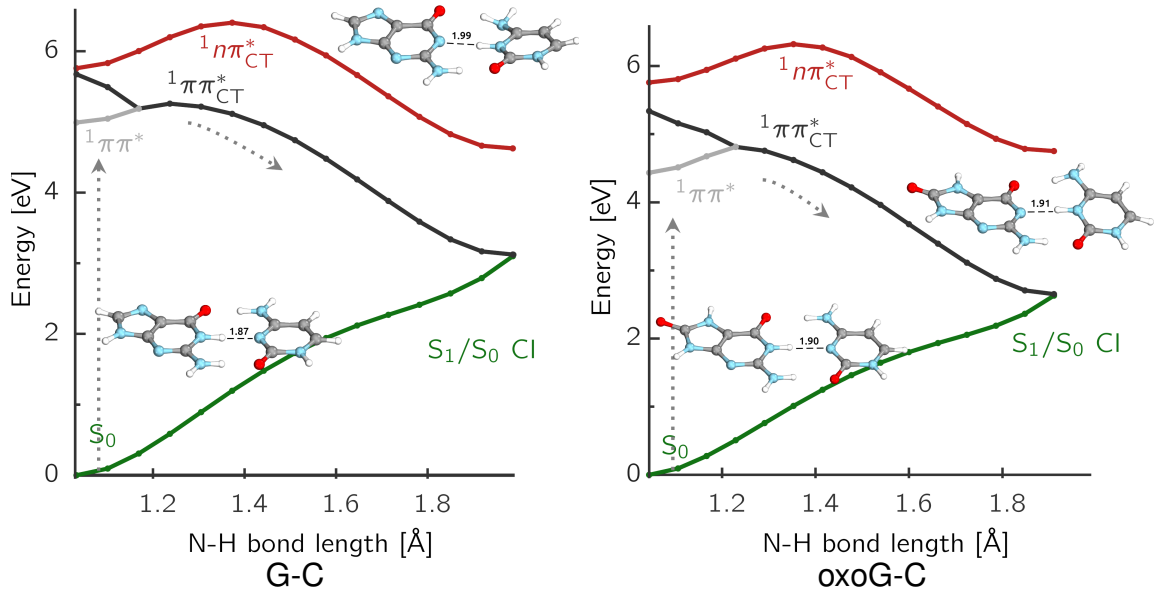

Figure 25. Interpolated PE surface cuts for G-C and oxo-G-C WC dimers illustrating the EDPT mechanism triggered on the $^1\pi\pi^*_{CT}$ state.

The differences between the G-C and oxo-G-C PE profiles are minor and include a red-shifted CT state and a slightly higher energy gap from the lowest bright state to the CT state. The S_1/S_0 MECP in oxo-G-C is located 0.47 eV lower than in G-C and for a slightly shorter elongation of the hydrogen bond. These findings are consistent with the results of studies on the protonated form of 8-oxo-G, which exhibits a very short (sub-picosecond) intrinsic excited-state lifetime, and its anionic form 8-oxo-G^- incorporated into the dimer with cytosine being too short-lived to be an efficient electron-transfer repair agent.[129] As it was already mentioned, G-C and oxo-G-C are the only base pairs with the dark $^1n\pi^*$ state lying above the charge-transfer state in the FC region and this remains true for the entire EDPT path. This dark state has a similar character in both complexes, although in oxo-G-C it has a significant admixture of the CT character (Ω_{CT} = 0.12) and lies slightly higher above the bright state than in G-C. However, a photodeactivation channel similar to that of G-C, involving stabilization of this state along the proton transfer coordinate, seems plausible.

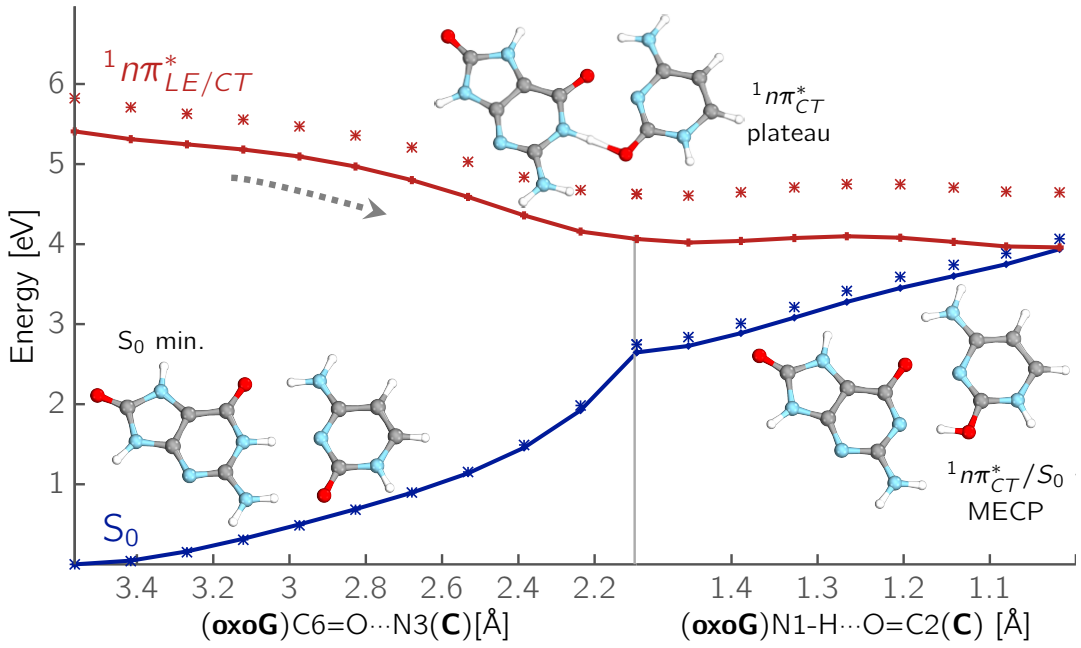

Figure 26. PE surface cuts presenting the EDPT process on the $^1n_{oxoG}\pi^*_C$. The PE surface calculated using the ADC(2)/cc-pVTZ is shown with lines and SCS-ADC(2)/cc-pVTZ results, obtained at the same geometries are shown with asterisks. The identical colors mark the same states.

Indeed, optimization of the geometry in the S_1 state that has $^1n\pi^*$ character revealed the spontaneous change in the pairing scheme from Watson-Crick to Wobble. The excitation energy dropped to 0.6 eV, indicating a nearby intersection with the ground state. This nonradiative deactivation mechanism presented in Figure 26 is virtually identical to the analogous one discussed earlier and shown in Figure 14 on page 60 for G-C. However, in contrast to the EDPT process occurring on the $^1\pi\pi^*_{CT}$ PE surface, which was more stable in the oxoG-C compared to G-C, the process involving the $^1n\pi^*_{CT}$ state is slightly less energetically favorable than in the canonical G-C base pair. Already in the FC region, the $^1n\pi^*_{CT}$ state has a higher excitation energy. The minimum energy structure in the plateau region is separated from the ground state by 1.42 eV, whereas the corresponding energy gap for the G-C amounts to 1.11 eV. Consequently, the MECP also lies slightly higher. Nonetheless, the PE profile shown in Figure 26 is qualitatively similar to that obtained for G-C and indicates that such a process is plausible in oxoG-C. Comparison with single-point calculations performed using the SCS-ADC(2) method shows a similar underestimation of the $^1n\pi^*_{CT}$ state excitation energies.

Two other base pairs within the studied set that have the lowest $^1n\pi^*$ state with a partial CT character are H-C and oxoH-C (see Table 8 on page 84). In H-C, the $^1n_C\pi^*_C$ state lies ~0.5 eV below $^1\pi_H\pi^*_C$ the CT state in the Franck-Condon region and in oxoH-C the respective

H-C and oxoH-C

energy gap is even smaller (~0.25 eV). The values of Ω_{CT} equal to 0.12 and 0.13 indicate a partial CT character of this transition in H-C and oxoH-C, respectively. Interestingly, in the FC region of H-C and oxoH-C, the CT state is separated from the lowest bright state by a large energy gap and a few other states, including the dark $^1n\pi^*$ state discussed. Thus, considering the apparent inaccessibility of the EDPT channel triggered on the $^1\pi\pi^*_{CT}$ PE surface, the alternative EDPT process comprising WC to Wobble rearrangement on the $^1n_C\pi^*_C$ PE surface could be even more plausible than in G-C. To investigate this hypothesis, optimization of the S_1 $n\pi^*$ minimum energy structure of H-C has been attempted. The calculations started with an imposed planar (C_s) symmetry constraints. The $^1n\pi^*$ state with a partial CT character was thus the lowest excited singlet state belonging to the A" irreducible representation. However, subsequent geometry optimization with no symmetry constraints led to $^1\pi\pi^*$ CoI. Given that the lowest $^1n\pi^*$ excited state is associated with the transition of electronic density from C_4 carbonyl lone-pair to the aromatic ring of cytosine, another attempt was to locate the S_1 minimum geometry of isolated cytosine, and then let the dimer relax. This approach led to a minimum of $^1n\pi^*$ state, but with a different character.

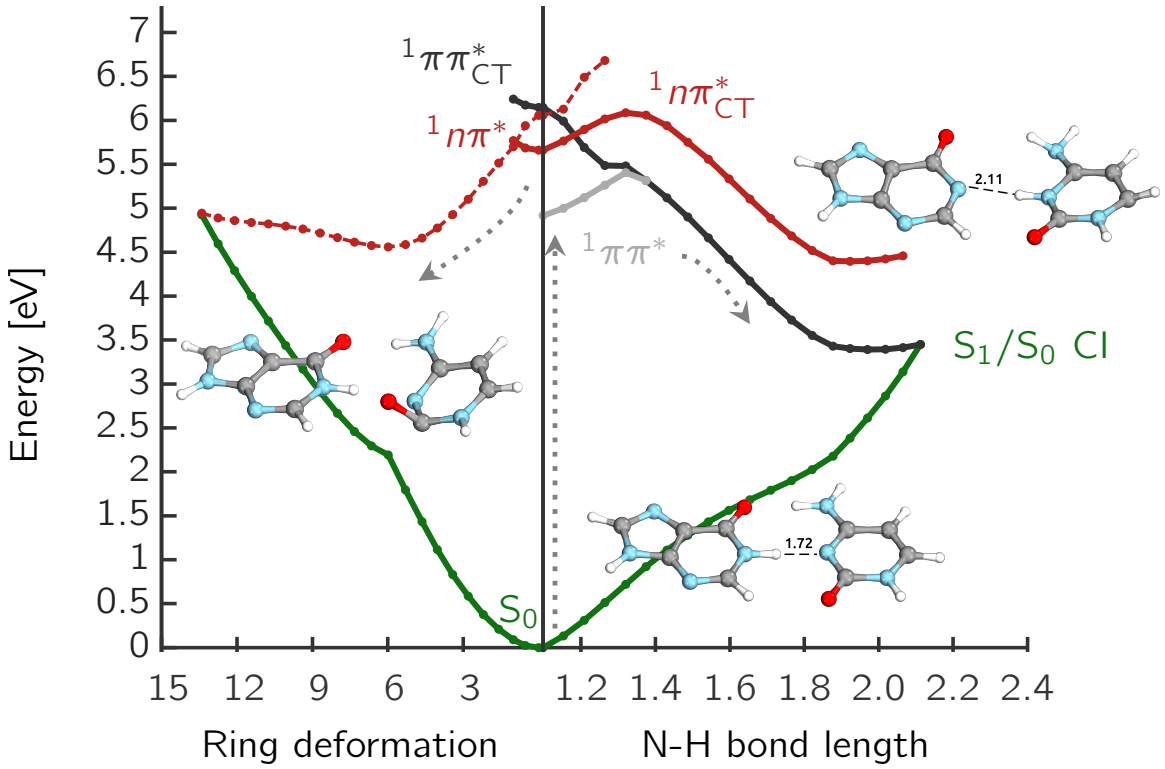

Figure 27. EDPT H-C on the $^1\pi\pi^*_{CT}$ state vs pyrimidine puckering on the $^1\pi\pi^*_{LE}$ state.

On the right-hand side of Figure 27, the EDPT process driven on the $^1\pi\pi^*_{CT}$ PE surface is shown, proceeding through a few state crossings. These include the crossing of bright LE and CT states ($^1\pi\pi^*_{LE}/\pi\pi^*_{CT}$) and CT/$S_0$. The $^1n\pi^*_{CT}$ state lies above the lowest-lying bright state but below the S_5 LE bright state; thus the former could be populated after crossing with the latter. There is yet another dark $^1n\pi^*_{LE}$, which is not involved in the relaxation along the N-H bond but its population could lead to ring puckering channel shown in the left panel of Figure 27. The crossing of the S_1 $^1n\pi^*_{LE}$ state with the ground state is characterized by a substantial elongation of the N2=O bond, resulting in its distortion out of the pyrimidine plane.

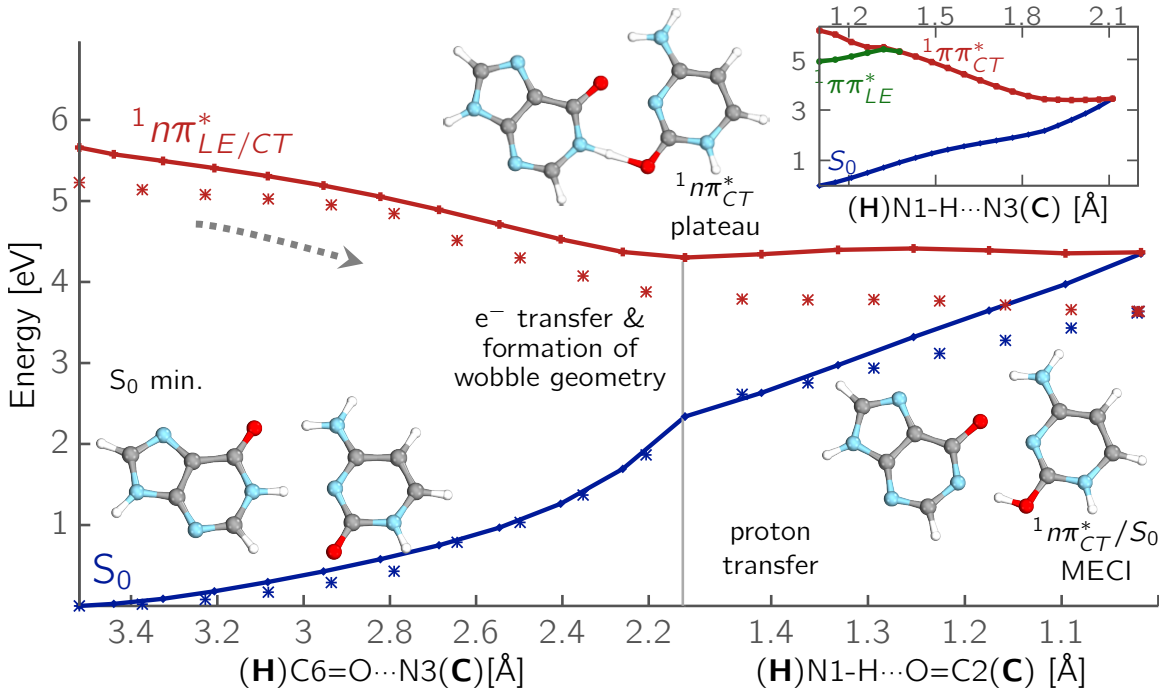

Figure 28. PE surface cuts presenting the EDPT process on the $^1n_H\pi^*_C$ PE surface calculated using SCS-ADC(2)/cc-pVTZ (lines with points) and ADC(2)/cc-pVTZ methods (points) by LIIC. The identical colors mark the same states.

The MECP of the bright $^1\pi\pi^*$ state (located on purine) with the ground state (not shown in the plot) is found at 4.28 eV. It is primarily associated with the puckering of the C2 atom of hypoxanthine, similar to the MECP located for the isolated nucleobase in the MR-CIS studies of Villabona-Monsalve et al.[268] Thus there are a few competing deactivation channels available in H-C and oxoH-C. Still, it is suspected that the EDPT chanel is plausible and may equally

be triggered by population of the $^1\pi\pi^*_{CT}$ and the $^1n\pi^*_{CT}$ states. The partial charge-transfer character of the latter state and the associated specific exciplex Wobble-like interaction indicate there should be a similar process to G-C and oxoG-C involving a change of pairing from WC to Wobble base pairing scheme. Indeed, calculations analogous to those performed earlier for G-C base pair allowed us to successfully locate the S_1 ($n\pi^*_{CT}$) plateau region and the corresponding MECP for H-C. The associated EDPT process is likely sequential since geometry optimization on the S_1 ($n\pi^*_{CT}$) hypersurface results in the formation of the Wobble H-C structure and further unconstrained optimization leads to a subsequent proton transfer (see Figure 28).

The electron-hole population analysis revealed that the fraction of the CT configuration increases to 0.34 in the region of the $^1n\pi^*_{CT}$ plateau. It is worth mentioning that the corresponding results of MP2/ADC(2) calculations indicate a lower fraction of CT configuration in the FC region than the SCS variant (only 0.08), which increases to 0.46 only in the plateau region. On the other hand, the S_1-S_0 energy gap in the plateau region calculated using MP2/ADC(2) amounts to 1.17 eV but increases to 1.96 eV when the SCS-variant of the methodology is applied. Consequently, the topography of the ground state PES is predicted to be steeper by the SCS-MP2 method, but otherwise the overall process remains the same. In the inset of Figure 28, the potential energy profile for EDPT relaxation triggered on the $^1\pi\pi^*_{CT}$ PE surface is presented, where it is again clear that the CT state is available at much higher excitation energies than in G-C. Thus, the EDPT process mediated by the dark $^1n\pi^*_{CT}$ state leading to the formation of the Wobble H-C exciplex may be more accessible and proceed in a barrier-free manner to the intersection with the ground electronic state. Notably, the $^1n\pi^*_{CT}$ state of H-C in the FC region is accessible at the same energy level (5.7 eV) as the $^1\pi\pi^*_{CT}$ state in the G-C. Thus, it is likely that excitation to the close bright state could trigger the ultrafast EDPT process mediated by the $^1n\pi^*_{CT}$ state. Comparison with the results obtained for oxoG-C and G-C indicates that the occurrence of the same mechanisms should be expected in the oxoH-C base pair.

The occurrence of this photostabilizing process in the base pairs of H-C and oxoH-C amplifies the plausibility of the prebiotic scenario involving the formation of inosine (nucleoside of hypoxanthine) and its hypothetical role as an agent, increasing the rate and fidelity of non-enzymatic replication of RNA template.[271,272]

[271] S. J. Roberts, R. Szabla, Z. R. Todd, S. Stairs, D.-K. Bučar, J. Šponer, D. Sasselov, and M. W. Powner, *Nat. Commun.*, **2018**, *9*, 4073.

[272] S. C. Kim, D. K. O'Flaherty, L. Zhou, V. S. Lelyveld, and J. W. Szostak, *Proceedings of the National Academy of Sciences*, **2018**, *115*, 13318–13323.

However, the question arises of whether the role of $^1n\pi^*$ states in these base pairs does not change in an aqueous environment. It is known that, as a result of a smaller dipole moment, the $n\pi^*$ states are often blueshifted with respect to the ground and the $\pi\pi^*$ states in the polarizable environment,[22,273] therefore they may not be energetically available in the nonradiative photorelaxation mechanisms. The $^1\pi\pi^*/S_0$ conical intersection may thus be easier to reach owing to the fact that the $\pi\pi^*$ states often experience a redshift in polar solvents.

The possible changes of the PE profile have been further studied with the solvation effects exerted by bulk solvents represented with the non-equilibrium Conductor-like Screening Model (COSMO) model implemented in TURBOMOLE 7.3 package. The vertical excitation energies of the solvated G-C and H-C base pairs were calculated using the ADC(2)/COSMO and SCS-ADC(2)/COSMO approaches assuming the non-equilibrium solvation. The single-point energies of the S_1 ($n\pi^*_{CT}$) minima were obtained assuming the reaction field equilibrated for the S_1 state. The comparison of selected vertical excitation energies for solvents with a dielectric constant of ϵ=78.34 and ϵ=4.80, representing polar (water) and apolar (chloroform) solvents, is presented in Table 9. Chloroform was previously suggested to be a good representative of the dielectric environment inside a DNA double helix.[274–276] For clarity, the results for G-C in the gas phase from Table 2 on page 57 are recalled in Table 9 and compared with the results obtained for H-C.

The ADC(2) results are shown mainly as a reference. In general, the SCS approach shifts all excitation energies toward higher values, but the $^1\pi\pi^*$ states are less affected than $^1n\pi^*$. In the following discussion, we focus on the SCS-ADC(2)/COSMO data. As expected, the $^1n\pi^*$ states are generally blue-shifted in the solvent. The calculations show that the lowest $^1n\pi^*$ state in the H-C base pair located on hypoxanthine is blueshifted by 0.06 eV and 0.10 eV in bulk chloroform and water, respectively. Larger shifts are observed for $^1n\pi^*$ states located on cytosine (0.21 and 0.31 eV, respectively). In contrast, the optically bright $^1\pi\pi^*$ states are less affected; although the ordering of these states is also affected by the solvation effects. Interestingly, the polar $^1\pi\pi^*_{CT}$ state in the G-C and H-C base pairs is also significantly

[273] C. M. Marian, *The Journal of Chemical Physics*, **2005**, *122*, 104314.
[274] J. Mazur and R. L. Jernigan, *Biopolymers*, **1991**, *31*, 1615–1629.
[275] K. Siriwong, A. A. Voityuk, M. D. Newton, and N. Rösch, *The Journal of Physical Chemistry B*, **2003**, *107*, 2595–2601.
[276] K. Röttger, H. J. B. Marroux, M. P. Grubb, P. M. Coulter, H. Böhnke, A. S. Henderson, M. C. Galan, F. Temps, A. J. Orr-Ewing, and G. M. Roberts, *Angewandte Chemie International Edition*, **2015**, *54*, 14719–14722.

Table 9. Vertical excitation energies (in eV) of G-C and H-C in the Franck–Condon region calculated with ADC(2) method in the gas phase and with the non-equilibrium Conductor-like Screening Model (COSMO) of bulk water, assuming imposed C_s symmetry.

State	Transition	E_{exc}/[eV]	f_{osc}
G-C ADC(2) C_S symmetry			
S_1(A')	$\pi_G\pi^*_G$ / $\pi_G\pi^*_C$ (CT)	4.857	$6.99 \cdot 10^{-2}$
S_2(A')	$\pi_C\pi^*_C$	4.906	$5.65 \cdot 10^{-2}$
S_3(A')	$\pi_G\pi^*_C$ (CT)	5.164	$2.84 \cdot 10^{-2}$
S_4(A")	$n_C\pi^*_C$/ $n_G\pi^*_C$ (CT)	5.369	$6.45 \cdot 10^{-4}$
S_5(A')	$\pi_C\pi^*_C$	5.370	0.234
S_6(A')	$\pi_G\pi^*_G$	5.416	0.407
S_7(A")	$n_G\pi^*_G$	5.583	$2.12 \cdot 10^{-4}$
S_8(A")	$n_C\pi^*_C$	5.684	$5.07 \cdot 10^{-5}$
S_9(A")	$n_C\pi^*_C$	6.171	$1.60 \cdot 10^{-6}$
S_{10}(A")	$n_G\pi^*_G$ / $n_G\pi^*_C$(CT)	6.312	$1.38 \cdot 10^{-3}$
S_{11}(A")	$n_C\pi^*_C$/ $n_G\pi^*_C$(CT)	6.343	$9.76 \cdot 10^{-5}$
S_{12}(A")	$\pi_G\sigma^*_G$	6.434	$8.80 \cdot 10^{-4}$
G-C ADC(2)-COSMO (ϵ = 4.80)			
S_1(A')	$\pi_G\pi^*_G$	4.833	0.124
S_2(A')	$\pi_C\pi^*_C$	4.926	0.142
S_3(A')	$\pi_G\pi^*_C$(CT)	5.197	$4.8 \cdot 10^{-4}$
S_4(A')	$\pi_G\pi^*_G$	5.364	0.488
S_5(A')	$\pi_C\pi^*_C$	5.386	0.212
S_6(A")	$n_G\pi^*_C$ (CT) / $n_G\pi^*_G$	5.586	$1.0 \cdot 10^{-3}$
S_7(A")	$n_G\pi^*_G$ / $n_C\pi^*_C$	5.661	$1.5 \cdot 10^{-5}$
S_8(A")	$n_C\pi^*_C$	5.863	$1.5 \cdot 10^{-4}$
S_9(A")	$n_C\pi^*_C$	6.286	$1.4 \cdot 10^{-5}$
S_{10}(A')	$\pi_C\pi^*_C$	6.357	0.281
S_{11}(A")	$n_G\pi^*_G$	6.368	$1.0 \cdot 10^{-3}$
S_{12}(A')	$\pi_G\pi^*_C$(CT)	6.494	$5.0 \cdot 10^{-3}$
G-C ADC(2)-COSMO (ϵ = 78.34)			
S_1(A')	$\pi_G\pi^*_G$	4.829	0.136
S_2(A')	$\pi_C\pi^*_C$	4.953	0.161
S_3(A')	$\pi_G\pi^*_G$	5.390	0.475
S_4(A')	$\pi_G\pi^*_C$ (CT)	5.427	$1.2 \cdot 10^{-4}$
S_5(A')	$\pi_C\pi^*_C$	5.474	0.192
S_6(A")	$n_G\pi^*_G$	5.663	$7.9 \cdot 10^{-4}$
S_7(A")	$n_C\pi^*_C$	5.744	$3.4 \cdot 10^{-4}$
S_8(A")	$n_C\pi^*_C$	6.018	$1.4 \cdot 10^{-4}$
S_9(A')	$\pi_C\pi^*_C$	6.309	0.274
S_{10}(A")	$n_C\pi^*_C$	6.379	$4.6 \cdot 10^{-5}$
S_{11}(A")	$n_G\pi^*_G$	6.409	$7.5 \cdot 10^{-4}$
S_{12}(A')	$\pi_G\pi^*_G$	6.511	$2.5 \cdot 10^{-2}$

State	Transition	E_{exc}/[eV]	f_{osc}
H-C ADC(2) C_S symmetry			
S_1(A')	$\pi_C\pi^*_C$	4.809	$7.60 \cdot 10^{-2}$
S_2(A')	$\pi_H\pi^*_H$	5.044	$8.70 \cdot 10^{-2}$
S_3(A")	$n_C\pi^*_C$ / $n_H\pi^*_C$(CT)	5.227	$2.97 \cdot 10^{-4}$
S_4(A')	$\pi_C\pi^*_C$	5.344	0.236
S_5(A")	$n_H\pi^*_H$	5.469	$4.24 \cdot 10^{-4}$
S_6(A')	$\pi_H\pi^*_H$	5.539	0.224
S_7(A")	$n_H\pi^*_C$(CT)	5.582	$2.49 \cdot 10^{-4}$
S_8(A")	$n_H\pi^*_H$	5.713	$2.39 \cdot 10^{-4}$
S_9(A")	$n_H\pi^*_H$	5.807	$5.15 \cdot 10^{-4}$
S_{10}(A')	$\pi_H\pi^*_C$(CT)	5.912	$4.31 \cdot 10^{-3}$
S_{11}(A")	$n_C\pi^*_C$	6.010	$7.64 \cdot 10^{-6}$
S_{12}(A")	$n_H\pi^*_H$	6.350	0.002
H-C ADC(2)-COSMO (ϵ = 4.80)			
S_1(A')	$\pi_C\pi^*_C$	4.870	0.146
S_2(A')	$\pi_H\pi^*_H$	5.047	0.109
S_3(A')	$\pi_H\pi^*_H$	5.363	0.268
S_4(A')	$\pi_C\pi^*_C$	5.474	0.256
S_5(A")	$n_H\pi^*_H$	5.496	$9.23 \cdot 10^{-4}$
S_6(A")	$n_H\pi^*_H$	5.571	$2.0 \cdot 10^{-7}$
S_7(A")	$n_C\pi^*_C$ / $n_H\pi^*_C$ (CT)	5.809	$8.31 \cdot 10^{-5}$
S_8(A")	$n_H\pi^*_H$	5.824	$9.59 \cdot 10^{-4}$
S_9(A")	$n_H\pi^*_H$	5.874	$5.67 \cdot 10^{-4}$
S_{10}(A')	$\pi_H\pi^*_C$ (CT)	5.923	$6.0 \cdot 10^{-2}$
S_{11}(A")	$n_C\pi^*_C$	6.160	$2.32 \cdot 10^{-5}$
S_{12}(A")	$n_H\pi^*_H$	6.396	$1.28 \cdot 10^{-3}$
H-C ADC(2)-COSMO (ϵ = 78.34)			
S_1(A')	$\pi_C\pi^*_C$	4.909	0.166
S_2(A')	$\pi_H\pi^*_H$	5.066	0.105
S_3(A')	$\pi_H\pi^*_H$	5.379	0.287
S_4(A')	$\pi_C\pi^*_C$	5.510	0.222
S_5(A")	$n_H\pi^*_H$ / $n_C\pi^*_C$	5.587	$7.0 \cdot 10^{-4}$
S_6(A")	$n_C\pi^*_C$	5.655	$3.3 \cdot 10^{-4}$
S_7(A")	$n_H\pi^*_H$	5.876	$1.18 \cdot 10^{-3}$
S_8(A")	$n_H\pi^*_H$	5.910	$2.6 \cdot 10^{-4}$
S_9(A")	$n_C\pi^*_C$	5.969	$3.4 \cdot 10^{-4}$
S_{10}(A")	$n_C\pi^*_C$	6.257	$2.9 \cdot 10^{-5}$
S_{11}(A')	$\pi_H\pi^*_C$ (CT)	6.362	$9.4 \cdot 10^{-2}$
S_{12}(A')	$\pi_C\pi^*_C$	6.377	0.286

Table 10. Vertical excitation energies (in eV) of G-C and H-C in the Franck–Condon region calculated with SCS-ADC(2) method in the gas phase and with the non-equilibrium Conductor-like Screening Model (COSMO) of bulk water, assuming imposed C_s symmetry.

State / Transition		E_{exc}/[eV]	f_{osc}
G-C SCS-ADC(2) C_S symmetry			
S_1(A')	$\pi_G\pi_G^*$	4.992	0.077
S_2(A')	$\pi_C\pi_C^*$	5.056	0.084
S_3(A')	$\pi_C\pi_C^*$	5.554	0.360
S_4(A')	$\pi_G\pi_G^*$	5.593	0.329
S_5(A')	$\pi_G\pi_C^*$ (CT)	5.673	0.029
S_6(A")	$n_C\pi_C^*$ / $n_G\pi_C^*$ (CT)	5.761	0.001
S_7(A")	$n_G\pi_G^*$/$n_C\pi_C^*$	5.837	$1.55 \cdot 10^{-5}$
S_8(A")	$n_C\pi_C^*$	6.303	$4.06 \cdot 10^{-5}$
S_9(A")	$n_C\pi_C^*$	6.384	$6.30 \cdot 10^{-7}$
S_{10}(A")	$n_G\pi_G^*$	6.603	0.003
S_{11}(A')	$\pi_C\pi_C^*$	6.631	0.265
S_{12}(A')	$\pi_G\pi_G^*$	6.691	0.074
G-C SCS-ADC(2)-COSMO (ϵ = 4.80)			
S_1(A')	$\pi_G\pi_G^*$	4.936	0.120
S_2(A')	$\pi_C\pi_C^*$	5.055	0.164
S_3(A')	$\pi_G\pi_G^*$	5.535	0.536
S_4(A')	$\pi_C\pi_C^*$	5.592	0.249
S_5(A')	$\pi_G\pi_C^*$ (CT)	5.703	$2.96 \cdot 10^{-4}$
S_6(A")	$n_G\pi_G^*$	5.833	0.001
S_7(A")	$n_C\pi_C^*$ / $n_G\pi_C^*$ (CT)	5.973	0.001
S_8(A")	$n_C\pi_C^*$	6.473	$6.65 \cdot 10^{-5}$
S_9(A")	$n_C\pi_C^*$	6.527	$2.12 \cdot 10^{-5}$
S_{10}(A')	$\pi_C\pi_C^*$	6.558	0.343
S_{11}(A')	$\pi_G\pi_G^*$	6.649	0.033
S_{12}(A")	$n_G\pi_G^*$	6.689	0.002
G-C SCS-ADC(2)-COSMO (ϵ = 78.34)			
S_1(A')	$\pi_G\pi_G^*$	4.925	0.131
S_2(A')	$\pi_C\pi_C^*$	5.067	0.179
S_3(A')	$\pi_G\pi_G^*$	5.553	0.519
S_4(A')	$\pi_C\pi_C^*$	5.666	0.235
S_5(A")	$n_G\pi_G^*$	5.863	$4.72 \cdot 10^{-4}$
S_6(A")	$n_C\pi_C^*$ / $n_G\pi_C^*$ (CT)	6.066	0.001
S_7(A')	$\pi_G\pi_C^*$ (CT)	6.130	0.013
S_8(A')	$\pi_C\pi_C^*$	6.516	0.340
S_9(A")	$n_C\pi_C^*$ / $n_G\pi_G^*$	6.560	$9.93 \cdot 10^{-5}$
S_{10}(A')	$\pi_G\pi_G^*$	6.631	0.054
S_{11}(A")	$n_C\pi_C^*$ /$n_G\pi_G^*$	6.674	$2.52 \cdot 10^{-5}$
S_{12}(A")	$n_G\pi_G^*$	6.733	0.002

State / Transition		E_{exc}/[eV]	f_{osc}
H-C SCS-ADC(2) C_S symmetry			
S_1(A')	$\pi_C\pi_C^*$	4.967	0.092
S_2(A')	$\pi_H\pi_H^*$	5.133	0.068
S_3(A')	$\pi_C\pi_C^*$	5.534	0.281
S_4(A")	$n_H\pi_H^*$	5.668	0.001
S_5(A')	$\pi_H\pi_H^*$ / $\pi_C\pi_C^*$	5.693	0.244
S_6(A")	$n_C\pi_C^*$ / $n_H\pi_C^*$ (CT)	5.736	$1.99 \cdot 10^{-4}$
S_7(A")	$n_H\pi_H^*$	5.992	0.001
S_8(A")	$n_C\pi_C^*$	6.110	$1.54 \cdot 10^{-4}$
S_9(A")	$n_C\pi_C^*$	6.199	$1.80 \cdot 10^{-7}$
S_{10}(A')	$\pi_H\pi_C^*$ (CT)	6.419	0.002
S_{11}(A")	$n_H\pi_H^*$	6.424	$1.81 \cdot 10^{-4}$
S_{12}(A")	$n_H\pi_H^*$	6.633	0.004
H-C SCS-ADC(2)-COSMO (ϵ = 4.80)			
S_1(A')	$\pi_C\pi_C^*$	4.996	0.154
S_2(A')	$\pi_H\pi_H^*$	5.136	0.085
S_3(A')	$\pi_H\pi_H^*$	5.514	0.335
S_4(A')	$\pi_C\pi_C^*$	5.640	0.277
S_5(A")	$n_H\pi_H^*$	5.731	0.001
S_6(A")	$n_H\pi_C^*$ (CT)	5.905	0.001
S_7(A")	$n_H\pi_H^*$	6.090	0.002
S_8(A")	$n_C\pi_C^*$	6.319	$1.07 \cdot 10^{-4}$
S_9(A")	$n_C\pi_C^*$	6.375	$1.03 \cdot 10^{-5}$
S_{10}(A")	$n_H\pi_H^*$	6.446	$1.03 \cdot 10^{-5}$
S_{11}(A')	$\pi_C\pi_C^*$	6.614	0.310
S_{12}(A")	$n_H\pi_H^*$	6.712	0.003
H-C SCS-ADC(2)-COSMO (ϵ = 78.34)			
S_1(A')	$\pi_C\pi_C^*$	5.023	0.170
S_2(A')	$\pi_H\pi_H^*$	5.153	0.083
S_3(A')	$\pi_H\pi_H^*$	5.515	0.344
S_4(A')	$\pi_C\pi_C^*$	5.689	0.251
S_5(A")	$n_H\pi_H^*$	5.771	$4.44 \cdot 10^{-4}$
S_6(A")	$n_H\pi_C^*$ (CT)	6.009	0.001
S_7(A")	$n_H\pi_H^*$	6.137	0.002
S_8(A")	$n_C\pi_C^*$	6.423	$1.24 \cdot 10^{-4}$
S_9(A")	$n_H\pi_H^*$	6.500	$1.98 \cdot 10^{-5}$
S_{10}(A')	$\pi_H\pi_C^*$ (CT)	6.539	0.009
S_{11}(A")	$n_C\pi_C^*$	6.541	$2.96 \cdot 10^{-5}$
S_{12}(A')	$\pi_C\pi_C^*$	6.575	0.324

destabilized in solvent (by up to 0.46 eV for G-C in bulk water). Regarding the excitation energies calculated for the S_1 minimum energy geometries, the S_1-S_0 energy gaps in the gas phase amount to 1.06 eV and 1.12 eV for G-C and H-C, respectively. Solvation shifts these towards higher values, as the $\Delta E_{S_1-S_0}$ in bulk water amounts to 1.48 eV for G-C and 1.47 eV for H-C. For both base pairs $\Delta E_{S_1-S_0}$ estimated in bulk chloroform is 1.38 eV.

Concluding the discussion of the solvation effects, the solvatochromic shifts of 0.2 to 0.4 eV for the $^1n\pi^*$ states are retained even outside the Franck-Condon region. This indicates that according to both the ADC(2) and the SCS-ADC(2) results, the discussed photodeactivation mechanisms are plausible in the gas phase and in both polar and apolar environments. Although in bulk water, the CT character of the $^1n\pi^*$ states in the Franck-Condon region was diminished because they tend to localize on a single base. Nonetheless, solvation effects did not affect the character or order of the relevant states in close proximity to the $^1n\pi^*_{CT}$ minimum. Thus, the sequential EDPT mechanism mediated by these states should be available also in the environment characteristic of the interior of a DNA double helix. However, the implicit solvation model is incapable of reproducing all of the environmental effects exerted by the interior of the DNA double helix. Presumably, taking into account stacking interactions along the bases in the horizontal interaction would provide a more comprehensive understanding of the environmental effects on the sequential EDPT process. Such calculations within the QM/MM framework would require significant computational effort. The addition of the sugar-phosphate backbone would be even more costly, since the most extensive QM/MM simulation that used the ADC(2) method included only four nucleobases.[277] Preliminary studies on various nucleobases and nucleosides generally suggest that the $^1n\pi^*$ states are stabilized after sugar substitution. Therefore, the EDPT process that occurs on the PE surface of the S_1 $n\pi^*_{CT}$ state might be feasible in a DNA duplex.

The studied set of base pairs includes complexes of isomerized guanine and cytosine (iG-iC) and isoguanine with guanine (G-iG), which are bound according to the same synthon scheme required for the exciplex N···O interaction, facilitating WC-to-wobble change of pairing, as in the G-C, oxoG-C, H-C and oxoH-C. The only exception is that the relevant $^1n\pi^*$ transition occurs locally on isocytosine or guanine. In the case of iG-iC, the search for a minimum of $^1n\pi^*$ excited state leads to a structure lying 2.53 eV above the ground state, thus

iG-iC

[277] R. Szabla, H. Kruse, P. Stadlbauer, J. Šponer, and A. L. Sobolewski, *Chemical Science*, **2018**, *9*, 3131–3140.

likely far from the MECI region. Furthermore, the photorelaxation process through the $^1n\pi^*_{\mathrm{LE}}$ state features a significant energy barrier of roughly 0.7 eV and does not involve a change in the pairing scheme.

The apparent inaccessibility of this channel is also supported by the presence of the lower-lying LE bright $^1\pi\pi^*$ state, which can be populated directly. The population of this state serves as a doorway to an independent radiationless mechanism associated with the puckering of the iG. Interestingly, optimization of the first excited state of the $^1\pi\pi^*$ character yields geometry with a puckered C6 atom of iG. The canonical base pairs and other alternative structures of G-C discussed earlier indicated changes involving mainly the C2 atom of purines, and the inversion of functional groups apparently changed this characteristic feature. The minimum energy structure of the S_1 $\pi\pi^*$ state characterized by the C2-atom puckering of the isoguanine is 0.77 eV above the more stable S_1 $\pi\pi^*$ minimum associated with the C6-NH_2 distortion, which is very close (0.04 eV) to the MECP with the ground state. Therefore, this mechanism is likely dominant within the spectral window of low-lying excitations of the iG-iC base pair. Regarding isolated iG, puckering at the C6 atom position has also been observed in a very recent MS-CASPT2 study reported by Ortín-Fernández et al.[278]

A pictorial representation of the identified nonradiative relaxation paths is presented in Figure 29. The mechanisms driven by the LE transitions are shown on the left-hand side of the graph. The scheme assumes the population of the lowest bright $^1\pi\pi^*$ state located on iG or the higher-lying transition located on iC. In the latter case, there are several competitive mechanisms triggered by the population of this state. The EDPT paths proceeding on the $^1\pi\pi^*_{\mathrm{CT}}$ PE surface are shown on the right-hand side of the graph. Although a PE barrier of about 0.7 eV is shown, this is only an estimate based on LIIC between the FC region and the corresponding S_1 minimum energy structures, and is likely overestimated.

The feasibility of proton transfer along two different hydrogen bonds (iG)N1-H$\cdots$N3(iC) and (iG)C6-$NH_2\cdots$O(iC) was investigated. The final intersections of the $^1\pi\pi^*_{\mathrm{CT}}$ and ground states are energetically close and differ only by 0.22 eV. These are easily accessible from the respective S_1 minima. Both MECPs lie significantly below the lowest bright state and lower than the $^1\pi\pi^*_{\mathrm{LE}}/S_0$ MECP associated with ring puckering at the C6 atom of isoguanine. It can thus be concluded that the electron-driven proton transfer may be an efficient radiationless mechanism of returning the iG-iC base pair to the ground state.

[278] J. Ortín-Fernández, N. E. Caldero-Rodríguez, C. E. Crespo-Hernández, L. Martínez-Fernández, and I. Corral, *Chemistry–A European Journal*, **2023**, *29*, e202203580.

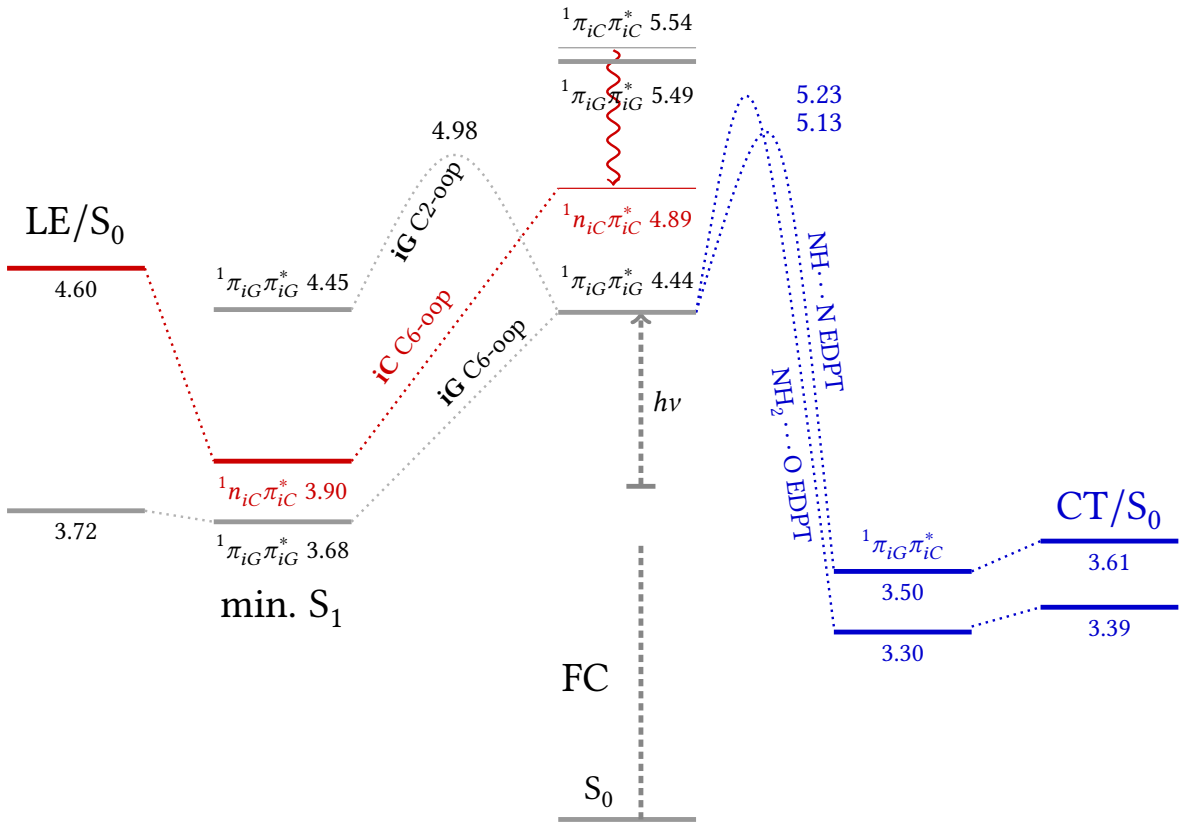

Figure 29. Pictorial presentation of the radiationless deactivation mechanisms in the iG-iC base pair.

The last isostere of the G-C base pair considered was the complex in which cytosine was replaced by isoguanine (G-iG). This base pair retains the same H-bonding synthon as the G-C, which could enable nonradiative relaxation of the excited state along the proton transfer coordinate. The vertical electronic spectrum in the FC region of the G-iG shows a negligible blueshift of the locally excited states compared to the G-C. However, the CT state is significantly shifted towards the higher energy, as it lies at 6.0 eV, which is ~1.0 eV above the optically allowed bright $^1\pi\pi^*$ state. Although the excitation energy to the lowest-lying $^1n\pi^*$ state appears similar, this transition is localized on the guanine. Thus, our calculations indicate that there are only two competing mechanisms of excitation decay available in G-iG, shown schematically in Figure 30. On the right-hand side of the graph the efficient barrierless EDPT mechanism is shown driven by the $^1\pi\pi^*_{CT}$ state. On the left-hand side of the graph, the mechanism of C2 guanine atom puckering is presented, which is virtually identical to the G-C. In the low-energy window of UV irradiation, this process will most likely dominate the photophysics of the G-iG base pair. A small PE barrier from the minimum of S_1 state should not affect these considerations.

G-iG

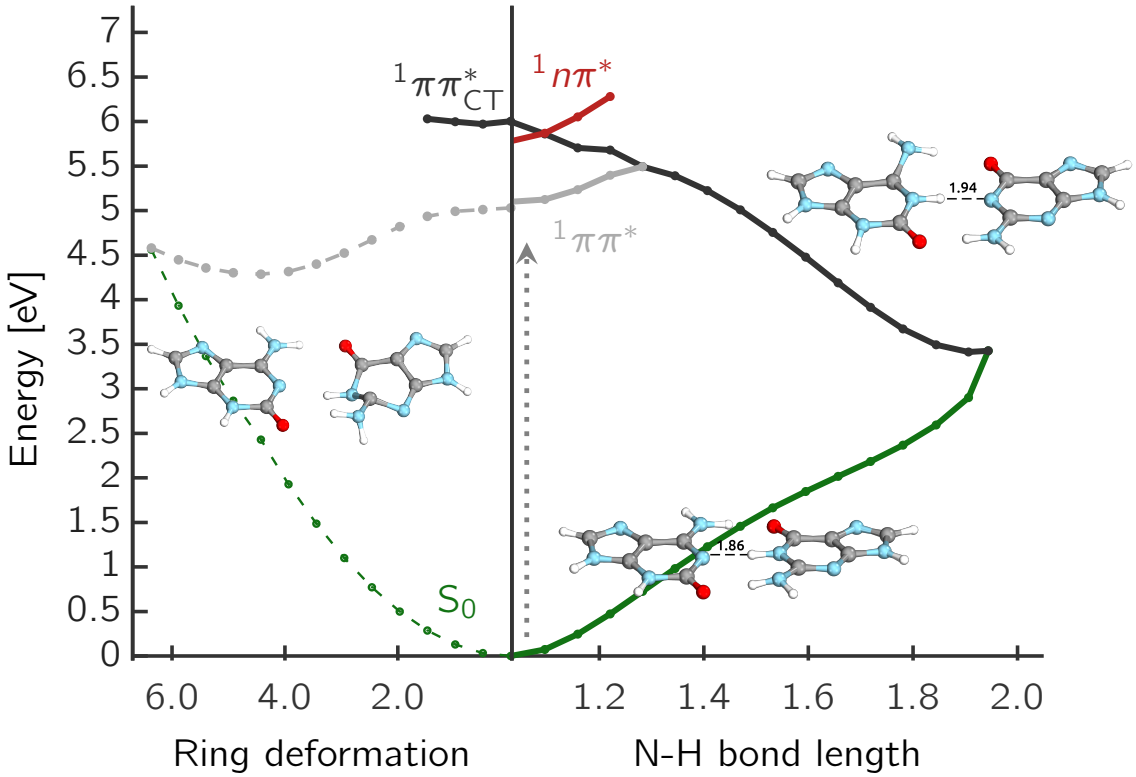

Figure 30. Potential energy surface calculated in the MP2/SCS-ADC(2) of G-iG base pair presents two competitive radiationless decay mechanisms.

In conclusion, the canonical G-C base pair appears to be the best suited for the EDPT process in comparison to the alternative complexes studied. This is an interesting observation in the context of prebiotic chemistry.

2.2.3 Isosteres of A-T/A-U

It has already been discussed that in the canonical base pairs of A-T and A-U the photorelaxation proceeds mostly through the LE $^1\pi\pi^*$ or $^1n\pi^*$ states. The question arises whether there exists a structural modification that may raise the importance of the EDPT channel in these dimers. The oxidative forms of purines generally are better electron donors, and the calculated PE profile of low-lying states in oxoG-C confirmed the feasibility of an efficient

oxoA-U

proton-coupled electron transfer. In the Franck-Condon region (see 8 on page 84), the 0.25 eV redshift of the CT state is found for the oxoA-U base pair. This modification also changes the position of the lowest-lying $^1n\pi^*$ state, which in oxoA-U lies 0.24 eV above the LE bright $^1\pi\pi^*$ state. This may affect the likelihood of the corresponding radiationless pathway.

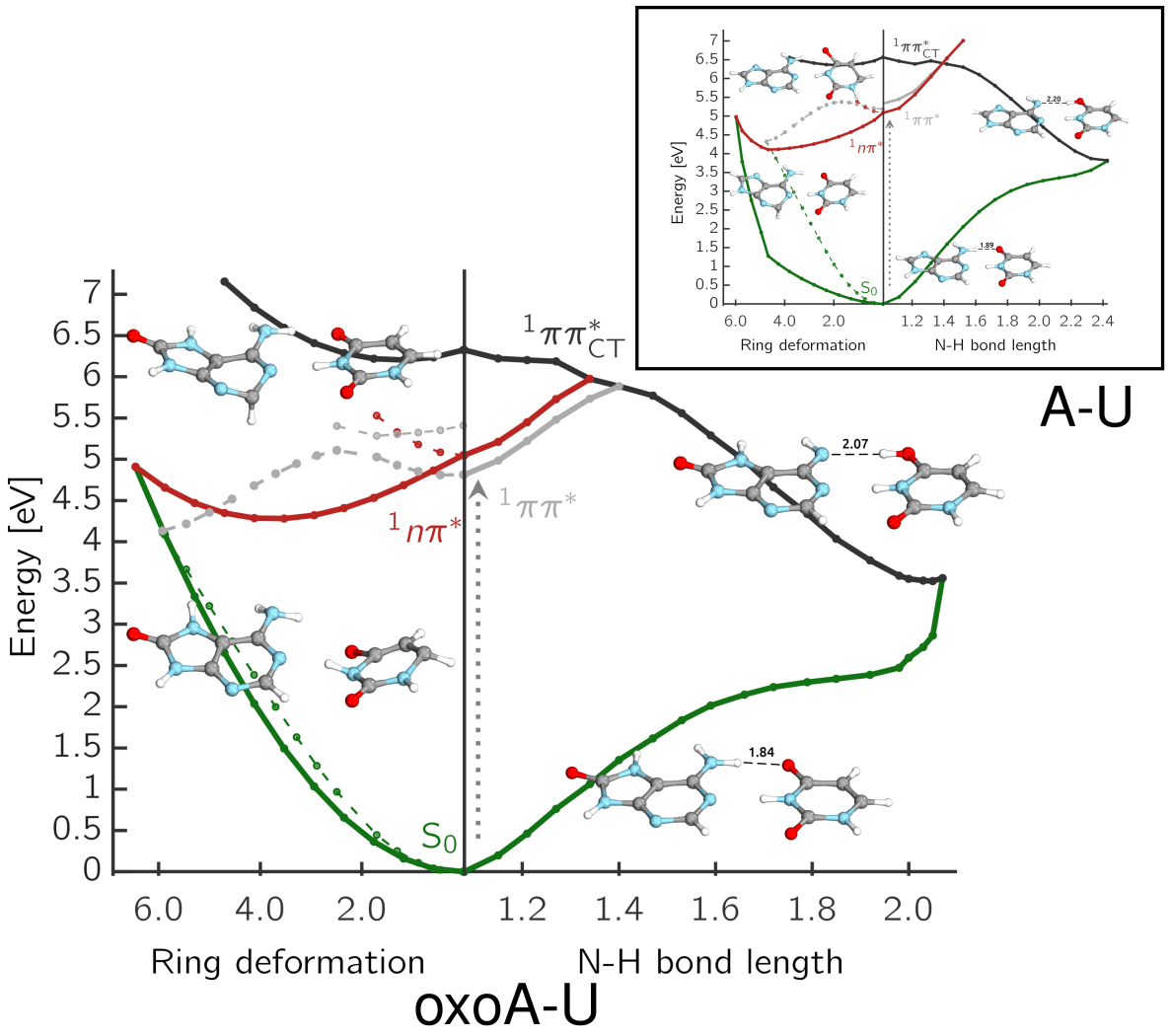

Figure 31. Potential energy cuts presenting selected deactivation mechanisms for oxo-A-U base pair. The corresponding plot for the A-U is shown as an inset for a reference.

The left-hand side of Figure 31 shows interpolated PES cuts between the equilibrium geometry of the ground state and the MECPs with the LE states. There are two plausible photorelaxation pathways that proceed on the hypersurfaces of the LE states of the oxoA-U base pair, both of which involve puckering of one of the nucleobases. The mass-weighted coordinates indicated on the horizontal axis reflect the changes within the purine or pyrimidine ring deformation. The puckering of U on the $^1n\pi^*$ PE surface leads to a sloped MECP with S_0. There is also a smaller energy gap between the minimum of the first excited state and the MECP found than in the canonical base pair. The puckering of the C2 atom of oxoA leads to a peaked MECP with S_0, however, through a small PE barrier. Therefore, even though the latter occurs on the PE surface of a bright state, both processes might be possible. On the right-hand

side of the plot, the EDPT process via (oxoA)NH_2···O(U) bond extension is presented. The EDPT process is due to the strong stabilization of the $^1\pi\pi^*_{CT}$ state along the proton transfer coordinate and leads to the barrierless crossing with the ground state. This MECP occurs at 3.81 eV, that is 0.25 eV lower than in the A-U. The CT state lies lower also in the FC region, but there is still a large barrier to reaching the MECP of the bright LE state with the CT state.

Since adding the carbonyl group to purine only slightly increased the chance to populate the $^1\pi\pi^*_{CT}$ excited state, further analysis included the substitution of a hydroxy group to uracil, forming the base pair of adenine-barbituric acid (A-B). However, the opposite effect was achieved since the $^1\pi\pi^*$ state of CT character in A-B is firmly blueshifted in the FC region. As a result, the EDPT process, which requires the population of the CT state at a higher excitation energy, is less likely to be reached in this system. Thus, similarly to that observed in oxoA-U, the intramolecular processes likely govern the non-radiative deactivation.

A-B

The population of the first excited state of $^1\pi\pi^*$ character through the efficient crossing with the lowest bright state (S_2) lying 0.16 eV above, can lead to the $S_1\pi\pi^*$ minimum associated with the puckering of the purine C2 atom. Unlike in A-U, reaching this minimum from the lowest-lying bright state is a barrier-free process, but the corresponding MECP lies 0.28 eV above it. The PE cuts presenting the described mechanisms are plotted in Figure 32, where the EDPT process is shown on the right-hand side of the graph and the purine (A)C2-oop path is shown on the left-hand side, plotted with lines with points.

Another efficient relaxation mechanism proceeds through the C6-atom puckering coordinate (dashed lines). It leads to the MECP with the ground state, exactly as in the former; except in the A-B dimer, this MECP is reached in an efficient barrierless manner and is located at lower excitation energy than the MECP associated with the C2-atom puckering. However, reaching the structure of the MECP associated with the (A)C6-oop requires a major geometrical change. This path leads to the propeller twist of the A-B dimer to 84.7°, thus it may not be possible in the nucleic acid duplex. This topic was thoroughly discussed on page 71 in Subsection 2.1.3.

The LE $^1n\pi^*$ state of the barbituric acid lies above the two discussed LE $^1\pi\pi^*$ states in the Franck-Condon region. However, when populated, it can efficiently evolve to the minimum energy S_1 of the $^1n\pi^*$ character with no PE energy barrier involved. From this point, the respective conical intersection can be reached; however, it has a steeply sloped character. This indicates that this process may extend the excited state lifetime of A-B and possibly lead to the population of the triplet manifold due to the long-living $^1n\pi^*$ state.

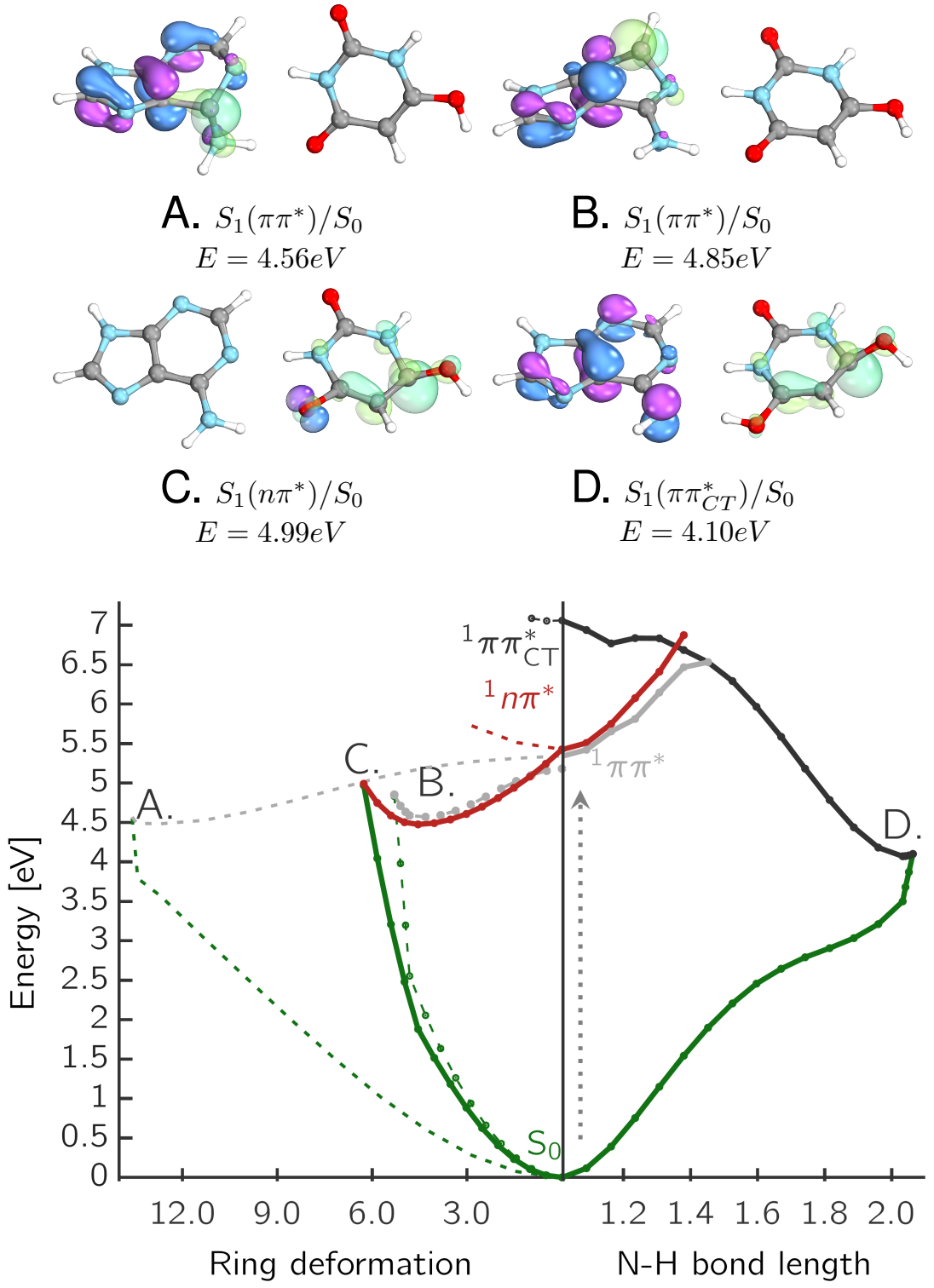

Figure 32. Potential energy cuts presenting selected deactivation mechanisms for A-B base pair.

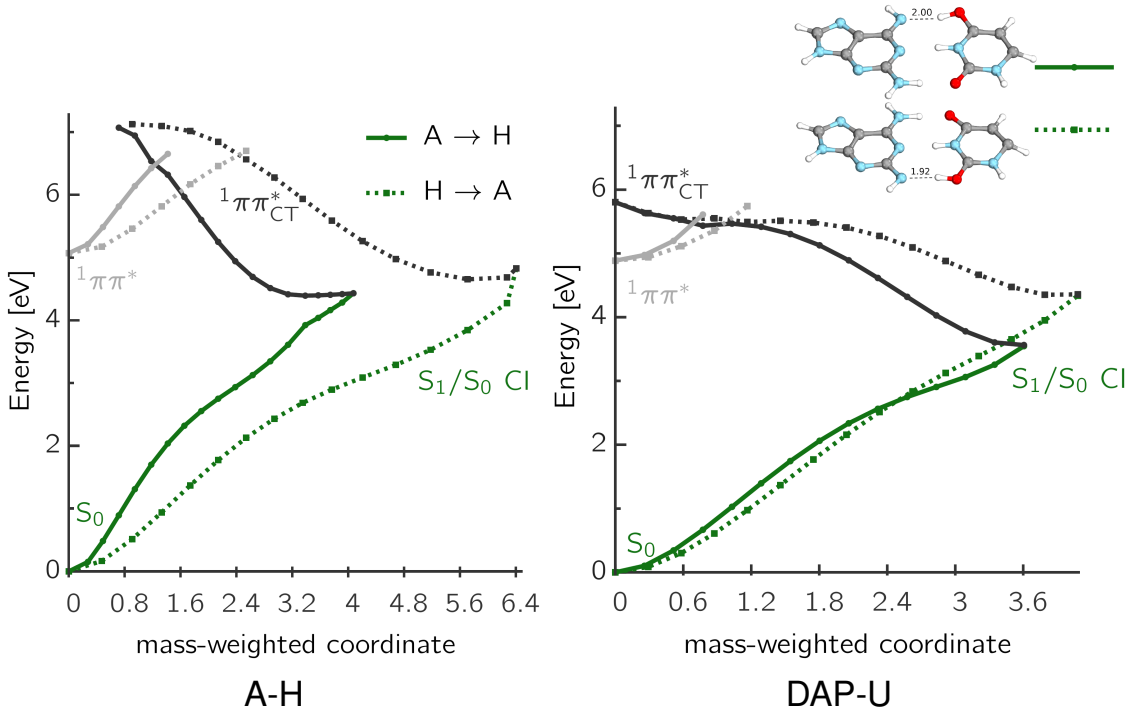

Figure 33. Potential energy cuts along mass-weighted coordinates for A-H and DAP-U base pairs, presenting two possible proton transfer processes along two different hydrogen bonds. The calculations were performed using the SCS-MP2/SCS-ADC(2) method.

A-H

Complementing adenine with another purine, hypoxanthine (A-H) yields only LE states within the 15 lowest-lying states in the Franck-Condon region. Since adenine and hypoxanthine have similar ionization potentials, the EDPT mechanism could in principle occur in both ways. Therefore, an attempt was made to locate the minima of the first excited state for both cases. The calculations returned geometries almost identical to the respective MECPs with the ground state (the excitation energies differ by less than 0.1 eV). The respective crossings of the optically bright and CT states along the proton transfer coordinate are found at a similar energy level; interpolation along the mass-weighted coordinates shown in Figure 33 indicates that the proton is transferred rather from the adenine to the hypoxanthine than in the reverse direction. The transfer along the central hydrogen bond is therefore not favorable in the A-H dimer. From this point of view, the vertical excitation energies in the Franck-Condon region of A-H are akin to those of the A-B base pair with the same H-bonding motif.

The MECP reached through the EDPT from A to H is located at 4.43 eV, which is 0.4 eV below the MECP corresponding to the opposite direction of proton transfer. Due to the apparent inaccessibility of the $^1\pi\pi^*_{CT}$ state from the Franck-Condon region, efficient photorelaxation of this dimer may be reached only through the LE states. In fact, adenine puckering at the C2

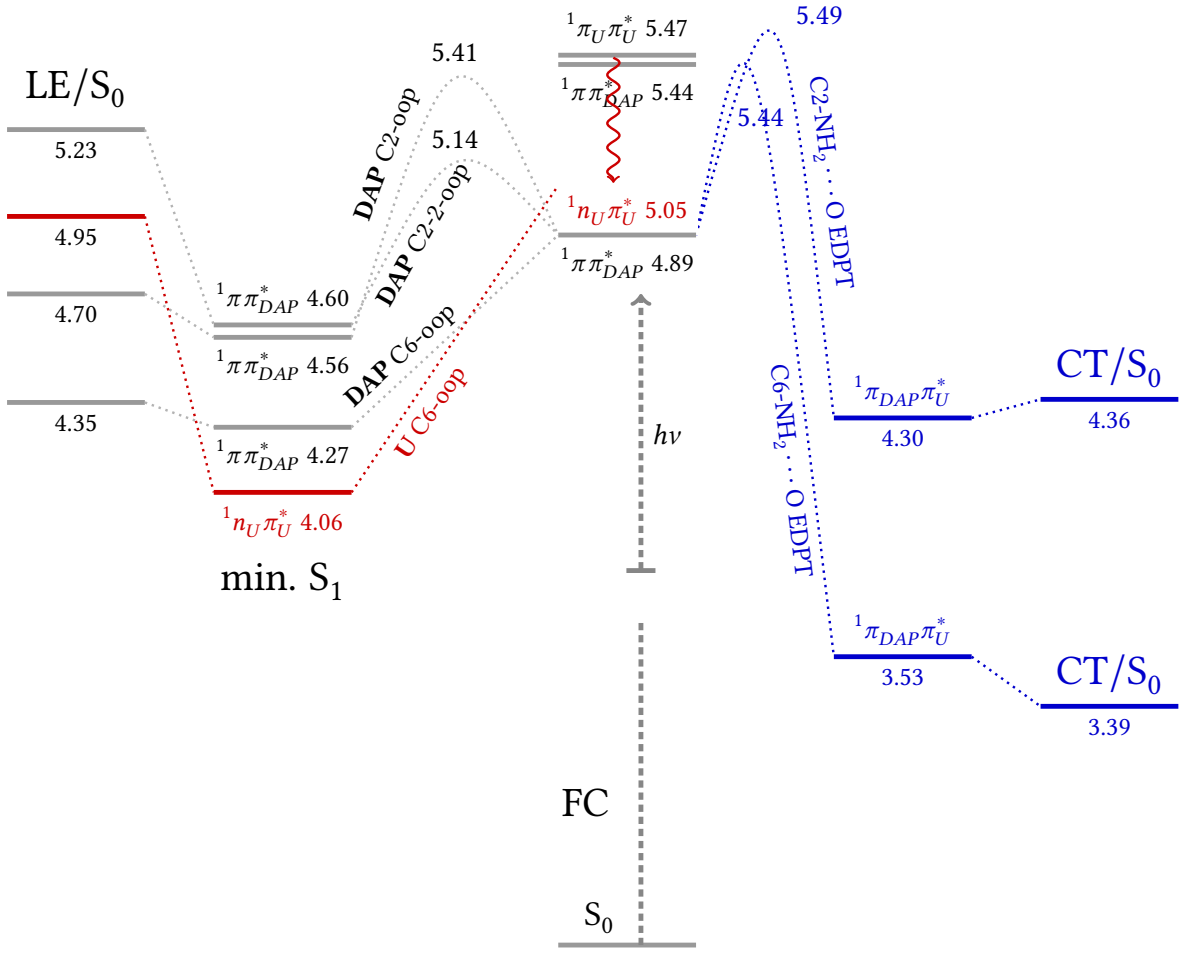

Figure 34. Schematic presentation of the radiationless deactivation mechanisms in the DAP-U base pair.

atom position leads to $\pi\pi^*_{\mathrm{LE}}/S_0$ MECP located at 4.19 eV. Therefore, the MECP of the EDPT lies higher on the potential energy profile than the MECP arising on the LE state hypersurface, which is rare. Notably, the $^1n\pi^*_{\mathrm{LE}}$ state in the FC region of A-H is also significantly separated from the lowest-lying $^1\pi\pi^*$ state, which is the effect of substitution of pyrimidine with the purine moiety in the complementary base pair. Therefore, this state likely does not participate in the photorelaxation of the A-H base pair.

Another mimetic of the A-U base pair considered is the non-biological 2-6-diaminopurine-uracil (DAP-U). It is yet another example of alteration of the photochemical behavior of a base pair by substitution in the C2 position of purine. The presence of the NH_2 functional group in this position lowers the energy of the bright and CT state in the Franck-Condon region and CT/S_0 MECP outside this region; it also changes the PE surface, which becomes more flat. In

DAP-U

the right panel of Figure 33, the cuts of the low-lying $^1\pi\pi^*$ PE surfaces of CT and LE character are presented along the mass-weighted coordinate that reflects the transfer of the protons along the two different hydrogen bonds, shown in the inset. Although both pathways lead to a crossing with the ground state in a virtually barrierless manner, the MECP arising along the (DAP)C6-$NH_2 \cdots$ O-C4(U) hydrogen bond lies significantly lower on the PE profile. As previously concluded, this proton transfer coordinate is preferable in all investigated systems if transfer along the central hydrogen bond is impossible (except for the iG-iC base pair).

The schematic representation of possible radiationless decay paths in the DAP-U base pair is shown in Figure 34. The population of the $^1n\pi^*$ state that lies above the bright state in the FC region leads to a minimum energy structure that is separated by 0.89 eV from the steeply sloped MECP with the ground state. This topology of the PE surface indicates that the trapping of the population in S_1 $^1n\pi^*$ may lead to ISC to a triplet manifold. The population of this state should extend the excited state lifetime.

Photorelaxation of DAP-U can also occur through the $^1\pi\pi^*_{LE}$ hypersurface. Indeed, MECPs characterized by puckering of DAP at either the C2 or C6 atoms positions were located that are virtually identical to those of the A-U. The first MECP lies 0.63eV above the corresponding PE minimum of the S_1 $\pi\pi^*$ state. However, to reach this minimum, the population of the higher-lying optically accessible state is required, precisely as in the A-U or oxo-A-U base pairs. Another path leads to an apparently more efficient conical intersection with the ground state at 4.70 eV which lies 0.14 eV above the S_1 minimum. However, even more energetically preferable is the path through puckering at the C6 atom of DAP, which is barrierless and the MECP with the ground state lies only 0.08 eV above the S_1 minimum. It should be noted that the corresponding structural changes involve significant displacement of the dimer; in particular, the propeller twist parameter totals 59.7°. Thus, as discussed in case of A-T results, it may not be accessible in the nucleic acid structure.

DAP-X

Substitution of pyrimidine with purine in 2,6-diaminopurine-xanthine (DAP-X), increased the energy gap between $^1n\pi^*$ and the lowest bright $^1\pi\pi^*$ states. However, the CT state is also blueshifted in this base pair. As a result, the EDPT process becomes available at higher excitation energies (see Figure 35). The $^1\pi\pi^*_{CT}$ state is strongly stabilized along the (DAP)C6-$NH_2 \cdots$ O(X) hydrogen bond and leads to a crossing with the ground state at 3.81 eV.

The alternative path involving DAP C6 atom puckering (dashed lines) appears to be easily accessible from the lowest optically allowed $^1\pi\pi^*$ state leading to the MECP located at 4.33 eV. This MECP is separated by less than 0.1 eV from the respective S_1 minimum. Similarly as in the A-B pair, there is also a path through the C2 atom of DAP (dashed lines with points) that

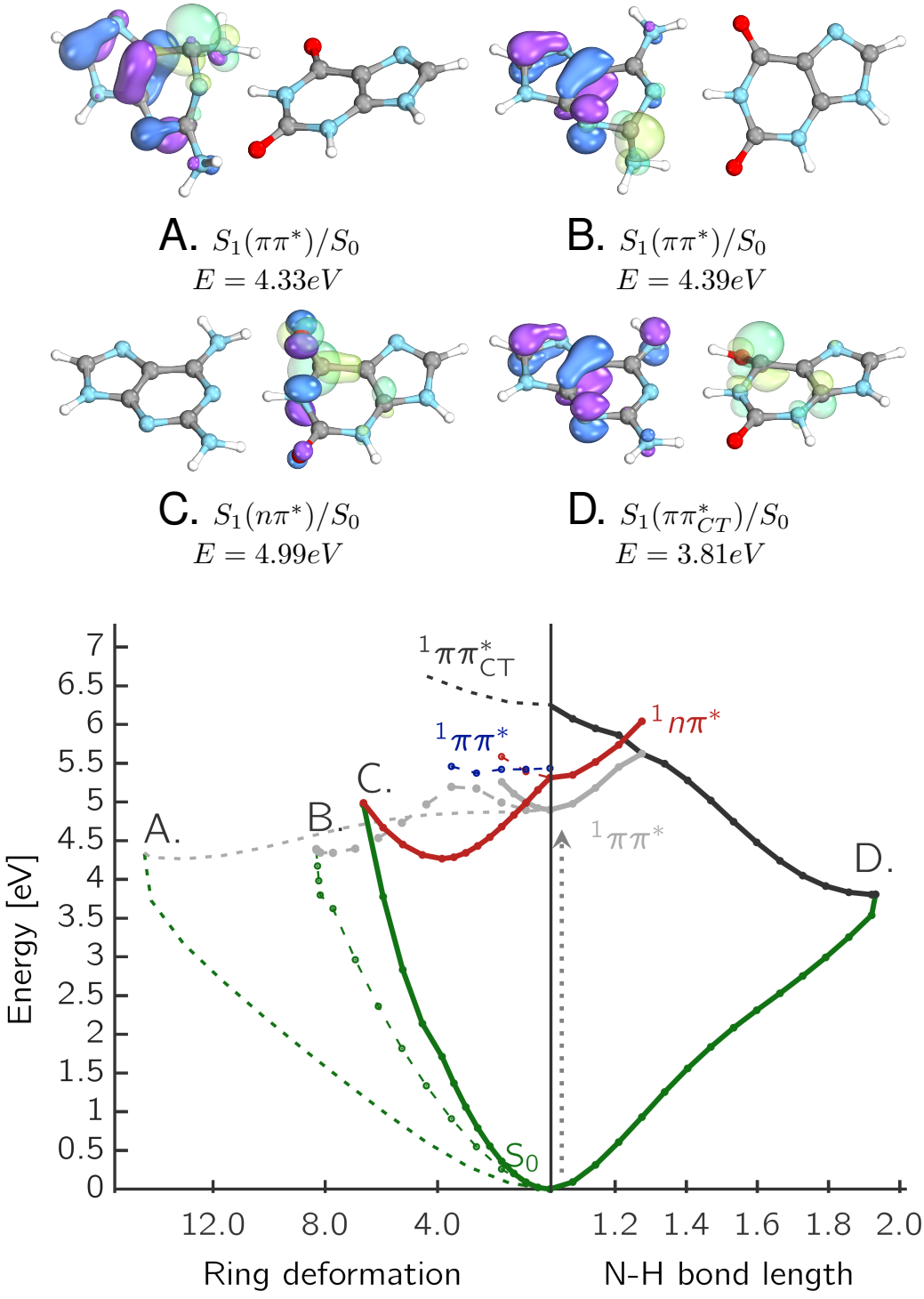

Figure 35. Potential energy cuts presenting selected deactivation mechanisms for DAP-X base pair.

proceeds through a small PE barrier. The least plausible seems to be the path that involves the $^{n}\pi^{*}$ transition localized on xanthine, but the population of this state should be detectable experimentally, as it would most likely lead to a slow component in a multiexponential decay and possibly ISC due to the steeply sloped MECP with the ground state. It should be noted that the decay path through the geometry of xanthine similar to that reported by Yamazaki, Sobolewski and Domcke[279] was not found in the DAP-X base pair.

oxoDAP-U

The 8-oxo-derivative of DAP concatenated with the uracil constitutes another isostere of the A-U base pair. The calculated vertical excitation energies (see Table 8 on page 84) and PE cuts (Figure 36) indicate that its photochemistry should be similar to that of DAP-U and DAP-X. The most noticeable difference is the increase in vertical excitation energy of the S_2 $n\pi^{*}$ state, located mainly on the uracil, which lies 0.55 eV above the lowest bright state, and the corresponding MECP has an even more steeply sloped character. On the left-hand side of Figure 36 the two ring-puckering paths on the $^{1}\pi\pi^{*}_{\mathrm{LE}}$ hypersurface are shown, of which the C6-NH_2 puckering is again more plausible. The crossing of the bright state with $^{1}\pi\pi^{*}_{\mathrm{CT}}$ is relatively close to the FC region and although it has a sloped character (as in other base pairs including G-C) it seems to be accessible, allowing the dimer to relax along the proton transfer coordinate through a very low-lying peaked MECP at 2.76 eV.

In the search for plausible components of primordial RNA, Cafferty and Hud[131,132] investigated 81 heterocycles that might be hypothetical protoRNA building blocks, capable of glycosylation and self-assembly. As the most promising in this context, they pointed to the complexes of melamine with uracil (M-U) and barbituric acid (M-B), as well as 2,4,6-triaminopyrimidine with barbituric acid (TAP-B).[166,280,281] These complexes could be considered as isosteres of A-T or A-U base pairs, consisting only of pyrimidine nucleobases. These molecules are also prone to spontaneous assemblage due to stacking interactions.[131,132]

M-U

The calculated vertical excitation energies of M-U (Table 8 on page 84) show that the $^{1}\pi\pi^{*}$ state located on the melamine lies 0.14 eV above the lowest bright state, which is $^{1}\pi\pi^{*}$ located on the uracil. Although the LE $^{1}\pi\pi^{*}_{\mathrm{M}}$ state has a relatively small oscillator strength, both states could be directly populated.

[279] S. Yamazaki, A. L. Sobolewski, and W. Domcke, *Physical Chemistry Chemical Physics*, **2009**, *11*, 10165–10174.
[280] C. Li, B. Cafferty, S. Karunakaran, G. Schuster, and N. Hud, *Physical Chemistry Chemical Physics*, **2016**, *18*, 20091–20096.
[281] M. C. Chen, B. J. Cafferty, I. Mamajanov, I. Gállego, J. Khanam, R. Krishnamurthy, and N. V. Hud, *Journal of the American Chemical Society*, **2013**, *136*, 5640–5646.

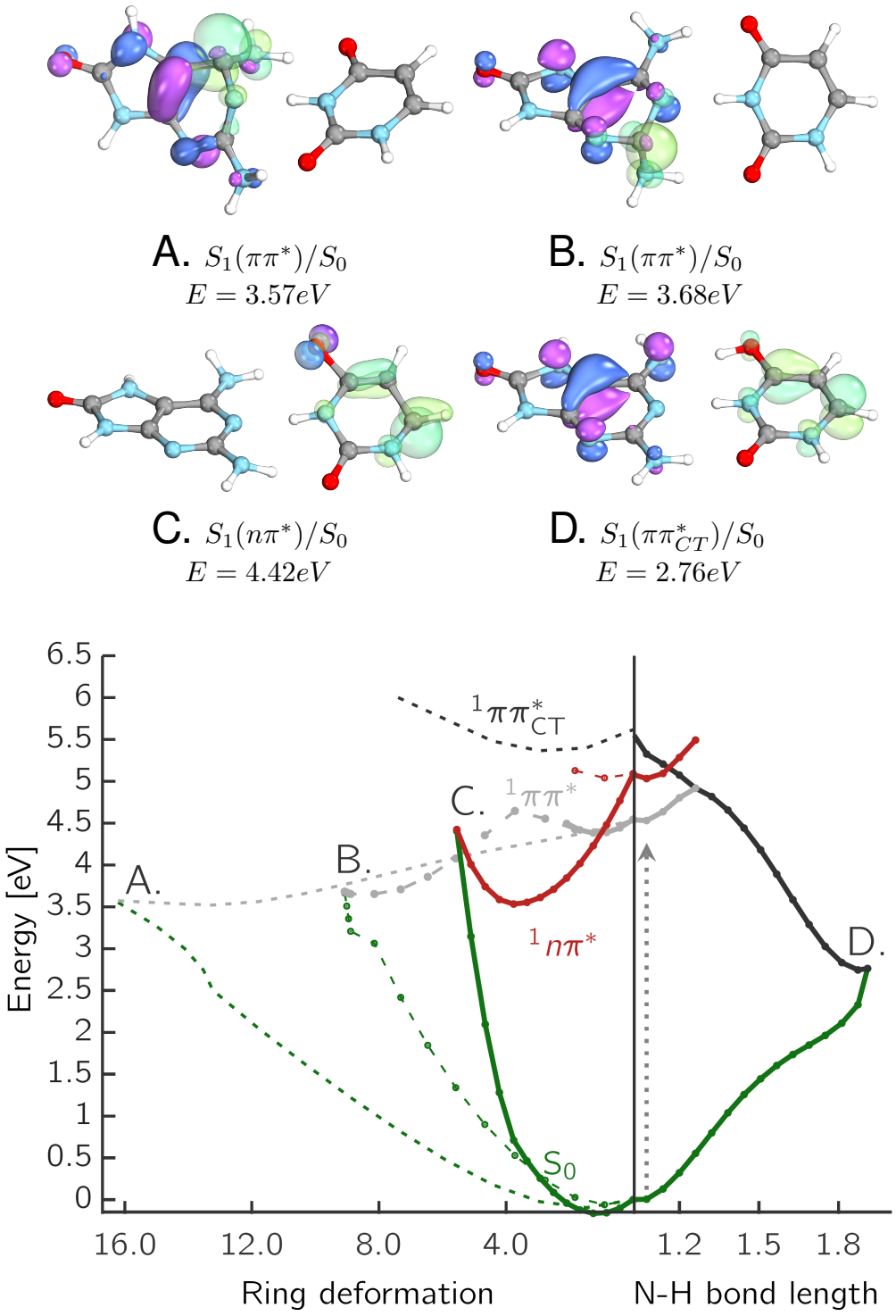

Figure 36. Potential energy cuts presenting selected deactivation mechanisms for oxoDAP-U base pair.

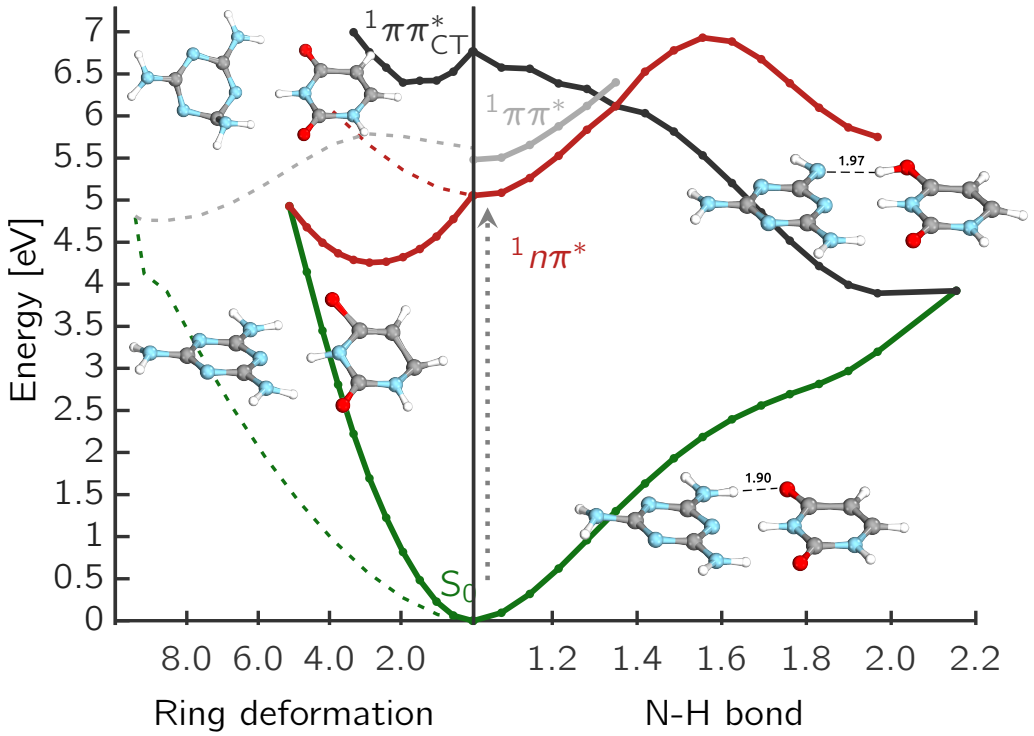

Figure 37. Potential energy cuts presenting selected deactivation mechanisms for M-U base pair.

Relaxation on the $^1\pi\pi^*_M$ PE surface manifests itself as puckering at the C4 atom of melamine (the labeling of atoms is preserved as in the other pyrimidines). The corresponding MECP is found at 4.81 eV. The relevant PE cuts are shown on the left-hand side of Figure 37. Since melamine has a highly symmetrical structure, it is interesting to note that the MECP associated with the puckering of the melamine ring at the position of the C2 atom is energetically unfavorable compared to the (M)C4-oop. The $^\pi\pi^*_{CT}$ state is found at 6.77 eV in the FC region. Once populated, the dark excited CT state should contribute to efficient photorelaxation to the ground state along the N-H bond elongation through MECP at 3.92 eV. The corresponding LIIC between the equilibrium geometry, minimum of the S_1 excited state and MECP is presented on the right-hand side of Figure 37.

This system is characterized by a low-lying dark $^1n\pi^*$ state (even below the lowest bright state). The population of this state located on the uracil should lead to a relatively efficient barrier-free population of the S_1 minimum at 4.07 eV. Similarly as in other studied base pairs, this could lead to population trapping and further deactivation either to the ground state through sloped MECP located 0.86 eV above the minimum or to the triplet manifold through ISC. Therefore, this pathway would certainly extend the lifetime of M-U.

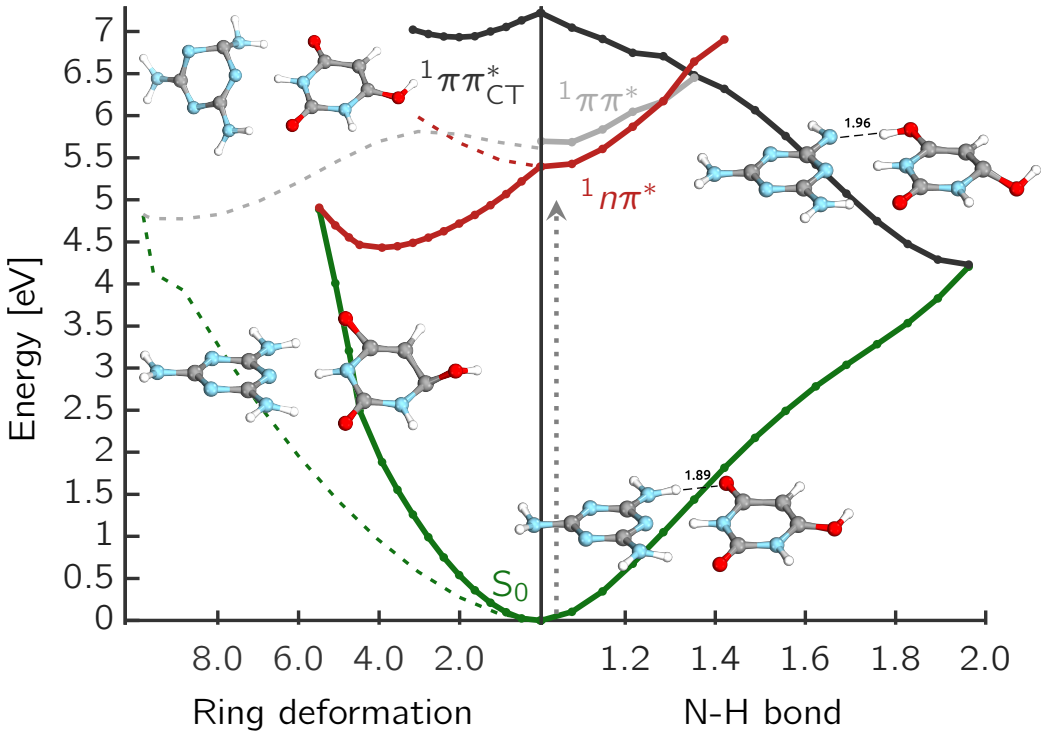

Figure 38. Potential energy cuts presenting selected deactivation mechanisms for M-B base pair.

The calculated PE cuts for the M-B dimer are quite similar (see Figure 38). However, the EDPT process becomes operative at even higher excitation energies. The MECP of $^1n\pi^*/S_0$ states can be reached through the population of the S_1 minimum and then a small barrier of 0.48 eV (shown in solid lines). It is mainly associated with the elongation of the barbituric acid C4=O bond. The efficiency of the described mechanism is amplified by the position of the $^1n\pi^*$ state below the lowest bright state located on barbituric acid. However, unlike in the M-U base pair, the $^1\pi\pi^*$ state on melamine also lies below the lowest bright state in the FC region. Thus, relaxation on the $^1\pi\pi^*_M$ LE state may be easily accessible from the FC region. The S_1 minimum of the $^1\pi\pi^*$ state, which lies close to the MECP with the ground state, can be populated along the coordinate manifesting itself as puckering of the melamine ring at the position of the C4 atom. This path shows a small PE barrier that might be an artifact of the LIIC procedure. M-B

S_1 excited state in the FC region of TAP-B is the lowest-lying bright state and involves the LE $^1\pi\pi^*$ transition occurring locally on the TAP nucleobase. Therefore, photorelaxation on the hypersurface of this state is easily accessible and leads to S_1 minimum connected with the ring puckering at the C4 atom of the TAP. Notably, the structural changes along this coordinate do not affect the planarity of the remaining structure, as the distorted amino group TAP-B

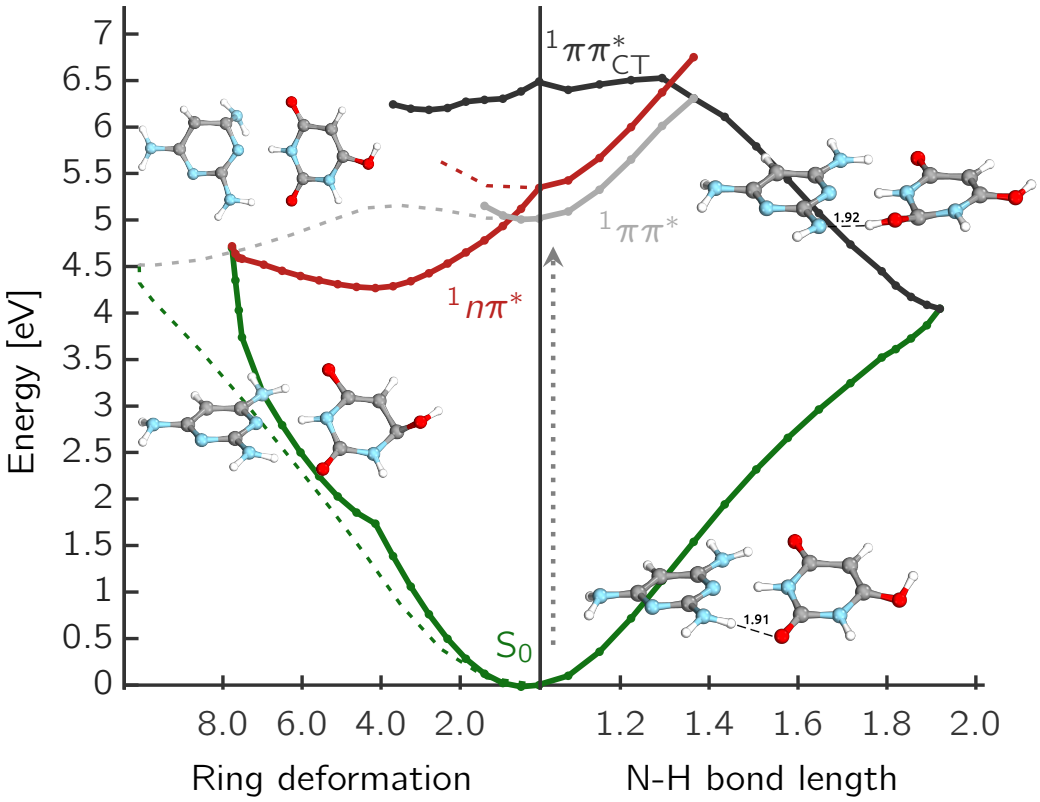

Figure 39. Potential energy cuts presenting selected deactivation mechanisms for TAP-B base pair.

does not interact with the carbonyl group of the barbituric acid. The discussed mechanism is shown on the left side of Figure 39. The minimum on the surface of the S_1 $\pi\pi^*$ state PE is energetically close to the corresponding MECP (0.02 eV). Thus, the conical intersection should be easily reached. The MECP associated with C2-atom puckering was also located, but is energetically unfavorable.

The population of the $^1n\pi^*$ minimum manifesting as the C4=O bond elongation and the out-of-plane distortion of the -OH group is a competing mechanism due to the highly repulsive character of this state. The corresponding sloped $^1n\pi^*/S_0$ MECP lies 0.44 eV above the S_1 minimum and can be reached through a rather flat PE surface. The EDPT process shown on the right-hand side of the graph leads to the lowest-lying MECP. Although the corresponding CT state is redshifted in comparison with the other pyrimidine-pyrimidine base pairs, it becomes available only at higher excitation levels.

3 Final remarks and conclusions

The research findings detailed in this thesis, obtained using quantum chemical computational methods, are twofold. First, Watson-Crick-type canonical base pairs were examined to investigate possible nonradiative relaxation mechanisms discussed earlier in the literature, with a particular focus on the electron-driven proton transfer pathway (EDPT) and processes that proceed through the population of $^1n\pi^*$ locally excited states (LE). This study is to our knowledge the first systematic comparative analysis of selected *intra-* and *intermolecular* channels in canonical base pairs. Second, the analysis was expanded to include base pairs of selected non-biological nucleobases and their analogous.

The results of calculations have supported previous findings regarding the availability of the EDPT photorelaxation channel for canonical base pairs on the surface of $^1\pi\pi^*$ states with intermolecular charge-transfer (CT) character. The intersections between this CT state and the locally excited $^1\pi\pi^*$ and $^1n\pi^*$ states, as well as the ground state, have been located. The earlier studies demonstrated through experimental and theoretical findings that the EDPT channel is accessible for the G-C canonical pair. However, no experimental evidence was found of its availability in the A-U and A-T pairs. According to earlier preliminary theoretical calculations, the population of the CT state could occur at a lower excitation energy level in the G-C, a conclusion that our results have strongly confirmed. Although the EDPT channel was also found in the base pairs A-U and A-T, the relevant $^1\pi\pi^*_{\mathrm{CT}}$ state is shifted in the Franck-Condon (FC) region toward higher energies, and in contrast to G-C, the $^1n\pi^*$ states located on the pyrimidine base lie below the bright states and are thus more accessible in A-U and A-T. It is also known that the WC hydrogen bonding scheme is not preferable in the gas phase complexes of A-U and A-T.

The photorelaxation channels that occur on the surface of the lowest-lying locally excited bright states $^1\pi\pi^*$ were also determined and characterized for the canonical base pairs. These

mechanisms are best described as nonradiative internal conversion through deformation of the purine or pyrimidine ring, with specific consideration given to puckering of the purine ring at the positions of the C2 and C6 atoms. This is particularly relevant to the ongoing debate in the literature on this phenomenon in isolated adenine. According to the analysis performed, despite similar energetics, the structural changes accompanying the internal conversion associated with the puckering of the ring at the C6 position may be too severe to be possible in the biological form of B-DNA. Furthermore, it has been established that the minimum energy crossing points (MECP) associated with the channels involving the locally excited states are located at a higher energy level compared to those resulting from the EDPT process. This is an interesting finding, as the availability of the latter has previously sparked controversy in the literature.[22,91]

Very intriguing photochemical pathways have been identified on the surface of LE $^1n\pi^*$ states located on pyrimidine. The canonical A-T and A-U pairs exhibit the potential for a barrierless population of these states; however, subsequent photorelaxation to the ground state proceeds through steeply sloped $^1n\pi^*/S_0$ MECP located roughly 0.9 eV above the S_1 minimum. These observations indicate that the system might be confined in this particular state, which might lead to subsequent intersystem crossing (ISC) to the triplet manifold. The estimated rate of an efficient intersystem crossing to triplet manifold is $1.6 \cdot 10^{10} s^{-1}$, which exceeds by an order of magnitude the corresponding internal conversion to the ground state.

It is interesting to note that by comparison of the ADC(2) and SCS-ADC(2) results with those obtained using NEVPT2 approach, it is evident that while both versions of the ADC(2) method consistently underestimate the excitation energy of the $^1n\pi^*$ states, the SCS-ADC(2) method provides results that are more consistent with the NEVPT2 reference values and provides a more balanced description of the LE and CT states.

Among the most intriguing findings of this thesis is the identification of a previously unreported deactivation pathway for the canonical WC G-C base pair. This mechanism involves proton transfer initiated on the $^1n\pi^*$ excited-state potential energy surface that is triggered by a substantial intermolecular transfer of electronic density. The reported sequential EDPT process is a consequence of interaction within a specific synthon, facilitating exciplex formation through the N—O interaction. This interaction leads to a change in the pairing mode from Watson-Crick to Wobble. Subsequently, the proton is spontaneously transferred from a purine to a pyrimidine. The potential energy profile along the proton transfer (PT) coordinate, which encompasses both phases of the EDPT process and involves the population of the locally excited $^1n\pi^*$ state of a partial CT character, was also validated using the XMS-CASPT2 method.

In the subsequent phase of the study, efforts were directed toward elucidating the potential mechanisms governing the nonradiative relaxation of noncanonical base pairs. Initial analysis of the interactions within the investigated complexes revealed a clear association between the determined interaction energy values and the pattern (synthon) of hydrogen bonds. These findings highlight the influence of the individual exocyclic groups that participate in proton exchange along the hydrogen bond on the strength of the intermolecular interactions. The analysis of interaction energy components revealed notable distinctions in the character of interactions within isosters of WC G-C and WC A-T/A-U. The former ones are predominantly governed by induction and charge-delocalization interactions. In contrast, in A-T/A-U biomimetics, the stabilization resulting from the electron correlation is increased, while the interactions of unperturbed monomers become repulsive. Therefore, the total interaction energy in the latter group of complexes typically shows relatively lower values.

The results of the calculations do not indicate that any correlation exists between the ionization potential (IP) of the base (or the redox potential within the studied base pairs) and the excitation energy of the CT state. However, IP alone seems to be a good predictor of the direction of electron and proton transfer from one base to another. Furthermore, the calculated vertical excitation energies in the Franck-Condon region supported the existence of alternative base pairs to the G-C that feature remarkably low-lying intermolecular CT states, which are recognized to play a role in the EDPT process. Our results also demonstrated that purine oxidation at the C8 position systematically reduces the energy of the aforementioned CT state in the Franck-Condon region.

Interestingly, we noticed that although the bioisosters of the G-C base pair exhibit the synthon characteristic for exciplex formation in the $^1n\pi^*_{\mathrm{CT}}$ state, similar to the Wobble G-C pair, the lowest singlet $^1n\pi^*$ state has a partial CT character only in the case of hypoxanthine-cytosine (H-C), 8-oxo-H-C (oxoH-C), and 8-oxo-G-C (oxoG-C) pairs. For the first time, the WC-to-Wobble photorelaxation path on the $^1n\pi^*_{\mathrm{CT}}$ potential energy surface was identified for the H-C and oxoG-C base pairs, indicating the accessibility of this channel. It is evident that concerted (non-sequential) proton transfer on the surface of the $^1n\pi^*_{\mathrm{CT}}$ state should occur spontaneously. However, the population of this excited state by crossing the LE and CT states necessitates overcoming a small energy barrier. In contrast, for the suggested sequential EDPT process occurring on the surface of the $^1n\pi^*_{\mathrm{CT}}$ state, a significant conformational change is required, despite its barrierless character. It should be noted that in the H-C and oxoH-C base pairs, the $^1n\pi^*$ state in the Franck-Condon region lies below the $^1\pi\pi^*_{\mathrm{CT}}$ state. Therefore, it is hypothesized that the sequential mechanism of EDPT with the change of pairing type

from Watson-Crick to Wobble may serve as a significant photorelaxation channel in these systems, particularly under lower-energy range UV irradiation.

In the context of bioisosters of the A-U and A-T base pairs, the results have led to the conclusion that the presence of low-lying long-living $^1n\pi^*$ states may be a significant factor in the relaxation handicap through the electron-driven proton transfer process. Evidently, unlike EDPT, photorelaxation on the surface of the electronic LE $^1n\pi^*$ state is not a barrierless process. The high energy barrier to reach the MECP with the ground state is expected to result in a longer lifetime of the $^1n\pi^*$ state, potentially leading to the population of the triplet manifold and, consequently, the formation of photoproducts and the photodegradation of nucleic acids. However, in the set of alternative base pairs considered, there are systems in which this energy barrier is relatively small (< 0.5 eV), suggesting, instead, the efficient photorelaxation through this channel. Our investigation of A-U and A-T isosteres revealed that the EDPT channel on the surface of the $^1\pi\pi^*_{\mathrm{CT}}$ state is present in all dimers studied. Furthermore, the MECPs associated with this process were the lowest-lying among all studied systems, with the exception of the unconventional base pair of two purines, adenine-hypoxanthine (A-H). Interestingly, the introduction of certain structural modifications, such as the addition of a functional group -NH2 at the C2 position and oxidation at the C8 position of adenine, leading to the oxoDAP-U base pair, appears to render the EDPT channel that should be accessible in the FC region, similarly to the canonical G-C base pair, upon exposure to UV light.

In conclusion, this thesis marks significant progress in our understanding of conical intersections between excited states that have $^1n\pi^*$ character with the ground state in both canonical and alternative base pairs. The findings of computational studies indicate that the long-lived, reactive $^1n\pi^*$ states, previously thought to contribute to photodamage in isolated pyrimidine nucleosides, may instead assist in efficient photodeactivation. The research identifies and characterizes two distinct categories of radiationless deactivation pathways that proceed through the potential energy surface of $^1n\pi^*$ states. One potential mechanism involves a single-step process in which the pyrimidine ring distorts upon excitation, eventually leading to photorelaxation of the base pair to the ground electronic state. Furthermore, in some WC-type base pairs, namely G-C and some of its bioisosteres, the population of the $^1n\pi^*$ states may trigger a two-step sequential EDPT process involving WC-to-Wobble isomerization. Moreover, in all systems studied, the $^1\pi\pi^*$ charge transfer state connects the LE states with the ground state through a cascade of conical intersections. Its availability may vary, and further studies are needed to investigate the nonadiabatic dynamics. However, considering the experimental evidence for the occurrence of an EDPT process in the G-C base pair in

the gas phase, the similar potential energy profile found in several of the base pairs studied indicates a high probability of the availability of this channel, which we hope will inspire further experimental work.

Extended abstract in Polish

Wstęp

Postęp technik spektroskopowych umożliwił na początku lat dwutysięcznych uzyskanie czasowo-rozdzielczych widm elektronowych i oscylacyjnych izolowanych par zasad kwasów nukleinowych.[3] Kompleksy te mogą występować w formie konformerów, różniących się geometrią i topologią wiązań wodorowych.[3,10,18] Dzięki wyrafinowanym technikom podwójnego rezonansu laserowego i obliczeniom z pierwszych zasad możliwe było przypisanie obserwowanych widm do określonych konformerów. Badania te doprowadziły do odkrycia nowego mechanizmu dezaktywacji stanu wzbudzonego, który jest specyficzny dla układów aromatycznych z wiązaniami wodorowymi. Niezwykle krótki czas życia stanu wzbudzonego konformeru Watsona-Cricka (WC) kanonicznej pary zasad guanina-cytozyna (G-C) oraz wyjątkowo słabe i szerokie pasmo w widmie wzmocnionej rezonansowo jonizacji wielofotonowej, wyraźnie różniące się od silnych i ostrych sygnałów obserwowanych dla innych konformerów, w połączeniu z obliczeniami z zasad pierwszych doprowadziły do zaproponowania tezy o dużym znaczeniu mechanizmów koncertowego przeniesienia elektronu i protonu dla fotofizyki tych układów.[97,104] Mechanizm ten nazwano wspomaganym elektronowo procesem przenoszenia protonu (ang. *electron-driven proton-transfer*, EDPT),[104] określanym niekiedy jako sprzężone przeniesienie elektronu i protonu (ang. *proton-coupled electron transfer*, PCET).[108,282]

Charakterystyczną cechą tego procesu jest obecność nieabsorbującego (określanego często w literaturze jako ciemny) stanu elektronowego o charakterze przeniesienia ładunku (ang. *charge-transfer*, CT). Obsadzenie tego stanu prowadzi do przeniesienia elektronu z jednej zasady na drugą. Wywołana tym procesem zmiana rozkładu gęstości elektronowej jest z kolei siłą napędową dla przeniesienia protonu. Powierzchnia energii potencjalnej (ang. *potential*

[282] S. Hammes-Schiffer, *Energy and Environmental Science*, **2012**, *5*, 7696–7703.

energy surface, PES) stanu CT, stabilizowanego silnie przez przeniesienie protonu, ma charakter repulsywny i przecina się zarówno ze stanem lokalnie wzbudzonym, obsadzonym w wyniku fotowzbudzenia, jak i stanem podstawowym, co umożliwia bezpromienistą relaksację.[26]

Cel i znaczenie badań

Zjawisko to jest szczególnie dobrze udokumentowane dla kanonicznej pary zasad kwasów nukleinowych WC G-C.[96,103–106] Jednak, analogiczny mechanizm EDPT, mimo doniesień teoretycznych o jego dostępności,[15,114] do dnia dzisiejszego nie został potwierdzony eksperymentalnie dla kanonicznej pary zasad WC adenina-tymina (A-T). Jednym z powodów może być fakt występowania niskoleżących stanów o charakterze $^1n\pi^*$,[116,172] których obsadzenie może wpływać na fotodynamikę tych układów poprzez konwersję wewnętrzną lub przejścia międzysystemowe na powierzchni stanów wzbudzonych zlokalizowanych na pirymidynie[67,176] lub purynie.[116] Ponieważ przeszkodą w efektywnej relaksacji na drodze wymiany protonu wzdłuż wiązania wodorowego mogą być procesy zachodzące z udziałem jednej z zasad, w niniejszej rozprawie przeprowadzono porównawczą analizę możliwych kanałów bezpromienistej dezaktywacji w kanonicznych i niekanonicznych parach zasad kwasów nukleinowych z uwzględnieniem procesów zarówno wewnątrzcząsteczkowych jak i międzycząsteczkowych. Zasadniczym celem tej analizy jest **określenie roli nisko-leżących singletowych stanów $n\pi^*$ w procesie fotorelaksacji badanych układów w odniesieniu do konkurencyjnych procesów fałdowania pierścienia zachodzących na powierzchni stanów $^1\pi\pi^*$ oraz kanału EDPT**.

Jeżeli odporność na promieniowanie ultrafioletowe (UV) była, jak się postuluje,[28] istotnym czynnikiem selekcyjnym na wczesnych etapach prebiotycznej chemicznej ewolucji polimerów informacyjnych, zbadanie fotostabilności nie tylko kanonicznych, ale również niekanonicznych zasad azotowych parowanych wedle schematu WC powinno dać odniesienie do tych założeń. Warto podkreślić, że fotostabilność kanonicznych par zasad została już szeroko opisana w literaturze, ale do tej pory badania relaksacji stanu wzbudzonego dla niekanonicznych par zasad wykonano jedynie dla par niebiologicznych typu WC, w których puryna jest utleniona w pozycji C8.[129,164,283] Analiza fotofizyki i fotochemii alternatywnych par niekanonicznych zasad azotowych może przyczynić się do wyjaśnienia roli procesów przeniesienia ładunku pomiędzy zasadami po absorpcji promieniowania UV. Tym samym, badania te pozwolą również na lepsze zrozumienie, dlaczego organizmy żywe wykorzystują tak wąski zestaw elementów budulcowych kodu genetycznego. Co ważne, wybór badanych w ramach rozprawy par niebiologicznych zasad został podyktowany po części doniesieniami zespołów pracujących nad syntezą hipotetycznych prekursorów nukleotydów w warunkach zbliżonych do tych panujących na młodej Ziemi.[131,142]

[283] Y. Zhang, J. Dood, A. A. Beckstead, X.-B. Li, K. V. Nguyen, C. J. Burrows, R. Improta, and B. Kohler, *The Journal of Physical Chemistry B*, **2015**, *119*, 7491–7502.

Zasadniczym celem badań prowadzonych w ramach niniejszej rozprawy doktorskiej jest zatem **określenie mechanizmów przeniesienia ładunku po absorpcji promieniowania UV pomiędzy zasadami azotowymi, a w konsekwencji identyfikacja nowych, nierozważanych wcześniej procesów bezpromienistej fotorelaksacji**. Według stawianej hipotezy badawczej, istnieją alternatywne kanały dezaktywacji par zasad azotowych poprzez międzycząsteczkowe przeniesienie ładunku wynikające z ich wzajemnego oddziaływania w stanach elektronowo wzbudzonych.

Opis rezultatów

Wyniki badań własnych opisanych w rozprawie, przeprowadzonych metodami obliczeniowymi chemii kwantowej, podzielić można na dwie zasadnicze części. W pierwszym etapie kanoniczne zasady azotowe typu WC zostały zbadane pod kątem występowania opisanych w literaturze prawdopodobnych mechanizmów relaksacji bezpromienistej zarówno wewnątrzcząsteczkowych jak i międzycząsteczkowych, ze szczególnym uwzględnieniem kanału EDPT oraz procesów zachodzących na powierzchni stanów $^1n\pi^*$. Po raz pierwszy przeprowadzono systematyczną analizę porównawczą wybranych kanałów wewnątrzcząsteczkowych i międzycząsteczkowych w kanonicznych parach zasad azotowych. W kolejnym etapie analizę tę uzupełniono o pary wybranych niebiologicznych zasad azotowych.

Metodologia

Struktura dimerów w stanie podstawowym została zoptymalizowana z wykorzystaniem metody rachunku zaburzeń Møllera–Plesseta drugiego rzędu (MP2) w atomowej bazie funkcyjnej typu cc-pVTZ.[214] Energie wzbudzeń wertykalnych w rejonie Francka–Condona (FC) oraz gometrie lokalnych minimów na powierzchni stanów wzbudzonych zostały wyznaczone za pomocą metody algebraicznej diagramatycznej konstrukcji do drugiego rzędu [ADC(2)][198,284,285] w wariancie skalowanych komponentów spinowych[233] [SCS-ADC(2)]. Charakter stanów wzbudzonych wyznaczono wykorzystując analizę naturalnych orbitali przejścia (ang. *natural transition orbitals*, NTOs). Aby przeanalizować bezpromieniste ścieżki dezaktywacji stanu wzbudzonego, skonstruowano przekroje PES dla stanu podstawowego i niskoleżących singletowych stanów wzbudzonych za pomocą liniowej interpolacji we współrzędnych wewnętrznych (ang. *Linear Interpolation in Internal Coordinates*, LIIC) pomiędzy kluczowymi punktami stacjonarnymi: regionem Francka–Condona, minimum PES stanu S_1 oraz punktem przecięcia tego stanu ze stanem podstawowym o minimalnej energii (ang. *minimum energy crossing point*, MECP). Punkty stacjonarne na powierzchniach energii potencjalnej

[284] J. Schirmer, *Physical Review A*, **1982**, *26*, 2395–2416.
[285] A. Dreuw and M. Wormit, *Wiley Interdiscip. Rev. Comput. Mol. Sci.*, **2014**, *5*, 82–95.

stanu wzbudzonego zlokalizowano przy użyciu metod ADC(2), SCS-ADC(2) oraz NEVPT2 z bazą funkcyjną cc-pVTZ. Geometrie w minimum szwu przecięcia stożkowego zostały zlokalizowane z wykorzystaniem optymalizacji funkcji celu dostępnej w pakiecie CIOpt,[12] sprzężonej z programem Turbomole 7.3, pozwalającym na obliczenia energii i jej analitycznych pochodnych względem zmian współrzędnych geometrycznych na poziomie metody SCS-MP2/SCS-ADC(2). Dzięki tak przeprowadzonym obliczeniom wykreślono profile powierzchni energii potencjalnej wzdłuż interpolowanych współrzędnych reakcji.

Kanoniczne pary zasad

W efekcie przeprowadzonych badań potwierdzono wcześniejsze rezultaty dotyczące dostępności kanału fotorelaksacji kanonicznych par zasad na powierzchni stanów $^1\pi\pi^*$ o charakterze międzycząsteczkowego przeniesienia ładunku (CT), poprzez przecięcia tego stanu z lokalnie wzbudzonymi stanami $^1\pi\pi^*$ oraz $^1n\pi^*$ i stanem podstawowym.[97,114] Wyniki otrzymane metodą SCS-ADC(2) są w tym względzie zgodne z wynikami obliczeń metodą NEVPT2, wykonanymi w pakiecie ORCA.[286,287] Zgodnie z przewidywaniami literaturowymi,[92,112,116] kanał EDPT w przypadku kanonicznej pary G-C wydaje się być łatwiej dostępny niż dla par A-U oraz A-T, ponieważ populacja stanu wzbudzonego CT jest możliwa na niższym poziomie energetycznym. Ponadto w WC G-C, poniżej stanu CT nie występują niskoleżące stany $^1n\pi^*$, których obsadzenie może prowadzić do konkurencyjnych procesów.[116] Energetyka kanału EDPT została porównanana z konkurencyjnymi kanałami fotorelaksacji na powierzchni niskoleżących lokalnie wzbudzonych stanów jasnych $^1\pi\pi^*$ oraz $^1n\pi^*$ prowadzących do bezpromienistej konwersji do stanu podstawowego poprzez deformację purynowego lub pirymidowego pierścienia. Uwzględniono przy tym zarówno fałdowanie pierścienia purynowego w pozycji atomów C2, jak i C6, odnosząc się do wciąż otwartej szerokiej dyskusji literaturowej na ten temat dla izolowanej adeniny.[288] Wykazano również, że pomimo dostępności wymienionych kanałów z regionu FC, ścieżki te mogą prowadzić do zmian strukturalnych, które nie będą dostępne w strukturze kwasów nukleinowych, jak również, że przecięcia stożkowe ze stanem podstawowym położone są wyżej energetycznie niż te wynikające z procesu EDPT, co również jest przedmiotem sporu w literaturze.[22,91]

Na powierzchni stanu $^1n\pi^*$ również zaobserwowano interesujące ścieżki fotochemiczne. Dla kanonicznych par A-T oraz A-U wykazano możliwość bezbarierowej populacji mini-

[286] F. Neese, *WIREs Computational Molecular Science*, **2012**, *2*, 73–78.
[287] F. Neese, *WIREs Computational Molecular Science*, **2018**, *8*, e1327.
[288] M. Barbatti, A. C. Borin, and S. Ullrich, *Photoinduced processes in nucleic acids*, Springer, 2015. DOI: 10.1007/128_2014_569.

mum stanu wzbudzonego. Jednak ewentualną fotorelaksację do stanu podstawowego na powierzchni stanu $^1n\pi^*$ utrudnia wysoka bariera energetyczna wynosząca około 0.9 eV. Wskazuje to na możliwość pułapkowania w tym stanie i przejścia międzysytemowego do stanu trypletowego. Co interesujące, porównanie wyników obliczeń metodami ADC(2) oraz SCS-ADC(2) względem metody NEVPT2 wskazuje, że mimo iż oba warianty metody ADC(2) systematycznie niedoszacowują energię wzbudzeń stanów $^1n\pi^*$, to wariant SCS-ADC(2) poprawia jakościowo zgodność z wartościami referencyjnymi.

Jednak najciekawszym wynikiem uzyskanym w ramach niniejszej rozprawy doktorskiej wydaje się odkrycie nowego, nieopisanego wcześniej kanału dezaktywacji dla kanonicznej pary WC G-C. Proces ten zachodzi na drodze przeniesienia protonu na powierzchni stanu $^1n\pi^*$ indukowanego międzycząsteczkowym przeniesieniem gęstości elektronowej. Ten sekwencyjny proces EDPT jest rezultatem oddziaływania w ramach specyficznego syntonu, który umożliwia powstanie ekscypleksu poprzez oddziaływanie N$\cdots$O i zmianę typu parowania zasad z typu WC na Wobble. Następnie dochodzi do spontanicznego przeniesienia protonu z puryny na pirymidynę. Profil energii potencjalnej wzdłuż współrzędnej przeniesienia tego protonu obejmujący oba etapy procesu EDPT poprzez obsadzenie lokalnie wzbudzonego stanu $^1n\pi^*$ o charakterze CT został zweryfikowany również na poziomie metody XMS-CASPT2.

Pary niekanonicznych zasad azotowych

W kolejnym etapie badań podjęto próbę określenia możliwych mechanizmów bezpromienistej relaksacji niekanonicznych par zasad azotowych. W tym celu wybrano zestaw cząsteczek heterocyklicznych, które mogą tworzyć pary zasad alternatywne do G-C oraz biomimetyki A-T lub A-U. Przeprowadzona na wstępie analiza natury oddziaływań w badanych kompleksach wykazała korelację pomiędzy wyznaczonymi wartościami energii oddziaływania a schematem (syntonem) wiązań wodorowych. Wyniki te ilustrują wpływ poszczególnych grup egzocyklicznych biorących udział w wymianie protonu wzdłuż wiazania wodorowego na siłę oddziaływania międzycząsteczkowego. Analiza składowych energii oddziaływania hybrydową metodą wariacyjno-perturbacyjną (HVPT-EDS) wykazała znaczną różnicę w naturze oddziaływania w kompleksach analogicznych do WC G-C oraz WC A-T/A-U. Te pierwsze zdominowane są przez oddziaływania indukcyjne, które odpowiadają za ok 85% stabilizacji w parach zasad alternatywnych do WC G-C. W przypadku bioizosterów A-T/A-U udział oddziaływań indukcyjnych spada do ok 60% przy czym relatywnie rośnie stabilizacja będąca efektem korelacji elektronowej przy jednoczesnej zmianie charakteru oddziaływań niezaburzonych monomerów na odpychające. W efekcie całkowita energia oddziaływania w tej ostatniej grupie kompleksów jest zwykle zdecydowanie niższa niż w bioizosterach WC G-C.

Aby przeanalizować donoro-akceptorowy charakter par zasad azotowych w kontekście przeniesienia ładunku w elektronowych stanach wzbudzonych, wykonano obliczenia potencjałów jonizacji izolowanych podukładów. Najlepszym donorem elektronu jest zgodnie z uzyskanymi wynikami 8-oxo-2,6-diaminopuryna (oxoDAP), zarówno w fazie gazowej jak i w fazie wodnej. Ciekawym spostrzeżeniem jest też to, że 2,4,6-triaminopirymidyna (TAP) plasuje się w tym zestawieniu na poziomie zbliżonym do puryn, czyli jest najlepszym donorem elektronu w analizowanej grupie pirymidyn. Dodatkowo, uzyskane wyniki wertykalnych energii wzbudzeń w regionie Francka-Condona zwracają uwagę na pary zasad alternatywne do G-C, dla których zaobserwowano wyjątkowo nisko leżące stany o charakterze międzycząsteczkowego przeniesienia ładunku (CT), a które biorą udział w procesie EDPT. Wyniki te wskazują także, że utlenienie puryn w pozycji atomu C8 systematycznie obniża energię wspomnianego stanu CT w regionie FC.

Pary zasad alternatywne do G-C

W związku z tym, że pary zasad alternatywnych do G-C posiadają synton charakterystyczny dla powstawania ekscypleksu w stanie $^1n\pi^*_{CT}$ opisanego dla pary Wobble G-C, zbadano dostępność analogicznego kanału dezaktywacji w tych układach. Jednakże przeprowadzone obliczenia wskazują, że najniższy singletowy stan $n\pi^*$ posiada częściowy charakter CT tylko w przypadku par hypoksantyna-cytozyna (H-C), 8-oxo-H-C (oxoH-C) oraz 8-oxo-G-C (oxoG-C). Dla par zasad H-C i oxoG-C wyznaczono analogiczne ścieżki relaksacji jak dla pary kanonicznej, które sugerują dostępność tego kanału. Zestawienie procesu EDPT zachodzącego na powierzchni stanów $^1n\pi^*$ oraz $^1\pi\pi^*$ z międzycząsteczkowym przeniesieniem ładunku wskazuje, że koncertowy (niesekwencyjny) transfer protonu na powierzchni stanu $^1\pi\pi^*_{CT}$ powinien zachodzić spontanicznie, jednak populacja tego stanu poprzez przecięcie LE/CT wiąże się z koniecznością pokonania niewielkiej bariery energetycznej. Z kolei w przypadku sekwencyjnego procesu EDPT zachodzącego na powierzchni stanu $^1n\pi^*_{CT}$, mimo iż jest on bezbarierowy, wymagana jest istotna zmiana konformacyjna. Warto jednak podkreślić, że w parach zasad H-C oraz oxoH-C, stan $^1n\pi^*$ w regionie FC leży poniżej stanu $^1\pi\pi^*_{CT}$. Postuluje się zatem, że sekwencyjny mechanizm EDPT ze zmianą typu parowania z WC na Wobble może być istotnym kanałem fotorelaksacji w tym układzie, w szczególności przy naświetlaniu promieniowaniem o niższej częstości.

Pary zasad alternatywne do A-U/A-T

W przypadku par zasad alternatywnych do A-U/A-T, wyniki optymalizacji geometrii lokalnych minimów na powierzchni stanów wzbudzonych $S_1(^1n\pi^*)$ i MECP $S_1(^1n\pi^*)/S_0$ przyczyniły się do zaproponowania konkurencyjnego dla EDPT mechanizmu relaksacji poprzez deformację pierścienia pirymidynowego na powierzchni stanów elektronowych o charakterze $^1n\pi^*$. Zgodnie z otrzymanymi wynikami, przecięcia stożkowe stanów $^1n\pi^*$ oraz S_0 są

odseparowane energetycznie od minimum stanu wzbudzonego i charakteryzują się topologią o stromym charakterze (ang. *peaked CI*). Oznacza to, że w przeciwieństwie do EDPT, nie jest to bezbarierowy kanał relaksacji stanu wzbudzonego. Przewiduje się także, że zważając na wysoką barierę energetyczną, dłuższe życie stanów singletowych o charakterze $n\pi^*$ może prowadzić do populacji stanu trypletowego, a w efekcie do otrzymania fotoproduktów i fotodegradacji kwasów nukleinowych. Jednak wśród przebadanych alternatywnych par zasad są takie, dla których bariera ta jest relatywnie mała (<0.5 eV) i postuluje się, że w tych układach stany $^1n\pi^*$ mogą przyczyniać się do efektywnej fotorelaksacji.

We wszystkich zbadanych mimetykach par A-U/A-T zidentyfikowano kanał EDPT na powierzchni stanu $^1\pi\pi^*_{CT}$. Za wyjątkiem pary adenina-hypoksantyna (A-H), MECP związany z tym procesem był najniżej leżącym przecięciem stożkowym ze stanem podstawowym spośród wszystkich przecięć zlokalizowanych w obrębie badanych kanałów fotorelaksacji tych układów. W przypadku pary zasad A-H mechanizm EDPT na powierzchni stanu $^1\pi\pi^*_{CT}$ wydaje się mało prawdopodobny z uwagi na wysokoleżący stan CT w rejonie FC i związaną z tym niekorzystną topologię przecięcia stożkowego LE/CT. Co ciekawe, dzięki modyfikacjom geometrycznym takim jak dodanie grupy funkcyjnej -NH_2 w pozycji atomu C2 oraz tlenu w pozycji atomu C8 adeniny w parze zasad oxoDAP-U, kanał EDPT po ekspozycji na światło UV wydaje się być równie dostępny z regionu FC jak dla kanonicznej pary G-C.

Podsumowanie

Podsumowując, w niniejszej rozprawie po raz pierwszy opisano przecięcia stożkowe stanów $S_1(n\pi^*)/S_0$ w kanonicznych i alternatywnych parach zasad azotowych, wskazujące na to, że długożyjące, reaktywne stany $^1n\pi^*$, uznawane dotąd jako potencjalne źródła fotouszkodzeń w izolowanych nukleozydach pirymidynowych, mogą w rzeczywistości ułatwiać wydajną fotodezaktywację. Zidentyfkowano i opisano dwa możliwe typy kanałów bezpromienistej dezaktywacji na powierzchni stanów $^1n\pi^*$. Może to być jednoetapowy proces, w którym podczas wzbudzenia dochodzi do odkształcenia pierścienia pirymidynowego i w efekcie do fotorelaksacji pary zasad. Stany $^1n\pi^*$ mogą mieć również udział w dwuetapowym procesie EDPT w niektórych parach zasad typu WC, w szczególności w parach G-C i oxoG-C. Zauważono również, że we wszystkich badanych układach, jeżeli tylko stan $^1\pi\pi^*$ o charakterze charge-transfer jest populowany w regionie Francka-Condona, zachodzi efektywna fotorelaksacja na powierzchni tego stanu stabilizowana przez przeniesienie protonu w procesie EDPT. Jednocześnie warto wspomnieć, że wartości minimum energetycznego przecięć stożkowych

MECP otrzymanych w nadmienionym procesie plasują się na najniższym poziomie energetycznym spośród wszystkich zbadanych kanałów dezaktywacji stanu wzbudzonego, z jednym wyjątkiem (para zasad A-H). Postuluje się, że wszystkie opisane mechanizmy występują w badanych układach po ekspozycji na promieniowanie UV i mogą aktywnie konkurować ze sobą, a ich wydajność ściśle zależy od zakresu UV, w jakim cząsteczka będzie pobudzana. Warto również odnotować, że w przypadku wszystkich badanych układów obserwowano znaczną poprawę w zakresie niedoszacowania energii wzbudzeń stanów o charakterze $n\pi^*$ i CT przez metodę ADC(2), gdy zastosowano w obliczeniach wariant uwzględniający skalowanie komponentów spinowych t.j. SCS-ADC(2).

Extended abstract in Czech

Úvod

Pokrok spektroskopických technik umožnil na počátku 21. století získat časově rozlišená elektronová a vibrační spektra izolovaných párů bází nukleových kyselin.[3] Tyto komplexy mohou existovat ve formě konformerů, lišících se geometrií a topologií vodíkových vazeb.[3,10,18] Díky sofistikovaným technikám duální laserové rezonance a ab initio výpočtům bylo možné přiřadit pozorovaná spektra ke konkrétním konformérům. Tyto studie vedly k objevu nového mechanismu deaktivace excitovaného stavu, který je specifický pro aromatické systémy s vodíkovými vazbami. Extrémně krátká životnost excitovaného stavu Watson-Crickova (WC) konformeru kanonického páru bází guanin-cytosin (G-C) a výjimečně slabý a široký pás v rezonančně zesíleném multifotonovém ionizačním spektru, jasně odlišný od silných a ostrých signálů pozorovaných u jiných konformerů, vedlo v kombinaci s ab initio výpočty k návrhu diplomové práce na téma významu mechanismů společného přenosu elektronů a protonů pro fotofyziku těchto systémů.[97,104] Tento mechanismus byl nazýván elektronově řízený přenos protonů (*electron-driven proton-transfer*, EDPT),[104] někdy označovaný jako spřažený přenos elektronů a přenos protonů (*proton-coupled electron transfer*, PCET).[108,282]

Charakteristickým rysem tohoto procesu je přítomnost neabsorbujícího (v literatuře často označovaného jako tmavý) elektronového stavu přenosu náboje (charge-transfer, CT). Obsazení tohoto stavu vede k přenosu elektronu z jedné báze na druhou. Změna v distribuci elektronové hustoty způsobená tímto procesem je zase hnací silou pro přenos protonů. Plocha potenciální energie (PES) CT stavu, silně stabilizovaného přenosem protonů, je odpudivá a protíná se jak s lokálně excitovaným stavem obsazeným v důsledku fotoexcitace, tak se základním stavem, který následně umožňuje nezářivou relaxaci.[26]

Tento jev je zvláště dobře zdokumentován pro kanonický WC pár bází G-C.[96,103–106] Avšak analogický mechanismus EDPT, navzdory teoretickým zprávám o jeho dostupnosti,[15,114] nebyl dosud experimentálně potvrzen pro kanonický WC pár bází adenin-thymin (A-T).

Smysl výzkumu

Jedním z důvodů může být existence nízko položených stavů $^1n\pi^*$,[116,172] jejichž přítomnost může ovlivnit fotodynamiku těchto systémů prostřednictvím vnitřní konverze nebo mezisystémových přechodů na ploše excitovaných stavů lokalizovaných na pyrimidinových[67,176] nebo purinových bázích.[116] Protože překážkou efektivní relaxace výměnou protonů podél vodíkové vazby mohou být procesy zahrnující jen jednu z dusíkatých bází, tato práce provádí srovnávací analýzu možných kanálů nezářivé deaktivace v kanonických a nekanonických párech bází nukleových kyselin, s přihlédnutím k intramolekulárním i intermolekulárním procesům. Hlavním cílem této analýzy je určit roli nízko položených singletových stavů $n\pi^*$ v procesu fotorelaxace studovaných systémů ve vztahu ke konkurenčním procesům puckeringu („prohýbání") kruhů probíhajících na povrchu stavy typu $\pi\pi^*$ a kanál EDPT.

Pokud byla odolnost vůči ultrafialovému (UV) záření, jak se předpokládá,[28] důležitým selekčním faktorem v raných fázích prebiotické chemické evoluce informačních polymerů, zkoumání fotostability nejen kanonických, ale i nekanonických dusíkatých bází spárovaných podle schématu WC, by mělo poskytnout vhled na oprávněnost těchto předpokladů. Stojí za zdůraznění, že fotostabilita kanonických párů bází již byla v literatuře široce popsána, ale dosud byly relaxační studie excitovaného stavu pro nekanonické páry bází provedeny pouze pro páry nebiologického typu WC, ve kterých byly purinové báze oxidované v poloze C8.[129,164,283] Analýza fotofyziky a fotochemie alternativních párů nekanonických dusíkatých bází může přispět k vysvětlení úlohy procesů přenosu náboje mezi bázemi po absorpci UV záření. Tento výzkum tedy také umožní lépe pochopit, proč živé organismy používají tak úzkou sadu stavebních kamenů genetického kódu.Důležité je, že výběr nebiologických párů bází studovaných v dizertační práci byl částečně diktován postupem týmů pracujících na syntéze hypotetických nukleotidových prekurzorů v podmínkách podobných těm, které převládali na rané Zemi.[131,142]

Hlavním cílem výzkumu realizovaného v rámci této doktorské disertační práce je zjistit mechanismy přenosu náboje po absorpci UV záření mezi dusíkatými bázemi a následně identifikovat nové, dříve neuvažované procesy nezářivé fotorelaxace. Podle výzkumné hypotézy existují alternativní kanály pro deaktivaci párů dusíkatých bází prostřednictvím mezimolekulárního přenosu náboje vyplývajícího z jejich interakce v elektronově excitovaných stavech.

Popis výsledku

Výsledky mého vlastního výzkumu popsaného v diplomové práci, provedeného pomocí kvantově chemických výpočetních metod, lze rozdělit do dvou hlavních částí. V první fázi byly testovány kanonické páry bazí typu WC na výskyt pravděpodobných intramolekulárních a

intermolekulárních nezářivých relaxačních mechanismů popsaných v literatuře, se zvláštním důrazem na kanál EDPT a procesy probíhající na povrchu stavu $n\pi^*$. Poprvé byla provedena systematická srovnávací analýza vybraných intramolekulárních a intermolekulárních kanálů v kanonických párech bází. V další fázi byla tato analýza doplněna o dvojice vybraných nebiologických dusíkatých bází.

Metodologie

Struktura dimerů v základním stavu byla optimalizována pomocí Møller–Plessetovy poruchové metody druhého řádu (MP2) s bází cc-pVTZ.[214] Energie vertikálních excitací ve Franck-Condonově oblasti (FC) a geometrie lokálních minim na povrchu excitovaných stavů byly určeny pomocí algebraické diagramatické konstrukce druhého řádu [ADC(2)][198,284,285] ve variantě škálovaných spinových komponent [SCS-ADC(2)].[233] Charakter excitovaných stavů byl stanoven pomocí analýzy přirozených přechodových orbitalů (*natural transition orbitals*, NTOs). Pro analýzu cest nezářivé deaktivace excitovaného stavu byly zkonstruovány PES průřezy pro základní stav a nízko položené singletové excitované stavy pomocí lineární interpolace ve vnitřních souřadnicích (LIIC) mezi klíčovými stacionárními body: Franck-Condonova oblast, minimum stavu S_1 a kónický průsečík tohoto stavu se základním stavem s minimální energií (MECP). Stacionární body na PES excitovaného stavu byly lokalizovány pomocí metod ADC(2), SCS-ADC(2) a NEVPT2 s bází cc-pVTZ. Geometrie v minimu kónického průsečíku byly lokalizovány pomocí optimalizace objektivní funkce dostupné v balíčku CIOpt[12] ve spojení s programem Turbomole 7.3. Tímto způsobem lze vypočítat energie a její analytické derivace metodou SCS-MP2/SCS-ADC(2). Na základě těchto výpočtů byly vyneseny profily PES podél interpolovaných reakčních souřadnic.

Kanonické páry bází

Získaná data potvrdila předchozí výsledky týkající se dostupnosti fotorelaxačního kanálu kanonických párů bází na povrchu $^1\pi\pi^*$ stavů povahy intermolekulárního přenosu náboje (charge-transfer, CT). Podařilo se nám lokalizovat průnik mezi tímto CT stavem s lokálně excitovanými stavy $^1\pi\pi^*$ a $^1n\pi^*$ a základním stavem.[97,114] V tomto ohledu jsou výsledky získané pomocí metody SCS-ADC(2) konzistentní s výsledky vypočítanými metodou NEVPT2, provedených v balíčku ORCA.[286,287] V souladu s předpovědí z literatury[92,112,116] se kanál EDPT pro kanonický pár G-C zdá být dostupnější než pro páry A-U a A-T, protože populace CT excitovaného stavu je na nižší energetické úrovni. Navíc ve WC G-C páru neexistují žádné nízko položené $^1n\pi^*$ stavy pod stavem CT, jejichž obsazení by mohlo vést ke konkurenčním procesům.[116] Energie kanálu EDPT byla porovnána s konkurenčními fotorelaxačními kanály na povrchu nízko položených, lokálně excitovaných jasných stavů $^1\pi\pi^*$ a $^1n\pi^*$ vedoucích k nezářivým přeměnám do základního stavu prostřednictvím deformace purinového nebo pyrimidového prsten. Bylo vzato v úvahu prohýbání purinového heterocyklu v poloze atomů C2 i C6 s ohledem na stále otevřenou diskusi v literatuře na toto téma pro izolovaný adenin.[288] Ukázalo se také, že navzdory dostupnosti výše uvedených kanálů z FC oblasti mohou tyto

cesty vést ke strukturálním změnám, které nebudou dostupné ve struktuře nukleových kyselin, a že kónické průsečíky se základním stavem jsou umístěny na vyšší energetické hladině než ty, které jsou výsledkem procesu EDPT, což je také předmětem sporů v literatuře.[22,91]

Zajímavé fotochemické dráhy byly také pozorovány na povrchu stavu $^1n\pi^*$. U kanonických párů A-T a A-U byla prokázána možnost bezbariérové populace minima excitovaného stavu. Nicméně možná fotorelaxace k základnímu stavu na povrchu stavu $^1n\pi^*$ je ztížena vysokou energetickou bariérou asi 0.9 eV. To naznačuje možnost zachycení v tomto stavu a mezisystémový přechod do tripletového stavu. Zajímavé je, že výsledky výpočtů pomocí metod ADC(2) a SCS-ADC(2) v porovnání s metodou NEVPT2 ukazují, že ačkoli obě varianty metody ADC(2) systematicky podhodnocují excitační energii $n\pi^*$, varianta SCS-ADC(2) kvalitativně zlepšuje shodu s referenčními hodnotami z NEVPT2.

Nejzajímavějším výsledkem získaným v rámci této disertační práce se však zdá být objev nového, dříve nepopsaného deaktivačního kanálu pro kanonický WC pár G-C. K tomuto procesu dochází přenosem protonu na povrch stavu $^1n\pi^*$ vyvolaným mezimolekulárním přenosem elektronové hustoty. Tento sekvenční proces EDPT je výsledkem interakce v rámci specifického synthonu, který umožňuje vytvoření exciplexu prostřednictvím interakce N$\cdots$O a změny typu párování bází z WC na wobble. Poté se proton spontánně přenese z purinu na pyrimidin. Profil PES podél přenosové souřadnice tohoto protonu pokrývající obě fáze procesu EDPT obsazením lokálně excitovaného $^1n\pi^*$ stavu CT povahy byl také ověřen metodou XMS-CASPT2.

Páry nekanonických dusíkatých bází

V další fázi výzkumu byl učiněn pokus o odhalení možných mechanismů nezářivé relaxace nekanonických párů dusíkatých bází. Pro tento účel byl vybrán soubor heterocyklických molekul, které mohou tvořit páry bází alternativní k párům G-C a A-T nebo A-U. Na začátku provedená analýza povahy interakcí ve studovaných komplexech ukázala korelaci mezi zjištěnými hodnotami interakční energie a uspořádáním (synthonem) vodíkových vazeb. Tyto výsledky ilustrují vliv jednotlivých exocyklických skupin zapojených do výměny protonů podél vodíkové vazby na sílu mezimolekulárních interakcí.

Analýza složek interakční energie pomocí hybridní variační-poruchové metody dekompozice interakční energie (HVPT-EDS) ukázala významný rozdíl v charakteru interakce v komplexech analogických WC G-C a A-T/A-U párům. Prvním z nich dominují indukční interakce, které jsou zodpovědné za přibližně 85% stabilizace v párech bází alternativních k WC G-C. V případě biomimetik A-T/A-U klesá podíl indukčních interakcí přibližně na 60%, přičemž stabilizace vyplývající z elektronické korelace relativně vzrůstá, zatímco charakter interakcí monomerů se mění na odpudivé. V důsledku toho je celková energie interakcí v

biomimetikách WC A-T/A-U párech obvykle mnohem nižší než v biomimetikách WC G-C páru.

Pro analýzu donor-akceptorové povahy párů dusíkatých bází v kontextu přenosu náboje v elektronově excitovaných stavech byly provedeny výpočty ionizačních potenciálů izolovaných bází. Podle získaných výsledků je nejlepším donorem elektronů 8-oxo-2,6-diaminopurin (oxo-DAP), a to jak v plynné fázi, tak ve vodě. Zajímavým pozorováním je, že 2,4,6-triaminopyrimidin (TAP) je v tomto žebříčku na úrovni podobné purinům, tj. je nejlepším donorem elektronů ve zkoumané skupině pyrimidinů. Získané výsledky vertikálních excitačních energií v FC oblasti navíc odhalují páry bází alternativní ke G-C, u kterých byly pozorovány mimořádně nízko položené stavy mezimolekulárního přenosu náboje (CT) a které se účastní procesu EDPT. Tyto výsledky také naznačují, že oxidace purinů v poloze atomu C8 systematicky snižuje energii uvedeného CT stavu v FC oblasti.

Vzhledem k tomu, že páry bází alternativní ke G-C mají synthonovou charakteristiku tvorby exciplexu v CT stavu $^1n\pi^*$ stejnou jako wobble pár G-C, byla zkoumána dostupnost analogického deaktivačního kanálu v těchto systémech. Provedené výpočty však ukazují, že nejnižší singletový stav $^1n\pi^*$ má částečný CT charakter pouze v případě párů hypoxanthin-cytosinu (H-C), 8-oxo-H-C (oxoH-C) a 8-oxo-G-C (oxoG-C). Pro páry bází H-C a oxoG-C byly zjištěny analogické relaxační dráhy jako pro kanonický pár, což naznačuje dostupnost tohoto kanálu. Srovnání procesu EDPT odehrávajícího se na povrchu stavů $^1n\pi^*$ a $^1\pi\pi^*$ s mezimolekulárním přenosem náboje ukazuje, že současný (nesekvenční) přenos protonů na povrchu $^1\pi\pi^*_{CT}$ stavu by měl nastat spontánně, ale populace tohoto excitovaného stavu přechodem přes LE a CT stav vyžaduje překonání malé energetické bariéry. Na druhou stranu v případě sekvenčního procesu EDPT probíhajícího na povrchu $^1n\pi^*_{CT}$ stavu, přestože je bezbariérový, je nutná významná konformační změna. Je však třeba zdůraznit, že v párech bází H-C a oxoH-C leží stav $^1n\pi^*$ v FC oblasti pod $^1\pi\pi^*_{CT}$ stavem. Proto se předpokládá, že sekvenční mechanismus EDPT se změnou párování z WC na wobble může být v těchto systémech důležitým fotorelaxačním kanálem, zejména při ozařování UV zářením s nižší energií.

V případě alternativních párů bází k A-U/A-T přispěly výsledky optimalizace geometrie lokálních minim na povrchu excitovaných stavů $S_1(^1n\pi^*)$ a MECP $S_1(^1n\pi^*)/S_0$ k navržení fotorelaxačního mechanismu kompetitivního k EDPT, který zahrnuje deformaci pyrimidinového kruhu na povrchu elektronového stavu $^1n\pi^*$. Podle získaných výsledků jsou kónické průsečíky stavů $^1n\pi^*$CT a S_0 energeticky odděleny od minima excitovaného stavu a vyznačují se strmou topologií (angl. *peaked CI*). To znamená, že na rozdíl od EDPT se nejedná o bezbar-

iérový relaxační kanál excitovaného stavu. Rovněž se očekává, že s ohledem na vysokou energetickou bariéru může delší životnost $n\pi^*$ singletových stavů vést k obsazení tripletového stavu a v důsledku toho k tvorbě fotoproduktů a fotodegradaci nukleových kyselin. Nicméně mezi testovanými alternativními páry bází jsou i takové, u kterých je tato bariéra relativně malá (< 0,5 eV) a předpokládá se, že v těchto systémech mohou stavy $^1n\pi^*$ přispívat k účinné fotorelaxaci.

U všech testovaných mimetik A-U/A-T páru byl na povrchu $^1\pi\pi^*_{CT}$ stavu identifikován kanál EDPT. S výjimkou páru adenin-hypoxanthin (A-H) byl kónický průsečík se základním stavem odpovídající tomuto procesu energeticky nejníže položeným ze všech MECP nalezených ve studovaných fotorelaxačních kanálech těchto systémů. V případě páru bází A-H se mechanismus EDPT na povrchu $^1\pi\pi^*_{CT}$ stavu zdá nepravděpodobný kvůli vysoko položenému CT stavu v FC oblasti. Souvisí to s nepříznivou topologií kónického průsečíku LE/CT. Zajímavé je, že díky modifikacím geometrie, jako je přidání funkční skupiny -NH_2 v poloze C2 a kyslíku v poloze C8 adeninu v páru bází oxoDAP-U, se kanál EDPT po vystavení UV záření jeví být z FC oblasti stejně dostupný jako pro kanonický pár G-C.

Shrnutí

Tato disertační práce poprvé popisuje kónické průsečíky stavů $S_1(^1n\pi^*)/S_0$ v kanonických a alternativních párech dusíkatých bází a naznačuje, že dlouho žijící, reaktivní stav $^1n\pi^*$, dříve považovaný za potenciální zdroj fotopoškození u izolovaných pyrimidinových nukleosidů, může ve skutečnosti usnadnit účinnou fotodeaktivaci.

Byly identifikovány a popsány dva možné typy nezářivých deaktivačních kanálů na povrchu $^1n\pi^*$ stavů. Může se jednat o jednokrokový proces, při kterém se během excitace pyrimidinový kruh deformuje a v důsledku toho se pár bází fotorelaxuje. Stavy $^1n\pi^*$ se mohou také účastnit dvoufázového procesu EDPT v případě některých párů bází typu WC, zejména G-C a oxoG-C. Ve všech studovaných systémech bylo také zjištěno, že pokud je v FC oblasti obsazen pouze stav $^1\pi\pi^*_{CT}$, dochází k účinné fotorelaxaci díky stabilizaci tohoto stavu přenosem protonu procesem EDPT. Zároveň stojí za zmínku, že kónické průsečíky s nejnižší energií spojené s tímto procesem jsou energeticky nejníže položené ze všech MECP ze všech zkoumaných kanálů deaktivace excitovaného stavu, s jedinou výjimkou (pár A-H).

Navrhujeme, že všechny popsané mechanismy se objevují ve zkoumaných systémech po vystavení UV záření a mohou si navzájem aktivně konkurovat, a že jejich účinnost silně závisí na UV oblasti, kterou je molekula excitována. Za zmínku také stojí, že u všech sledovaných

systémů bylo z hlediska podcenění excitačních energií $n\pi^*$ a CT stavů pozorováno výrazné zlepšení při výpočtech s použitím varianty škálování spinové složky, tzn SCS-ADC(2), oproti nemodifikované ADC(2).

Bibliography

[1] J. A. Barltrop and J. D. Coyle, *Principles of photochemistry*, Wiley, 1978.

[2] P. Atkins, *Shriver and Atkins' inorganic chemistry*, Oxford University Press, USA, 2010.

[3] S. Boldissar and M. S. d. Vries, "How nature covers its bases", *Physical Chemistry Chemical Physics* **2018**, *20*, 9701–9716. DOI: 10.1039/C8CP01236A.

[4] C. J. Cramer, *Essentials of computational chemistry: theories and models*, John Wiley & Sons, 2013.

[5] L. González and R. Lindh, eds., *Quantum Chemistry and Dynamics of Excited States: Methods and Applications*, 1st edition. Wiley, 2021.

[6] E. Lewars, "Computational chemistry", *Introduction to the theory and applications of molecular and quantum mechanics* **2011**, *318*. DOI: 10.1007/978-90-481-3862-3.

[7] L. Piela, *Ideas of quantum chemistry*, Elsevier, 2006.

[8] R. Crespo-Otero and M. Barbatti, "Recent Advances and Perspectives on Nonadiabatic Mixed Quantum–Classical Dynamics", *Chemical Reviews* **2018**, *118*, 7026–7068. DOI: 10.1021/acs.chemrev.7b00577.

[9] W. Domcke, D. Yarkony, and H. Köppel, *Conical intersections: electronic structure, dynamics & spectroscopy*, vol. 15. World Scientific, 2004.

[10] C. E. Crespo-Hernández, B. Cohen, P. M. Hare, and B. Kohler, "Ultrafast excited-state dynamics in nucleic acids", *Chemical Reviews* **2004**, *104*, 1977–2020. DOI: 10.1021/cr0206770.

[11] S. H. Lin, "Rate of interconversion of electronic and vibrational energy", *The Journal of Chemical Physics* **1966**, *44*, 3759–3767. DOI: 10.1063/1.1726531.

[12] B. G. Levine, J. D. Coe, and T. J. Martinez, "Optimizing Conical Intersections without Derivative Coupling Vectors: Application to Multistate Multireference Second-Order Perturbation Theory (MS-CASPT2)", *The Journal of Physical Chemistry B* **2008**, *112*, 405–413. DOI: 10.1021/jp0761618.

[13] K. Röttger, H. J. B. Marroux, M. P. Grubb, P. M. Coulter, H. Böhnke, A. S. Henderson, M. C. Galan, F. Temps, A. J. Orr-Ewing, and G. M. Roberts, "Ultraviolet Absorption Induces Hydrogen-Atom Transfer in G-C Watson-Crick DNA Base Pairs in Solution", *Angewandte Chemie International Edition* **2015**, *54*, 14719–14722. DOI: 10.1002/anie.201506940.

[14] A. Francés-Monerris, H. Gattuso, D. Roca-Sanjuán, I. Tuñón, M. Marazzi, E. Dumont, and A. Monari, "Dynamics of the excited-state hydrogen transfer in a (dG)·(dC) homopolymer: intrinsic photostability of DNA", *Chemical Science* **2018**, *9*, 7902–7911.

[15] J. P. Gobbo, V. Sauri, D. Roca-Sanjuan, L. Serrano-Andres, M. Merchan, and A. C. Borin, "On the deactivation mechanisms of adenine–thymine base pair", *The Journal of Physical Chemistry B* **2012**, *116*, 4089–4097. DOI: 10.1021/jp300583h.

[16] V. Sauri, J. P. Gobbo, J. J. Serrano-Perez, M. Lundberg, P. B. Coto, L. Serrano-Andres, A. C. Borin, R. Lindh, M. Merchan, and D. Roca-Sanjuan, "Proton/Hydrogen Transfer mechanisms in the Guanine–Cytosine base pair: photostability and tautomerism", *Journal of Chemical Theory and Computation* **2013**, *9*, 481–496. DOI: 10.1021/ct3006166.

[17] C. T. Middleton, K. d. L. Harpe, C. Su, Y. K. Law, C. E. Crespo-Hernández, and B. Kohler, "DNA Excited-State Dynamics: From Single Bases to the Double Helix", *Annual Review of Physical Chemistry* **2009**, *60*, 217–239. DOI: 10.1146/annurev.physchem.59.032607.093719.

[18] K. Kleinermanns, D. Nachtigallová, and M. S. de Vries, "Excited state dynamics of DNA bases", *International Reviews in Physical Chemistry* **2013**, *32*, 308–342. DOI: 10.1080/0144235X.2012.760884.

[19] M. Barbatti, A. C. Borin, and S. Ullrich. "Photoinduced Processes in Nucleic Acids". In: *Photoinduced Phenomena in Nucleic Acids I.* Ed. by M. Barbatti, A. C. Borin, and S. Ullrich. Vol. 355. Cham: Springer International Publishing, 2014. 1–32. DOI: 10.1007/128_2014_569.

[20] A. Giussani, J. Segarra-Martí, D. Roca-Sanjuán, and M. Merchán. "Excitation of Nucleobases from a Computational Perspective I: Reaction Paths". In: *Photoinduced Phenomena in Nucleic Acids I: Nucleobases in the Gas Phase and in Solvents*. Ed. by M. Barbatti, A. C. Borin, and S. Ullrich. Topics in Current Chemistry. Cham: Springer International Publishing, 2015. 57–97. DOI: 10.1007/128_2013_501.

[21] S. Mai, M. Richter, P. Marquetand, and L. González. "Excitation of Nucleobases from a Computational Perspective II: Dynamics". In: *Photoinduced Phenomena in Nucleic Acids I: Nucleobases in the Gas Phase and in Solvents*. Ed. by M. Barbatti, A. C. Borin, and S. Ullrich. Topics in Current Chemistry. Cham: Springer International Publishing, 2015. 99–153. DOI: 10.1007/128_2014_549.

[22] R. Improta, F. Santoro, and L. Blancafort, "Quantum Mechanical Studies on the Photophysics and the Photochemistry of Nucleic Acids and Nucleobases", *Chemical Reviews* **2016**, *116*, 3540–3593. DOI: 10.1021/acs.chemrev.5b00444.

[23] P. R. Callis, "Electronic States and Luminescence of Nucleic Acid Systems", *Annual Review of Physical Chemistry* **1983**, *34*, 329–357. DOI: 10.1146/annurev.pc.34.100183.001553.

[24] N. Ismail, L. Blancafort, M. Olivucci, B. Kohler, and M. A. Robb, "Ultrafast decay of electronically excited singlet cytosine via a π, π^* to no, π^* state switch", *Journal of the American Chemical Society* **2002**, *124*, 6818–6819. DOI: 10.1021/ja0258273.

[25] M. Barbatti, A. J. A. Aquino, J. J. Szymczak, D. Nachtigallová, P. Hobza, and H. Lischka, "Relaxation mechanisms of UV-photoexcited DNA and RNA nucleobases", *Proceedings of the National Academy of Sciences* **2010**, *107*, 21453–21458. DOI: 10.1073/pnas.1014982107.

[26] A. L. Sobolewski and W. Domcke, "The chemical physics of the photostability of life", *Europhysics News* **2006**, *37*, 20–23. DOI: 10.1051/epn:2006405.

[27] D. Shemesh, A. L. Sobolewski, and W. Domcke, "Efficient excited-state deactivation of the gly-phe-ala tripeptide via an electron-driven proton-transfer process", *Journal of the American Chemical Society* **2009**, *131*, 1374–1375. DOI: 10.1021/ja808485b.

[28] N. J. Green, J. Xu, and J. D. Sutherland, "Illuminating Life's Origins: UV Photochemistry in Abiotic Synthesis of Biomolecules", *Journal of the American Chemical Society* **2021**, *143*, 7219–7236. DOI: 10.1021/jacs.1c01839.

[29] H. Langer, N. L. Doltsinis, and D. Marx, "Excited-State Dynamics and Coupled Proton–Electron Transfer of Guanine", *ChemPhysChem* **2005**, *6*, 1734–1737. DOI: 10.1002/cphc.200400578.

[30] D. Tuna, A. L. Sobolewski, and W. Domcke, "Mechanisms of Ultrafast Excited-State Deactivation in Adenosine", *The Journal of Physical Chemistry A* **2014**, *118*, 122–127. DOI: 10.1021/jp410121h.

[31] A. Alexandrova, J. Tully, and G. Granucci, "Photochemistry of DNA fragments via semiclassical nonadiabatic dynamics", *Biophysical Journal* **2010**, *98*, 43a. DOI: 10.1021/jp103322c.

[32] S. Ullrich, T. Schultz, M. Z. Zgierski, and A. Stolow, "Electronic relaxation dynamics in DNA and RNA bases studied by time-resolved photoelectron spectroscopy", *Physical Chemistry Chemical Physics* **2004**, *6*, 2796–2801. DOI: 10.1039/B316324E.

[33] C. Canuel, M. Mons, F. Piuzzi, B. Tardivel, I. Dimicoli, and M. Elhanine, "Excited states dynamics of DNA and RNA bases: Characterization of a stepwise deactivation pathway in the gas phase", *The Journal of Chemical Physics* **2005**, *122*, 074316. DOI: 10.1063/1.1850469.

[34] H. Chen and S. Li, "Ab initiostudy on deactivation pathways of excited 9H-guanine", *The Journal of Chemical Physics* **2006**, *124*, 154315. DOI: 10.1063/1.2186998.

[35] C. M. Marian, "The guanine tautomer puzzle: quantum chemical investigation of ground and excited states", *The Journal of Physical Chemistry A* **2007**, *111*, 1545–1553. DOI: 10.1021/jp068620v.

[36] L. Serrano-Andrés, M. Merchán, and A. C. Borin, "A Three-State Model for the Photophysics of Guanine", *Journal of the American Chemical Society* **2008**, *130*, 2473–2484. DOI: 10.1021/ja0744450.

[37] Z. Lan, E. Fabiano, and W. Thiel, "Photoinduced nonadiabatic dynamics of 9H-guanine", *ChemPhysChem* **2009**, *10*, 1225–1229. DOI: 10.1002/cphc.200900030.

[38] N. L. Doltsinis, P. R. L. Markwick, H. Nieber, and H. Langer. "Ultrafast Radiationless Decay in Nucleic Acids: Insights From Nonadiabatic Ab Initio Molecular Dynamics". In: *Radiation Induced Molecular Phenomena in Nucleic Acids: A Comprehensive Theoretical and Experimental Analysis*. Ed. by M. K. Shukla and J. Leszczynski. Challenges and Advances In Computational Chemistry and Physics. Dordrecht: Springer Netherlands, 2008. 265–299. DOI: 10.1007/978-1-4020-8184-2_10.

[39] M. Barbatti, J. J. Szymczak, A. J. Aquino, D. Nachtigallová, and H. Lischka, "The decay mechanism of photoexcited guanine- A nonadiabatic dynamics study", *The Journal of Chemical Physics* **2011**, *134*, 01B606. DOI: 10.1063/1.3521498.

[40] S. Yamazaki, W. Domcke, and A. L. Sobolewski, "Nonradiative decay mechanisms of the biologically relevant tautomer of guanine", *The Journal of Physical Chemistry A* **2008**, *112*, 11965–11968. DOI: 10.1021/jp806622m.

[41] N. L. Evans and S. Ullrich, "Wavelength dependence of electronic relaxation in isolated adenine using UV femtosecond time-resolved photoelectron spectroscopy", *The Journal of Physical Chemistry A* **2010**, *114*, 11225–11230. DOI: 10.1021/jp1029097.

[42] L. Serrano-Andres, M. Merchan, and A. C. Borin, "Adenine and 2-aminopurine: paradigms of modern theoretical photochemistry", *Proceedings of the National Academy of Sciences* **2006**, *103*, 8691–8696. DOI: 10.1073/pnas.060299110.

[43] H. Chen and S. Li, "Theoretical study toward understanding ultrafast internal conversion of excited 9H-adenine", *The Journal of Physical Chemistry A* **2005**, *109*, 8443–8446. DOI: 10.1021/jp0537207.

[44] S. Perun, A. L. Sobolewski, and W. Domcke, "Ab Initio Studies on the Radiationless Decay Mechanisms of the Lowest Excited Singlet States of 9H-Adenine", *Journal of the American Chemical Society* **2005**, *127*, 6257–6265. DOI: 10.1021/ja044321c.

[45] L. Blancafort, "Excited-state potential energy surface for the photophysics of adenine", *Journal of the American Chemical Society* **2006**, *128*, 210–219. DOI: 10.1021/ja054998f.

[46] M. Barbatti, Z. Lan, R. Crespo-Otero, J. J. Szymczak, H. Lischka, and W. Thiel, "Critical appraisal of excited state nonadiabatic dynamics simulations of 9 H-adenine", *The Journal of Chemical Physics* **2012**, *137*, 22A503. DOI: 10.1063/1.4731649.

[47] A. L. Sobolewski and W. Domcke, "On the mechanism of nonradiative decay of DNA bases: ab initio and TDDFT results for the excited states of 9H-adenine", *The European Physical Journal D-Atomic, Molecular, Optical and Plasma Physics* **2002**, *20*, 369–374. DOI: 10.1140/epjd/e2002-00164-5.

[48] A. L. Sobolewski, W. Domcke, C. Dedonder-Lardeux, and C. Jouvet, "Excited-state hydrogen detachment and hydrogen transfer driven by repulsive $^1\pi\sigma^*$ states: A new paradigm for nonradiative decay in aromatic biomolecules", *Physical Chemistry Chemical Physics* **2002**, *4*, 1093–1100. DOI: 10.1039/B110941N.

[49] M. Barbatti and H. Lischka, "Nonadiabatic Deactivation of 9 H-Adenine: A Comprehensive Picture Based on Mixed Quantum- Classical Dynamics", *Journal of the American Chemical Society* **2008**, *130*, 6831–6839. DOI: 10.1021/ja800589p.

[50] I. Hünig, C. Plützer, K. A. Seefeld, D. Löwenich, M. Nispel, and K. Kleinermanns, "Photostability of Isolated and Paired Nucleobases: N-H Dissociation of Adenine and Hydrogen Transfer in its Base Pairs Examined by Laser Spectroscopy", *A European Journal of Chemical Physics and Physical Chemistry* **2004**, *5*, 1427–1431. DOI: 10.1002/cphc.200400142.

[51] J. W. Park and T. Shiozaki, "On-the-Fly CASPT2 Surface-Hopping Dynamics", *Journal of Chemical Theory and Computation* **2017**, *13*, 3676–3683. DOI: 10.1021/acs.jctc.7b00559.

[52] F. Plasser, R. Crespo-Otero, M. Pederzoli, J. Pittner, H. Lischka, and M. Barbatti, "Surface hopping dynamics with correlated single-reference methods: 9H-adenine as a case study", *Journal of chemical theory and computation* **2014**, *10*, 1395–1405. DOI: 10.1021/ct4011079.

[53] Y. Lu, Z. Lan, and W. Thiel, "Monomeric adenine decay dynamics influenced by the DNA environment", *Journal of computational chemistry* **2012**, *33*, 1225–1235. DOI: 10.1002/jcc.22952.

[54] Y. Lu, Z. Lan, and W. Thiel, "Hydrogen bonding regulates the monomeric nonradiative decay of adenine in DNA strands", *Angewandte Chemie* **2011**, *123*, 6996–6999. DOI: 10.1002/anie.201008146.

[55] K. L. Wells, D. J. Hadden, M. G. Nix, and V. G. Stavros, "Competing $\pi\sigma^*$ States in the Photodissociation of Adenine", *The Journal of Physical Chemistry Letters* **2010**, *1*, 993–996. DOI: 10.1021/jz100050y.

[56] J.-W. Ho, H.-C. Yen, W.-K. Chou, C.-N. Weng, L.-H. Cheng, H.-Q. Shi, S.-H. Lai, and P.-Y. Cheng, "Disentangling Intrinsic Ultrafast Excited-State Dynamics of Cytosine Tautomers", *The Journal of Physical Chemistry A* **2011**, *115*, 8406–8418. DOI: 10.1021/jp205603w.

[57] M. Merchán and L. Serrano-Andrés, "Ultrafast internal conversion of excited cytosine via the lowest $\pi\pi^*$ electronic singlet state", *Journal of the American Chemical Society* **2003**, *125*, 8108–8109.

[58] L. Blancafort, "Energetics of Cytosine Singlet Excited-State Decay Paths—A Difficult Case for CASSCF and CASPT2", *Photochemistry and Photobiology* **2007**, *83*, 603–610.

[59] K. A. Kistler and S. Matsika, "Radiationless decay mechanism of cytosine: an ab initio study with comparisons to the fluorescent analogue 5-methyl-2-pyrimidinone", *The Journal of Physical Chemistry A* **2007**, *111*, 2650–2661.

[60] L. Blancafort and M. A. Robb, "Key role of a threefold state crossing in the ultrafast decay of electronically excited cytosine", *The Journal of Physical Chemistry A* **2004**, *108*, 10609–10614.

[61] M. Z. Zgierski, S. Patchkovskii, T. Fujiwara, and E. C. Lim, "On the Origin of the Ultrafast Internal Conversion of Electronically Excited Pyrimidine Bases", *The Journal of Physical Chemistry A* **2005**, *109*, 9384–9387. DOI: 10.1021/jp054158n.

[62] R. Gonzalez-Luque, T. Climent, I. Gonzalez-Ramirez, M. Merchan, and L. Serrano-Andres, "Singlet- Triplet States Interaction Regions in DNA/RNA Nucleobase Hypersurfaces", *Journal of Chemical Theory and Computation* **2010**, *6*, 2103–2114.

[63] A. Nakayama, Y. Harabuchi, S. Yamazaki, and T. Taketsugu, "Photophysics of cytosine tautomers: new insights into the nonradiative decay mechanisms from MS-CASPT2 potential energy calculations and excited-state molecular dynamics simulations", *Physical Chemistry Chemical Physics* **2013**, *15*, 12322–12339. DOI: 10.1039/C3CP51617B.

[64] H. R. Hudock and T. J. Martinez, "Excited-State Dynamics of Cytosine Reveal Multiple Intrinsic Subpicosecond Pathways", *ChemPhysChem* **2008**, *9*, 2486–2490.

[65] M. Barbatti, A. J. Aquino, J. J. Szymczak, D. Nachtigallova, and H. Lischka, "Photodynamical simulations of cytosine: characterization of the ultrafast bi-exponential UV deactivation", *Physical Chemistry Chemical Physics* **2011**, *13*, 6145–6155.

[66] M. Merchán, L. Serrano-Andrés, M. A. Robb, and L. Blancafort, "Triplet-state formation along the ultrafast decay of excited singlet cytosine", *Journal of the American Chemical Society* **2005**, *127*, 1820–1825.

[67] A. J. Pepino, J. Segarra-Martí, A. Nenov, I. Rivalta, R. Improta, and M. Garavelli, "UV-induced long-lived decays in solvated pyrimidine nucleosides resolved at the MS-CASPT2/MM level", *Physical Chemistry Chemical Physics* **2018**, *20*, 6877–6890.

[68] M. Merchan, R. Gonzalez-Luque, T. Climent, L. Serrano-Andres, E. Rodríguez, M. Reguero, and D. Pelaez, "Unified model for the ultrafast decay of pyrimidine nucleobases", *The Journal of Physical Chemistry B* **2006**, *110*, 26471–26476.

[69] Z. Lan, E. Fabiano, and W. Thiel, "Photoinduced nonadiabatic dynamics of pyrimidine nucleobases: on-the-fly surface-hopping study with semiempirical methods", *The Journal of Physical Chemistry B* **2009**, *113*, 3548–3555.

[70] J. J. Szymczak, M. Barbatti, J. T. Soo Hoo, J. A. Adkins, T. L. Windus, D. Nachtigallová, and H. Lischka, "Photodynamics simulations of thymine: Relaxation into the first excited singlet state", *The Journal of Physical Chemistry A* **2009**, *113*, 12686–12693. DOI: 10.1021/jp905085x.

[71] D. Asturiol, B. Lasorne, M. A. Robb, and L. Blancafort, "Photophysics of the π, π^* and n, π^* states of thymine: MS-CASPT2 minimum-energy paths and CASSCF on-the-fly dynamics", *The Journal of Physical Chemistry A* **2009**, *113*, 10211–10218.

[72] H. R. Hudock, B. G. Levine, A. L. Thompson, H. Satzger, D. Townsend, N. Gador, S. Ullrich, A. Stolow, and T. J. Martinez, "Ab initio molecular dynamics and time-resolved photoelectron spectroscopy of electronically excited uracil and thymine", *The Journal of Physical Chemistry A* **2007**, *111*, 8500–8508.

[73] S. Perun, A. L. Sobolewski, and W. Domcke, "Conical Intersections in Thymine", *The Journal of Physical Chemistry A* **2006**, *110*, 13238–13244. DOI: 10.1021/jp0633897.

[74] S. Yamazaki and T. Taketsugu, "Nonradiative deactivation mechanisms of uracil, thymine, and 5-fluorouracil: A comparative ab initio study", *The Journal of Physical Chemistry A* **2012**, *116*, 491–503. DOI: 10.1021/jp206546g.

[75] L. Blancafort, B. Cohen, P. M. Hare, B. Kohler, and M. A. Robb, "Singlet excited-state dynamics of 5-fluorocytosine and cytosine: An experimental and computational study", *The Journal of Physical Chemistry A* **2005**, *109*, 4431–4436.

[76] G. Zechmann and M. Barbatti, "Photophysics and Deactivation Pathways of Thymine", *The Journal of Physical Chemistry A* **2008**, *112*, 8273–8279. DOI: 10.1021/jp804309x.

[77] W. Park, S. Lee, M. Huix-Rotllant, M. Filatov, and C. H. Choi, "Impact of the dynamic electron correlation on the unusually long excited-state lifetime of thymine", *The Journal of Physical Chemistry Letters* **2021**, *12*, 4339–4346.

[78] A. Nakayama, G. Arai, S. Yamazaki, and T. Taketsugu, "Solvent effects on the ultrafast nonradiative deactivation mechanisms of thymine in aqueous solution: Excited-state QM/MM molecular dynamics simulations", *The Journal of Chemical Physics* **2013**, *139*, 214304. DOI: 10.1063/1.4833563.

[79] J. J. Serrano-Pérez, I. Gonzalez-Ramirez, P. B. Coto, M. Merchan, and L. Serrano-Andres, "Theoretical insight into the intrinsic ultrafast formation of cyclobutane pyrimidine dimers in UV-irradiated DNA: Thymine versus cytosine", *The Journal of Physical Chemistry B* **2008**, *112*, 14096–14098.

[80] N. J. Kim, J. Chang, H. M. Kim, H. Kang, T. K. Ahn, J. Heo, and S. K. Kim, "Femtosecond decay dynamics of intact adenine and thymine base pairs in a supersonic jet", *ChemPhysChem* **2011**, *12*, 1935–1939.

[81] M. Kotur, T. C. Weinacht, C. Zhou, and S. Matsika, "Following Ultrafast Radiationless Relaxation Dynamics With Strong Field Dissociati ve Ionization: A Comparison Between Adenine, Uracil, and Cytosine", *IEEE Journal of Selected Topics in Quantum Electronics* **2012**, *18*, 187–194. DOI: 10.1109/JSTQE.2011.2107892.

[82] S. Matsika, M. Spanner, M. Kotur, and T. C. Weinacht, "Ultrafast Relaxation Dynamics of Uracil Probed via Strong Field Dissociative Ionization", *The Journal of Physical Chemistry A* **2013**, *117*, 12796–12801. DOI: 10.1021/jp408073d.

[83] S. Matsika, "Radiationless Decay of Excited States of Uracil through Conical Intersections", *The Journal of Physical Chemistry A* **2004**, *108*, 7584–7590. DOI: 10.1021/jp048284n.

[84] Y. Mercier, F. Santoro, M. Reguero, and R. Improta, "The decay from the dark nπ^* excited state in uracil: an integrated CASPT2/CASSCF and PCM/TD-DFT study in the gas phase and in water", *The Journal of Physical Chemistry B* **2008**, *112*, 10769–10772.

[85] D. Nachtigallová, A. J. Aquino, J. J. Szymczak, M. Barbatti, P. Hobza, and H. Lischka, "Nonadiabatic dynamics of uracil: population split among different decay mechanisms", *The Journal of Physical Chemistry A* **2011**, *115*, 5247–5255.

[86] M. Richter, S. Mai, P. Marquetand, and L. González, "Ultrafast intersystem crossing dynamics in uracil unravelled by ab initio molecular dynamics", *Physical Chemistry Chemical Physics* **2014**, *16*, 24423–24436.

[87] T. Gustavsson, A. Bányász, E. Lazzarotto, D. Markovitsi, G. Scalmani, M. J. Frisch, V. Barone, and R. Improta, "Singlet excited-state behavior of uracil and thymine in aqueous solution: a combined experimental and computational study of 11 uracil derivatives", *Journal of the American Chemical Society* **2006**, *128*, 607–619. DOI: 10.1021/ja056181s.

[88] D. Picconi, V. Barone, A. Lami, F. Santoro, and R. Improta, "The Interplay between $\pi\pi^*$/nπ^* Excited States in Gas-Phase Thymine: A Quantum Dynamical Study", *ChemPhysChem* **2011**, *12*, 1957–1968.

[89] M. Dargiewicz, M. Biczysko, R. Improta, and V. Barone, "Solvent effects on electron-driven proton-transfer processes: adenine–thymine base pairs", *Physical Chemistry Chemical Physics* **2012**, *14*, 8981–8989. DOI: 10.1039/C2CP23890J.

[90] M. J. Janicki, R. Szabla, J. Šponer, and R. W. Góra, "Photoinduced water–chromophore electron transfer causes formation of guanosine photodamage", *Physical Chemistry Chemical Physics* **2022**, *24*, 8217–8224.

[91] B. Marchetti, T. N. V. Karsili, M. N. R. Ashfold, and W. Domcke, "A 'bottom up', ab initio computational approach to understanding fundamental photophysical processes in nitrogen containing heterocycles, DNA bases and base pairs", *Physical Chemistry Chemical Physics* **2016**, *18*, 20007–20027. DOI: 10.1039/c6cp00165c.

[92] L. Martinez Fernandez, F. Santoro, and R. Improta, "Nucleic Acids as a Playground for the Computational Study of the Photophysics and Photochemistry of Multichromophore Assemblies", *Accounts of Chemical Research* **2022**, *55*, 2077–2087.

[93] C. E. Crespo-Hernández, B. Cohen, and B. Kohler, "Base stacking controls excited-state dynamics in A-T DNA", *Nature* **2005**, *436*, 1141–1144. DOI: 10.1038/nature03933.

[94] Y. Zhang, K. de La Harpe, A. A. Beckstead, R. Improta, and B. Kohler, "UV-induced proton transfer between DNA strands", *Journal of the American Chemical Society* **2015**, *137*, 7059–7062. DOI: 10.1021/jacs.5b03914.

[95] V. A. Spata, W. Lee, and S. Matsika, "Excimers and exciplexes in photoinitiated processes of oligonucleotides", *The Journal of Physical Chemistry Letters* **2016**, *7*, 976–984.

[96] A. Abo-Riziq, L. Grace, E. Nir, M. Kabelac, P. Hobza, and M. S. De Vries, "Photochemical selectivity in guanine-cytosine base-pair structures", *Proceedings of the National Academy of Sciences* **2005**, *102*, 20–23.

[97] A. L. Sobolewski, W. Domcke, and C. Hattig, "Tautomeric selectivity of the excited-state lifetime of guanine/cytosine base pairs: The role of electron-driven proton-transfer processes", *Proceedings of the National Academy of Sciences* **2005**, *102*, 17903–17906. DOI: 10.1073/pnas.0504087102.

[98] A. L. Sobolewski and W. Domcke, "Relevance of Electron-Driven Proton-Transfer Processes for the Photostability of Proteins", *A European Journal of Chemical Physics and Physical Chemistry* **2006**, *7*, 561–564.

[99] E. Nir, K. Kleinermanns, and M. S. de Vries, "Pairing of isolated nucleic-acid bases in the absence of the DNA backbone", *Nature* **2000**, *408*, 949–951. DOI: 10.1038/35050053.

[100] F. Plasser, A. J. A. Aquino, H. Lischka, and D. Nachtigallová. "Electronic Excitation Processes in Single-Strand and Double-Strand DNA: A Computational Approach". In: *Photoinduced Phenomena in Nucleic Acids II: DNA Fragments and Phenomenological Aspects*. Ed. by M. Barbatti, A. C. Borin, and S. Ullrich. Topics in Current Chemistry. Cham: Springer International Publishing, 2015. 1–37. DOI: 10.1007/128_2013_517.

[101] P. R. Markwick and N. L. Doltsinis, "Ultrafast repair of irradiated DNA: Nonadiabatic ab initio simulations of the guanine-cytosine photocycle", *The Journal of Chemical Physics* **2007**, *126*, 05B603.

[102] G. Groenhof, L. V. Schäfer, M. Boggio-Pasqua, M. Goette, H. Grubmüller, and M. A. Robb, "Ultrafast deactivation of an excited cytosine- guanine base pair in DNA", *Journal of the American Chemical Society* **2007**, *129*, 6812–6819.

[103] A. L. Sobolewski and W. Domcke, "Ab initio studies on the photophysics of the guanine–cytosine base pair", *Physical Chemistry Chemical Physics* **2004**, *6*, 2763–2771.

[104] T. Schultz, E. Samoylova, W. Radloff, I. V. Hertel, A. L. Sobolewski, and W. Domcke, "Efficient Deactivation of a Model Base Pair via Excited-State Hydrogen Transfer", *Science* **2004**, *306*, 1765–1768. DOI: 10.1126/science.1104038.

[105] N. K. Schwalb and F. Temps, "Ultrafast electronic relaxation in guanosine is promoted by hydrogen bonding with cytidine", *Journal of the American Chemical Society* **2007**, *129*, 9272–9273.

[106] V. G. Stavros and J. R. Verlet, "Gas-phase femtosecond particle spectroscopy: a bottom-up approach to nucleotide dynamics", *Annual Review of Physical Chemistry* **2016**, *67*, 211–232. DOI: 10.1146/annurev-physchem-040215-112428.

[107] S. Hammes-Schiffer, "Theoretical Perspectives on Proton-Coupled Electron Transfer Reactions", *Accounts of Chemical Research* **2001**, *34*, 273–281. DOI: 10.1021/ar9901117.

[108] S. Hammes-Schiffer, "Proton-coupled electron transfer: Moving together and charging forward", *Journal of the American Chemical Society* **2015**, *137*, 8860–8871.

[109] J. A. Green, S. Gómez, G. Worth, F. Santoro, and R. Improta, "Solvent Effects on Ultrafast Charge Transfer Population: Insights from the Quantum Dynamics of Guanine-Cytosine in Chloroform", *Chemistry–A European Journal* **2022**, *28*, e202201731.

[110] L. Biemann, S. A. Kovalenko, K. Kleinermanns, R. Mahrwald, M. Markert, and R. Improta, "Excited state proton transfer is not involved in the ultrafast deactivation of guanine–cytosine pair in solution", *Journal of the American Chemical Society* **2011**, *133*, 19664–19667.

[111] P. R. Markwick, N. L. Doltsinis, and J. Schlitter, "Probing irradiation induced DNA damage mechanisms using excited state Car-Parrinello molecular dynamics", *The Journal of Chemical Physics* **2007**, *126*, 01B623.

[112] J. A. Green, M. Yaghoubi Jouybari, H. Asha, F. Santoro, and R. Improta, "Fragment Diabatization Linear Vibronic Coupling Model for Quantum Dynamics of Multichromophoric Systems: Population of the Charge-Transfer State in the Photoexcited Guanine–Cytosine Pair", *Journal of Chemical Theory and Computation* **2021**, *17*, 4660–4674. DOI: 10.1021/acs.jctc.1c00416.

[113] G. Villani, "Theoretical investigation of hydrogen transfer mechanism in the adenine–thymine base pair", *Chemical Physics* **2005**, *316*, 1–8. DOI: 10.1016/j.chemphys.2005.04.030.

[114] S. Perun, A. L. Sobolewski, and W. Domcke, "Role of Electron-Driven Proton-Transfer Processes in the Excited-State Deactivation of the Adenine-Thymine Base Pair", *The Journal of Physical Chemistry A* **2006**, *110*, 9031–9038. DOI: 10.1021/jp061945r.

[115] K. Röttger, H. J. Marroux, A. F. Chemin, E. Elsdon, T. A. Oliver, S. T. Street, A. S. Henderson, M. C. Galan, A. J. Orr-Ewing, and G. M. Roberts, "Is UV-induced electron-driven proton transfer active in a chemically modified A· T DNA base pair?", *The Journal of Physical Chemistry B* **2017**, *121*, 4448–4455.

[116] M. Y. Jouybari, J. A. Green, R. Improta, and F. Santoro, "The Ultrafast Quantum Dynamics of Photoexcited Adenine–Thymine Basepair Investigated with a Fragment-based Diabatization and a Linear Vibronic Coupling Model", *The Journal of Physical Chemistry A* **2021**, *125*, 8912–8924.

[117] J. Cerezo, Y. Liu, N. Lin, X. Zhao, R. Improta, and F. Santoro, "Mixed quantum/classical method for nonadiabatic quantum dynamics in explicit solvent models: The $\pi\pi^*$/nπ^* decay of thymine in water as a test case", *Journal of Chemical Theory and Computation* **2018**, *14*, 820–832.

[118] F. Santoro, V. Barone, and R. Improta, "Absorption Spectrum of A–T DNA Unraveled by Quantum Mechanical Calculations in Solution on the (dA) 2(dT) 2 Tetramer", *ChemPhysChem* **2008**, *9*, 2531–2537.

[119] F. Santoro, V. Barone, and R. Improta, "Excited States Decay of the A- T DNA: A PCM/TD-DFT Study in Aqueous Solution of the (9-Methyl-adenine) 2·(1-methyl-thymine) 2 Stacked Tetramer", *Journal of the American Chemical Society* **2009**, *131*, 15232–15245.

[120] L. Stojanović, S. Bai, J. Nagesh, A. F. Izmaylov, R. Crespo-Otero, H. Lischka, and M. Barbatti, "New Insights into the State Trapping of UV-Excited Thymine", *Molecules* **2016**, *21*, 1603. DOI: 10.3390/molecules21111603.

[121] H. Lischka, M. Barbatti, F. Siddique, A. Das, and A. J. Aquino, "The effect of hydrogen bonding on the nonadiabatic dynamics of a thymine-water cluster", *Chemical Physics* **2018**, *515*, 472–479.

[122] R. C.-T. Chan, C. Ma, A. K.-W. Wong, C. T.-L. Chan, J. C.-L. Chow, and W.-M. Kwok, "Dual Time-Scale Proton Transfer and High-Energy, Long-Lived Excitons Unveiled by Broadband Ultrafast Time-Resolved Fluorescence in Adenine–Uracil RNA Duplexes", *The Journal of Physical Chemistry Letters* **2022**, *13*, 302–311.

[123] K. H. Johnson, D. M. Gray, and J. C. Sutherland, "Vacuum UV CD spectra of homopolymer duplexes and triplexes containing AT or AU base pairs", *Nucleic Acids Research* **1991**, *19*, 2275–2280.

[124] M. Pollum, L. Martinez-Fernandez, and C. E. Crespo-Hernandez, "Photochemistry of nucleic acid bases and their thio-and aza-analogues in solution", *Photoinduced Phenomena in Nucleic Acids I: Nucleobases in the Gas Phase and in Solvents* **2015**, 245–327.

[125] S. Reiter, D. Keefer, and R. de Vivie-Riedle, "RNA environment is responsible for decreased photostability of uracil", *Journal of the American Chemical Society* **2018**, *140*, 8714–8720.

[126] R. Szabla, H. Kruse, J. Šponer, and R. W. Góra, "Water–chromophore electron transfer determines the photochemistry of cytosine and cytidine", *Physical Chemistry Chemical Physics* **2017**, *19*, 17531–17537. DOI: 10.1039/C7CP02635H.

[127] R. Mansour, J. M. Toldo, and M. Barbatti, "Role of the hydrogen bond on the internal conversion of photoexcited adenosine", *The Journal of Physical Chemistry Letters* **2022**, *13*, 6194–6199.

[128] A. Kumar and M. D. Sevilla, "Excited state proton-coupled electron transfer in 8-oxoG–C and 8-oxoG–A base pairs: a time dependent density functional theory (TD-DFT) study", *Photochemical & Photobiological Sciences* **2013**, *12*, 1328. DOI: 10.1039/c3pp25430e.

[129] X. Wu, T. Karsili, and W. Domcke, "Role of Electron-Driven Proton-Transfer Processes in the Ultrafast Deactivation of Photoexcited Anionic 8-oxoGuanine-Adenine and 8-oxoGuanine-Cytosine Base Pairs", *Molecules* **2017**, *22*, 135. DOI: 10.3390/molecules22010135.

[130] T. Carell, C. Brandmayr, A. Hienzsch, M. Müller, D. Pearson, V. Reiter, I. Thoma, P. Thumbs, and M. Wagner, "Structure and Function of Noncanonical Nucleobases", *Angewandte Chemie International Edition* **2012**, *51*, 7110–7131. DOI: 10.1002/anie.201201193.

[131] N. V. Hud, B. J. Cafferty, R. Krishnamurthy, and L. D. Williams, "The Origin of RNA and "My Grandfather's Axe"", *Chemistry & Biology* **2013**, *20*, 466–474. DOI: 10.1016/j.chembiol.2013.03.012.

[132] B. J. Cafferty, I. Gállego, M. C. Chen, K. I. Farley, R. Eritja, and N. V. Hud, "Efficient Self-Assembly in Water of Long Noncovalent Polymers by Nucleobase Analogues", *Journal of the American Chemical Society* **2013**, *135*, 2447–2450. DOI: 10.1021/ja312155v.

[133] A. C. Rios and Y. Tor, "On the origin of the canonical nucleobases: an assessment of selection pressures across chemical and early biological evolution", *Israel journal of chemistry* **2013**, *53*, 469–483.

[134] S. Becker, C. Schneider, A. Crisp, and T. Carell, "Non-canonical nucleosides and chemistry of the emergence of life", *Nature Communications* **2018**, *9*, 5174. DOI: 10.1038/s41467-018-07222-w.

[135] C. Switzer, S. E. Moroney, and S. A. Benner, "Enzymatic incorporation of a new base pair into DNA and RNA", *Journal of the American Chemical Society* **1989**, *111*, 8322–8323. DOI: 10.1021/ja00203a067.

[136] J. A. Piccirilli, S. A. Benner, T. Krauch, S. E. Moroney, and S. A. Benner, "Enzymatic incorporation of a new base pair into DNA and RNA extends the genetic alphabet", *Nature* **1990**, *343*, 33–37. DOI: 10.1038/343033a0.

[137] C. Roberts, R. Bandaru, and C. Switzer, "Theoretical and Experimental Study of Isoguanine and Isocytosine: Base Pairing in an Expanded Genetic System", *Journal of the American Chemical Society* **1997**, *119*, 4640–4649. DOI: 10.1021/ja970123s.

[138] K. Groebke, J. Hunziker, W. Fraser, L. Peng, U. Diederichsen, K. Zimmermann, A. Holzner, C. Leumann, and A. Eschenmoser, "Warum Pentose- und nicht Hexose-Nucleinsäuren??. Teil V. (Purin-Puri n)-Basenpaarung in der homo-DNS-Reihe: Guanin, Isoguanin, 2,6-Diaminopurin und Xanthin", *Helvetica Chimica Acta* **1998**, *81*, 375–474. DOI: 10.1002/hlca.19980810302.

[139] B. D. Heuberger and C. Switzer, "An Alternative Nucleobase Code: Characterization of Purine-Purine DNA Double Helices Bearing Guanine-Isoguanine and Diaminopurine 7-Deaza-Xanthine Base Pairs", *ChemBioChem* **2008**, *9*, 2779–2783. DOI: 10.1002/cbic.200800450.

[140] F. Crick, "The origin of the genetic code", *Journal of Molecular Biology* **1968**, *38*, 367–379. DOI: 10.1016/0022-2836(68)90392-6.

[141] S. Miyakawa, H. J. Cleaves, and S. L. Miller, "The Cold Origin of Life: B. Implications Based on Pyrimidines and Purines Produced From Frozen Ammonium Cyanide Solutions", *Origins of Life and Evolution of the Biosphere* **2002**, *32*, 209–218. DOI: 10.1023/a:1019514022822.

[142] J. Xu, V. Chmela, N. J. Green, D. A. Russell, M. J. Janicki, R. W. Góra, R. Szabla, A. D. Bond, and J. D. Sutherland, "Selective prebiotic formation of RNA pyrimidine and DNA purine nucleosides", *Nature* **2020**, *582*, 60–66. DOI: 10.1038/s41586-020-2330-9.

[143] C. Hartel and M. Göbel, "Substitution of Adenine by Purine-2, 6-diamine Improves the Nonenzymatic Oligomerization of Ribonucleotides on Templates Containing Thymidine", *Helvetica Chimica Acta* **2000**, *83*, 2541–2549. DOI: 10.1002/1522-2675(20000906)83:9<2541::aid-hlca2541>3.0.co;2-8.

[144] Y. Y. Guan, N. Fray, P. Coll, F. Macari, D. Chaput, F. Raulin, and H. Cottin, "UVolution: compared photochemistry of prebiotic organic compounds in low Earth orbit and in the laboratory", *Planetary and Space Science* **2010**, *58*, 1327–1346.

[145] M. P. Callahan, K. E. Smith, H. J. Cleaves, J. Ruzicka, J. C. Stern, D. P. Glavin, C. H. House, and J. P. Dworkin, "Carbonaceous meteorites contain a wide range of extraterrestrial nucleobases", *Proceedings of the National Academy of Sciences* **2011**, *108*, 13995–13998. DOI: 10.1073/pnas.1106493108.

[146] J. Šponer, P. Jurečka, and P. Hobza, "Accurate Interaction Energies of Hydrogen-Bonded Nucleic Acid Base Pairs", *Journal of the American Chemical Society* **2004**, *126*, 10142–10151. DOI: 10.1021/ja048436s.

[147] Z. Gengeliczki, M. P. Callahan, N. Svadlenak, C. I. Pongor, B. Sztaray, L. Meerts, D. Nachtigallova, P. Hobza, M. Barbatti, H. Lischka, et al., "Effect of substituents on the excited-state dynamics of the modified DNA bases 2, 4-diaminopyrimidine and 2, 6-diaminopurine", *Physical Chemistry Chemical Physics* **2010**, *12*, 5375–5388.

[148] M. M. Brister, M. Pollum, and C. E. Crespo-Hernández, "Photochemical etiology of promising ancestors of the RNA nucleobases", *Physical Chemistry Chemical Physics* **2016**, *18*, 20097–20103. DOI: 10.1039/c6cp00639f.

[149] Y. Zhang, A. A. Beckstead, Y. Hu, X. Piao, D. Bong, and B. Kohler, "Excited-state dynamics of melamine and its lysine derivative investigated by femtosecond transient absorption spectroscopy", *Molecules* **2016**, *21*, 1645. DOI: 10.3390/molecules21121645.

[150] J. Peon and A. H. Zewail, "DNA/RNA nucleotides and nucleosides: direct measurement of excited-state lifetimes by femtosecond fluorescence up-conversion", *Chemical physics letters* **2001**, *348*, 255–262. DOI: 10.1016/S0009-2614(01)01128-9.

[151] B. Cohen, P. M. Hare, and B. Kohler, "Ultrafast excited-state dynamics of adenine and monomethylated adenines in solution: Implications for the nonradiative decay mechanism", *Journal of the American Chemical Society* **2003**, *125*, 13594–13601.

[152] R. J. Malone, A. M. Miller, and B. Kohler, "Singlet Excited-state Lifetimes of Cytosine Derivatives Measured by Femtosecond Transient Absorption¶", *Photochemistry and photobiology* **2003**, *77*, 158–164.

[153] H. Kang, K. T. Lee, B. Jung, Y. J. Ko, and S. K. Kim, "Intrinsic lifetimes of the excited state of DNA and RNA bases", *Journal of the American Chemical Society* **2002**, *124*, 12958–12959.

[154] A. M. Rijs and J. Oomens, *Gas-phase IR spectroscopy and structure of biological molecules*, vol. 364. Springer, 2015.

[155] J. Chen and B. Kohler, "Ultrafast nonradiative decay by hypoxanthine and several methylxanthines in aqueous and acetonitrile solution", *Physical Chemistry Chemical Physics* **2012**, *14*, 10677–10682. DOI: 10.1039/C2CP41296A.

[156] D. Nachtigallova, H. Lischka, J. J. Szymczak, M. Barbatti, P. Hobza, Z. Gengeliczki, G. Pino, M. P. Callahan, and M. S. De Vries, "The effect of C5 substitution on the photochemistry of uracil", *Physical Chemistry Chemical Physics* **2010**, *12*, 4924–4933.

[157] L. Martinez-Fernandez, S. Arslancan, D. Ivashchenko, C. E. Crespo-Hernandez, and I. Corral, "Tracking the origin of photostability in purine nucleobases: the photophysics of 2-oxopurine", *Physical Chemistry Chemical Physics* **2019**, *21*, 13467–13473.

[158] M. Barbatti and H. Lischka, "Why water makes 2-aminopurine fluorescent?", *Physical Chemistry Chemical Physics* **2015**, *17*, 15452–15459.

[159] A. Jaworski, J. S. Kwiatkowski, and B. Lesyng, "Why isoguanine and isocytosine are not the components of the genetic code", *International Journal of Quantum Chemistry* **2009**, *28*, 209–216. DOI: 10.1002/qua.560280720.

[160] R. Szabla, R. W. Góra, and J. Šponer, "Ultrafast excited-state dynamics of isocytosine", *Physical Chemistry Chemical Physics* **2016**, *18*, 20208–20218. DOI: 10.1039/C6CP01391K.

[161] G. Gate, R. Szabla, M. R. Haggmark, J. Šponer, A. L. Sobolewski, and M. S. de Vries, "Photodynamics of alternative DNA base isoguanine", *Physical Chemistry Chemical Physics* **2019**, *21*, 13474–13485. DOI: 10.1039/C9CP01622H.

[162] H. Böhnke, K. Röttger, R. A. Ingle, H. J. Marroux, M. Bohnsack, N. K. Schwalb, A. J. Orr-Ewing, and F. Temps, "Electronic relaxation dynamics of UV-photoexcited 2-aminopurine–thymine base pairs in Watson–Crick and Hoogsteen conformations", *The Journal of Physical Chemistry B* **2019**, *123*, 2904–2914.

[163] S. Kanvah, J. Joseph, G. B. Schuster, R. N. Barnett, C. L. Cleveland, and U. Landman, "Oxidation of DNA: Damage to Nucleobases", *Accounts of Chemical Research* **2010**, *43*, 280–287. DOI: 10.1021/ar900175a.

[164] Y. Zhang, J. Dood, A. A. Beckstead, X.-B. Li, K. V. Nguyen, C. J. Burrows, R. Improta, and B. Kohler, "Efficient UV-induced charge separation and recombination in an 8-oxoguanine-containing dinucleotide", *Proceedings of the National Academy of Sciences* **2014**, *111*, 11612–11617. DOI: 10.1073/pnas.1404411111.

[165] S. Steenken, S. V. Jovanovic, M. Bietti, and K. Bernhard, "The Trap Depth (in DNA) of 8-Oxo-7,8-dihydro-2'deoxyguanosine as Derived from Electron-Transfer Equilibria in Aqueous Solution", *Journal of the American Chemical Society* **2000**, *122*, 2373–2374. DOI: 10.1021/ja993508e.

[166] B. J. Cafferty, D. M. Fialho, J. Khanam, R. Krishnamurthy, and N. V. Hud, "Spontaneous formation and base pairing of plausible prebiotic nucleotides in water", *Nature communications* **2016**, *7*, 11328.

[167] J. D. Sutherland, "The Origin of Life—Out of the Blue", *Angew. Chem. Int. Ed.* **2016**, *55*, 104–121. DOI: 10.1002/anie.201506585.

[168] P. Ehrenfreund, M. Bernstein, J. Dworkin, S. Sandford, and L. Allamandola, "The photostability of amino acids in space", *The Astrophysical Journal* **2001**, *550*, L95.

[169] R. Szabla, D. Tuna, R. W. Góra, J. Šponer, A. L. Sobolewski, and W. Domcke, "Photochemistry of 2-aminooxazole, a hypothetical prebiotic precursor of RNA nucleotides", *The Journal of Physical Chemistry Letters* **2013**, *4*, 2785–2788. DOI: 10.1021/jz401315e.

[170] S. A. Sandford, P. P. Bera, T. J. Lee, and M. Nuevo. "Photosynthesis and photostability of nucleic acids in prebiotic extraterrestrial environments". In: *Photoinduced Phenomena in Nucleic Acids II*. Springer, 2014. 123–164.

[171] C. Plützer, I. Hünig, K. Kleinermanns, E. Nir, and M. S. de Vries, "Pairing of Isolated Nucleobases: Double Resonance Laser Spectroscopy of Adenine-Thymine", *ChemPhysChem* **2003**, *4*, 838–842. DOI: 10.1002/cphc.200300648.

[172] E. Samoylova, H. Lippert, S. Ullrich, I. V. Hertel, W. Radloff, and T. Schultz, "Dynamics of photoinduced processes in adenine and thymine base pairs", *Journal of the American Chemical Society* **2005**, *127*, 1782–1786.

[173] E. Samoylova, T. Schultz, I. Hertel, and W. Radloff, "Analysis of ultrafast relaxation in photoexcited DNA base pairs of adenine and thymine", *Chemical Physics* **2008**, *347*, 376–382.

[174] K. Röttger, H. J. B. Marroux, A. F. M. Chemin, E. Elsdon, T. A. A. Oliver, S. T. G. Street, A. S. Henderson, M. C. Galan, A. J. Orr-Ewing, and G. M. Roberts, "Is UV-Induced Electron-Driven Proton Transfer Active in a Chemically Modified A-T DNA Base Pair?", *The Journal of Physical Chemistry B* **2017**, *121*, 4448–4455. DOI: 10.1021/acs.jpcb.7b02679.

[175] R. Szabla, R. W. Góra, M. Janicki, and J. Šponer, "Photorelaxation of imidazole and adenine via electron-driven proton transfer along H2O wires", *Faraday Discussions* **2016**, *195*, 237–251. DOI: 10.1039/C6FD00131A.

[176] P. M. Hare, C. E. Crespo-Hernández, and B. Kohler, "Internal conversion to the electronic ground state occurs via two distinct pathways for pyrimidine bases in aqueous solution", *Proceedings of the National Academy of Sciences* **2007**, *104*, 435–440. DOI: 10.1073/pnas.0608055104.

[177] A. Szabo and N. S. Ostlund, *Modern quantum chemistry: introduction to advanced electronic structure theory*, Courier Corporation, 2012.

[178] F. Jensen. *Introduction to computational chemistry*. 2016.

[179] B. O. Roos, P. R. Taylor, and P. E. Sigbahn, "A complete active space SCF method (CASSCF) using a density matrix formulated super-CI approach", *Chemical Physics* **1980**, *48*, 157–173.

[180] P.-Å. Malmqvist and B. O. Roos, "The CASSCF state interaction method", *Chemical Physics Letters* **1989**, *155*, 189–194.

[181] K. P. Lawley, *Ab Initio Methods in Quantum Chemistry, Volume 69, Part 2*, John Wiley & Sons, 2009.

[182] V. Veryazov, P. Å. Malmqvist, and B. O. Roos, "How to select active space for multi-configurational quantum chemistry?", *International Journal of Quantum Chemistry* **2011**, *111*, 3329–3338. DOI: 10.1002/qua.23068.

[183] B. O. Roos, K. Andersson, M. P. Fülscher, P.-â. Malmqvist, L. Serrano-Andrés, K. Pierloot, and M. Merchán. "Multiconfigurational Perturbation Theory: Applications in Electronic Spectroscopy". In: *Advances in Chemical Physics*. Ed. by I. Prigogine and S. A. Rice. John Wiley & Sons, Inc., 1996. 219–331.

[184] H. Lischka, M. Dallos, P. G. Szalay, D. R. Yarkony, and R. Shepard, "Analytic Evaluation of Nonadiabatic Coupling Terms at the MR-CI Level. I. Formalism", *The Journal of Chemical Physics* **2004**, *120*, 7322–7329. DOI: 10.1063/1.1668615.

[185] F. Plasser, "Quantum mechanical simulations of defect dynamics in DNA and model systems", PhD Thesis, University of Vienna, **2012**.

[186] M. R. Silva-Junior, M. Schreiber, S. P. A. Sauer, and W. Thiel, "Benchmarks of electronically excited states: Basis set effects on CASPT2 results", *The Journal of Chemical Physics* **2010**, *133*, 174318. DOI: 10.1063/1.3499598.

[187] R. Sarkar, P.-F. Loos, M. Boggio-Pasqua, and D. Jacquemin, "Assessing the Performances of CASPT2 and NEVPT2 for Vertical Excitation Energies", *Journal of Chemical Theory and Computation* **2022**, *18*, 2418–2436. DOI: 10.1021/acs.jctc.1c01197.

[188] J. P. Zobel, J. J. Nogueira, and L. González, "The IPEA dilemma in CASPT2", *Chemical Science* **2017**, *8*, 1482–1499. DOI: 10.1039/C6SC03759C.

[189] S. Battaglia and R. Lindh, "Extended dynamically weighted CASPT2: The best of two worlds", *Journal of Chemical Theory and Computation* **2020**, *16*, 1555–1567.

[190] Ł. Wolański, D. Grabarek, and T. Andruniów, "Is the choice of a standard zeroth-order hamiltonian in CASPT2 ansatz optimal in calculations of excitation energies in protonated and unprotonated schiff bases of retinal?", *Journal of Computational Chemistry* **2018**, *39*, 1470–1480. DOI: 10.1002/jcc.25217.

[191] C. Angeli, R. Cimiraglia, and J.-P. Malrieu, "n-electron valence state perturbation theory: A spinless formulation and an efficient implementation of the strongly contracted and of the partially contracted variants", *The Journal of Chemical Physics* **2002**, *117*, 9138–9153.

[192] C. Angeli, R. Cimiraglia, and J.-P. Malrieu, "N-electron valence state perturbation theory: a fast implementation of the strongly contracted variant", *Chemical Physics Letters* **2001**, *350*, 297–305.

[193] C. Angeli, R. Cimiraglia, S. Evangelisti, T. Leininger, and J.-P. Malrieu, "Introduction of n-electron valence states for multireference perturbation theory", *The Journal of Chemical Physics* **2001**, *114*, 10252–10264.

[194] A. A. Granovsky, "Extended multi-configuration quasi-degenerate perturbation theory: The new approach to multi-state multi-reference perturbation theory", *The Journal of Chemical Physics* **2011**, *134*, 214113. DOI: 10.1063/1.3596699.

[195] T. Shiozaki, W. Győrffy, P. Celani, and H.-J. Werner, "Communication: Extended multi-state complete active space second-order perturbation theory: Energy and nuclear gradients", *J. Chem. Phys.* **2011**, *135*, 081106. DOI: 10.1063/1.3633329.

[196] Q. M. Phung, Y. Komori, T. Yanai, T. Sommerfeld, and M. Ehara, "Combination of a Voronoi-type complex absorbing potential with the XMS-CASPT2 method and pilot applications", *Journal of Chemical Theory and Computation* **2020**, *16*, 2606–2616.

[197] M. Musiał. "Equation-of-Motion Coupled-Cluster Models". In: *Quantum Chemistry and Dynamics of Excited States.* John Wiley & Sons, Ltd, 2020. 77–108. DOI: 10.1002/9781119417774.ch4.

[198] C. Hättig. "Structure Optimizations for Excited States with Correlated Second-Order Methods: CC2 and ADC(2)". In: *Advances in Quantum Chemistry.* Ed. by H. J. A. Jensen. Vol. 50. Response Theory and Molecular Properties (A Tribute to Jan Linderberg and Poul Jørgensen). Academic Press, 2005. 37–60. DOI: 10.1016/S0065-3276(05)50003-0.

[199] A. B. Trofimov and J. Schirmer, "An efficient polarization propagator approach to valence electron excitation spectra", *Journal of Physics B: Atomic, Molecular and Optical Physics* **1995**, *28*, 2299. DOI: 10.1088/0953-4075/28/12/003.

[200] A. Dreuw and M. Wormit, "The algebraic diagrammatic construction scheme for the polarization propagator for the calculation of excited states", *Wiley Interdisciplinary Reviews: Computational Molecular Science* **2015**, *5*, 82–95. DOI: 10.1002/wcms.1206.

[201] R. Lindh and L. González, *Quantum Chemistry and Dynamics of Excited States: Methods and Applications*, John Wiley & Sons, 2020.

[202] A. Dreuw, A. Papapostolou, and A. L. Dempwolff, "Algebraic Diagrammatic Construction Schemes Employing the Intermediate State Formalism: Theory, Capabilities, and Interpretation", *The Journal of Physical Chemistry A* **2023**.

[203] S. Grimme, "Improved second-order Møller–Plesset perturbation theory by separate scaling of parallel- and antiparallel-spin pair correlation energies", *J. Chem. Phys.* **2003**, *118*, 9095–9102. DOI: 10.1063/1.1569242.

[204] S. Grimme, L. Goerigk, and R. F. Fink, "Spin-component-scaled electron correlation methods", *Wiley Interdisciplinary Reviews: Computational Molecular Science* **2012**, *2*, 886–906. DOI: 10.1002/wcms.1110.

[205] A. Tajti and P. G. Szalay, "Accuracy of Spin-Component-Scaled CC2 Excitation Energies and Potential E nergy Surfaces", *Journal of Chemical Theory and Computation* **2019**, *15*, 5523–5531. DOI: 10.1021/acs.jctc.9b00676.

[206] S. Boys and F. Bernardi, "The Calculation of Small Molecular Interactions by the Differences of Separate Total Energies. Some Procedures with Reduced Errors", *Molecular Physics* **1970**, *19*, 553–566. DOI: 10.1080/00268977000101561.

[207] M. J. Frisch, G. W. Trucks, H. B. Schlegel, G. E. Scuseria, M. A. Robb, J. R. Cheeseman, G. Scalmani, V. Barone, G. A. Petersson, H. Nakatsuji, X. Li, M. Caricato, A. V. Marenich, J. Bloino, B. G. Janesko, R. Gomperts, B. Mennucci, H. P. Hratchian, J. V. Ortiz, A. F. Izmaylov, J. L. Sonnenberg, D. Williams-Young, F. Ding, F. Lipparini, F. Egidi, J. Goings, B. Peng, A. Petrone, T. Henderson, D. Ranasinghe, V. G. Zakrzewski, J. Gao, N. Rega, G. Zheng, W. Liang, M. Hada, M. Ehara, K. Toyota, R. Fukuda, J. Hasegawa, M. Ishida, T. Nakajima, Y. Honda, O. Kitao, H. Nakai, T. Vreven, K. Throssell, J. A. Montgomery Jr., J. E. Peralta, F. Ogliaro, M. J. Bearpark, J. J. Heyd, E. N. Brothers, K. N. Kudin, V. N. Staroverov, T. A. Keith, R. Kobayashi, J. Normand, K. Raghavachari, A. P. Rendell, J. C. Burant, S. S. Iyengar, J. Tomasi, M. Cossi, J. M. Millam, M. Klene, C. Adamo, R. Cammi, J. W. Ochterski, R. L. Martin, K. Morokuma, O. Farkas, J. B. Foresman, and D. J. Fox. *Gaussian~16 Revision C.01.* Gaussian Inc. Wallingford CT. 2016.

[208] M. W. Schmidt, K. K. Baldridge, J. A. Boatz, S. T. Elbert, M. S. Gordon, J. H. Jensen, S. Koseki, N. Matsunaga, K. A. Nguyen, S. Su, et al., "General atomic and molecular electronic structure system", *Journal of Computational Chemistry* **1993**, *14*, 1347–1363.

[209] M. Gutowski, F. B. Van Duijneveldt, G. Chałasiński, and L. Piela, "Proper correction for the basis set superposition error in SCF calculations of intermolecular interactions", *Molecular Physics* **1987**, *61*, 233–247. DOI: 10.1080/00268978700101101.

[210] W. A. Sokalski, S. Roszak, and K. Pecul, "An efficient procedure for decomposition of the SCF interaction energy into components with reduced basis set dependence", *Chemical physics letters* **1988**, *153*, 153–159. DOI: 10.1016/0009-2614(88)85203-5.

[211] G. Chałasiński and M. Szcześniak, "On the connection between the supermolecular Møller-Plesset treatment of the interaction energy and the perturbation theory of intermolecular forces", *Molecular Physics* **1988**, *63*, 205–224. DOI: 10.1080/00268978800100171.

[212] S. Cybulski, G. Chal/asiński, and R. Moszyński, "On decomposition of second-order Mo/ller–Plesset supermolecular interaction energy and basis set effects", *The Journal of chemical physics* **1990**, *92*, 4357–4363. DOI: 10.1063/1.457743v.

[213] R. W. Gora, W. Bartkowiak, S. Roszak, and J. Leszczynski, "Intermolecular interactions in solution: Elucidating the influence of the solvent", *The Journal of chemical physics* **2004**, *120*, 2802–2813. DOI: 10.1063/1.1636155.

[214] T. H. Dunning, "Gaussian basis sets for use in correlated molecular calculations. I. The atoms boron through neon and hydrogen", *The Journal of Chemical Physics* **1989**, *90*, 1007–1023. DOI: 10.1063/1.456153.

[215] *TURBOMOLE v7.3 2018, a development of University of Karlsruhe and Forschungszentrum Karlsruhe GmbH, 1989-2007, TURBOMOLE GmbH, since 2007; available from www.turbomole.com.*

[216] J. Tomasi, B. Mennucci, and R. Cammi, "Quantum mechanical continuum solvation models", *Chemical reviews* **2005**, *105*, 2999–3094. DOI: 10.1021/cr9904009.

[217] F. Plasser, M. Wormit, and A. Dreuw, "New tools for the systematic analysis and visualization of electronic excitations. I. Formalism", *The Journal of Chemical Physics* **2014**, *141*, 024106. DOI: 10.1063/1.4885819.

[218] F. Plasser, S. A. Bäppler, M. Wormit, and A. Dreuw, "New tools for the systematic analysis and visualization of electronic excitations. II. Applications", *The Journal of Chemical Physics* **2014**, *141*, 024107. DOI: 10.1063/1.4885820.

[219] F. Plasser, "TheoDORE: A toolbox for a detailed and automated analysis of electronic excited state computations", *The Journal of Chemical Physics* **2020**, *152*, 084108. DOI: 10.1063/1.5143076.

[220] R. S. Mulliken, "Electronic population analysis on LCAO–MO molecular wave functions. I", *The Journal of chemical physics* **1955**, *23*, 1833–1840. DOI: 10.1063/1.1740588.

[221] Q. Peng, Y. Yi, Z. Shuai, and J. Shao, "Excited state radiationless decay process with Duschinsky rotation effect: Formalism and implementation", *The Journal of Chemical Physics* **2007**, *126*, 114302. DOI: 10.1063/1.2710274.

[222] Y. Niu, Q. Peng, C. Deng, X. Gao, and Z. Shuai, "Theory of Excited State Decays and Optical Spectra: Application to Polyatomic Molecules", *The Journal of Physical Chemistry A* **2010**, *114*, 7817–7831. DOI: 10.1021/jp101568f.

[223] Z. Shuai, "Thermal Vibration Correlation Function Formalism for Molecular Excited State Decay Rates", *Chinese Journal of Chemistry* **2020**, *38*, 1223–1232. DOI: 10.1002/cjoc.202000226.

[224] Y. Niu, W. Li, Q. Peng, H. Geng, Y. Yi, L. Wang, G. Nan, D. Wang, and Z. Shuai, "MOlecular MAterials Property Prediction Package (MOMAP) 1.0: a software package for predicting the luminescent properties and mobility of organic functional materials", *Molecular Physics* **2018**, *116*, 1078–1090. DOI: 10.1080/00268976.2017.1402966.

[225] Y. Shao, Z. Gan, E. Epifanovsky, A. T. Gilbert, M. Wormit, J. Kussmann, A. W. Lange, A. Behn, J. Deng, X. Feng, et al., "Advances in molecular quantum chemistry contained in the Q-Chem 4 program package", *Molecular Physics* **2015**, *113*, 184–215. DOI: 10.1080/00268976.2014.952696.

[226] S. Kotaru, P. Pokhilko, and A. I. Krylov, "Spin–orbit couplings within spin-conserving and spin-flipping time-dependent density functional theory: Implementation and benchmark calculations", *The Journal of Chemical Physics* **2022**, *157*, 224110. DOI: 10.1063/5.0130868.

[227] R. L. Martin, "Natural transition orbitals", *The Journal of Chemical Physics* **2003**, *118*, 4775–4777. DOI: 10.1063/1.1558471.

[228] P. G. Szalay, T. Watson, A. Perera, V. Lotrich, and R. J. Bartlett, "Benchmark Studies on the Building Blocks of DNA. 3. Watson–Crick and Stacked Base Pairs", *The Journal of Physical Chemistry A* **2013**, *117*, 3149–3157. DOI: 10.1021/jp3100975.

[229] Z. Benda and P. G. Szalay, "Characterization of the excited states of DNA building blocks: a coupled cluster computational study", *Physical Chemistry Chemical Physics* **2016**, *18*, 23596–23606. DOI: 10.1039/C6CP02969H.

[230] J. Dezalay, M. Broquier, S. Soorkia, and G. Grégoire, "Excited state dynamics of protonated keto uracil: intersystem crossing pathways in competition", *The European Physical Journal D* **2021**, *75*, 1–11. DOI: 10.1140/epjd/s10053-020-00017-z.

[231] J. Ray and S. G. Ramesh, "Excited-state proton transfer in a 2-aminopyridine dimer: a surface hopping study", *Physical Chemistry Chemical Physics* **2022**, *24*, 7274–7292. DOI: 10.1039/D1CP05517H.

[232] X. Zhang, J. Jie, D. Song, and H. Su, "Deprotonation of Guanine Radical Cation G•+ Mediated by the Protonated Water Cluster", *The Journal of Physical Chemistry A* **2020**, *124*, 6076–6083. DOI: 10.1021/acs.jpca.0c03748.

[233] A. Hellweg, S. A. Grün, and C. Hättig, "Benchmarking the performance of spin-component scaled CC2 in ground and electronically excited states", *Physical Chemistry Chemical Physics* **2008**, *10*, 4119–4127. DOI: 10.1039/B803727B.

[234] A. L. Sobolewski and W. Domcke, "Computational Studies of the Photophysics of Hydrogen-Bonded Molecular Systems", *The Journal of Physical Chemistry A* **2007**, *111*, 11725–11735. DOI: 10.1021/jp075803o.

[235] S. Mouret, C. Baudouin, M. Charveron, A. Favier, J. Cadet, and T. Douki, "Cyclobutane pyrimidine dimers are predominant DNA lesions in whole human skin exposed to UVA radiation", *Proceedings of the National Academy of Sciences* **2006**, *103*, 13765–13770. DOI: 10.1073/pnas.0604213103.

[236] O. Christiansen, H. Koch, and P. Jørgensen, "The second-order approximate coupled cluster singles and doubles model CC2", *Chemical Physics Letters* **1995**, *243*, 409–418. DOI: 10.1016/0009-2614(95)00841-q.

[237] O. Kennard, "Structural Studies of DNA Fragments: The G·T Wobble Base Pair in A, B and Z DNA; The G·A Base Pair in B-DNA", *Journal of Biomolecular Structure and Dynamics* **1985**, *3*, 205–226. DOI: 10.1080/07391102.1985.10508412.

[238] T. Brown, O. Kennard, G. Kneale, and D. Rabinovich, "High-resolution structure of a DNA helix containing mismatched base pairs", *Nature* **1985**, *315*, 604–606. DOI: 10.1038/315604a0.

[239] J. E. Ladner, A. Jack, J. D. Robertus, R. S. Brown, D. Rhodes, B. F. Clark, and A. Klug, "Structure of yeast phenylalanine transfer RNA at 2.5 A resolution.", *Proceedings of the National Academy of Sciences* **1975**, *72*, 4414–4418. DOI: 10.1073/pnas.72.11.4414.

[240] G. Varani and W. H. McClain, "The G·U wobble base pair", *EMBO reports* **2000**, *1*, 18–23. DOI: 10.1093/embo-reports/kvd001.

[241] *BAGEL, Brilliantly Advanced General Electronic-structure Library. http:// www.nubakery.org under the GNU General Public License.*

[242] R. Szabla, J. Campos, J. E. Šponer, J. Šponer, R. W. Góra, and J. D. Sutherland, "Excited-state hydrogen atom abstraction initiates the photochemistry of β-2′-deoxycytidine", *Chemical Science* **2015**, *6*, 2035–2043. DOI: 10.1039/C4SC03761H.

[243] X. Wu, T. N. V. Karsili, and W. Domcke, "Excited-State Deactivation of Adenine by Electron-Driven Proton-Transfer Reactions in Adenine–Water Clusters: A Computational Study", *ChemPhysChem* **2016**, *17*, 1298–1304. DOI: 10.1002/cphc.201501154.

[244] P. M. Keane, M. Wojdyla, G. W. Doorley, G. W. Watson, I. P. Clark, G. M. Greetham, A. W. Parker, M. Towrie, J. M. Kelly, and S. J. Quinn, "A Comparative Picosecond Transient Infrared Study of 1-Methylcytosine and 5'-dCMP That Sheds Further Light on the Excited States of Cytosine Derivatives", *Journal of the American Chemical Society* **2011**, *133*, 4212–4215. DOI: 10.1021/ja1106089.

[245] C. Ma, C. C.-W. Cheng, C. T.-L. Chan, R. C.-T. Chan, and W.-M. Kwok, "Remarkable effects of solvent and substitution on the photo-dynamics of cytosine: a femtosecond broadband time-resolved fluorescence and transient absorption study", *Physical Chemistry Chemical Physics* **2015**, *17*, 19045–19057. DOI: 10.1039/C5CP02624E.

[246] G. W. Doorley, D. A. McGovern, M. W. George, M. Towrie, A. W. Parker, J. M. Kelly, and S. J. Quinn, "Picosecond Transient Infrared Study of the Ultrafast Deactivation Processes of Electronically Excited B-DNA and Z-DNA Forms of [poly (dG-dC)] 2", *Angewandte Chemie* **2009**, *121*, 129–133. DOI: 10.1002/anie.200803904.

[247] K. E. Szkaradek, P. Stadlbauer, J. Šponer, R. W. Góra, and R. Szabla, "UV-induced hydrogen transfer in DNA base pairs promoted by dark nπ^* states", *Chemical Communications* **2020**, *56*, 201–204. DOI: 10.1039/C9CC06180K.

[248] S. M. Cybulski and M. L. Lytle, "The origin of deficiency of the supermolecule second-order Mö ller-Plesset approach for evaluating interaction energies", *The Journal of Chemical Physics* **2007**, *127*, 141102–141102–4. DOI: 10.1063/1.2795693.

[249] P. R. Horn, Y. Mao, and M. Head-Gordon, "Probing non-covalent interactions with a second generation energy decomposition analysis using absolutely localized molecular orbitals", *Physical Chemistry Chemical Physics* **2016**, *18*, 23067–23079. DOI: 10.1039/C6CP03784D.

[250] M. Etinski, "The role of Duschinsky rotation in intersystem crossing: a case study of uracil", *Journal of the Serbian Chemical Society* **2011**, *76*, 1649–1660. DOI: 10.2298/JSC110713147E.

[251] C. Canuel, M. Mons, F. Piuzzi, B. Tardivel, I. Dimicoli, and M. Elhanine, "Excited states dynamics of DNA and RNA bases: Characterization of a stepwise deactivation pathway in the gas phase", *The Journal of Chemical Physics* **2005**, *122*, 074316. DOI: 10.1063/1.1850469.

[252] H. M. Berman, W. K. Olson, D. L. Beveridge, J. Westbrook, A. Gelbin, T. Demeny, S.-H. Hsieh, A. Srinivasan, and B. Schneider, "The nucleic acid database. A comprehensive relational database of three-dimensional structures of nucleic acids.", *Biophysical Journal* **1992**, *63*, 751. DOI: 10.1016/S0006-3495(92)81649-1.

[253] B. Coimbatore Narayanan, J. Westbrook, S. Ghosh, A. I. Petrov, B. Sweeney, C. L. Zirbel, N. B. Leontis, and H. M. Berman, "The Nucleic Acid Database: new features and capabilities", *Nucleic Acids Research* **2014**, *42*, D114–D122. DOI: 10.1093/nar/gkt980.

[254] A. Hospital, P. Andrio, C. Cugnasco, L. Codo, Y. Becerra, P. D. Dans, F. Battistini, J. Torres, R. Goni, M. Orozco, et al., "BIGNASim: a NoSQL database structure and analysis portal for nucleic acids simulation data", *Nucleic Acids Research* **2016**, *44*, D272–D278. DOI: 10.1093/nar/gkv1301.

[255] A. Hospital, I. Faustino, R. Collepardo-Guevara, C. Gonzalez, J. L. Gelpí, and M. Orozco, "NAFlex: a web server for the study of nucleic acid flexibility", *Nucleic Acids Research* **2013**, *41*, W47–W55. DOI: 10.1093/nar/gkt378.

[256] C. E. Crespo-Hernández, L. Martínez-Fernández, C. Rauer, C. Reichardt, S. Mai, M. Pollum, P. Marquetand, L. González, and I. Corral, "Electronic and structural elements that regulate the excited-state dynamics in purine nucleobase derivatives", *Journal of the American Chemical Society* **2015**, *137*, 4368–4381. DOI: 10.1021/ja512536c.

[257] P. Jurečka, J. Šponer, J. Černỳ, and P. Hobza, "Benchmark database of accurate (MP2 and CCSD (T) complete basis set limit) interaction energies of small model complexes, DNA base pairs, and amino acid pairs", *Physical Chemistry Chemical Physics* **2006**, *8*, 1985–1993. DOI: 10.1039/B600027D.

[258] A. Hesselmann, G. Jansen, and M. Schütz, "Interaction energy contributions of H-bonded and stacked structures of the AT and GC DNA base pairs from the combined density functional theory and intermolecular perturbation theory approach", *Journal of the American Chemical Society* **2006**, *128*, 11730–11731. DOI: 10.1021/ja0633363.

[259] Y. Mo, "Probing the nature of hydrogen bonds in DNA base pairs", *Journal of Molecular Modeling* **2006**, *12*, 665–672. DOI: 10.1007/s00894-005-0021-y.

[260] A. Alparone, "Linear and nonlinear optical properties of nucleic acid bases", *Chemical Physics* **2013**, *410*, 90–98. DOI: 10.1016/j.chemphys.2012.11.005.

[261] R. W. Góra. *EDS package, revision 2.8.3*. 1998.

[262] S. Śmiga, S. Siecińska, and I. Grabowski, "From simple molecules to nanotubes. Reliable predictions of ionization potentials from the ΔMP2-SCS methods", *New Journal of Physics* **2020**, *22*, 083084. DOI: 10.1088/1367-2630/abaa00.

[263] V. Orlov, A. Smirnov, and Y. M. Varshavsky, "Ionization potentials and electron-donor ability of nucleic acid babes and their analogues", *Tetrahedron Letters* **1976**, *17*, 4377–4378. DOI: 10.1016/0040-4039(76)80120-7.

[264] K. B. Bravaya, O. Kostko, S. Dolgikh, A. Landau, M. Ahmed, and A. I. Krylov, "Electronic structure and spectroscopy of nucleic acid bases: ionization energies, ionization-induced structural changes, and photoelectron spectra", *The Journal of Physical Chemistry A* **2010**, *114*, 12305–12317. DOI: 10.1021/jp1063726.

[265] A. Trofimov, J. Schirmer, V. Kobychev, A. Potts, D. Holland, and L. Karlsson, "Photoelectron spectra of the nucleobases cytosine, thymine and adenine", *Journal of Physics B: Atomic, Molecular and Optical Physics* **2005**, *39*, 305. DOI: 10.1088/0953-4075/39/2/007.

[266] S. Farid, J. P. Dinnocenzo, P. B. Merkel, R. H. Young, D. Shukla, and G. Guirado, "Reexamination of the Rehm–Weller data set reveals electron transfer quenching that follows a Sandros–Boltzmann dependence on free energy", *Journal of the American Chemical Society* **2011**, *133*, 11580–11587. DOI: 10.1021/ja2024367.

[267] D. Rehm and A. Weller, "Kinetics of fluorescence quenching by electron and H-atom transfer", *Israel Journal of Chemistry* **1970**, *8*, 259–271. DOI: 10.1002/ijch.197000029.

[268] J. P. Villabona-Monsalve, R. Noria, S. Matsika, and J. Peón, "On the accessibility to conical intersections in purines: hypoxanthine and its singly protonated and deprotonated forms", *Journal of the American Chemical Society* **2012**, *134*, 7820–7829. DOI: 10.1021/ja300546x.

[269] T. Takaya, C. Su, K. de La Harpe, C. E. Crespo-Hernández, and B. Kohler, "UV excitation of single DNA and RNA strands produces high yields of exciplex states between two stacked bases", *Proceedings of the National Academy of Sciences* **2008**, *105*, 10285–10290. DOI: 10.1073/pnas.0802079105.

[270] L. J. Karas, C.-H. Wu, H. Ottosson, and J. I. Wu, "Electron-driven proton transfer relieves excited-state antiaromaticity in photoexcited DNA base pairs", *Chemical Science* **2020**, *11*, 10071–10077. DOI: 10.1039/D0SC02294B.

[271] S. J. Roberts, R. Szabla, Z. R. Todd, S. Stairs, D.-K. Bučar, J. Šponer, D. Sasselov, and M. W. Powner, "Selective Prebiotic Conversion of Pyrimidine and Purine Anhydronucleosides into Watson-Crick Base-pairing arabino-Furanosyl Nucleosides in Water", *Nat. Commun.* **2018**, *9*, 4073. DOI: 10.1038/s41467-018-06374-z.

[272] S. C. Kim, D. K. O'Flaherty, L. Zhou, V. S. Lelyveld, and J. W. Szostak, "Inosine, but none of the 8-oxo-purines, is a plausible component of a primordial version of RNA", *Proceedings of the National Academy of Sciences* **2018**, *115*, 13318–13323. DOI: 10.1073/pnas.1814367115.

[273] C. M. Marian, "A new pathway for the rapid decay of electronically excited adenine", *The Journal of Chemical Physics* **2005**, *122*, 104314. DOI: 10.1063/1.1861452.

[274] J. Mazur and R. L. Jernigan, "Distance-dependent dielectric constants and their application to double-helical DNA", *Biopolymers* **1991**, *31*, 1615–1629. DOI: 10.1002/bip.360311316.

[275] K. Siriwong, A. A. Voityuk, M. D. Newton, and N. Rösch, "Estimate of the Reorganization Energy for Charge Transfer in DNA", *The Journal of Physical Chemistry B* **2003**, *107*, 2595–2601. DOI: 10.1021/jp027052q.

[276] K. Röttger, H. J. B. Marroux, M. P. Grubb, P. M. Coulter, H. Böhnke, A. S. Henderson, M. C. Galan, F. Temps, A. J. Orr-Ewing, and G. M. Roberts, "Ultraviolet Absorption Induces Hydrogen-Atom Transfer in G·C Watson–Crick DNA Base Pairs in Solution", *Angewandte Chemie International Edition* **2015**, *54*, 14719–14722. DOI: 10.1002/anie.201506940.

[277] R. Szabla, H. Kruse, P. Stadlbauer, J. Šponer, and A. L. Sobolewski, "Sequential electron transfer governs the UV-induced self-repair of DNA photolesions", *Chemical Science* **2018**, *9*, 3131–3140. DOI: 10.1039/C8SC00024G.

[278] J. Ortín-Fernández, N. E. Caldero-Rodríguez, C. E. Crespo-Hernández, L. Martínez-Fernández, and I. Corral, "Photophysical Characterization of Isoguanine in a Prebiotic-Like Environment", *Chemistry–A European Journal* **2023**, *29*, e202203580. DOI: 10.1002/chem.202203580.

[279] S. Yamazaki, A. L. Sobolewski, and W. Domcke, "Photophysics of xanthine: computational study of the radiationless decay mechanisms", *Physical Chemistry Chemical Physics* **2009**, *11*, 10165–10174. DOI: 10.1039/B913131K.

[280] C. Li, B. Cafferty, S. Karunakaran, G. Schuster, and N. Hud, "Formation of supramolecular assemblies and liquid crystals by purine nucleobases and cyanuric acid in water: Implications for the possible origins of RNA", *Physical Chemistry Chemical Physics* **2016**, *18*, 20091–20096. DOI: 10.1039/C6CP03047E.

[281] M. C. Chen, B. J. Cafferty, I. Mamajanov, I. Gállego, J. Khanam, R. Krishnamurthy, and N. V. Hud, "Spontaneous prebiotic formation of a β-ribofuranoside that self-assembles with a complementary heterocycle", *Journal of the American Chemical Society* **2013**, *136*, 5640–5646. DOI: 10.1021/ja410124v.

[282] S. Hammes-Schiffer, "Proton-coupled electron transfer: Classification scheme and guide to theoretical methods", *Energy and Environmental Science* **2012**, *5*, 7696–7703. DOI: 10.1039/C2EE03361E.

[283] Y. Zhang, J. Dood, A. A. Beckstead, X.-B. Li, K. V. Nguyen, C. J. Burrows, R. Improta, and B. Kohler, "Photoinduced electron transfer in DNA: Charge shift dynamics between 8-oxo-guanine anion and adenine", *The Journal of Physical Chemistry B* **2015**, *119*, 7491–7502. DOI: 10.1021/jp511220x.

[284] J. Schirmer, "Beyond the random-phase approximation: A new approximation scheme for the polarization propagator", *Physical Review A* **1982**, *26*, 2395–2416. DOI: 10.1103/PhysRevA.26.2395.

[285] A. Dreuw and M. Wormit, "The algebraic diagrammatic construction scheme for the polarization propagator for the calculation of excited states", *Wiley Interdiscip. Rev. Comput. Mol. Sci.* **2014**, *5*, 82–95. DOI: 10.1002/wcms.1206.

[286] F. Neese, "The ORCA program system", *WIREs Computational Molecular Science* **2012**, *2*, 73–78. DOI: 10.1002/wcms.81.

[287] F. Neese, "Software update: the ORCA program system, version 4.0", *WIREs Computational Molecular Science* **2018**, *8*, e1327. DOI: 10.1002/wcms.1327.

[288] M. Barbatti, A. C. Borin, and S. Ullrich, *Photoinduced processes in nucleic acids*, Springer, 2015. DOI: 10.1007/128_2014_569.

Published Articles

- K. Szkaradek, K. Buzar, E. A. Pidko, and B. M. Szyja, "Supported Ru metalloporphyrins for electrocatalytic CO2 conversion", ChemCatChem 2018, 10, 1814–1820. doi: 10.1002/cctc.201701045.

- K. E. Szkaradek, P. Stadlbauer, J. Šponer, R. W. Góra, and R. Szabla, "UV-induced hydrogen transfer in DNA base pairs promoted by dark $n\pi^*$ states", Chemical Communications 2020, 56, 201–204. doi: 10.1039/C9CC06180K.

- K. Szkaradek, and R. Góra, Theoretical insight into adenine-uracil and adenine-thymine photodeactivation mechanisms., ChemRxiv, 2024. doi:10.26434/chemrxiv-2024-d3fhc This content is a preprint and has not been peer-reviewed. (submitted to Physical Chemistry Chemical Physics).

- D. Wiczew, A. Borowska, K. Szkaradek, T. Biegus, K. Wozniak, M. Pyclik, M. Sitarska, L. Jaszewski, L. Radosinski, B. Hanus-Lorenz, et al., "Molecular mechanism of vSGLT inhibition by gneyulin reveals antiseptic properties against multidrug-resistant gram-negative bacteria", Journal of Molecular Modeling 2019, 25, 1–9. doi: 10.1007/s00894-019-4073-9.

- M. Dudek, M. Deiana, K. Szkaradek, M. J. Janicki, Z. Pokładek, R. W. Góra, and K. Matczyszyn, "Light-induced modulation of chiral functions in G-quadruplex–photochrome systems", The Journal of Physical Chemistry Letters 2021, 12, 9436–9441.doi: 10.1021/acs.jpclett.1c02207.